Beyond SOD1: Detailed Characterisation of a TDP-43 Transgenic Mouse Model of Motor Neurone Disease

By

Jodie Stephenson

Sheffield Institute for Translational Neuroscience

University of Sheffield

Submitted for the degree of Doctor of Philosophy (PhD)

January 2017

Acknowledgments

First and foremost I wish to thank Professor Dame Pamela Shaw for her faith in giving me the opportunity to do a PhD in the first place, and her guidance throughout. A huge thank you to Dr Richard Mead for his everlasting confidence in my abilities and capacity to see the positives in everything. I also wish to thank Dr James Alix, Dr Aneurin Kennerley and Dr Thomas Jenkins for generously contributing their specialist expertise and time.

Past and present members of the Mead group have all been a great team throughout my project and I would especially like to thank Dr Nazia Maroof, Dr Matthew Sellwood, Dr Matthew Stopford, Heledd Brown-Wright and Yuri Ciervo for their support and help. The nursing team and my office colleagues have all played a massive part in keeping me sane throughout my PhD, particularly by listening to my rants, and I can't thank them enough.

I'd also like to thank my family for the beer and laughter, especially my nephew Jake who has always provided a ray of sunshine, even in the hardest of times. Thank you also to the Watkins family who have provided wine and supportive words throughout. Last but not least, an incredibly enormous thank you to my boyfriend Matthew Watkins who has endured a lot of panic and stress from me but has always remained positive, supportive and encouraging.

Abstract

Background: Motor neurone disease (MND) is a fatal, progressive, neurodegenerative disease causing muscle weakness, spasticity and paralysis. No small molecule drugs have translated from MND mouse models to MND patients, possibly because of MND mouse models being based on SOD1 mutations, representing only a small proportion of patients. Nearly all non-SOD1 patients have TDP-43 pathology, whereas SOD1 patients do not, suggesting a mechanistic difference between non-SOD1 and SOD1-related MND. A TDP-43 model may be more representative of the patient population and lead to better translation of treatments. There is also a need for translational biomarkers in MND to further improve translation.

Methods: A colony of mice transgenic for mutant human TDP-43 (TDP-43^{Q331K}) was established, alongside a control line (TDP-43^{WT}). The mice were characterised for motor function including rotarod, gait analysis, and neuroscoring. Immunohistochemical, mRNA and protein level studies were also carried out. Increased weight was noted in the TDP-43^{Q331K} mice, leading to a study of voluntary activity and food intake. A further study investigated electrophysiological parameters, apathy, and riluzole treatment. Preclinical 31P-MRS imaging was carried out in $SOD1^{G93A}$ mice in an attempt to find a translational biomarker.

Results: TDP-43^{Q331K} mice developed a progressive phenotype, whilst TDP-43^{WT} mice showed none. TDP-43^{Q331K} mice showed signs of motor dysfunction, increased TDP-43 in the nucleus and cytoplasm of motor neurons (supported by increased mRNA and protein levels), astrogliosis, and microgliosis in the spinal cord, apathy, overeating and electrophysiological findings suggestive of denervation. Riluzole may have had a mild treatment effect in TDP-43^{Q331K} mice, measured by electrophysiology. No conclusions could be drawn from the preclinical 31P-MRS due to animal welfare issues.

Conclusions: TDP-43^{Q331K} mice have a progressive motor phenotype of low variability with reliable motor, pathological and cognitive readouts of disease and may provide a useful model for evaluating potential neuroprotective therapies.

Table of Contents

List of Figures

List of Tables

Abbreviations	
ACh	acetylcholine
ADP	adenosine diphosphate
ALS	amyotrophic lateral sclerosis
ALS-FRS-R	ALS functional rating scale revised
ATP	adenosine triphosphate
C9ORF72	chromosome 9 open reading frame 72
CMAP	compound muscle action potential
CNS	central nervous system
CSF	cerebrospinal fluid
DAPI	4',6-diamidino-2-phenylindole
ddPCR	droplet digital PCR
dH_2O	distilled water
Dot1l	disruptor of telomeric silencing 1-like
DTI	diffusion tensor imaging
ECL	enhanced chemiluminescence
EMG	electromyography
EPP	endplate potential
FTD	frontotemporal dementia
FUS	fused in sarcoma
GAPDH	glyceraldehyde 3-phosphate dehydrogenase
GFAP	glial fibrillary acidic protein
GLUT4	glucose transporter type 4
hnRNP	heterogeneous ribonucleoprotein
HRP	horseradish peroxidase
MEPs	motor evoked potentials
MND	motor neurone disease
MRI	magnetic resonance imaging
MRS	magnetic resonance spectroscopy
MUNE	motor unit number estimation
MUNIX	motor unit number index

NES	nuclear export signal
NIV	non-invasive ventilation
NLS	nuclear localisation signal
NMJ	neuromuscular junction
NTg	non-transgenic
PBP	progressive bulbar palsy
PBS	phosphate buffered saline
PCr	phosphocreatine
PCR	polymerase chain reaction
PFA	paraformaldehyde
Pi	inorganic phosphate
PK	pharmacokinetic
PLS	primary lateral sclerosis
PMS	progressive muscular atrophy
qPCR	real-time PCR
RT	room temperature
SOD1	superoxide dismutase 1
SPF	specified pathogen free
TARDBP	transactivating response DNA binding protein 43
TBC1D1	TBC1 domain family member 1
TIC	total ion current
TR	repetition time
WT	wild type

1. Introduction

1.1. Motor Neurone Disease (MND)

Motor neurone disease (MND) is a progressive neurodegenerative disease causing muscle weakness, wasting, spasticity and eventual paralysis. The lifetime risk of developing MND is approximately 1 in 400 (van Rheenen et al., 2016). 50% of patients die within 2 years of diagnosis (Hoppitt et al., 2011), most commonly from respiratory failure due to weakening of the diaphragm and intercostal muscles (Berlowitz et al., 2016).

1.1.1. Clinical Presentation

The majority of patients present with the disease aged 55-75 years (Bergman et al., 2015), however, the disease is frequently identified in patients of all ages, occasionally as young as in the third or fourth decade of life (Beghi et al., 2006). Although 50% of patients die within 2 years of diagnosis (Hoppitt et al., 2011), 5-10% of patients live over a decade beyond diagnosis (Chio et al., 2009).

MND has a tendency to affect a larger proportion of men than women, more so in the younger generations, with as many as 80% of patients under 40 being male (del Aguila et al., 2003).

The majority of patients (66%) present with limb onset MND (Gordon, 2013) in which a particular limb is affected by weakness, fasciculations and/or spasticity, usually followed by symptoms in the contralateral limb or the other limb on the same side of the body. Approximately 30% of patients present with bulbar onset MND in which they experience dysarthria and/or dysphagia (Mitchell and Borasio, 2007). The remaining patients (approximately 5%) present with respiratory onset MND in which they have difficulty breathing (Gautier et al., 2010). The disease will usually progress from the site of onset to eventually involve limb, bulbar, and respiratory symptoms.

The majority of patients show signs of upper and lower motor neurone degeneration such as weakness, fasciculation, spasticity, stiffness, muscle wasting and hyperreflexia and are therefore diagnosed with amyotrophic lateral sclerosis (ALS). However, the disease is occasionally confined to an upper or lower motor neurone variant. Two percent of patients are diagnosed with the upper motor neurone variant, primary lateral

sclerosis (PLS), and experience spasticity, brisk reflexes, stiffness and weakness (Rowland and Shneider, 2001). Approximately 20 percent of patients are diagnosed with the lower motor neurone variant, progressive muscular atrophy (PMA), and experience fasciculations, muscle wasting and weakness (Rowland and Shneider, 2001). Patients are occasionally diagnosed with progressive bulbar palsy (PBP) in which their symptoms are initially confined to the bulbar area, however, these patients usually go on to develop ALS (Karam et al., 2010).

It is now well recognised that MND is on a disease continuum with frontotemporal dementia (FTD) and current data suggest that at least 50% of MND patients demonstrate cognitive/behavioural changes (Ringholz et al., 2005). 10-15% of MND patients fulfil the criteria for ALSFTD, as diagnosed using a battery of psychological tests (Ringholz et al., 2005). The symptoms of FTD include behavioural changes including apathy, disinhibition, compulsive behaviour, changes in eating habits and loss of empathy (Chan et al., 2015).

1.1.2. Diagnosis and Biomarkers of MND

Diagnosis of MND requires the experience and knowledge of a specialist neurologist due to a lack of diagnostic tools/biomarkers. There is no specific test for MND and diagnosis therefore requires elimination of other potential diseases or health problems which may have caused the patient's symptoms. Patients tend to present to a Neurologist approximately 12 months from symptom onset (Mitchell et al., 2010) and will usually undergo an MRI scan, blood tests and electrophysiological testing before a diagnosis can be given.

There is an ongoing effort to find a suitable biomarker of MND and this is a rapidly evolving field which has shown progress over recent years (Turner et al., 2013). A definitive biomarker is not only required for diagnosis but also to monitor disease progression and prognosis. A biomarker of progression would be beneficial in therapeutic trials as it would enable a more accurate gauge of survival than the current measures of survival, such as ALS functional rating scale revised (ALS-FRS-R) (Brooks et al., 2000) and strength testing. The identification of translational biomarkers (a biological measurement which can be reliably measured in MND models as well as patients) would be extremely useful for monitoring the effect of drugs in both preclinical

and clinical trials, allowing for easier determination of appropriate dosage by matching the change in biomarker levels found in models, to those found in patients.

Potential biomarkers have been investigated in many areas including imaging, electrophysiology, blood sampling and cerebrospinal fluid (CSF) sampling (Turner et al., 2013, Rosenfeld and Strong, 2015).

1.1.3. Mechanisms of MND

The principal mechanisms underlying the pathophysiology of MND have not been definitively identified. However, many mechanisms have been implicated including oxidative stress (Cookson and Shaw, 1999), protein aggregation (Wood et al., 2003), axonal transport dysfunction (El-Kadi et al., 2007), neuroinflammation (Hooten et al., 2015), microglial activation (Turner et al., 2004), defects of RNA processing (Polymenidou et al., 2012), excitotoxicity (Shaw, 1994) and energy metabolism dysfunction (Dupuis et al., 2011), including mitochondrial dysfunction (Beretta et al., 2003). It is unclear whether each of these mechanisms occurs simultaneously or as part of a sequential cascade. It is also unclear whether particular disease mechanisms relate to specific phenotypes, subgroups or genetic mutations of the disease.

1.1.4. Treatment of MND

The lack of a well-defined mechanistic understanding of disease pathogenesis has hampered efforts to develop effective therapies. Riluzole, a drug which reduces glutamate excitotoxicity, was first described as a therapeutic agent for MND in 1994 (Bensimon et al., 1994) and has been shown to extend life by several months (Stewart et al., 2001, Miller et al., 2003). However, in the $SOD1^{G93A}$ mouse model of MND (the most commonly used animal model of MND), riluzole appears to improve motor function but has little effect on lifespan (Gurney et al., 1998). These findings fit with a common hypothesis that riluzole may be very beneficial for a subgroup of patients, but not necessarily effective for all patients (Georgoulopoulou et al., 2013).

Patients experiencing respiratory failure are usually given non-invasive ventilation (NIV) to aid respiratory function. NIV is commonly believed to improve quality of life,

particularly by improving quality of sleep (Bourke et al., 2006), and has also been shown to extend life by an estimated 13 months (Berlowitz et al., 2016).

A recent study of diaphragm pacing has found this treatment to be detrimental as it was associated with decreased survival in comparison to treatment with NIV alone (McDermott et al., 2015a).

Insertion of a feeding tube is a useful symptomatic treatment, enabling patients to maintain their body weight after losing the ability to swallow. Maintenance of body weight is highly correlated with increased survival in MND patients (Desport et al., 2000) and it appears to be crucial that patients receive a feeding tube earlier on in disease to prevent major loss of body weight (McDermott et al., 2015b).

1.2. Causes of MND

Approximately 5-10% of MND cases are familial, leading to the identification of many causal mutations in several genes. Currently, causal genetic mutations have been implicated in approximately two thirds of familial MND cases and 11% of sporadic cases (Renton et al., 2014).

The first gene to be linked to MND was superoxide dismutase 1 (*SOD1*) (Rosen et al., 1993). Following this initial discovery, causal mutations were identified in many other genes including fused in sarcoma (*FUS*), transactivating response DNA binding protein 43 (*TARDBP*) and a G_4C_2 repeat expansion was identified in *C9ORF72* (DeJesus-Hernandez et al., 2011), all of which have been found to cause MND and/or FTD (see *table 1.1*).

Table 1. 1: Causal genetic mutations in MND. *Table adapted from (Taylor et al., 2016).*

Locus	Gene	Protein	Protein function	Mutations	Proportion of MND		Reference
					Familial	Sporadic	
21q22.1	*SOD1*	Cu–Zn superoxide dismutase	Superoxide dismutase	>150	20%	2%	(Rosen et al., 1993)
2p13	*DCTN1*	Dynactin subunit 1	Component of dynein motor complex	10	1%	<1%	(Puls et al., 2003)
14q11	*ANG*	Angiogenin	Ribonuclease	>10	<1%	<1%	(Greenway et al., 2006)
1q36	*TARDBP*	TDP-43	RNA-binding protein	>40	4-5%	<1%	(Sreedharan et al., 2008, Kabashi et al., 2008)
16p11.2	*FUS*	FUS	RNA-binding protein	>40	5%	<1%	(Vance et al., 2009, Kwiatkowski et al., 2009)
9p13.3	*VCP*	Transitional endoplasmic reticulum ATPase	Ubiquitin segregase	5	1–2%	<1%	(Johnson et al., 2010)
10p15-p14	*OPTN*	Optineurin	Autophagy adaptor	1	4%	<1%	(Maruyama et al., 2010)
9p21-22	*C9orf72*	C9orf72	Possible guanine nucleotide exchange factor	Intronic GGGGCC repeat	25%	10%	(DeJesus-Hernandez et al., 2011, Renton et al., 2011)
Xp11.23-Xp13.1	*UBQLN2*	Ubiquilin 2	Autophagy adaptor	5	<1%	<1%	(Deng et al., 2011)
5q35	*SQSTM1*	Sequestosome 1	Autophagy adaptor	10	<1%	unknown	(Fecto et al., 2011, Teyssou et al., 2013)
17p13.2	*PFN1*	Profilin-1	Actin-binding protein	5	<1%	<1%	(Wu et al., 2012a)
12q13.1	*HNRNPA1*	hnRNP A1	RNA-binding protein	3	<1%	<1%	(Kim et al., 2013, Liu et al., 2016a)2013
5q31.2	*MATR3*	Matrin 3	RNA-binding protein	4	<1%	<1%	(Johnson et al., 2014)
2q36.1	*TUBA4A*	Tubulin α-4A chain	Microtubule subunit	7	<1%	<1%	(Smith et al., 2014)

22q11.23	*CHCHD10*	Coiled-coil-helix-coiled-coil-helix domain-containing protein 10	Mitochondrial protein of unknown function	2	<1%	<1%	(Bannwarth et al., 2014)
12q14.1	*TBK1*	Serine/threonine-protein kinase TBK1	Regulates autophagy and inflammation	10	unknown	unknown	(Freischmidt et al., 2015)

1.2.1. SOD1

SOD1 codes for copper/zinc superoxide dismutase and over 160 causal mutations have since been identified in *SOD1*, most of which are missense mutations with varying locations in the gene (Rosenfeld and Strong, 2015, Al-Chalabi et al., 2012). Most *SOD1* cases show a dominant inheritance in families and dismutase activity has been found to be reduced in most, but not all cases, showing no correlation between dismutase activity and severity of disease (Brotherton et al., 2011, Andersen et al., 1995). *SOD1* mutations are associated with a wide range of heterogeneity and are rarely associated with cognitive deficits (Renton et al., 2014).

The main function of SOD1 is to protect cells from oxidative stress (Rosen et al., 1993). However, when a mutation in *SOD1* occurs, the SOD1 protein becomes misfolded in the motor neurons and glia of the spinal cord (Nagai et al., 2007).

Causal mutations in *SOD1* account for approximately 12% of familial MND cases, and 1-2% of sporadic cases (Renton et al., 2014). In recent years, SOD1-linked MND cases have been considered as distinct from other MND cases as SOD1 patient pathology lacks the TDP-43 proteinopathy found in almost all other cases (Mackenzie et al., 2007). Post-mortem SOD1 patient cord shows ubiquitin and p62-positive skeins or inclusions in the motor neurons without TDP-43 pathology (Mackenzie et al., 2007).

1.2.2. TARDBP

The *TARDBP* gene is located on chromosome 1 (Stover et al., 2001) and consists of 6 exons. *TARDBP* codes for TDP-43, a DNA-/RNA-binding protein (Ou et al., 1995, Buratti and Baralle, 2012). Originally described as an HIV-1 protein (Ou et al., 1995), TDP-43 has more recently been uncovered as a key player in neurodegenerative disease, including MND and FTD (Neumann et al., 2006, Tollervey et al., 2011).

1.2.2.1. TDP-43 Structure and Location

The TDP-43 protein is 414 amino acids long and is a highly conserved heterogeneous ribonucleoprotein (hnRNP) (Krecic and Swanson, 1999). As shown in *figure 1.1* TDP-43 contains two RNA recognition motifs (Neumann et al., 2006), a nuclear export signal

(NES) (Winton et al., 2008), a nuclear localisation signal (NLS) (Winton et al., 2008), and a glycine-rich C-terminal sequence (Wang et al., 2004).

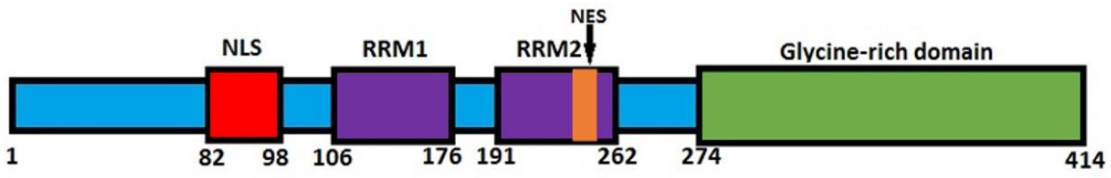

Figure 1. 1: TDP-43 structure (NLS = nuclear localisation signal, RRM = RNA recognition motif, NES = nuclear export signal).

TDP-43 is predominantly nuclear, but also shuttles between the nucleus and cytoplasm (Winton et al., 2008), in a transcription-dependent manner (Ayala et al., 2008). Efflux of TDP-43 from the nucleus to the cytoplasm is associated with cellular stress (Barmada et al., 2010).

The C-terminus of TDP-43 is critically involved in the cellular localisation, interactions with other proteins, and solubility of TDP-43 (Ayala et al., 2008, Budini et al., 2015, Chang et al., 2013). Whereas, the N-terminus is involved in promoting oligomerisation and enhancing DNA-binding affinity (Chang et al., 2012). The N-terminus is vital for the folded structure and splicing of TDP-43 (Zhang et al., 2013), and is integral to the function of the second RNA-recognition motif (Wang et al., 2013).

1.2.2.2. TDP-43 Function

TDP-43 is involved in multiple functions including DNA/RNA-binding, transcription, translational regulation, RNA splicing, transportation, mRNA stability, stress granule response, and microRNA biogenesis (Buratti and Baralle, 2010, Buratti and Baralle, 2012). TDP-43 can regulate its own mRNA levels via a negative feedback loop and therefore autoregulates TDP-43 protein levels (Ayala et al., 2011, Koyama et al., 2016) via the ubiquitin proteasome system and autophagy (Scotter et al., 2014, Wang et al., 2010). TDP-43 binds to the 3' UTRs of over 1000 transcripts, regulating splicing and stability and therefore influencing many cellular processes (Tollervey et al., 2011, Polymenidou et al., 2011). TDP-43 also has numerous binding sites on non-coding RNAs, which may be involved in many processes including transcription regulation and posttranscriptional processing (Tollervey et al., 2011).

TDP-43 is an important component of RNA transport granules and protein synthesis in dendrites, which are key facets of neuronal plasticity and development (Tollervey et al., 2011). A likely synaptic role for TDP-43 stems from observations that TDP-43 binds to many RNA targets which are involved in synaptic function, and deletion of TDP-43 in cultured neurons causes abnormal dendrite morphology. It therefore appears likely that TDP-43 plays a key role in synaptic function (Fujii et al., 2005).

Under cellular stress, TDP-43 forms cytoplasmic stress granules from protein complexes of redundant mRNA's (Colombrita et al., 2009) and TDP-43 tends to relocate to the cytoplasm (Barmada et al., 2010).

1.2.2.3. TDP-43 Pathology in MND-FTD

Discovery of TDP-43 as a key part of ubiquitinated cytoplasmic neuronal inclusions in both MND and FTD (Neumann et al., 2006), was crucial in identifying these diseases as existing on a continuum.

Approximately 97% of MND patients (including most non-SOD1 MND patients) have inclusions of ubiquitinated TDP-43 protein in motor neurons (Mackenzie et al., 2007). In the hippocampus, neocortex and spinal cord of both MND and FTD patients, TDP-43 mislocalises from the nucleus to the cytoplasm and forms detergent-resistant aggregates, containing hyper-phosphorylated, ubiquitinated, and C-terminal truncated, TDP-43 (Neumann et al., 2006, Tollervey et al., 2011). The nuclear content of TDP-43 becomes depleted.

Neuronal aggregates and inclusions of TDP-43 in the cytoplasm of motor neurons have become a pathological hallmark of MND. These aggregates and inclusions tend to be immunoreactive for ubiquitin and p62 (a marker of autophagy) but negative for tau and α-synuclein (Neumann et al., 2006, Arai et al., 2006). These inclusions are also found in around 50% of FTD patients (Ling et al., 2013), regardless of whether they carry a mutation in the *TARDBP* gene. TDP-43 pathology in non-primary motor areas appears highly correlated with cognitive functioning in MND-FTD (Prudlo et al., 2016).

Aggregation of TDP-43 may not be necessary for neurodegeneration, or could be an occurrence at the very end stage of cell death, as several TDP-43 mouse models have shown neurodegeneration without aggregates (Arnold et al., 2013, Kraemer et al., 2010,

Ricketts et al., 2014). A recent study of cultured cells and primary neurons showed that the extreme N-terminus of TDP-43 regulates the formation of TDP-43 aggregates and deletion of the N-terminus reduces aggregation (Sasaguri et al., 2016).

Disruption of the NLS or NES causes cytoplasmic mislocalisation and aggregation of TDP-43, regardless of whether a mutation is present in the C-terminus (Winton et al., 2008). Cleavage of TDP-43 results in C-terminal fragments moving out of the nucleus and in to the cytoplasm. This occurrence is enhanced by the presence of C-terminal mutations (Sreedharan et al., 2008, Rutherford et al., 2008) and cellular stress (Dormann et al., 2009). Misfolded TDP-43 may cause further misfolding and aggregation of wild-type TDP-43, suggesting the pathology can spread throughout cells and intercellularly across axon terminals, in a prion-like manner (Zhu et al., 2014, Feiler et al., 2015).

A recent study suggested that cytoplasmic TDP-43 of motor neurons may accumulate predominantly within the mitochondria, binding mRNAs and therefore, preventing translation, impairing aerobic energy metabolism by reducing complex I activity (Wang et al., 2016).

1.2.2.4. MND-FTD Causal Mutations in TARDBP

Following the discovery of TDP-43 pathology in MND, mutations in *TARDBP* were investigated. Over 40 known mutations in *TARDBP* have been associated with MND (Renton et al., 2014), most of which have been identified in the C-terminal glycine rich domain of TARDBP (Gitcho et al., 2008, Sreedharan et al., 2008), which is associated with protein-protein interactions and cellular localisation (Ayala et al., 2008).

Causal mutations in *TARDBP* account for approximately 4-5% of familial MND cases, and 1% of sporadic cases (Renton et al., 2014, Millecamps et al., 2010). Mutations in *TARDBP* are inherited in an autosomal dominant manner and have been found to cause both MND and FTD. Within the one family, members with the same mutation may present with MND and no signs of FTD, whereas others present with FTD and no signs of MND (Sreedharan et al., 2008).

Patients with causal mutations in *TARDBP* have a tendency to present with upper limb onset disease at a slightly earlier age when compared to sporadic cases, and show a moderately prolonged duration of disease (Corcia et al., 2012). The pathology of

patients with *TARDBP* mutations is similar to that of sporadic patients (Yokoseki et al., 2008) with neuronal loss, gliosis and TDP-43 positive cytoplasmic inclusions in both the upper and lower motor neurons.

1.2.2.5. TDP-43 Loss and/or Gain of Function in MND-FTD

Although it is well established that TDP-43 aggregates are a key pathological finding in MND, it is unclear whether they are a causal mechanism of neuronal death, or a consequence of upstream events. It is possible that TDP-43 aggregates cause toxicity, either via a gain and/or loss of function of TDP-43.

Several studies have suggested that a loss of nuclear TDP-43 causes disease via loss-of-function. In support of this splicing defects have been found in neuronal cell cultures (De Conti et al., 2015), post-mortem MND patient spinal cord and patient-derived cells (Highley et al., 2014), and mouse embryonic stem cells (Ling et al., 2015). Additionally, knockout of TDP-43 in mice was shown to be embryonic lethal (Chiang et al., 2010, Kraemer et al., 2010, Sephton et al., 2010), highlighting the importance of TDP-43 in development. Whereas partial or post-developmental knockout of TDP-43 produces progressive motor phenotypes and proteinopathy (Wu et al., 2012b, Iguchi et al., 2013, Yang et al., 2014).

Conversely, the aggregation of TDP-43 in the cytoplasm may cause a toxic gain-of-function. Multiple TDP-43 models have shown that an increase in wild type TDP-43 causes neurodegeneration and proteinopathy (Wils et al., 2010, Tsai et al., 2010, Stallings et al., 2010, Xu et al., 2010, Shan et al., 2010, Igaz et al., 2011, Swarup et al., 2011), despite the fact that no overexpression has been found in MND patients. The most logical explanation for this finding is a toxic gain of function in patients, replicated by an increased expression of TDP-43 in the models. Furthermore, the cytoplasmic level of TDP-43 has been shown to be highly associated with neuronal death in primary rat cortical neurons (Barmada et al., 2010), also suggestive of toxic gain-of-function.

However, other TDP-43 models have shown a role of loss and gain of splicing function (Arnold et al., 2013) and altered TDP-43 structure by misfolding (Zhu et al., 2014), which may indicate both loss and gain-of-function mechanisms being involved in the disease process.

1.2.3. FUS

Causal mutations in FUS account for approximately 4% of familial MND cases, and 1% of sporadic cases (Renton et al., 2014).

The FUS protein binds to RNA and has multiple functions including transcription, RNA splicing and transport (Vance et al., 2009). The FUS protein is predominantly located in the nucleus, with a very similar role and location to TDP-43. Mutations in FUS cause similar pathology to that of TDP-43 as the FUS protein aggregates in the cytoplasm of neurons without the presence of TDP-43 and ubiquitin (Kwiatkowski et al., 2009, Vance et al., 2009).

1.2.4. C9ORF72

The most commonly found causal mutations are in the chromosome 9 open reading frame 72 (C9ORF72) gene, which are responsible for 40-50% of familial MND cases and around 7% of apparently sporadic cases (Renton et al., 2014). The genetic alterations consist of a hexanucleotide (GGGGCC) repeat expansion in intron 1 of the C9ORF72 gene. Many patients with these mutations also show signs of FTD (DeJesus-Hernandez et al., 2011, Renton et al., 2011). Mutations in C9ORF72 have also been found in 25% of patients with FTD without signs of MND (Majounie et al., 2012).

A higher proportion of patients with repeat expansions in C9ORF72 present with bulbar onset MND compared to other genetic subgroups and there appears to be an anticipation effect in families, meaning that subsequent generations carrying a C9ORF72 expansion will develop MND-FTD progressively earlier (Cooper-Knock et al., 2014).

The mechanisms linked to C9ORF72 pathogenesis include RNA toxicity, loss-of function, and accumulation of RNA-foci repeat associated non-ATG translated dipeptide repeat proteins (Haeusler et al., 2016, Hayes and Rothstein, 2016).

1.2.5. Genetic Risk Factors

The investigation of genetic risk factors has been a broadening field in recent years, culminating with the onset of Project MinE, a large-scale worldwide project to identify genetic mutations involved in MND.

Several studies have found genetic risk factors for both familial and sporadic MND. It often appears that genetic susceptibility variants (e.g. ATXN2, SMN1 and UNC13A) are found in familial cases in which a causal mutation already exists (Dekker et al., 2016, Elden et al., 2010). This may influence the age of onset of disease, explaining why members of the same family with the same causal mutation may present with MND at different ages and sites of onset.

Genetic susceptibility variants are now being identified in sporadic patients, such as TUBA4A (Pensato et al., 2015) and UNC13A (Manuel Vidal-Taboada et al., 2015), suggesting that a genetic risk factor combined with environmental factors, may be a trigger for sporadic MND.

1.2.6. Environmental Risk Factors

Environmental risk factors are implicated not only in sporadic MND cases but also in familial cases, since family members who share causal genetic mutations will often develop disease at very difference ages, and show a propensity to develop FTD or MND. Therefore, it is likely that the occurrence, timing and severity of MND is dependent on a combination of genetic and environmental risk factors. A wide variety of environmental factors have been proposed over time, mostly from epidemiological studies.

Military service has been identified as a potential risk factor for MND in several studies (Haley, 2003, Weisskopf et al., 2005), which may be linked to exposure of BMAA and cyanobacteria (Cox et al., 2009). A high proportion of MND in Italian football players was highlighted over a decade ago (Chio et al., 2005), adding to the debate over whether high levels of physical activity may be a risk factor for MND (Harwood et al., 2009, Harwood et al., 2016, Longstreth et al., 1998, Armon, 2003, Sutedja et al., 2009). Several studies and reviews have found smoking to be a risk factor for MND (Armon, 2003, Armon, 2009, Weisskopf et al., 2004), as well as exposure to toxins (Gunnarsson et al., 1992) and exposure to magnetic fields (Sutedja et al., 2009).

1.3. Modelling of MND

Modelling of MND is crucial to increase understanding of the disease and find potential therapies. A wide variety of model types have been used to model MND, each with distinct advantages and limitations for use *(see table 1.2)*.

Table 1. 2: Features and limitations of modelling methods. *Table adapted from (Clerc et al., 2016).*

Methods	**Examples**	**Features**	**Limitations**
In vivo	*Caenorhabditis elegans*	Cellular focus without systemic complexity	Lacks spinal cord and lower motor neurons affected by MND
	Drosophila	More complexity than *C. elegans*, but less than vertebrates	Wild-type human gene expression is toxic; relatively simple nervous system structure compared with human
	Zebrafish	Cheap, quick, simple; vertebrate	Not mammalian; relatively new models
	Mouse	Many different models; short lifespan and disease length	Overexpression artefacts; unique biological properties compared to humans (lifespan, metabolism,*etc.*)
	Rat	Larger size; short lifespan and disease length	Disease phenotype differences from mouse
	Dog	Naturally occurring disease (Canine Degenerative Myelopathy)	Disease similar to, but not same as MND
	Nonhuman primates	Better disease mimic than other species	Expensive, long lived, ethical issues
In vitro cultures	Yeast	Simple, models protein aggregation well	Not neuronal, or human
	Patient dissociated motor neurons	Natural disease gene expression; easy, direct drug application	Finite lifespan; difficult to transfect

Methods	Examples	Features	Limitations
	NSC34	Immortal motor neuron-like cell line; manipulable	Induced disease phenotype; not true motor neuron line
	Stem cells	Can transplant or differentiate for study/transplant	Transplantation still experimental
	Induced pluripotent stem cells	Can differentiate into motor neurons or glia	Expensive; low neuronal yields; clonal issues.
	Tissue slice culture (animal)	Easily manipulated; more systemic than cell cultures	Same issues as whole animal in trying to find good model; distant connections severed

1.3.1. Non-mouse *in Vivo* Models of MND

Mice are often the model of choice for testing potential drug therapies once a drug has shown promise in vitro.

At the less complex end of the spectrum *Drosophila melangoster* (fruit fly), *Caenorhabditis elegans* (nematode) and *Danio rerio* (zebrafish) models can be used for relatively fast, cheap and simple drug screening. This is because development and breeding periods are very short and assays can be carried out very effectively using quantification of fluorescence, without dissecting the animals. Nematode models have been produced carrying mutations in *SOD1* (Wang et al., 2009) and *FUS* (Murakami et al., 2012). Fly models of *SOD1* (Watson et al., 2008), *TARDBP* (Diaper et al., 2013), *FUS* (Chen et al., 2011) and *C9ORF72* (Mizielinska et al., 2014) have also shown the effects of these mutations on various mechanisms and pathways. However, fruit flies and nematodes lack spinal cords and the structure of disease-related genes may differ from human genes, so findings in these models may not be well replicated in vertebrate models.

In comparison, zebrafish have an orthologue for approximately 82% of genes which are associated with human diseases (Howe et al., 2013). Several zebrafish models have been developed modelling a variety of causal genetic mutations including *SOD1*

(Lemmens et al., 2007, Ramesh et al., 2010), *TARDBP* (Kabashi et al., 2010), *FUS* (Acosta et al., 2014) and *C9ORF72* (Ciura et al., 2013). Zebrafish may be a more promising model for identifying potentially effective compounds, before moving on to the more costly and time consuming mammalian models.

At the more complex, human-like end of the model spectrum we have non-human primates, which are very costly, time consuming and carry a heavy ethical burden. Despite this, a cynomolgus monkey overexpression model of TARDBP has been produced, showing many of the signs of human MND symptoms and pathology (Uchida et al., 2012).

Several rat models have been created including models with *SOD1* (Llado et al., 2006), *TARDBP* (Zhou et al., 2010) and *FUS* mutations (Huang et al., 2011). Rat models can be very useful, especially because they are considerably larger than mice and this can be key for imaging studies and surgeries. However, rats are more costly than mice and are less easy to use for genetic manipulation.

Consequently, most MND in vivo studies use mouse models, particularly for testing potential drug therapies.

1.3.2. Mouse Models of MND

The first mouse proposed as a model of MND was the Wobbler mouse (Duchen and Strich, 1968), which arose by spontaneous mutation in 1955. The Wobbler mouse carries a mutation in the Vps54 gene (Schmitt-John et al., 2005), which is not associated with MND. This mouse has an MND-like phenotype including muscle atrophy, unsteady gait, reduced body weight, and tremor, however, it does not carry an MND-linked mutation and pathological studies have identified prominent vacuoles in the motor neurons, which is not a typical feature of MND (Moser et al., 2013). Since the discovery of the Wobbler mouse, many models have been created, some of which model mutations found in only a small number of patients. The following table provides a summary of MND models for the most commonly implicated genes *SOD1, TARDBP, FUS* and *C9ORF72* (described previously).

Table 1. 3: Summary of mouse models of SOD1, TARDBP, FUS and C9ORF72. + demonstrates one or two features of MND (e.g. phenotype: muscle atrophy; pathology: neuronal loss), ++ demonstrates several features of MND (e.g. phenotype: muscle atrophy, weakness, anxiety; pathology: neuronal loss, astrogliosis, decreased brain volume), +++ demonstrates most features of MND (phenotype: muscle atrophy, weakness, progression to paralysis, anxiety, antisocial behaviour; pathology: neuronal loss, astrogliosis, microgliosis, cytoplasmic inclusions, poor NMJ morphology, decreased brain volume).

Implicated gene	Gene status	Phenotype	Pathology	Reference
SOD1	Human $SOD1^{G93A}$ transgenic	+++	+++	(Gurney et al., 1994)
	Human $SOD1^{G37R}$ transgenic	+++	+++	(Wong et al., 1995)
	Endogenous $SOD1^{G85R}$ mutation	+++	+++	(Bruijn et al., 1997, Ripps et al., 1995)
	GFAP-$SOD1^{G86R}$ transgenic (astrocytes only)	none	+	(Gong et al., 2000)
	Human $SOD1^{H46R/H48Q}$ transgenic	++	+++	(Wang et al., 2002)
	Human $SOD1^{WT}$ transgenic	+	none	(Lino et al., 2002)
	Endogenous $SOD1^{D83G}$ mutation	++	++	(Joyce et al., 2015)
TARDBP	Human TDP-43^{A315T} transgenic	++	+++	(Wegorzewska et al., 2009)

	Human TDP-43^{WT} transgenic	+++	+++	(Wils et al., 2010)
	Endogenous TDP-43^{WT}	++	++	(Tsai et al., 2010)
	Human TDP-43^{WT} transgenic	None	+	(Stallings et al., 2010)
	Human TDP-43^{A315T} transgenic	+	++	(Stallings et al., 2010)
	Human TDP-43^{M337V} transgenic	++	++	(Stallings et al., 2010)
	Human TDP-43^{WT} transgenic	+	++	(Xu et al., 2010)
	Human TDP-43^{WT} transgenic	++	++	(Shan et al., 2010)
	Conditional knockout	unknown	unknown	(Chiang et al., 2010)
	Heterozygous knockout	+	none	(Kraemer et al., 2010)
	Human TDP-43^{WT} transgenic	+	++	(Igaz et al., 2011)
	ΔNLS partial knockout	+	++	(Igaz et al., 2011)
	Human TDP-43^{M337V} transgenic	+++	++	(Xu et al., 2011)
	Human TDP-43^{WT} transgenic	++	+	(Swarup et al., 2011)
	Human TDP-43^{A315T} transgenic	++	++	(Swarup et al., 2011)

	Human TDP-43^{G348C} transgenic	++	+++	(Swarup et al., 2011)
	Conditional knockout	+++	++	(Wu et al., 2012b)
	Human TDP-43^{M337V} transgenic	+++	+++	(Janssens et al., 2013)
	Human TDP-43^{WT} transgenic	++	++	(Janssens et al., 2013)
	Partial knockout	++	++	(Iguchi et al., 2013)
	Human TDP-43^{Q331K} transgenic	++	++	(Arnold et al., 2013)
	Human TDP-43$^{Q331K\text{-}low}$ transgenic	+	+	(Arnold et al., 2013)
	Human TDP-43^{M337V} transgenic	+	+	(Arnold et al., 2013)
	Partial knockout	+++	+	(Yang et al., 2014)
	Endogenous TDP-43^{Q10X} mutation	+	none	(Ricketts et al., 2014)
	Conditional ΔNLS knockout	+++	+++	(Walker et al., 2015)
FUS	Human FUS^{WT} transgenic	+++	++	(Mitchell et al., 2013)
	Partial ΔNLS knockout	+++	++	(Shiihashi et al., 2016)
C9ORF72	Anti-sense oligonucleotide injection	none	+	(Lagier-Tourenne et al., 2013)

	Inducible human $(G_4C_2)_{80}$ repeat expansion transgenic	none	++	(Hukema et al., 2014)
	Human $(G_4C_2)_{500}$ repeat expansion transgenic	none	++	(Peters et al., 2015)
	Human $(G_4C_2)_{100\text{-}1000}$ repeat expansion transgenic	none	++	(O'Rourke et al., 2015)
	Endogenous $(G_4C_2)_{66}$ repeat expansion	++	+++	(Chew et al., 2015)
	Conditional knockout	none	none	(Koppers et al., 2015)
	Human $(G_4C_2)_{450}$ repeat expansion transgenic	++	++	(Jiang et al., 2016)
	Heterozygous knockout	+	none	(Jiang et al., 2016)
	Homozygous knockout	++	none	(Atanasio et al., 2016)
	Homozygous knockout	none	none	(O'Rourke et al., 2016)
	Human $(G_4C_2)_{37\text{-}500}$ repeat expansion transgenic	+++	+++	(Liu et al., 2016b)

1.3.2.1. Lack of Translation from Mouse to Human

The SOD1^{G93A} mouse model is by far the most commonly used mouse model in therapeutic trials of MND (Benatar, 2007, Ludolph et al., 2007). However, compounds found to be effective in the SOD1^{G93A} mice may not then prove effective in human disease, as has been shown with several therapeutics including creatine (Klivenyi et al., 1999, Groeneveld et al., 2003), vitamin E (Gurney et al., 1996, Desnuelle et al., 2001, Graf et al., 2005) and gabapentin (Gurney et al., 1996, Miller et al., 2001). There are several potential reasons for this lack of translation including validity of the model, study design and a lack of translational biomarkers.

1.3.2.1.1. Reliance on One Mouse Model

A key reason for a lack of translation is that the SOD1^{G93A} model is only representative of a very small proportion of familial MND (Ittner et al., 2015). Therefore, a compound found to be effective in this model may also be effective in patients affected by SOD1. However, when given to a wide variety of patients (familial and sporadic), the potential effect on SOD1 patients is lost.

As has been highlighted in recent years, SOD1-based MND appears to be rather distinct from non-SOD1 MND due to the lack of TDP-43 pathology (Mackenzie et al., 2007). The treatment of SOD1 MND separate to non-SOD1 MND may therefore be key to finding effective compounds and the first SOD1-specific drug trial is currently underway.

1.3.2.1.2. Poor Preclinical Study Design

Another key reason for lack of translation is that many trials have used a SOD1^{G93A} model on a mixed genetic background, increasing the variability of disease (Mead et al., 2011) and combined with poor study design this has led to a large number of false positive studies (Scott et al., 2008).

Also, many preclinical trials are carried out without checking the pharmacokinetic (PK) properties of the drug in the model. PK studies should be carried out to ensure the drug is penetrating the blood brain barrier (Ludolph et al., 2010) and accessing the drug target directly in neurons. This PK data can later be used to match an effective dose in mice, to an effective dose in humans as plasma levels of the drug in patient trials can be tested

and compared to the mouse data. One issue with this is that compound levels within the human brain and spinal cord will remain unknown. However, matching the plasma drug levels may lead to more appropriate dosing.

Furthermore, in most pre-clinical drug trials, the compound is administered prior to symptom onset (Benatar, 2007, Ittner et al., 2015, Ludolph et al., 2007) and therefore at a very early stage of the disease. In comparison, patients will not be put on a drug trial until they are far beyond symptom onset and even diagnosis, at which point the disease may be too advanced for the drug to effectively rescue the target disease mechanism. On this note, it can be argued that if a drug was found effective by pre-symptomatic dosing, familial MND could be treated by administering the drug to unaffected family members to delay disease onset or reduce the pace of disease progression (Benatar, 2007). However, no MND patient drug trials have been carried out in this manner and the study design for such an approach would require a prolonged follow-up phase.

Preclinical trial outcomes are frequently assessed by survival of the mice (Benatar, 2007), disregarding the effect of a drug on quality of life and symptom severity. However, patients would undoubtedly welcome a drug which improved their quality of life without an effect on survival. Preclinical investigators are rarely blinded to which group is the treated group (Benatar, 2007) and this leads to a potential bias when collecting data. Randomisation of mice to treatment groups is often neglected, creating potential for confounding factors to emerge (Benatar, 2007).

A key example of these issues is in the case of minocycline, an inhibitor of microglial activation, which was found to extend survival of $SOD1^{G93A}$ mice when administered pre-symptomatically (Kriz et al., 2002). However, when a phase III human clinical trial was carried out, minocycline appeared to accelerate disease progression in patients (Gordon et al., 2007). Subsequently, a preclinical trial was carried out in which $SOD1^{G93A}$ mice were administered minocycline post symptom onset and no effect on survival was found (Keller et al., 2011).

1.3.2.1.3. Lack of Translational Biomarkers

As mentioned previously (1.1.2.), there is a lack of reliable biomarkers in MND, which are required not only for diagnosis but also disease monitoring. This need extends to preclinical biomarkers which will translate from animal models to patients (Ludolph et al., 2010). If biomarkers could be used in both preclinical and patient trials this could offer invaluable insights into the disease pathophysiology and, importantly, reduce the duration and cost of clinical trials. A translatable biomarker would be incredibly valuable in translational studies to gauge the dose administered to patients if the effect of the drug on a biomarker could be matched between models and patients.

Whilst the search for reliable biomarkers continues in patients, no previous reports of translational biomarker investigations could be found. One area under constant investigation is imaging biomarkers, including magnetic resonance imaging (MRI), magnetic resonance spectroscopy (MRS) and diffusion tensor imaging (DTI) (Chio and Traynor, 2015).

New research is currently underway at the institute, investigating 31P-MRS as a biomarker in MND patients. 31P-MRS measures phosphorous containing compounds, many of which are involved in energy metabolism, which is known to be dysregulated in MND (Dupuis et al., 2011). Therefore, a minor part of this project was to investigate 31P-MRS as a translational biomarker in a mouse model of MND.

1.3.2.2. Identifying a Mouse Model More Likely to Translate

A mouse model with a genetic mutation known to cause MND may only be representative of patients with mutations in the same gene, possibly even the same mutation in that gene. However, if a mouse model was representative of sporadic MND, or at least a large proportion of MND, it would be far more likely to show translation of therapeutics to humans.

As mentioned previously, familial cases represent approximately 5-10% of MND, hence modelling familial MND has limitations with translation. Sporadic MND can have genetic elements (Renton et al., 2014) and may also be significantly influenced by the environment and therefore very hard to model as an entity. However, 97% of patients can be 'grouped' in that they all show TDP-43 pathology (Mackenzie et al., 2007), so

although a variety of upstream causes may be present, they all share a common pathway/mechanism related to TDP-43 biology, resulting in this pathology. If this TDP-43 pathomechanism could be modelled, this may be an ideal way to target a mechanism affecting nearly all MND patients, creating a model with high translational potential.

The overall aim of this PhD was to identify and characterise a *TARDBP* mouse model to increase the likelihood of successful therapeutic trials translating to patients.

1.3.2.3. Choosing a TARDBP Mouse Model

Many *TARDBP* models have been created over the past 7 years and several others are known to be under investigation at the moment. A thorough review of *TARDBP* mouse models was made (see *table 1.4*), in order to choose the most appropriate model to set up in our institute.

In general, a mouse model for disease research should be on a defined genetic background, have a reproducible phenotype, disease homogeneity, a mild-moderate disease severity, a moderate length of disease course and an appropriate control line. These qualities ensure that meaningful, statistically robust data can be collected whilst keeping the number of mice required in studies relatively low, reducing the time and cost of studies as well as suffering of the mice.

A *TARDBP* mouse model should ideally have a degenerative phenotype due to loss of motor neurons and replicate MND pathology. For our purposes the model also needed to be readily available and carry a mutated *TARDBP* gene. Overexpression and knockout models were avoided as this is not seen in MND patients.

Table 1. 4: Summary of TARBP mouse models of MND.

Reference	Promoter, transgene, expression (Ax = A-fold expression)	Genetic background	Pathology	Phenotype	Symptom Onset	Survival	Reason(s) not to use as our chosen model
(Wegorzewska et al., 2009)	mPrp, huTDP-43 ^{A315T}, 3xflag tag	B6.Cg-Tg(Prnp-*TARDBP**A315T) 95Balo/J C57BL6/J x CBA, backcrossed to C57BL6/J for two generations	Motor neuron and motor axon loss, astrogliosis, nuclear loss of TDP-43	Muscular atrophy in hind legs, gait abnormality (3-4 months), weight loss and 'swimming gait' at 4.5 months	91d	155d due to gastrointestinal problems (Hatzipetros et al., 2014)	Concerns over gastrointestinal problems
(Tsai et al., 2010)	CaMKII, mTDP-43 cDNA ^{WT} 2x	FVB/N	Some TDP-43-positive cytoplasmic inclusions, loss of cortical neurons, astrogliosis in cortex and hippocampus, reduced brain weight	Impaired learning/memory, abnormal gait and reduced rotarod performance	60d	Normal	Overexpression of wild type may not be representative of disease
(Stallings et al., 2010)	mPRP, TDP-43^{A315T} 4x	STOCK Tg(Prnp-*TARDBP*)4Jlel/J B6SJLF1 x CD1, backcrossed with CD1 or mixed background	Astrogliosis in spinal cord, rare ubiquitinated, TDP-43+ inclusions	Muscular atrophy, gait abnormality	4 wks	14d-37.5 wks	Very short disease course, mixed background
	mPRP, TDP-43^{M337V} >10x		Neuronal morphological abnormalities, rare	Reduced grip, weakness, spasticity	Not recorded	16-42d	Very short disease course, mixed background

			ubiquitinated TDP-43+ inclusions, astrogliosis				
	mPRP, huTDP-43 ^{WT} 3x		Rare ubiquitinated inclusions, mild astrogliosis	None	None	Normal	No phenotype, overexpression of wild type may not be representative of disease
(Xu et al., 2010)	mPRP, huTDP-43 cDNA ^{WT} 2.5x	C57BL/6-Tg(Prnp-*TARDBP*)3cPtrc/J	Astrogliosis, rare cytoplasmic phospho-TDP-43 aggregates, mitochondrial neuronal aggregates, rare nuclear clearance of TDP-43 and reduced brain weight	Reduced body weight, gait abnormality and tremor	2 wks	4.5-8.5 wks	Very short disease course, overexpression of wild type may not be representative of disease
(Wils et al., 2010)	Thy1.2, huTDP-43 cDNA ^{WT} 3.8-5.1x	B6;SJL-Tg(Thy1-*TARDBP*)4Singh/J C57BL/6 x SJL/J founders backcrossed to C57BL/6, n not stated	Loss of motor neurons and motor axons, astrogliosis, nuclear loss of TDP-43 and rare ubiquitinated TDP-43+ aggregates	Abnormal hind-limb reflex, reduced rotarod performance, gait abnormalities, paralysis, fasciculations and spasm of facial muscles	2-8.5 wks (variation in phenotype proportional to TDP-43 expression)	4-29 wks (variation in phenotype proportional to TDP-43 expression)	High variability, overexpression of wild type may not be representative of disease
(Shan et al., 2010)	Thy1.2, huTDP-43 cDNA ^{WT} 2.3-4.6x	C57BL/6;SJL, backcrossed with C57BL/6.	Cytoplasmic mitochondrial aggregation, intranuclear TDP-43, FUS inclusions, reduced large motor neurons, TDP-43+	Reduced body weight, gait abnormality, tremor, abnormal hindlimb reflex.	M: 2-2.5 wks F: 13 wks	normal	Overexpression of wild type may not be representative of disease

			inclusions, abnormal NMJ morphology.				
(Chiang et al., 2010)	Rosa26 ubiquitous promoter, depletion of TDP-43 using Cre/lox knockout	*floxed TARDBP x Rosa26-ErCre* to generate inducible *TARDBP*-KO	None reported	Rapid weight loss and death	Not recorded	9 days post tamoxifen induction	No pathology, very rapid disease progression
(Kraemer et al., 2010)	Knockout using gene trap insertion vector pGT1lxf	*Tardbp*$^{Gt(RBO30)Byg}$ chimeric mice were generated and backcrossed x5 on to C57Bl/6	None	Reduced grip strength	Not recorded	Normal	No pathology, little phenotype
(Swarup et al., 2011)	Endogenous promoter, huTDP-43 ^{A315T} 3x	C3H x C57Bl/6 backcrossed to C57Bl/6	Cytoplasmic accumulation of TDP-43, increase in small motor axons; decrease in larger axons. Astrogliosis and microgliosis in the brain and spinal cord (pathology milder than that of TDP-43^{G348C})	Impaired learning, impaired memory, reduced rotarod function	30 wks	Normal	Very late onset

	Endogenous promoter, huTDP-43 ^{G348C} 3x		Cytoplasmic accumulation of TDP-43, cytoplasmic ubiquitinated TDP-43-positive aggregates, neurofilament disorganisation, increase in small motor axons; decrease in larger axons, astrogliosis and microgliosis in the brain and spinal cord	Impaired learning, impaired memory, reduced rotarod performance	30 wks	Normal	Very late onset
	Endogenous promoter, huTDP-43 ^{WT} 3x		Astrogliosis and microgliosis in the brain and spinal cord (similar to that found in TDP-43 ^{A315T})	Impaired learning, impaired memory, reduced rotarod performance	30 wks	Normal	Overexpression of wild type may not be representative of disease
(Igaz et al., 2011)	CaMKII TRE, ΔNLS 1.7x	C57BL/6J x C3HeJ Crossed with tTa mice and tetO mice	Time-dependent cerebral atrophy, astrogliosis, axon loss, nuclear loss of TDP-43 and rare TDP-43+ aggregates	Spasticity (more PLS-like than ALS-like), abnormal hindlimb clasping	7 d post induction	Not recorded	Lack of information on survival
	CaMKII TRE, huTDP-43 ^{WT}		Cerebral atrophy, gliosis, nuclear loss of	Spasticity (more PLS-like than ALS-like),	8-49 wks	Not recorded	Lack of information on survival

	8-9x		TDP-43 and rare TDP-43+ aggregates	abnormal hindlimb clasping			
(Xu et al., 2011)	mPRP, huTDP-43 ^{M337V} 1-2x	C57BL/6-Tg(Prnp-*TARDBP**M337V) 4Ptrc/J C57BL/6 (B6) x B6	Cytoplasmic phosphorylated TDP-43 aggregates, reactive gliosis, widespread ubiquitination, cytoplasmic mitochondrial aggregates, abnormal phosphorylated tau, reduced brain weight	Gait abnormalities, limb weakness, body tremors and difficulty recruiting hind-limbs	3 wks	4 wks	Very rapid disease course
(Wu et al., 2012b)	HB9-promoter, targeted knockout of TDP-43 using Cre/lox	C57BL/6J x HB9:Cre	Motor neuron loss, astrocytosis of the spinal cord, cytoplasmic ubiquitinated protein accumulations in TDP-43 negative motor neurons	Kyphosis, motor dysfunction, muscular atrophy, reduced body weight, weakness, abnormal hind limb clasping, reduced rotarod function	20wks	10m	Knockout may not be representative of disease
(Janssens et al., 2013)	Thy-1.2, huTDP-43^{M337V} 1.7x	Bl6/SJL backcrossed to C57BL/6J	Cytoplasmic, ubiquitinated TDP-43 inclusions, phosphorylated TDP-43, C-terminal fragments, gliosis, reduced brain weight	Hindlimb clasping, muscular atrophy, paralysis, muscle twitches, reduced body weight	11d	17-18d	Very rapid disease course
	Thy-1.2, huTDP-43^{WT} 2x		Cytoplasmic, ubiquitinated TDP-43 inclusions, phosphorylated TDP-	Hindlimb clasping, muscular atrophy, paralysis	14d	25-26d	Very rapid disease course

			43, C-terminal fragments, gliosis				
(Arnold et al., 2013)	mPRP, huTDP-43 ^{Q331K} cDNA, myc-tagged 3x	B6N.Cg-Tg(Prnp-*TARDBP**Q331K)103 Dwc/J B6N.Cg-Tg(Prnp-*TARDBP**Q331K)109 Dwc/J B6N.Cg-Tg(Prnp-*TARDBP*)96Dwc/J	LMN degeneration but no loss of UMNs, astrogliosis and microgliosis in the spinal cord, vacuolisation and myelin defects in motor axons, loss of motor axons, reduced neuromuscular junction endplates	Tremor, hindlimb clasping, decreased hindlimb grip strength, decreased rotarod performance.	3 months	Normal	Chosen model
	mPRP, huTDP-43 $^{Q331K\text{-}low}$ cDNA, myc-tagged lower than endogenous	C57Bl6/C3H backcrossed to C57Bl6 at least 4 times	Age-dependent decrease in LMNs.	Significant age-dependent motor deficits (less so than TDP-43 ^{Q331K})	Not recorded	Not recorded	Lack of pathology and phenotype
	mPRP, huTDP-43 ^{M337V} cDNA, myc-tagged similar to endogenous		Age-dependent decrease in LMNs	Significant age-dependent motor deficits (less so than TDP-43 ^{Q331K})	Not recorded	Not recorded	Lack of pathology and phenotype
(Iguchi et al., 2013)	Motor neuron specific knockout of TDP-43 using Cre/lox	En1flox-neo x C57BL/6 backcrossed with C57BL/6 at least 5 times, then crossed with CAChT-Cre	Degeneration of large motor axons, denervation in the neuromuscular junction, autophagy-related structures accumulated in cell	Progressive weight loss and motor impairment, muscular atrophy, tremor, reduced rotarod performance and grip strength	50 wks	Normal	Knockout may not be representative of disease

			bodies of motor neurons				
(Yang et al., 2014)	Knockout using transgenic RNAi and Cre/lox	amiR–TDP43u x CMV–Cre	Progressive neurodegeneration, predominantly in cortical layer V and the spinal cord	Hyperactivity, motor dysfunction, weakness, paralysis, reduced body weight	5wks	44-100d	Unpublished at the time
(Ricketts et al., 2014)	*TARDBP-^{43Q10X} from a N*-ethyl-*N*-nitrosourea (ENU) mutant mouse archive endogenous	(C3H/HeH.C57BL/6J) backcrossed on to C57BL/6J x 3-4	None	Limb clasping, lack of body tone	32wks	Normal	Unpublished at the time
(Walker et al., 2015)	NEFH promoter doxycycline (Dox)-suppressible expression of huTDP-43 with defective nuclear localization signal (ΔNLS) 50% reduction in expression	Mixed C57BL/6J × C3HeJ F1	Brain atrophy, insoluble cytoplasmic TDP-43 in the brain and spinal cord, muscle denervation, motor neuron loss	Hindlimb clasping, tremor, reduced grip strength and rotarod performance, reduced body weight	4 wks off dox	10.3 wks off dox	Unpublished at the time

After careful consideration, the TDP-43^{Q331K} mouse model (Arnold et al., 2013) was imported from Jackson laboratories (USA) along with the wild-type control line (huTDP-43^{Q331K} Jax #017933 and huTDP-43^{WT} Jax #017907).

This mouse model was chosen as it met most of the criteria described previously by having a degenerative phenotype due to motor neuron loss, a defined genetic background, a mild disease severity, a moderate length of disease course (10 months), and an appropriate control line (TDP-43^{WT}) which lacked a phenotype. In addition, unlike most other transgenic TDP-43 models, this model has been developed with the idea of creating a line with transgenic expression similar to the endogenous mouse gene, avoiding the issues seen in highly overexpressing models where both mutant and wild type TDP-43 overexpression cause neurodegeneration.

The TDP-43^{WT} mouse line is transgenic for human *TARDBP* and the TDP-43^{Q331K} mouse line is transgenic for human *TARDBP* with a glutamine to lysine mutation at position 331 (Q331K). The Q331K mutation has been identified in exon 6 of the *TARDBP* gene in a 72 year old male patient who developed limb-onset MND with a 3 year disease duration (Sreedharan et al., 2008). In this mouse model, the human *TARDBP* gene is expressed under the murine prion promoter, which is mainly expressed in the astrocytes and motor neurons of the CNS (Wang et al., 2005) as well as the heart (Borchelt et al., 1996). The human *TARDBP* gene is also c-myc-tagged.

Previous work with this mouse model showed widespread alterations in gene splicing, motor neuron and motor axon loss, reduced rotarod performance and grip strength, and a mild disease course which plateaus at 10 months of age (Arnold et al., 2013).

The mice were backcrossed on to a C57BL/6NJ background before being deposited at Jackson laboratories. Therefore, the mouse colonies established are on a slightly different genetic background compared to those in the original paper (C57BL/6NCrl), which may have a significant effect on disease severity (Heiman-Patterson et al., 2005).

Subsequently, in 2015 a further study was published in which a different line of the TDP-43^{Q331K} mice was crossed with the TDP-43^{WT} mice, causing a very rapid disease progression (Mitchell et al., 2015). It is hypothesised that this cross pushed the level of TARDBP expression over a 'threshold', causing the disease to become far more aggressive. However, the TDP-43^{Q331K} mice used in this publication were a different line

compared to the mice in our colony as well as now being on a slightly different genetic background. Therefore, comparison of data between this project and previous studies should be approached with caution.

1.4. Aims of the project

The overall aims of the project were to:

1. Establish a breeding colony of a translationally relevant mouse model of MND.
2. Identify quantitative readouts of disease progression with low variability, suitable for use in pre-clinical therapeutic trials.
3. Carry out the first known drug trial of riluzole in the selected mouse model.
4. Investigate 31P-MRS as a potential preclinical biomarker of MND.

2. Motor Phenotypic Characterisation of the TDP-43^{Q331K} Mouse

2.1. Introduction

Upon receiving the TDP-43^{Q331K} and TDP-43^{WT} mice, colonies were established and a characterisation study was initiated. This mouse model has been investigated previously on a C57BL/6NCrl background which had been backcrossed for a minimum of 4 generations (Arnold et al., 2013) but has subsequently been backcrossed on to a different genetic background (C57BL/6NJ). A difference in genetic background can have a large impact on disease severity, as found in the SOD1^{G93A} mouse model (Heiman-Patterson et al., 2005). It was therefore of great importance to ensure the TDP-43^{Q331K} colony we were establishing carried the described mutation and that there would be genetic homogeneity within the colonies.

Previously, the TDP-43^{Q331K} mouse model was described as developing a rotarod deficit and reduced grip strength with age, worsening over a period of 10 months (Arnold et al., 2013). However, the difference in genetic background between the published model and the TDP-43^{Q331K} model in use here, may cause a differing motor phenotype. It is therefore appropriate to test for a motor phenotype in this TDP-43^{Q331K} model.

As discussed previously (chapter 1), homogeneity and reproducibility of disease is key in a disease model, especially when planning to carry out therapeutic trials, as minimal variability is crucial to identifying treatment effects with small group sizes (Mead et al., 2011). Carrying out a phenotypic study allowed for assessment of these parameters and for comparison of non-transgenic and TDP-43^{WT} mice with TDP-43^{Q331K} mice to identify mutant specific effects, as well as the effects of WT TDP-43 expression.

Analysis of motor phenotype defines the disease severity and onset. This is useful for therapeutic trials as users may wish to administer drugs from the onset of symptoms rather than from maturity (Benatar, 2007, Ittner et al., 2015). Assessment of motor phenotype may also provide an indication of the degree of distress suffered by the mice, with the possibility of identifying humane disease endpoints, if relevant for the model. Motor function can be assessed in a variety of ways including grip strength, rotarod, the raised beam test, open field and gait analysis (Brooks and Dunnett, 2009). Rotarod, grip strength, weight, gait analysis and neurological scoring are commonly used for the assessment of the motor phenotype in the SOD1^{G93A} model (Weydt et al., 2003, Mead et al., 2011). Practically, the accessibility of equipment must be considered when

designing a study and the readily available equipment for this study consisted of a rotarod and the Catwalk gait analysis system. Weight was also monitored and the overall neurological deficit was scored. For the purposes of maintaining and managing colonies, it is always helpful to know the expected litter statistics for mouse models, and importantly, the breeding life of the mice. In many models, including SOD1^{G93A}, fertility is impaired. Males have a short window of fertility from adulthood (50-60 days of age) to approximately 90 days of age (in-house data) and females are infertile. Therefore, breeding statistics for TDP-43^{Q331K} mice were also investigated, as these had not been reported previously.

As described previously in chapter 1, approximately 97% of MND patients develop TDP-43 pathology in motor neurons, including ubiquitinated inclusions and cytoplasmic mislocalisation (Mackenzie et al., 2007). Ideally, the TDP-43^{Q331K} mice would replicate this pathology, however, the previously published data showed small TDP-43 positive inclusions but no cytoplasmic mislocalisation (Arnold et al., 2013). It is well established that inflammation is a key component of disease in humans, often reflected in the activation of astrocytes and microglia. Both these cell types are activated in MND, as shown by microgliosis and astrocytosis, both *in vitro* and *in vivo* (Boillee et al., 2006, Ferraiuolo et al., 2011, Yamanaka et al., 2008b). Previous investigation of the TDP-43^{Q331K} model found signs of astrogliosis with increased glial fibrillary acidic protein (GFAP) immunoreactivity, and microgliosis demonstrated by increased levels of IBA-1 immunoreactivity (Arnold et al., 2013). Therefore, it is important to establish whether these findings are also evident in the TDP-43^{Q331K} model on a C57BL/6NJ background.

2.2. Aims

1. To assess the motor function of TDP-43^{Q331K} and TDP-43^{WT} mice over a period of 10 months.

2. To establish whether the TDP-43^{WT} motor phenotype is similar/different to non-transgenic mice of the same background strain.

3. To assess the variability of the motor phenotype in TDP-43^{Q331K} and TDP-43^{WT} mice.

4. To assess breeding and litter statistics in the TDP-43^{Q331K} and TDP-43^{WT} mice.

5. To investigate the TDP-43 pathology, astrogliosis and microgliosis in the spinal cord of TDP-43^{Q331K} mice.

2.3. Materials and Methods

2.3.1. Ethics Statement

All mouse experiments were carried out under the terms of the UK Animals (Scientific Procedures) Act 1986 and under a UK Home Office project license. Mice were housed and cared for in accordance with the Home Office Code of Practice for Housing and Care of Animals Used in Scientific Procedures. All procedures were carried out under an appropriate UK Project Licence by personal licence holders. ARRIVE guidelines (Kilkenny et al., 2010) have been followed for the work described in this thesis.

2.3.2. Transgenic C57BL/6NJ Mice

TDP-43^{WT} and TDP-43^{Q331K} mice *(Mus musculus)* were originally generated on a C57BL/6NCrl background by insertion of c-myc-tagged human *TARDBP* cDNA constructs, injected in to the pronuclei of C57Bl6/C3H blastocysts and implanted in to pseudopregnant female mice (Arnold et al., 2013). Offspring were subsequently backcrossed on to a C57BL/6NJ background before being deposited at the Jackson Laboratory (stock numbers 017907 and 017933, respectively).

The basic characterisation tests were carried out with 5-7 males and 5-7 females per group (TDP-43^{WT} and TDP-43^{Q331K}), based on power calculations from rotarod data in SOD1^{G93A} mice. Non-transgenic littermates of each mouse were also tested, the data for which were pooled to create the non-transgenic (NTg) group. Mice were recruited at 25 days of age and remained on the study until 300 days of age.

Colonies were established using 3 male breeders and 6 female breeders in each colony. Transgenic males were mated with non-transgenic females from within the same colony. All mice were fertile and remained as breeding stock up to 12 months of age.

2.3.3. Housing

Mice were bred in a specified pathogen free (SPF) environment, and transferred to a conventional facility for the studies described here. The facility uses a 12 h light/dark cycle, and room temperature set to 21˚C. Cages were lined with fine sawdust (eco-pure flakes 6, Datesand, UK), which was changed weekly, and a plastic house was placed in each cage with paper wool (Datesand, UK) as bedding material. Mice were fed 2018 rodent diet (Harlan, UK) ad libitum. Water was provided ad libitum and changed weekly. Fresh bottles were provided every four weeks.

All mice were housed in same-sex littermate pairs or quadruplets. However, some male pairs were separated at around six months of age due to fighting.

2.3.4. Genotyping

Mice were identified by ear clipping and the ear clip was then used for genotyping. DNA was extracted by incubating ear clips at 65˚C for 15 minutes in a 20 µl volume of QuickExtract DNA Extraction Solution (Epicentre, Cambridge, UK), followed by a 2 minute incubation at 98˚C. 1 µl of DNA was then placed in solution with 4 µl of Firepol (Solis Biodyne, Estonia), 11 µl of water, 0.5 µm of each huTDP-43 primer (forward 5'-AGAGGTGTCCGGCTGGTAG-3', reverse 5'-CCTGCACCATAAGAACTTCTCC-3') and 0.5 µm of each interleukin-4 receptor control primer (forward 5'-CTAGGCCACAGAATTGAAAGATCT-3', reverse 5'-GTAGGTGGAAATTCTAGCATCATCC-3'), (Sigma-Aldrich, UK).

This polymerase chain reaction (PCR) mix was then run on a PCR machine (G-Storm, UK) with a 2 min incubation period at 94°C, followed by 10 cycles of 94°C for 20 seconds, 65-50°C for 15 seconds and 68°C for 10 seconds. This was followed by 28 cycles of 94°C for 15 seconds, 50°C for 15 seconds, and 72°C for 10 seconds. Following this was a 2 minute period at 72°C. Samples were then held at 10°C.

A 2% w/vol agarose/1xTAE solution was microwaved until the agarose was fully dissolved. Once cooled, 1% ethidium bromide was added and the solution was poured into a gel mould. Once set, the gel was placed in to a gel tank filled with 1xTAE. 4µl of 100bp hyperladder (Bioline, UK) was loaded in the first well of each row and 8µl of PCR

product was then added to each subsequent well. The gel was then run for 40 mins at 120mV.

Transgenic samples are represented by a predominant PCR product for the human TDP-43 transgene at 228bp as well as the control IL4R PCR product at 324bp, whereas non-transgenic samples are represented by a single band at 324bp.

2.3.5. Sequence Analysis

DNA was extracted by incubating ear clips at 65˚C for 15 minutes in a 20 µl volume of QuickExtract DNA Extraction Solution (Epicentre, Cambridge, UK), followed by a 2 minute incubation at 98˚C.

A 1 µl volume of DNA was then placed in solution with 4 µl of Firepol (Solis Biodyne, Estonia), 11 µl of water, 0.5 µm of each huTDP-43 primer (forward 5'-AGAGGTGTCCGGCTGGTAG-3', reverse 5'-CCTGCACCATAAGAACTTCTCC-3') and 0.5 µm of each interleukin-4 receptor control primer (forward 5'-CTAGGCCACAGAATTGAAAGATCT-3', reverse 5'-GTAGGTGGAAATTCTAGCATCATCC-3'), (Sigma-Aldrich, UK).

This solution was then run on a PCR machine (G-storm, UK) with a 2 min incubation period at 94°C, followed by 94°C for 20 seconds, 65-50°C for 15 seconds and 68°C for 10 seconds, repeated for 10 cycles. This was followed by 28 cycles of 94°C for 15 seconds, 50°C for 15 seconds, and 72°C for 10 seconds. Following this was a 2 minute period at 72°C. Samples were then held at 10°C.

5µl of each PCR product was then placed in a 0.2ml Eppendorf with 0.05µl of exonuclease I (Thermo Fisher, UK), 1µl of shrimp alkaline phosphatase (Thermo Fisher, UK) and 4µl of nuclease-free water. This solution was then incubated in a PCR machine (G-Storm, UK) at 37 ^{o}C for 45 mins, followed by 80 ^{o}C for 15 mins.

These samples were then sent to the Core Genomic Facility, Medical School, University of Sheffield for sequencing using an Abi 3730 instrument (ThermoFisher Scientific, UK) and PTC-200 cyclers (ThermoFisher Scientific, UK) and a manufacturer-recommended BigDye Terminator kit (ThermoFisher Scientific, UK).

2.3.6. Copy Number Analysis

Ear clips were taken from mice at 10 months of age (1 non-transgenic, 3 TDP-43^{WT}, 12 TDP-43^{Q331K}) and sent to the Mary Lyon Centre, MRC Harwell, Didcot for analysis of human *TARDBP* copy number.

A VIC-labelled reference assay (disruptor of telomeric silencing 1-like [Dot1l]) set at 2 copies (CNV2) on the Bio-Rad QX200 droplet digital PCR (ddPCR) system (Bio-Rad, CA) was performed using a Taqman assay specific to human *TARDBP* cDNA to estimate the number of transgene integrations. Reaction mixtures (20 µl) contained 1 µl crude DNA lysate, 1x ddPCR Supermix for probes (Bio-Rad, CA, USA), 225 nM of each primer (two primers/assay) and 50nM of each probe (one VIC-labelled probe for the reference gene assay and one FAM-labelled for the transgene target assay). These reaction mixes were loaded into DG8 cartridges with 70 µl droplet oil per sample and droplets produced using the QX100 Droplet Generator, or alternatively were loaded in plate format into the Bio-Rad QX200 AutoDG and droplets produced as per the manufacturer's instructions. After droplet generation, the oil/reagent emulsion was transferred to a 96 well semi-skirted plate (Eppendorf AG, Hamburg, Germany) and the samples were amplified on the Bio-Rad C1000 Touch thermocycler (95°C for 10 min, then 40 cycles of 94°C for 30s and 58°C for 60s, followed by a final elongation step of 98°C for 10 min). The plate was then loaded into the QX200 Droplet Reader (Bio-Rad, CA, USA). Standard reagents and consumables supplied by Bio-Rad were used, including cartridges and gaskets, droplet generation oil and droplet reader oil.

2.3.7. Neuroscoring and Weighing

Neuroscores and weight were monitored weekly in the morning, measuring forelimb and hindlimb tremor on a subjective scale of 0-3 (normal-strong) adapted from the in-house SOD1^{G93A} neuroscoring system. A 'neuroscore' scale was used to delineate motor dysfunction (0-normal, 1-significant hindlimb tremor, 2-abnormal gait, 3-severe waddle, 4-dragging of one hindlimb). Whenever possible, this scoring was carried out by the same investigator (JS).

Weight was monitored by placing the mice in a box on a set of scales (Kern, Germany) pre-set to zero. These measurements were taken immediately prior to rotarod testing and in the same procedure room as the rotarod.

2.3.8. Accelerating Rotarod Test

Mice were placed on the accelerating rotarod (Jones & Roberts for mice 7650) for a period of 300 seconds. In this time the rotarod accelerates from 4 to 40 rpm and latency to fall was recorded for each mouse. All rotarod testing was carried out at a similar time of day (am) and all testing consisted of two trials, with the highest score being recorded for analysis.

Mice were initially trained on the rotarod over 3 days (27-29 days of age) and underwent the first testing day at 30 days of age, being tested each week thereafter. For each mouse at each time point the ratio of rotarod performance/weight was also plotted to account for the effect of weight.

2.3.9. Catwalk Gait Analysis

The catwalk gait analysis system 7.1 (Noldus Information Technology B.V., Netherlands) was used to capture gait parameters at 1, 3, 6 and 10 months of age. Mice were placed on the glass floor of the catwalk system in complete darkness and left to walk/run freely. Whenever possible, 6 straight continuous runs were recorded and the 3 best runs were selected for analysis. Catwalk software 7.1 was used to label each paw print of each run (as shown in *figure 2.1*) and analyse the gait parameters of the mice. Microsoft Excel was used to collate data within groups and select data which may be informative.

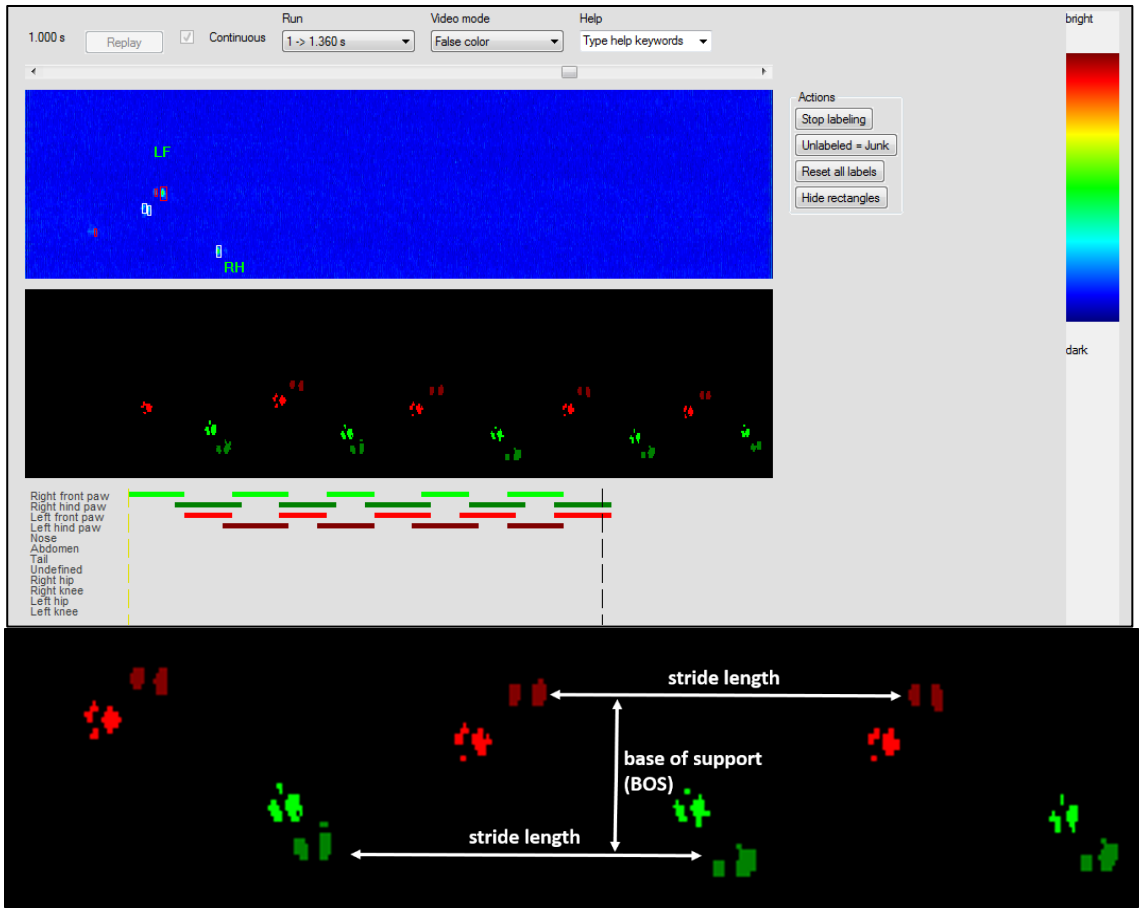

Figure 2. 1: Demonstration of catwalk gait analysis software.

As shown in the top panel (blue) each individual paw print was labelled and colour co-ordinated for analysis. Forepaws are bright; hindpaws are dull. Left paws are red; right paws are green. The bottom panel demonstrates the definition of stride length and base of support.

2.3.10. Litter Statistics

Throughout maintenance of the TDP-43^{WT} and TDP-43^{Q331K} mouse colonies, data for each mouse was monitored and each litter was assessed for size, percentage of transgenic pups, and percentage of male pups. Data for savaged pups was unavailable.

2.3.11. qPCR

Primer pairs were mixed and diluted to 5µM (see table 2.1 for primer sequences).

Samples were plated in duplicate in non-skirted, frosted, thin-wall 0.2ml low profile 96 well plates (P3-0402, Geneflow, UK) and covered with optical wide area 8-cap strips (P3-0051, Geneflow, UK). Each well contained 1µl cDNA, 1µl primer mix, 3µl water and 5µl brilliant III ultra-fast SYBR® green qPCR master mix (600882, Agilent Technologies, USA). Glyceraldehyde 3-phosphate dehydrogenase (GAPDH) was used as the house-keeping gene. A non-template control was plated for each primer pair.

Samples were placed in the qPCR machine (Mx 3000P, Stratagene, USA) and run on the following protocol: 95˚C for 10 mins, 45 cycles (95˚C for 30s, 58˚C for 1 min, 72˚C for 1 min), 95˚C for 1 min, 55˚C for 30s, 95˚C for 30s.

Table 2. 1: Primer sequences. Forward and reverse primer sequences used for qPCR analysis.

Primer pair	Forward	Reverse
huTDP-43	TGGGATGAACTTTGGTGCGT	TTTGGCTCCCTCTGCATGTT
Mouse (total) TDP-43	TACCGGAATCCCGTGTCTCA	GAGGAAGCATCTGTCTCATCCA
GAPDH	ATGGTGAAGGTCGGTGTGAA	TGGCAACAATCTCCACTTTGC

2.3.12. qPCR Analysis

Cycle threshold (Ct) values were extracted using MxPro Mx3000P software version 4.10 (Stratagene, USA). Further analysis was carried out using Microsoft Excel 2013 (Microsoft, USA) and GraphPad Prism 6 (GraphPad, USA).

Mean Ct values were calculated for each sample from the duplicates. Data were not used if duplicate Ct values differed by ≥1. The relative concentration was calculated using the equation: $1/2^{(\text{gene of interest Ct} - \text{GAPDH Ct})}$. Values were presented as a percentage

of the mean TDP-43^{WT} value for each sample, or as a percentage of the mean non-transgenic value wherever possible.

2.3.13. Preparation of Lysates for Western Blotting

Cortex samples (n = 3 male, 3 female/group, 10 months of age) were homogenised in 700µl of RIPA buffer (150mM sodium chloride, 50mM Tris, 1% triton x-100, 0.5% SDS, 0.5% sodium deoxycholate, pH 8.0), whilst spinal cord samples (n = 3 male, 3 female/group, 10 months of age) were homogenised in 350µl of RIPA buffer. Samples were homogenised using a plastic pestle in the Eppendorf, followed by passage through a syringe and needle at least 3 times. Samples were then rolled at 4˚C for 30 mins and left on ice for a further hour.

Samples were centrifuged at 18000 x g (14000rpm) for 10 mins at 4˚C and the supernatant was collected in aliquots and frozen at -80˚C. Pellets were discarded.

2.3.14. Western Blotting

2.3.14.1. SDS-Polyacrylamide Gel Preparation

Resolving gels were made at a concentration of 12% by mixing 3.5ml distilled water (dH_20), 4ml acrylamide (30% w/v), 2.5ml resolving buffer (1.5M Trizma, 13.9mM SDS, pH 8.8), 50µl APS (10% w/v) and 20µL TEMED. This solution was placed into 1mm spacer plates and short plates (Bio-Rad), assembled on the Mini-PROTEAN® Tetra Cell Casting Stand and clamps with gaskets (Bio-Rad). A layer of isopropanol was left on the top of the gel whilst setting and poured/blotted off afterwards.

Stacking gels were made at a concentration of 5% by mixing 5.8ml dH_20, 1.7ml acrylamide (30% w/v), 2.5ml stacking buffer (0.5M Trizma, 13.9mM SDS, pH 6.8), 50µl APS (10% w/v) and 20µL TEMED. This solution was then poured in to the gel cast to sit above the resolving gel. A 1mm 10-well Mini-PROTEAN® comb (Bio-Rad) was inserted in to the top of the gel during setting (at least 10 mins).

2µl of 4x Laemmli buffer (228mM Tris-HCl, 38% (v/v) glycerol, 277mM SDS, 0.038% (w/v) bromophenol blue, 5% (v/v) β-mercaptoethanol, pH 6.8) was added to 6µl of each sample and heated at 95˚C for 5 mins. The protein gels were loaded in to a Mini-

PROTEAN® Tetra Vertical Electrophoresis Cell (Bio-Rad), and the tank was filled with running buffer (25mM Tris, 3.5mM SDS, 20mM glycine). 2µl of pre-stained protein ladder was loaded in to one well of each gel and samples were then loaded in the remaining wells. Electrophoresis was run at 50V for 30 mins, followed by 150V for 90 mins.

2.3.14.2. Transfer of SDS-Polyacrylamide Gel to Nitrocellulose Membrane

Gels were removed from the electrophoresis apparatus and placed over a nitrocellulose membrane saturated in transfer buffer (47.9mM Tris, 38.6mM glycine, 1.38mM SDS, 20% (v/v) methanol) and placed between 6 layers of Whatman paper, also saturated in transfer buffer. These layers were then placed in the semi-dry apparatus (Biometra, Germany) and electrophoretic transfer was performed at 0.15A/gel for 1 hour.

Membranes were then stained with Ponceau (0.1% (w/v) Ponceau S, 5% (v/v) acetic acid) to check for proteins, and then washed in TBST (20mM Tris, 137mM NaCl, 0.2% (v/v) Tween® 20, pH 7.6).

2.3.14.3. Immunoblotting

Membranes were blocked in 5% (w/v) milk/TBST for 20 mins at room temperature (RT) on a roller. Membranes were then incubated with the rabbit anti-TDP-43 primary antibody (10782-2-AP, Proteintech, UK, 1/1000) in 5% (w/v) milk/TBST for 1 hour at RT on a roller followed by 3 x 5 min washes in TBST. The horseradish peroxidase (HRP) anti-rabbit secondary antibody (W401B, Promega, UK, 1/5000) in 5% (w/v) milk/TBST was then applied for 1 hour at RT on a roller followed by 3 x 5 min washes in TBST. Membranes were then incubated in enhanced chemiluminescence (ECL) for 1 min and imaged on the G:BOX (Syngene, UK).

For the loading control, membranes were incubated with the mouse anti-β-actin primary antibody (ab6276, Abcam, UK, 1/1000) in 5% (w/v) milk/TBST for 1 hour at RT on a roller followed by 3 x 5 min washes in TBST. The anti-mouse HRP conjugate secondary antibody (W402B, Promega, UK, 1/5000) in 5% (w/v) milk/TBST was then applied for 1 hour at RT on a roller followed by 3 x 5 min washes in TBST. Membranes

were then incubated in ECL for 1 min and imaged on the G:BOX (Syngene, UK) using GeneSnap software (Syngene, UK).

2.3.15. Western Blot Analysis

GeneTools software (Syngene, UK) was used to quantify the signal of each band on the membrane. Signal was quantified relative to the first band on the membrane and adjusting for the loading control (β-actin) and normalised to the mean non-transgenic total TDP-43 value for each gel.

2.3.16. Tissue Collection for Immunohistochemical Staining

Mice were sacrificed at 10 months of age by trans-cardiac perfusion following anaesthetic overdose using an intraperitoneal injection of pentobarbitone (2.5ml/kg). Under deep anaesthesia (checked by absence of pedal reflex) and prior to cessation of cardiac function, a thoracotomy was performed, in which the left ventricle was cannulated with a syringe containing phosphate buffered saline (PBS) and mild pressure applied to distend the right auricle, which was then cut. The mouse was then perfused with PBS via the left ventricle of the heart, followed by perfusion with 4% paraformaldehyde (PFA)/PBS.

Spinal columns were then extracted and placed in 4% PFA/PBS overnight. The spinal cord was then extracted from the spinal column and cryoprotected by immersion through a gradient of 5, 10, 15 and 20% sucrose/PBS for 5 minutes in each concentration before incubation in 20% sucrose overnight. The spinal cords were then dissected into cervical, thoracic, lumbar and sacral segments, and frozen in OCT embedding matrix (CellPath, UK) over dry ice, then stored at -80˚C.

For sectioning of the lumbar spinal cord, samples were acclimatised at -20˚C for at least 30 mins. Lumbar sections were sliced at 14 µm using a cryostat and mounted on to uncoated, charged slides (CellPath, UK). Sections were mounted serially over series' of 5 slides, with 5 sections per slide (total length of cord between sections on a slide being 70 µm) for a total of 50 slides, then stored at -20˚C.

2.3.17. Immunohistochemical Staining

Slides were placed at 37˚C for 30 minutes and then washed three times in PBS at room temperature with shaking. Sections were then permeabilised in 5% BSA, 0.5% triton X-100/PBS for 90 minutes at 37˚C and subsequently placed in an antigen access unit (A. Menarini Diagnostics, UK) submerged in Access Revelation pH 6.5 (MP-607-x500, A. Menarini Diagnostics, UK) for a 30 minute cycle at 125˚C, with a pressure of 20 psi.

After 3 x 5 min washes in PBS with shaking, slides were blocked with 5% BSA, 0.25% triton X-100/PBS for 10 minutes and then incubated with the primary antibodies (see *table 2.2*) diluted in 0.25% Triton X-100/PBS overnight at 4˚C.

Following 6 quick washes and 3 x 5 min washes in PBS with shaking, slides were blocked in 5% BSA/PBS for 10 mins and then incubated with secondary antibodies (see *table 2.2*) at RT for 90 mins.

Slides were then given 2 quick washes with PBS, 3 x 5 min washes in PBS and 1 x 5 min wash in filtered water, with shaking and in darkness. Sections were mounted in Vectashield hard set aqueous mountant with 4',6-diamidino-2-phenylindole (DAPI) (Vector Laboratories, Peterborough, UK) and left to dry at 4˚C overnight in the dark.

Table 2. 2: Table of antibodies used for immunohistochemical analysis.

Primary/ secondary	**Antibody**	**To aid visualisation of**	**Monoclonal/ polyclonal**	**Animal raised in**	**Supplier**	**Supplier code**	**Concentration**
primary	anti-c-myc	c-myc tagged huTDP-43	polyclonal	rabbit	Sigma, UK	C3956	1/1000
primary	anti-NeuN	Neurons	monoclonal	mouse	Merck Millipore, UK	MAB377	1/1000
primary	anti-GFAP	Astrocytes	polyclonal	chicken	Abcam, UK	Ab4674	1/1000
primary	anti-IBA-1	Microglia	polyclonal	rabbit	Alpha Laboratories, UK	019-19741	1/500
secondary	Alexa fluor anti-rabbit 488	anti-rabbit primary	polyclonal	donkey	Thermo Fisher Scientific, UK	A21206	1/1000
secondary	Alexa fluor anti-mouse 555	anti-mouse primary	polyclonal	donkey	Thermo Fisher Scientific, UK	A31570	1/1000
secondary	Alexa fluor anti-chicken 488	anti-chicken primary	polyclonal	goat	Thermo Fisher Scientific, UK	A11039	1/1000

2.3.18. Immunohistochemical Staining Image Analysis

Images were captured using the IN Cell Analyzer 2000 (GE Healthcare, UK) and analysed using GE Developer Toolbox 1.9 (GE Healthcare, UK).

NeuN and c-myc staining was captured at 20x magnification within each ventral horn of each spinal cord section. NeuN staining was detected by object segmentation with kernel size 45 and sensitivity 23, followed by a sieve filter for an object size of over 19.44µm^2. DAPI staining was filtered by intensity segmentation (grey level 55 - 4095) with a sieve filter for an object size of over 0.55µm^2 to identify the nuclei of the motor neurons. Staining intensity of c-myc was then recorded for the cytoplasm (in which there was NeuN and no DAPI staining), and the nucleus (in which there was DAPI staining). TDP-43^{WT} and TDP-43^{Q331K} tissue was then compared for analysis.

GFAP staining was captured at 60x magnification within each ventral horn of each spinal cord section. GFAP staining was segmented by intensity level with a threshold of greater than 12500 grey levels and staining index ([unstained pixels-stained pixels]/2xSD) was recorded. The mean staining index was calculated for each mouse. Non-transgenic and TDP-43^{Q331K} tissue was compared for analysis. TDP-43^{WT} tissue was of poor quality and appeared fragmented, the reason for which is unknown.

IBA-1 staining was captured at 60x magnification within each ventral horn of each spinal cord section. IBA-1 staining was detected by object segmentation with a kernel size of 21 and sensitivity of 1, followed by a sieve filter for objects over 3µm^2. The mean staining area (µm^2) for each mouse was then recorded. Non-transgenic and TDP-43^{Q331K} tissue was compared for analysis. Image montage figures were contrast adjusted and produced using ImageJ.

2.3.19. Statistics

GraphPad Prism 6 was used for all statistical analyses (GraphPad, San Diego, CA, USA). Two-way ANOVA with Tukey's post-test was used unless otherwise stated. All data are represented as a mean and standard deviation, unless otherwise stated.

Power analysis was carried out using G*Power Version 3.1.9.2. (Faul et al., 2009) using a student's t-test, two-tailed, $\alpha = 0.05$, $\beta = 0.8$.

2.4. Results

2.4.1. Confirmation of the Q331K Mutation

DNA sequencing was carried out to ensure that TDP-43^{WT} and TDP-43^{Q331K} mice carried the correct gene sequence.

DNA sequencing of the *TARDBP* gene in a TDP-43^{Q331K} mouse (*figure 2.2B*) shows cytosine (C) replaced by adenine (A) at codon position 331 of the sequenced PCR product (highlighted in blue) when compared to the sequence of a TDP-43^{WT} mouse (*figure 2.2A*).

The triplet CAG in the TDP-43^{WT} sequence encodes glutamine (Q), whereas the triplet AAG in the TDP-43^{Q331K} sequence encodes lysine (K) at amino acid position 331.

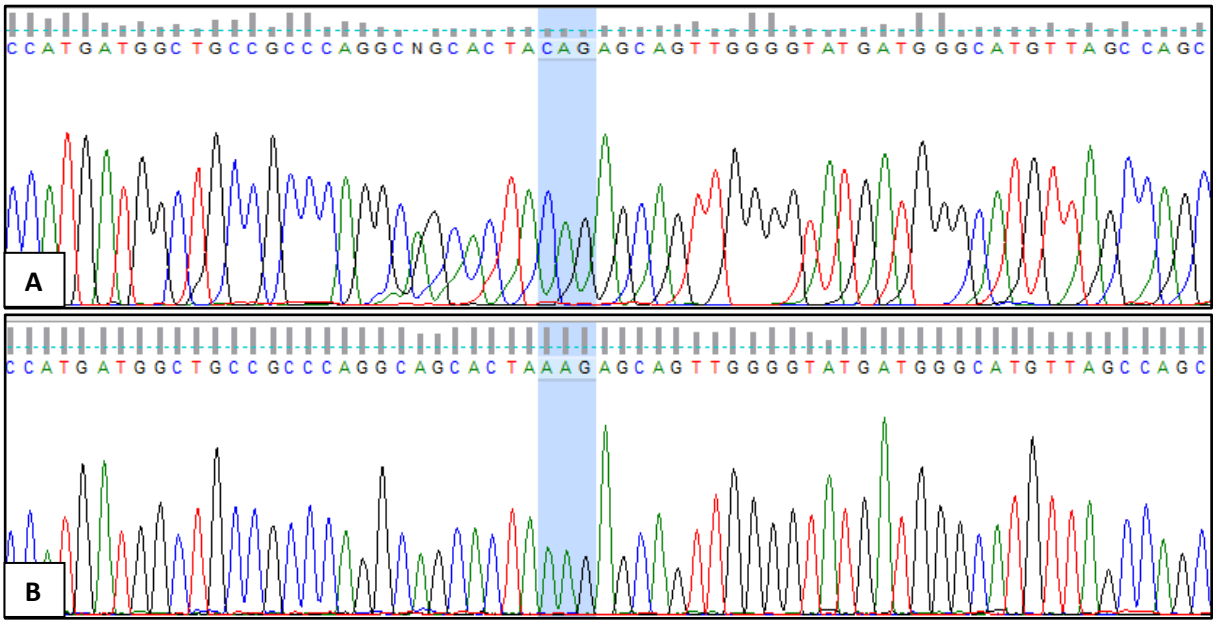

Figure 2. 2: DNA sequence of TDP43^{WT} and TDP43^{Q331K} transgenic mice.

Raw chromatographs show sequences from the human TARDBP gene in the TDP43^{WT} transgenic mice, in which the nucleotides CAG form glutamine (A); and the sequence of the TDP43^{Q331K} mice, in which nucleotides AAG form lysine (B).

2.4.2. Human *TARDBP* Copy Number Estimation

Human *TARDBP* copy number was investigated in each mouse line. The non-transgenic mouse showed no sign of human *TARDBP* (*table 2.3*). All TDP-43^{WT} mice appear to carry one copy of the human *TARDBP* gene. TDP-43^{Q331K} mice appear to express a range of copy numbers between one and five. Samples for which the copy number estimation is non-specific (e.g. 4/5) indicate an uncertainty in the prediction of copy number.

Table 2. 3: Human TARDBP copy number estimation. *Estimated copy number of human TARDBP in 1 non-transgenic mouse, 3 TDP-43^{WT}mice and 12 TDP-43^{Q331K}mice. Mouse numbers 11 and 12 presented with a typical weight and rotarod for TDP-43^{Q331K} mice, despite apparently having only one copy of the mutated gene.*

Mouse number	Genotype	Copy number	M/F
1	Non-transgenic	0	M
2	*TDP-43^{WT}*	1	F
3	*TDP-43^{WT}*	1	F
4	*TDP-43^{WT}*	1	M
5	*TDP-43^{Q331K}*	4/5	F
6	*TDP-43^{Q331K}*	2/3	F
7	*TDP-43^{Q331K}*	3	F
8	*TDP-43^{Q331K}*	3	F
9	*TDP-43^{Q331K}*	4	F
10	*TDP-43^{Q331K}*	3	F
11	*TDP-43^{Q331K}*	1	F
12	*TDP-43^{Q331K}*	1	M
13	*TDP-43^{Q331K}*	4	M
14	*TDP-43^{Q331K}*	5	M
15	*TDP-43^{Q331K}*	5	M
16	*TDP-43^{Q331K}*	4	M

2.4.3. Abnormal Gait Evident at 27 Weeks of Age in TDP-43^{Q331K} Mice

Male and female TDP-43^{Q331K} mice develop a neuroscore of 2 (abnormal gait) around 27 weeks of age and progress to develop a waddling gait. Female TDP-43^{Q331K} mice produce more consistent neuroscores with less variation amongst mice compared to male TDP-

43^{Q331K} mice. Conversely, TDP-43^{WT} and non-transgenic mice show no significant sign of tremor or an abnormal gait (*figure 2.3*).

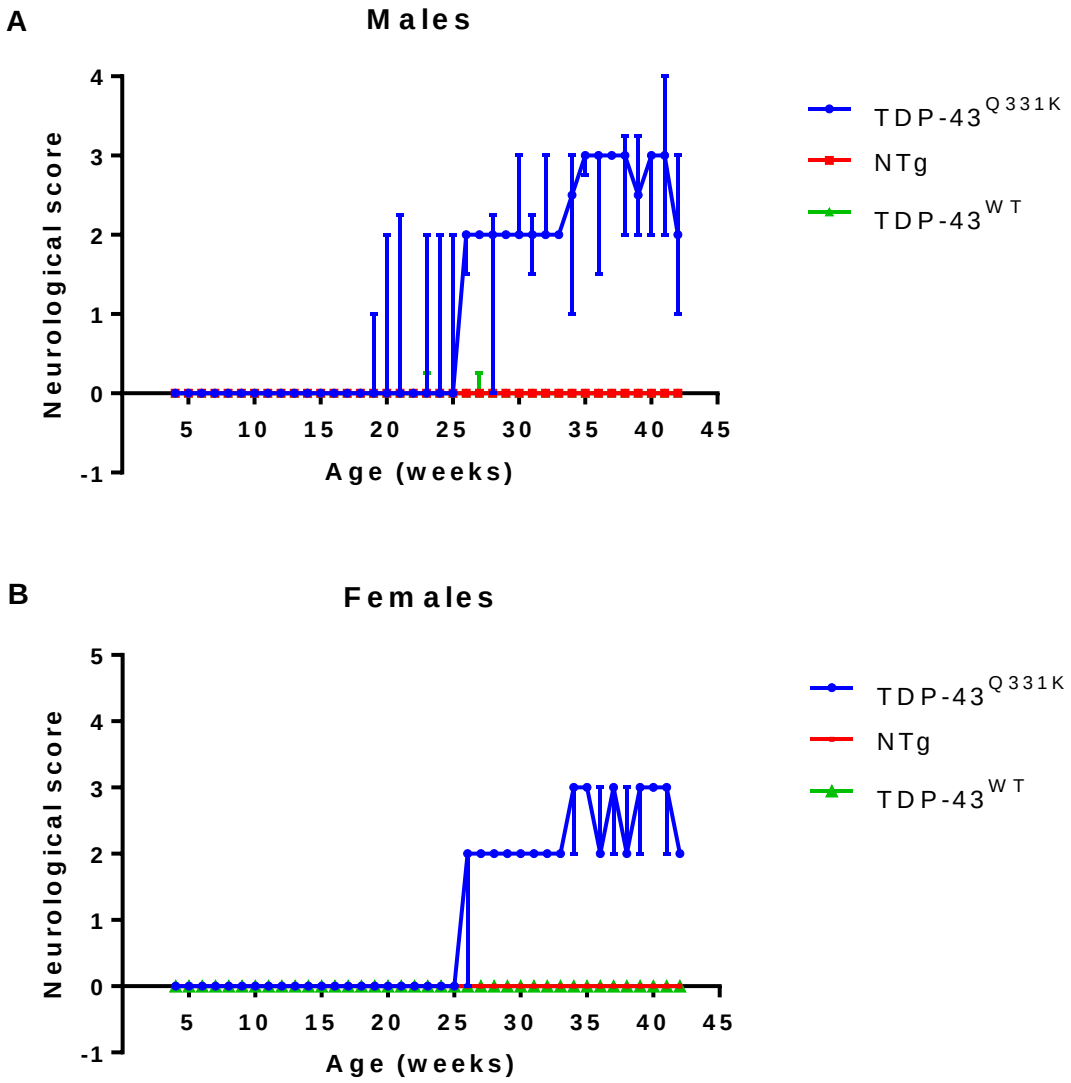

Figure 2. 3: Neuroscores.

Median neuroscores (± interquartile range) for male (A) and female (B) TDP-43^{Q331K} mice (n = 6/7) compared to TDP-43^{WT} (n = 6) and non-transgenic (NTg, n = 12) mice. 0 = normal, 1 = significant hindlimb tremor, 2 = abnormal gait, 3 = severe waddle, 4 = dragging of one hindlimb.

2.4.4. TDP-43^{Q331K} Mice are Heavier than TDP-43^{WT} Mice

TDP-43^{Q331K} mice are significantly heavier than the TDP-43^{WT} and non-transgenic mice (see *figure 2.4*) from 10 weeks of age in males (n = 6/7 TDP-43^{Q331K}; 6 TDP-43^{WT}; 12 NTg, 29±3.3g TDP-43^{Q331K} vs 24.4±0.7g TDP-43^{WT}, $p<0.05$) and 9 weeks of age in females (n =

5-12, 21.5±2g TDP-43^{Q331K} vs 17.4±1.3g TDP-43^{WT}, p<0.05). On a two-way ANOVA with repeated measures and Tukey's post-test, all groups get significantly heavier with age (p<0.0001) and TDP-43^{Q331K} mice were significantly heavier than TDP-43^{WT} and non-transgenic mice in males (p<0.001) and females (p<0.0001).

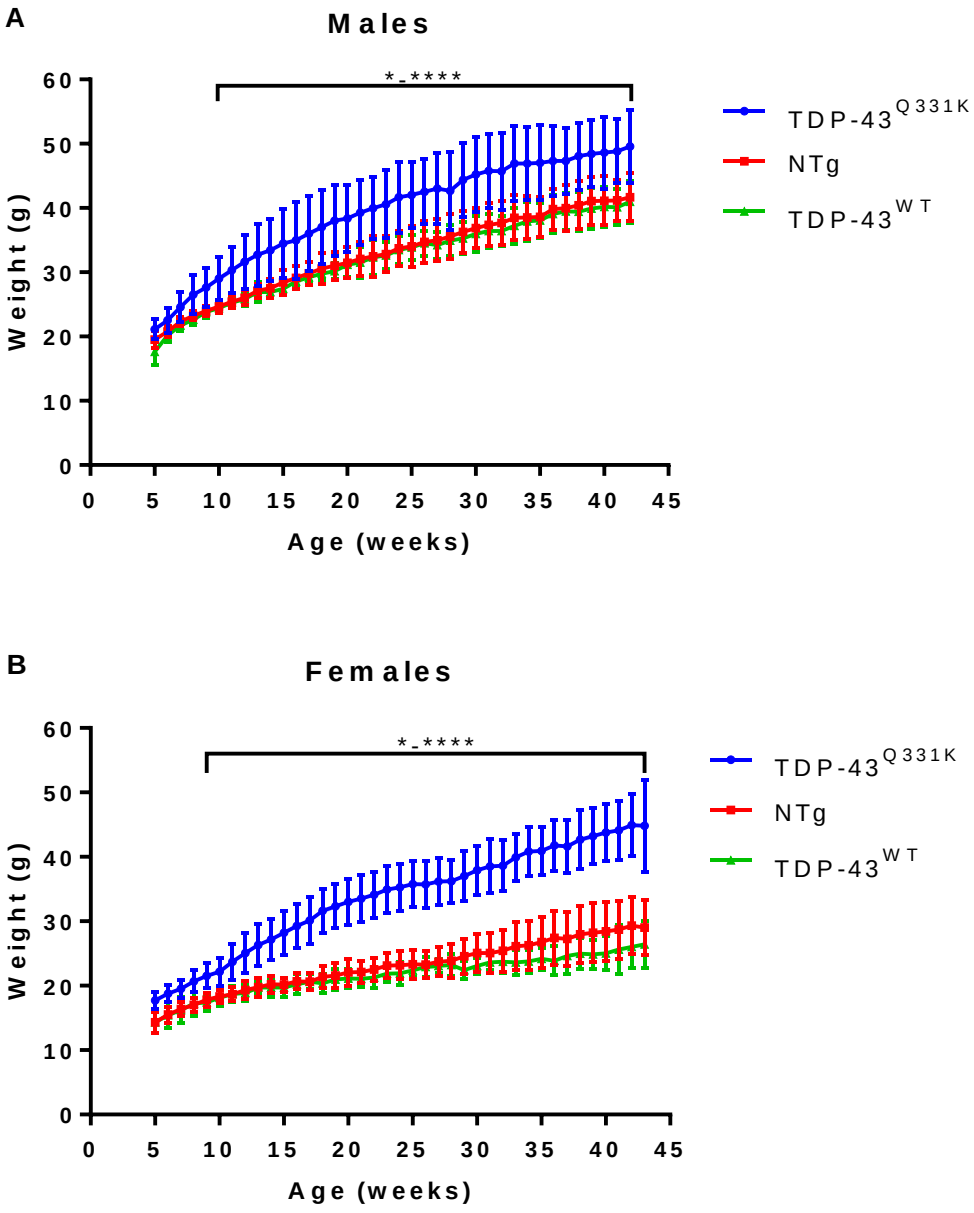

Figure 2. 4: Body weight of the TDP-43^{Q331K}, TDP-43^{WT} and non-transgenic mice.

*Mean weight (± SD) for male (A) and female (B) TDP-43^{Q331K} mice (n = 6/7) compared to TDP-43^{WT} (n = 6) and non-transgenic (NTg, n = 12) mice. TDP-43^{Q331K} mice were significantly heavier than the other groups. *p<0.05 vs all other groups, ****p<0.0001 vs all other groups, two-way ANOVA with repeated measures and Tukey's post-tests.*

2.4.5. Rotarod Performance Decreases with Age in the TDP-43^{Q331K} Mice

TDP-43^{Q331K} mice show a significantly decreased latency to fall compared to the TDP-43^{WT} and non-transgenic mice (see *figure 2.5*) by 7 weeks of age in males (n = 5-12, 147.8±34.6s TDP-43^{Q331K} vs 261±49.4s TDP-43^{WT}, $p<0.01$) and 10 weeks of age in females (n = 5-12, 201.6±36.9s TDP-43^{Q331K} vs 264.8±40.8 TDP-43^{WT}, $p<0.01$) (*figure 2.5*). On a two-way ANOVA with repeated measures and Tukey's post-test rotarod performance reduced significantly with age in all groups ($p<0.0001$) and TDP-43^{Q331K} mice had a significantly decreased latency to fall compared to non-transgenic and TDP-43^{WT} mice ($p<0.0001$).

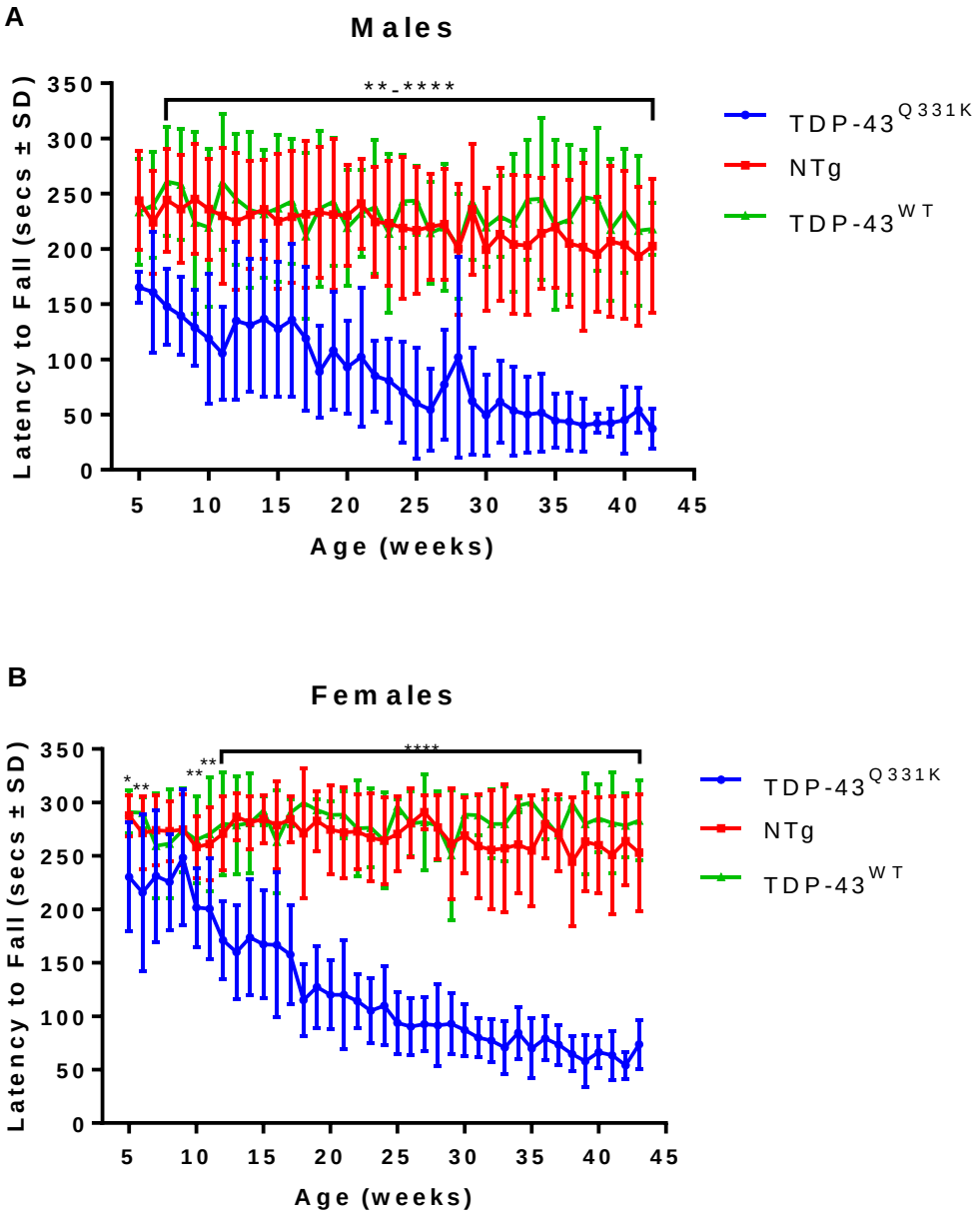

Figure 2. 5: Rotarod performance.

*Mean latency to fall (± SD) for male and female TDP-43^{Q331K} mice compared to TDP-43^{WT} and non-transgenic (NTg) mice. TDP-43^{Q331K} mice had a significantly decreased latency to fall compared to the other groups. *p<0.05 vs all other groups, **p<0.01 vs all other groups, ****p<0.0001 vs all other groups, two-way ANOVA with repeated measures and Tukey's post-test.*

2.4.6. Rotarod Performance Decreases Despite Weight

Weight may have a significant influence on rotarod performance, so a correlation of mean rotarod performance and mean weight (n = 5-12) was therefore calculated for each group (*figure 2.6*). In the TDP-43^{Q331K} male and female mice, the correlation between weight and rotarod was highly significant (males r = -0.9507, p<0.0001; females r = -0.9799, p<0.0001). There was also a strong correlation between weight and rotarod in the non-transgenic male and female mice (males r = -0.2875, p>0.05; females r = 0.09947, p>0.05) but interestingly, no correlation was found in the male and female TDP-43^{WT} data (males r = -0.8483, p<0.0001; females r = -0.5919, p<0.0001). This may suggest that if weight alone influenced rotarod performance then some correlation with rotarod performance for TDP-43^{WT} mice may have been observed but was not. However, it may still be the case that weight influences rotarod performance, as suggested by the TDP-43^{Q331K} and non-transgenic correlations.

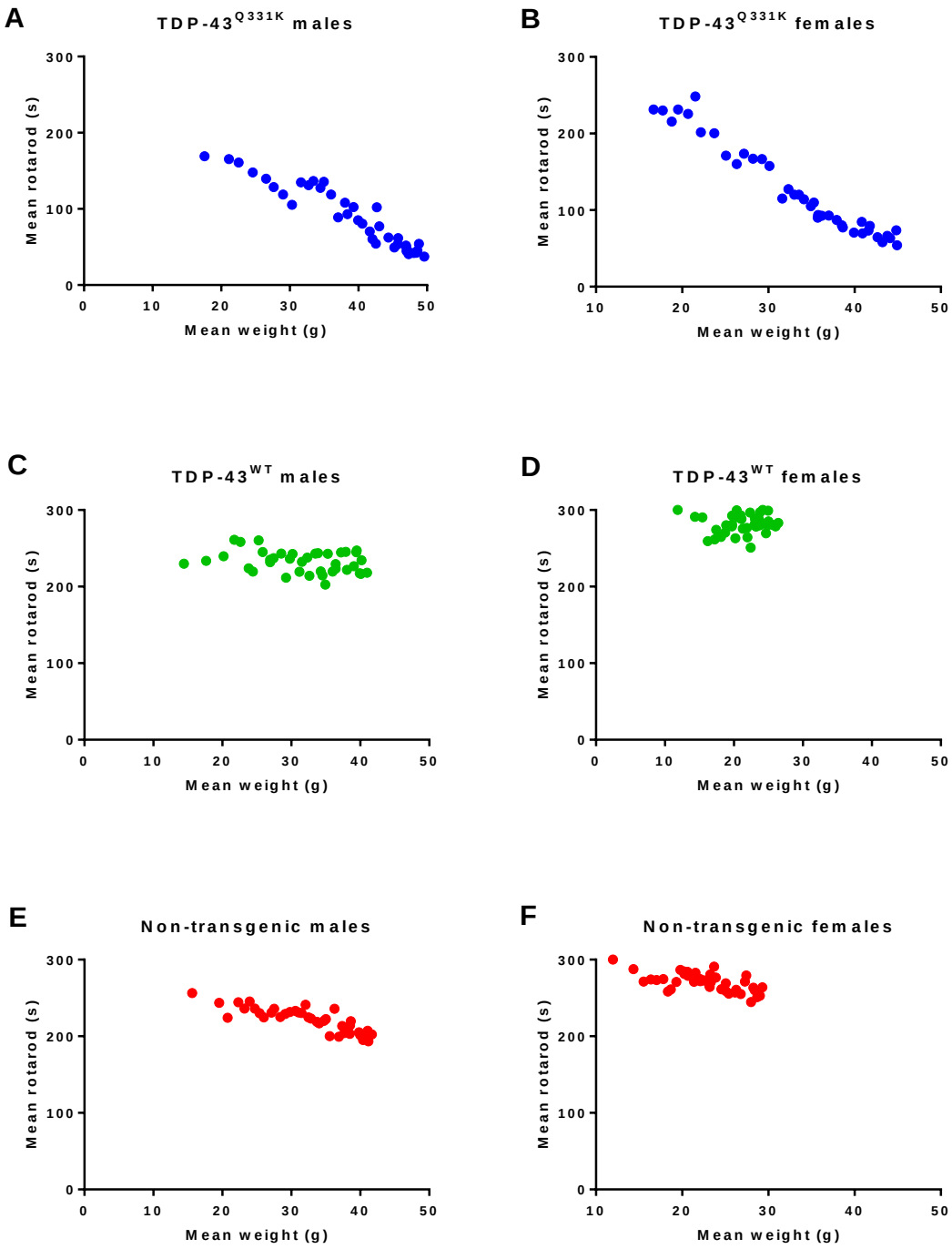

Figure 2. 6: Spearman correlation of weight vs rotarod.

Spearman correlation of mean weight vs mean rotarod for male TDP-43^{Q331K} mice (A, r = -0.9507, p<0.0001), male TDP-43^{WT} mice (C, r = -0.2875, p>0.05), male non-transgenic mice (E, r = -0.8483, p<0.0001), female TDP-43^{Q331K} mice (B, r = -0.9799, p<0.0001), female TDP-43^{WT} mice (D, r = 0.09947, p>0.05), and female non-transgenic mice (F, r = -0.5919, p<0.0001).

After consultation with several statisticians to devise a method which would account for the influence of weight on the rotarod, several methods of analysis were considered including a regression analysis, a general linear model, a mixed model, and an analysis of covariance. After much deliberation, the simple method of normalising the rotarod to weight through division was used.

To eliminate the influence of weight, rotarod performance was normalised for weight by generating a ratio of rotarod performance/weight as shown in *figure 2.7*. A two-way ANOVA with repeated measures and Tukey's post-test revealed that the TDP-43^{Q331K} mice performed considerably worse than the TDP-43^{WT} and non-transgenic mice. The ratio of rotarod performance/weight decreases over time in all groups, in both males and females ($p<0.0001$) and the TDP-43^{Q331K} mice show a significant reduction in rotarod/weight compared to the other groups ($p<0.0001$) on a two-way ANOVA with Tukey's post-tests. The non-transgenic and TDP-43^{WT} mice show a similar starting point with a similar decline, whereas the TDP-43^{Q331K} mice have a lower rotarod/weight value from the beginning and throughout the disease course, in both male and female mice (*figure 2.7A*).

The female rotarod/weight values are higher compared to the male data in both TDP-43^{WT} and non-transgenic mice. The female decline in rotarod/weight in TDP-43^{Q331K} mice is more pronounced than in males and more significantly different when compared to the other groups (*figure 2.7B*).

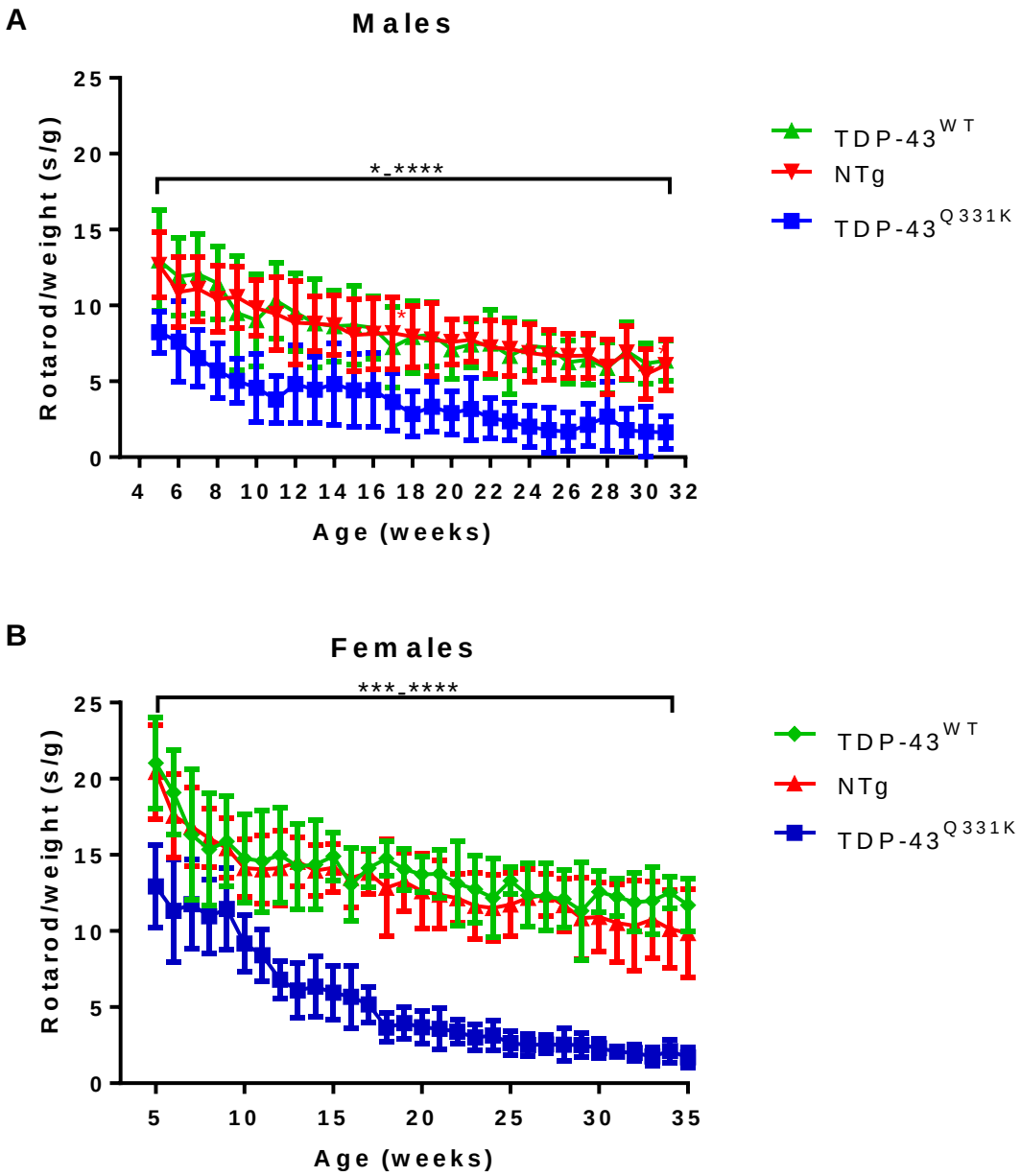

Figure 2. 7: Rotarod performance/weight.

Mean latency to fall/weight (± SD) for male and female TDP-43^{Q331K} mice compared to TDP-43^{WT} and non-transgenic (NTg) mice. TDP-43^{Q331K} mice show a significantly lower rotarod/weight ratio compared to all other groups. **p<0.05 vs all other groups, **p<0.01 vs all other groups, ***p<0.001 vs all other groups, ****p<0.0001 vs all other groups, two way ANOVA with Tukey's post-tests.*

2.4.7. huTARDBP Copy Number vs Rotarod Performance

Plotting of the rotarod performance for each mouse with a known huTARDBP copy number estimation shows no clear difference between the rotarod performances of mice with a higher or lower huTARDBP copy number estimation (*figure 2.8*).

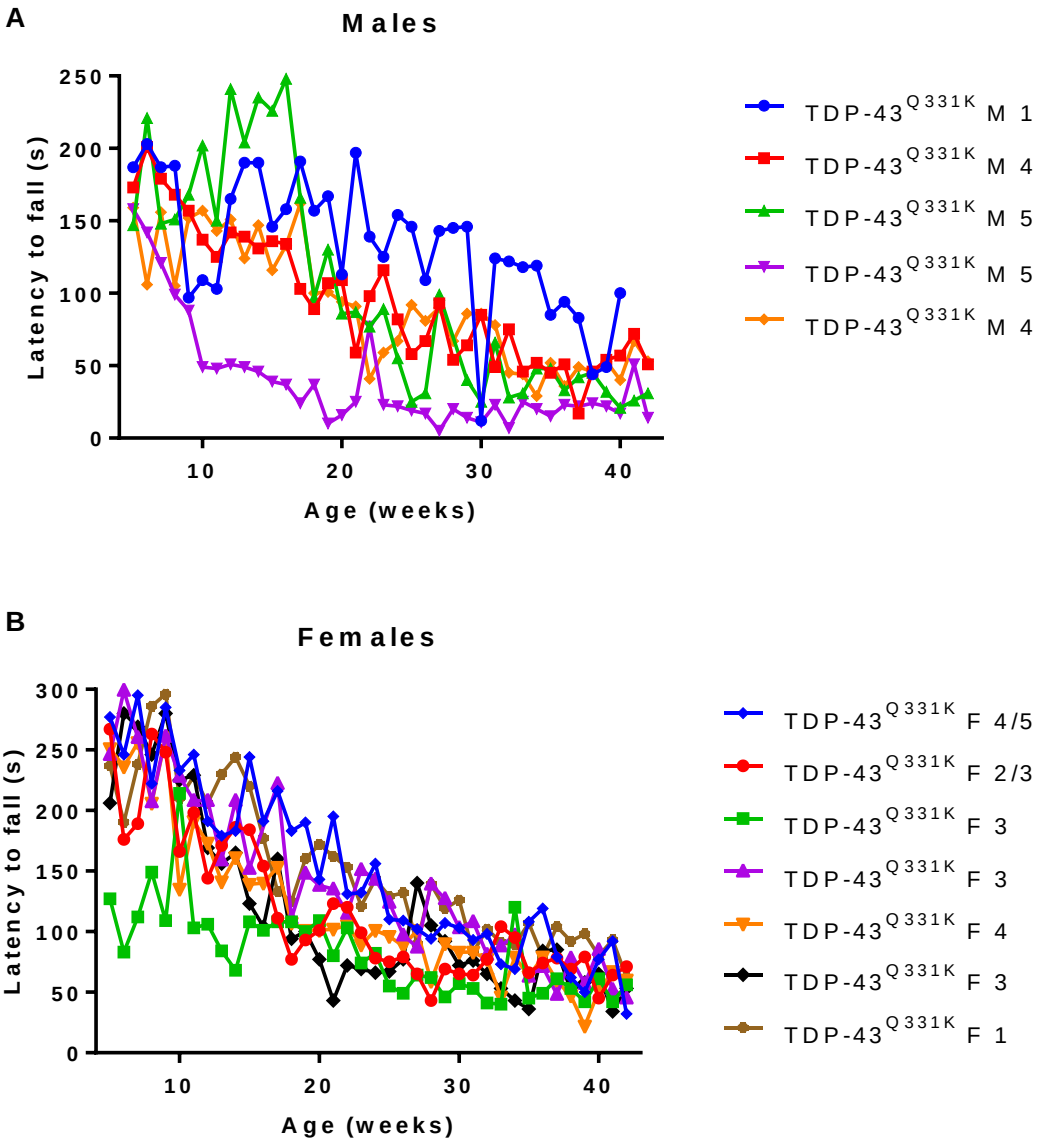

Figure 2. 8: Rotarod performance and huTARDBP copy number estimation.

Latency to fall on the rotarod is plotted for each of the mice with a known copy number estimation for males (A) and females (B). Copy number estimation is shown in the legend. All mice are TDP-43^{Q331K}.

Rotarod performance of the male mouse with an estimated human *TARDBP* copy number of one shows a slightly increased rotarod performance compared to the mean TDP-43^{Q331K} rotarod data (*figure 2.9A*). The female mouse with an estimated human *TARDBP* copy number of one shows no obvious difference in rotarod performance when compared to the mean TDP-43^{Q331K} rotarod data (*figure 2.9B*).

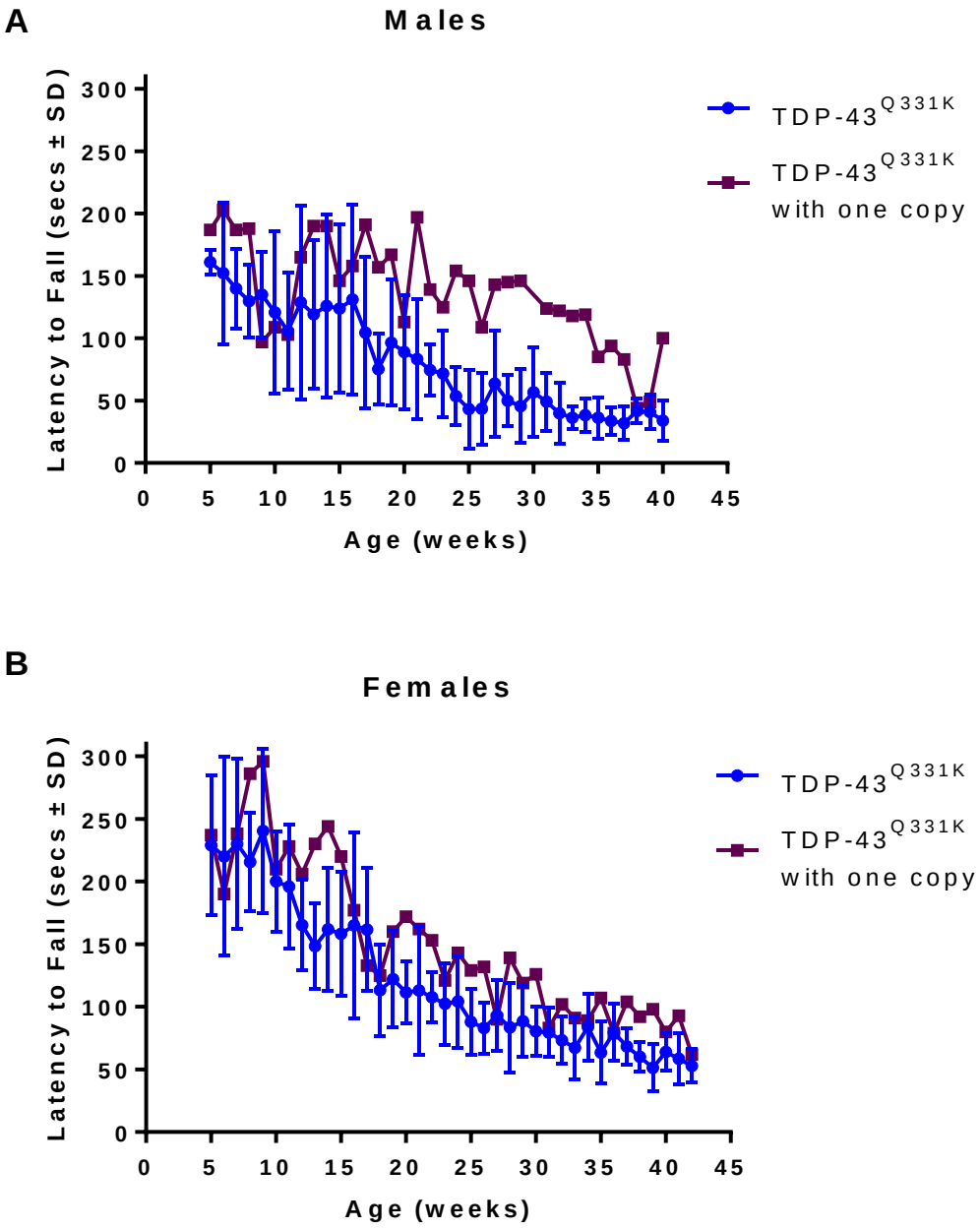

Figure 2. 9: Rotarod performance of all TDP-43^{Q331K} mice compared to those with an estimated copy number of one.

Latency to fall on the rotarod is plotted for each of the TDP-43^{Q331K} mice with the low copy number mouse data plotted as a separate line in males (A) and females (B).

2.4.8. Gait Analysis

Gait parameters were analysed at 1, 3, 6, and 10 months of age in the TDP-43^{Q331K}, TDP-43^{WT} and non-transgenic mice. Pawprint images display a wider gait with larger pawprints in the TDP-43^{Q331K} mice (*figure 2.10C*), compared to the gait of non-transgenic (*figure 2.10A*) and TDP-43^{WT} mice (*figure 2.10B*).

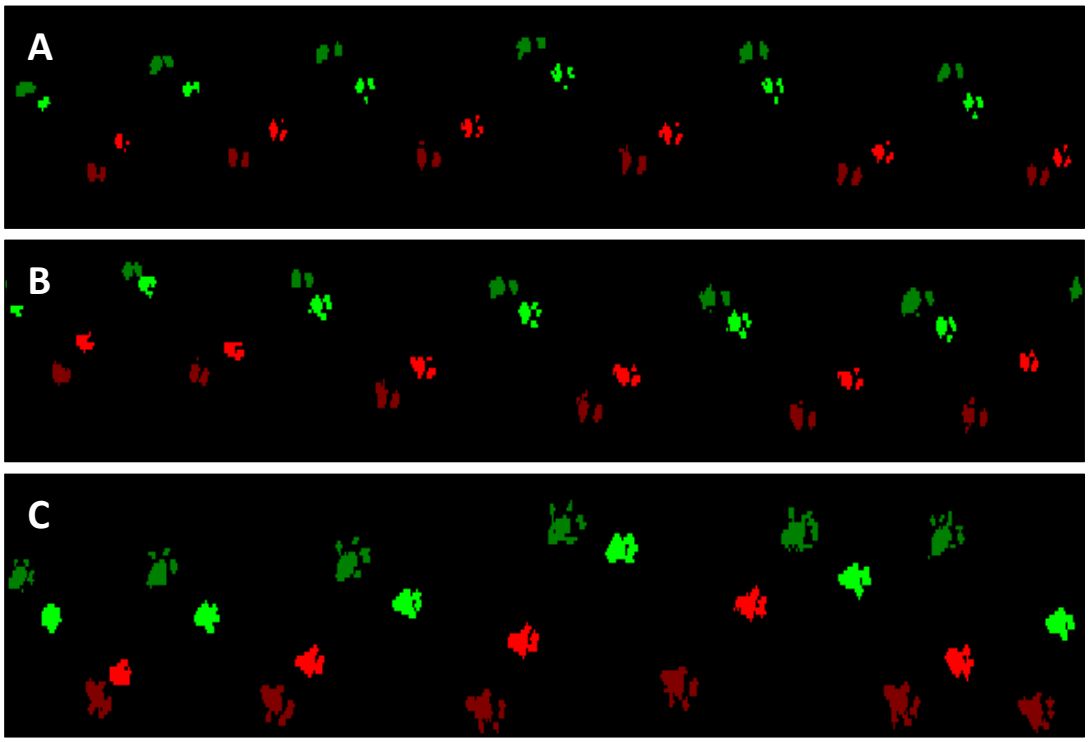

Figure 2. 10: Catwalk gait analysis.

Footprint traces of non-transgenic (A), TDP-43^{WT} (B) and TDP-43^{Q331K} (C) mice, as seen by the camera from below. Red prints = left hand limbs, green prints = right hand limbs, bright prints = forelimbs, darker prints = hindlimbs.

All statistics for significant findings are reported in *table 2.4.*

Forelimb intensity (*figure 2.11A & B*) is a measure of weight support in the forepaws. Forelimb intensity is increased at 10 months of age compared to 1, 3 and 6 months of age in all groups of male mice (*figure 2.11A*). However, there is no significant difference between groups at any age in males. The female data show a significantly increased forelimb intensity at 3 months of age in the TDP-43^{Q331K} mice compared to the TDP-43^{WT} and non-transgenic mice (*figure 2.11B*). This increase is not evident at 6 months of age but is shown again at 10 months of age.

Print length (*figure 2.11C & D*) is a measure of the paw print length. The forelimb print length does not appear to change significantly over time, nor does it show any differences between groups in males or females.

Stride length (*figure 2.11E & F*) is a measure of the distance covered by each stride, or the distance between paw prints of the same paw. In male mice, the forelimb stride length data do not show any significant changes over time and no differences between groups of mice. However, in female mice, the forelimb stride length increases with age in the TDP-43^{WT} and non-transgenic mice, whilst remaining the same in the TDP-43^{Q331K} mice, presenting as a non-significantly shorter stride length at 6 months of age, and a significantly shorter stride length at 10 months of age.

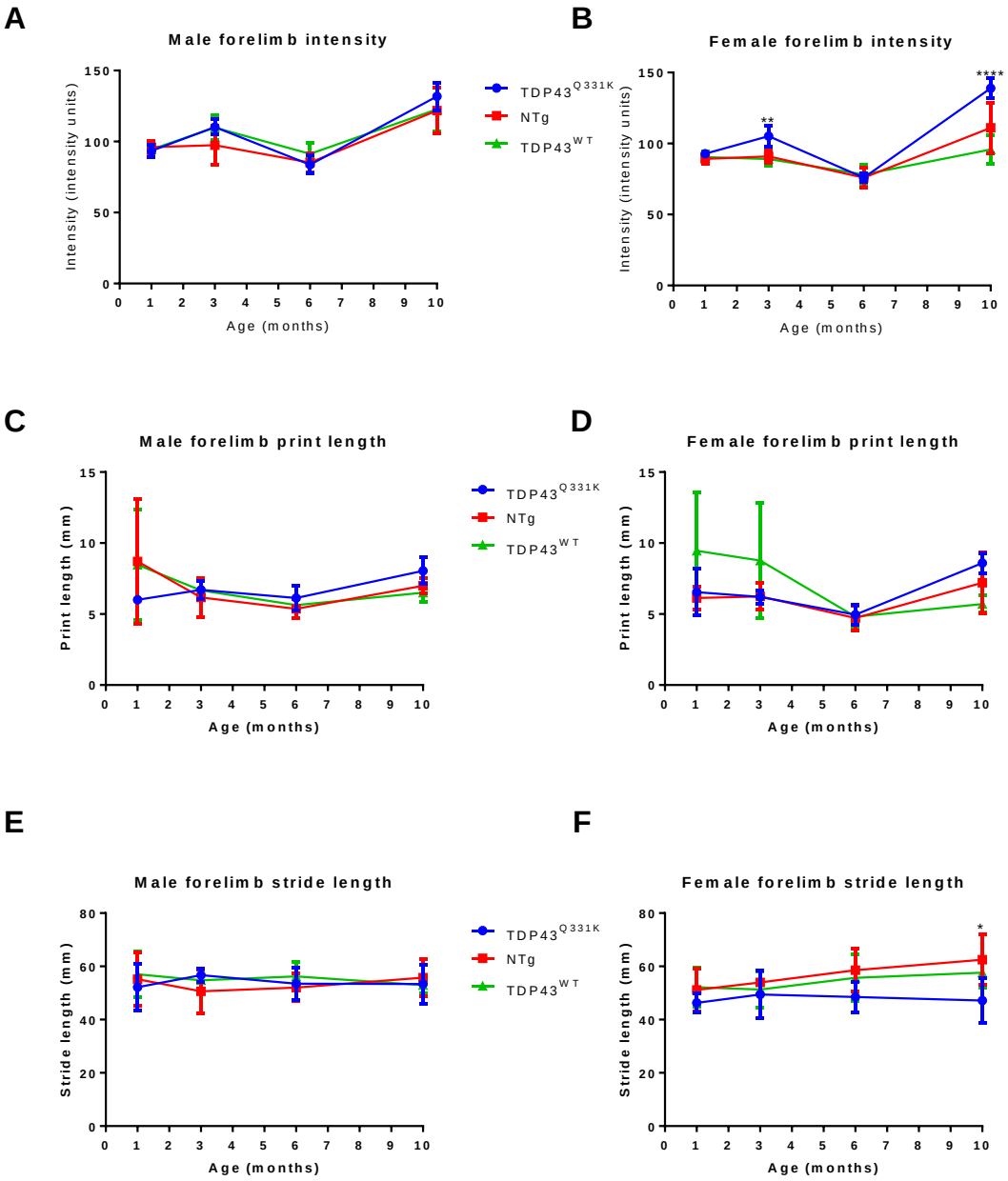

Figure 2. 11: Catwalk gait analysis of male and female forelimb intensity (A, B), print length (C, D) and stride length (E, F).

*Intensity is a measure of weight support in the paws. Print length is a measure of the paw print length. Stride length is a measure of the distance covered by each stride. Numbers are presented as a mean of the right and left side for each mouse, mean (±SD), n = 4-12, *p<0.05, **p<0.01, ***p<0.001, ****p<0.0001 TDP-43^{Q331K} vs all other groups, two way ANOVA with Tukey's post-tests.*

Duty cycle (*figure 2.12A & B*) is the length of time a paw is on the floor, expressed as a percentage of the total time taken for each stride. The forelimb duty cycle does not appear to change significantly over time, nor does it show any differences between groups in males. However, in females the forelimb duty cycle is decreased at 6 months of age in all groups compared to all other time points. At 6 months of age the female TDP-43^{Q331K} mice have a significantly increased forelimb duty cycle, and this is more significantly increased at 10 months of age.

Swing time (*figure 2.12C & D*) is the length of time between placements of each individual paw. In both males and females the forelimb swing time appears to increase at 6 months of age in all groups compared to all other time points. Male forelimb swing time is significantly increased at 3 months of age in the TDP-43^{Q331K} mice. This increase is more significant at 6 and 10 months of age. Similarly, female forelimb swing time is significantly increased at 3 months of age in the TDP-43^{Q331K} mice. This increase is more significant at 6 and 10 months of age.

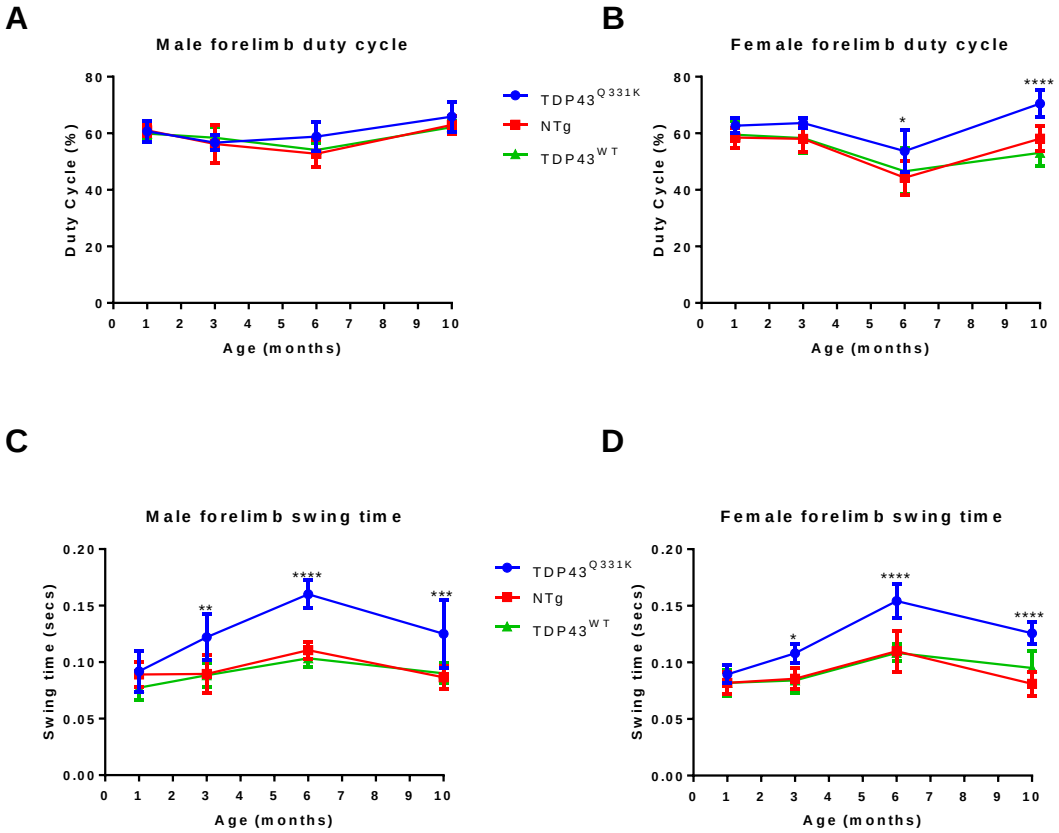

Figure 2. 12: Catwalk gait analysis of male and female forelimb duty cycle (A, B) and swing time (C, D).

*Duty cycle is the length of time a paw is on the floor, expressed as a percentage of the total time taken for each stride. Swing time is the length of time between placements of each paw. Numbers are presented as a mean of the right and left side for each mouse, mean (±SD), n = 6/7 TDP-43^{Q331K}; 6 TDP-43^{WT}; 12 NTg, *p<0.05, **p<0.01, ***p<0.001, ****p<0.0001 TDP-43^{Q331K} vs all other groups, two way ANOVA with Tukey's post-tests.*

Hindlimb intensity (*figure 2.13A & B*) is a measure of weight support in the hindpaws. The hindlimb intensity is decreased at 6 months of age and increased at 10 months of age compared to 1 and 3 months of age in all groups, in both male and female mice. The male data show a decreased hindlimb intensity throughout in the TDP-43^{Q331K} mice and this is significant at 10 months of age. However, there is no significant difference between groups at any age in the female hindlimb intensity.

Print length (*figure 2.13C & D*) is a measure of the paw print length. The hindlimb print length does not appear to change significantly over time, nor does it show any

differences between groups in males. However, in females, the hindlimb print length is significantly increased in the TDP-43^{Q331K} hindlimb at 10 months of age.

Stride length (*figure 2.13E & F*) is a measure of the distance covered by each stride, meaning the distance between paw prints of the same paw. In male mice, the hindlimb stride length data do not show any significant changes over time and no differences between groups of mice. However, in female mice, the hindlimb stride length increases with age in the TDP-43^{WT} and non-transgenic mice, whilst remaining the same in the TDP-43^{Q331K} mice, presenting as a non-significantly shorter hindlimb stride length at 6 months of age, and a significantly shorter stride length at 10 months of age.

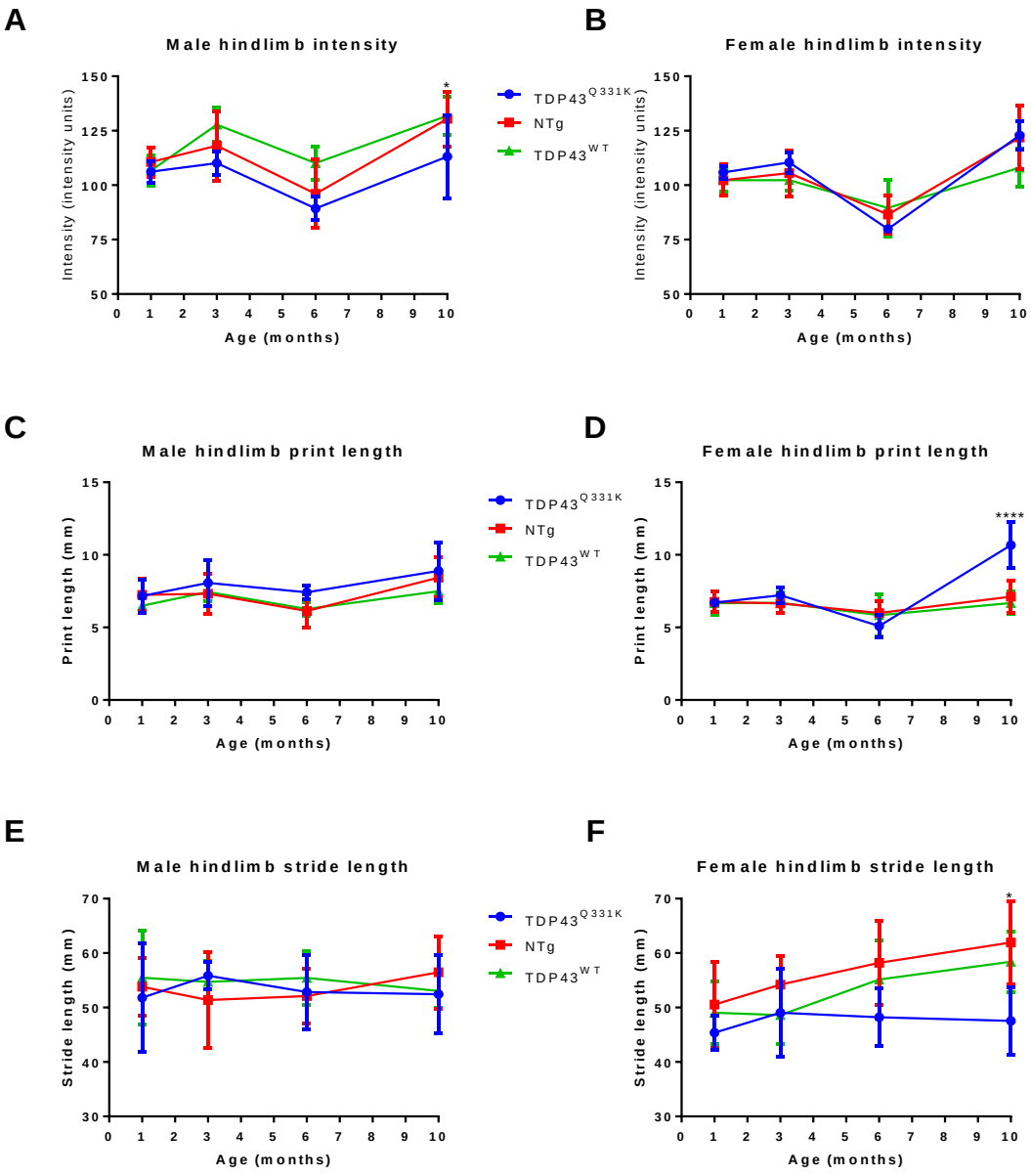

Figure 2. 13: Catwalk gait analysis of male and female hindlimb intensity (A, B), print length (C, D) and stride length (E, F).

*Intensity is a measure of weight support in the paws. Print length is a measure of the paw print length. Stride length is a measure of the distance covered by each stride. Numbers are presented as a mean of the right and left side for each mouse, mean (±SD), n = 4-12, *p<0.05, **p<0.01, ***p<0.001, ****p<0.0001 TDP-43^{Q331K} vs all other groups, two way ANOVA with Tukey's post-tests.*

Duty cycle (*figure 2.14A & B*) is the length of time a paw is on the floor, expressed as a percentage of the total time taken for each stride. The hindlimb duty cycle shows a slight increase at 10 months of age in males compared to 1, 3 and 6 months. The male data show no differences between groups other than a decreased duty cycle in TDP-43^{Q331K} mice at 3 months of age. However, in females the hindlimb duty cycle is decreased at 6 months of age in all groups compared to all other time points and at 10 months of age the female TDP-43^{Q331K} mice have a significantly increased hindlimb duty cycle.

Swing time (*figure 2.14C & D*) is the length of time between placements of each individual paw. In both males and females the hindlimb swing time appears to increase at 6 months of age in all groups compared to all other time points. Male hindlimb swing time is significantly increased at 6 and 10 months of age in the TDP-43^{Q331K}. Similarly, female hindlimb swing time is significantly increased at 6 months of age in the TDP-43^{Q331K} mice. However, there is no significant difference in hindlimb swing time between female groups at 10 months of age.

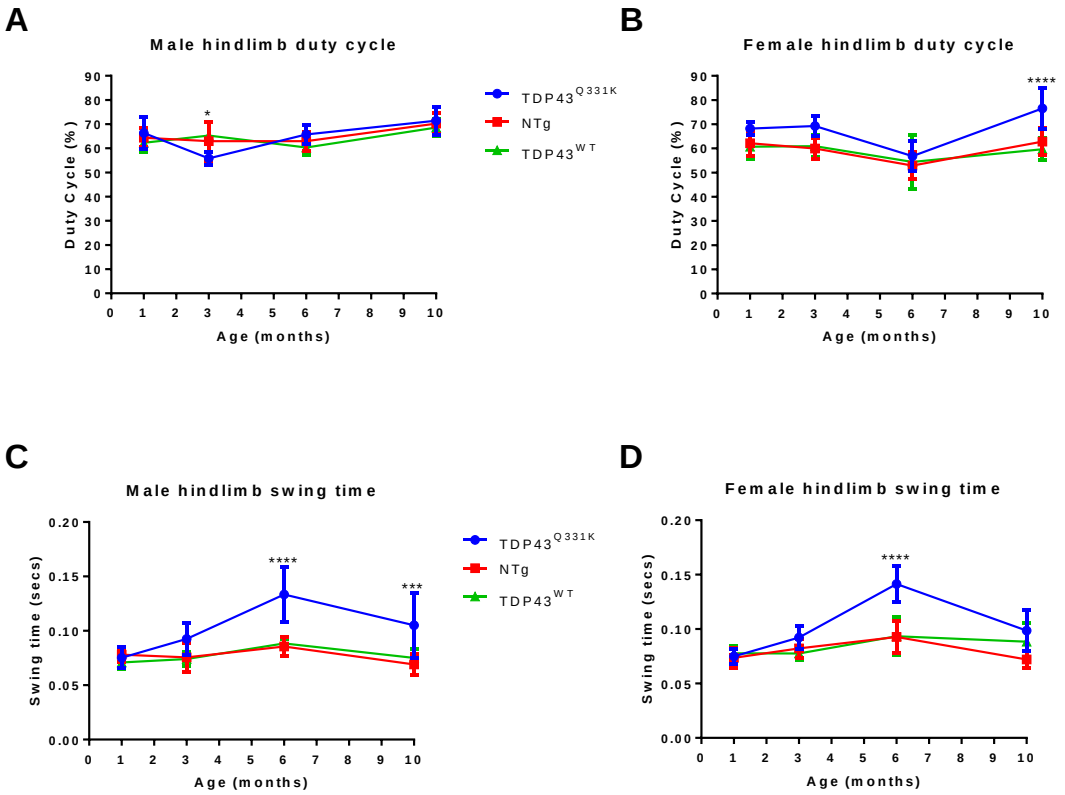

Figure 2. 14: Catwalk gait analysis of male and female hindlimb duty cycle (A, B) and swing time (C, D).

*Duty cycle is the length of time a paw is on the floor, expressed as a percentage of the total time taken for each stride. Swing time is the length of time between placements of each foot. Numbers are presented as a mean of the right and left side for each mouse, mean (±SD), n = 4-12, *p<0.05, **p<0.01, ***p<0.001, ****p<0.0001 TDP-43^{Q331K} vs all other groups, two way ANOVA with Tukey's post-tests.*

Base of support (BOS) is the distance between the two paws. The forelimb BOS (*figure 2.15A & B*) has a tendency to increase with age in both males and females. However, there are no significant differences between groups at any age in the male mice. Female TDP-43^{Q331K} mice show a significantly larger forelimb BOS at 10 months of age.

Hindlimb BOS (*figure 2.15C & D*) is increased at 6 and 10 months in all groups compared to 1 and 3 months in both males and females. In males, the hindlimb BOS is significantly larger in the TDP-43^{Q331K} mice at 6 and 10 months. In females, the hindlimb BOS is significantly larger in the TDP-43^{Q331K} mice at 6 and 10 months. This appears to be the

most consistent and useful measure of gait abnormalities in these mice and reflects well the 'waddling gait' observed.

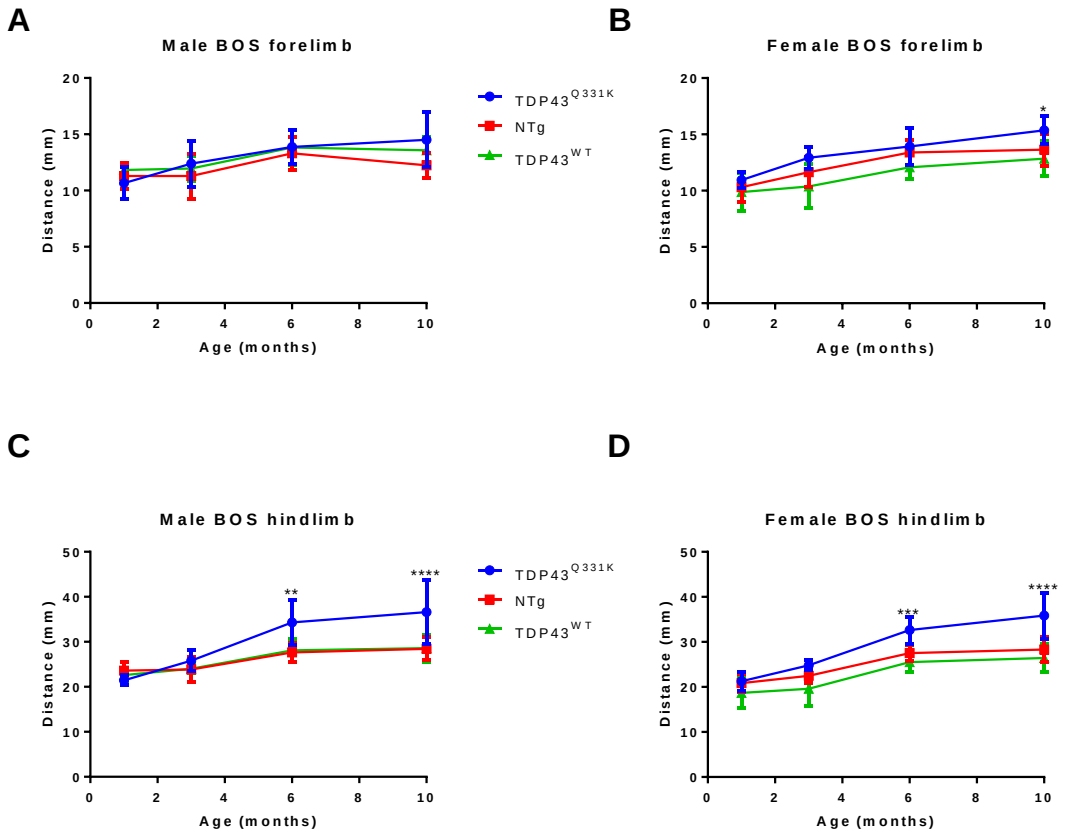

Figure 2. 15: Catwalk gait analysis of male and female hindlimb base of support in the forelimb (A, B) and hindlimb (C, D).

*Base of support (BOS) is the distance between the two paws. Mean (±SD), n = 4-12, *p<0.05, **p<0.01, ***p<0.001, ****p<0.0001 TDP-43^{Q331K} vs all other groups, two way ANOVA with Tukey's post-tests.*

Walking duration (*figure 2.16A & B*) is the time taken to cross the length of the recording area (43.8cm). Walking remains similar in TDP-43^{WT} and non-transgenic mice at 1, 3, 6 and 10 months of age, in both males and females. However, walking duration is increased by 3 months of age in males, significantly so by 6 months of age and more so by 10 months of age. In female mice, the walking duration is significantly increased at 3 months of age, 6 months of age and 10 months of age.

The percentage of time spent walking with a diagonal step pattern is shown in *figure 2.16C & D* (left forepaw placed down in time with right hindpaw; right forepaw placed

down in time with left hindpaw). In males and females the percentage of diagonal stepping pattern shows no obvious trends with age in the TDP-43^{WT} and non-transgenic mice. However, the percentage of diagonal stepping is decreased in the TDP-43^{Q331K} male mice at 6 and 10 months of age. In females, the percentage of diagonal stepping is significantly decreased in the TDP-43^{Q331K} mice at 10 months of age.

The percentage of time spent walking with three paws on the ground at any one time is also shown in *figure 2.16E & F*. In males and females the percentage of three paw step pattern shows no obvious trends with age in the TDP-43^{WT} and non-transgenic mice. However, the percentage of three paw stepping is non-significantly decreased in the TDP-43^{Q331K} mice at 6 and 10 months of age. In females, the percentage of three paw stepping is significantly decreased in the TDP-43^{Q331K} mice at 10 months of age.

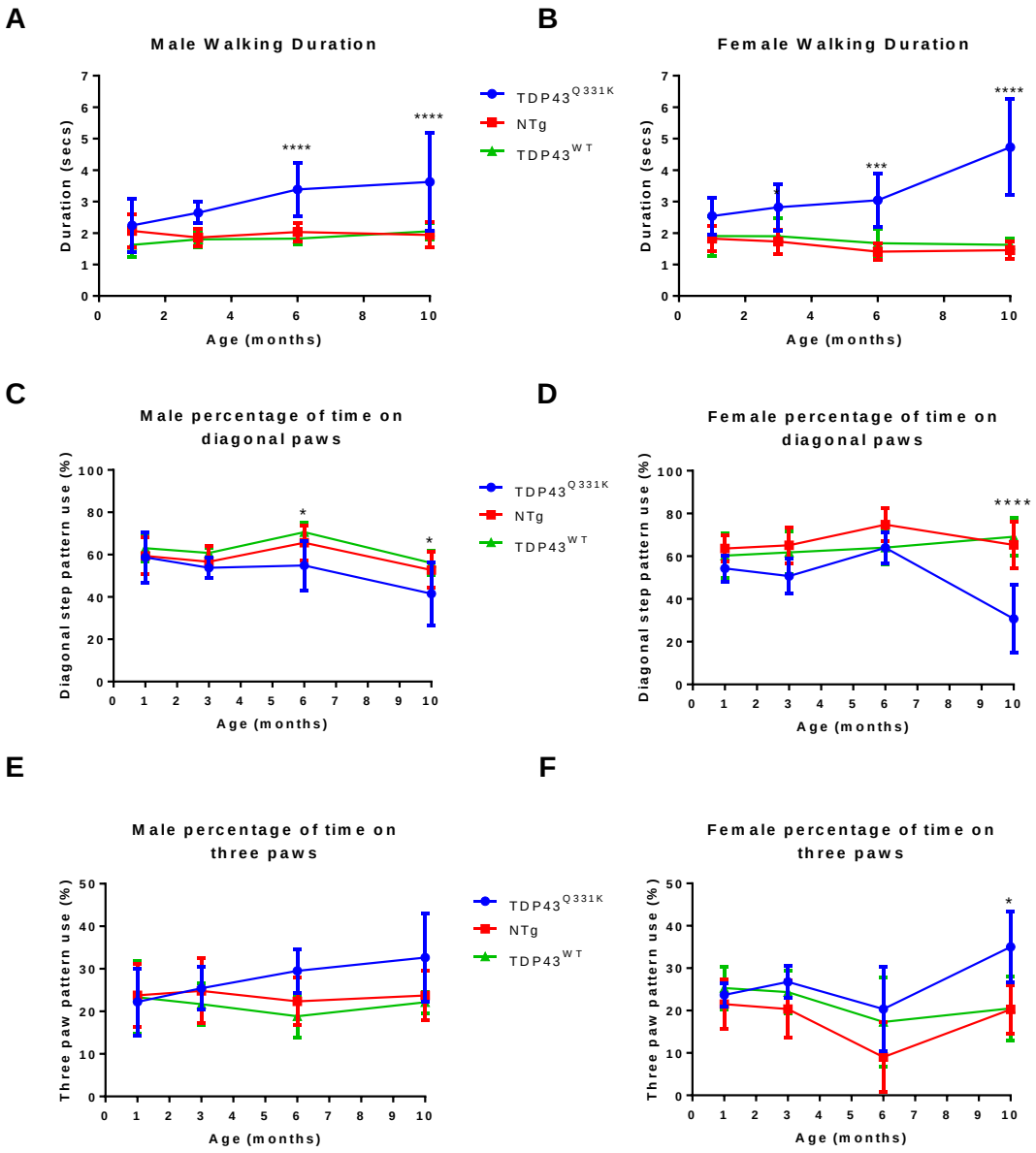

Figure 2. 16: Catwalk gait analysis of male and female duration (A, B), percentage of time on diagonal paws (C, D) and percentage of time on three paws (E, F).

*Duration is the time it takes the mice to walk the distance of the catwalk (43.8cm). For the percentage of time spent walking with a diagonal step pattern and the percentage of time spent on 3 paws, statistics are also based on logit transformation. Mean (±SD), n=4-12, *p<0.05, **p<0.01, ***p<0.001, ****p<0.0001 TDP-43^{Q331K} vs all other groups, two way ANOVA with Tukey's post-tests.*

Table 2. 4: Table of significant statistics for catwalk gait analysis. **=p<0.05, **=p<0.01, ***=p<0.001, ****=p<0.0001, IU=intensity units. All differences are between the TDP-43^{Q331K} and control groups, there were no significant differences between the non-transgenic and TDP-43^{WT} groups.*

Catwalk parameter	**Age (months)**	**Gender**	**TDP-43^{Q331K}**	**TDP-43^{WT}**	**Non-transgenic**	**Significance of the difference between the TDP-43^{Q331K} and control groups**
Forelimb intensity	3	Females	105.2±7.9IU	89.1±4.9IU	90.9±4.6IU	**
	10	Females	139±7.1IU	95.8±10.1IU	111.1±17.8IU	****
Forelimb stride length	10	Females	47.2±8.5mm	57.6±5.8mm	62.5±9.5mm	*
Forelimb duty cycle	6	Females	53.7±7.6%	46.6±8.2%	44.3±6%	*
	10	Females	70.5±4.8%	53.1±4.5%	58.1±4.4%	****
Forelimb swing time	3	Males	0.122±0.02s	0.088±0.011s	0.09±0.017s	**
	6	Males	0.16±0.013s	0.103±0.008s	0.111±0.007s	****
	10	Males	0.125±0.03s	0.095±0.009s	0.087±0.01s	****
	3	Females	0.108±0.008s	0.084±0.011s	0.086±0.009s	**
	6	Females	0.154±0.015s	0.108±0.008s	0.11±0.018s	****
	10	Females	0.126±0.01s	0.095±0.015s	0.081±0.11s	***
Hindlimb intensity	10	Males	113.2±19.2IU	131.9±9IU	130.4±12.6IU	*

Hindlimb print length	10	Females	10.7±1.6mm	6.7±0.8mm	7.1±1.1mm	****
Hindlimb stride length	10	Females	47.6±6.2mm	58.4±5.6mm	61.9±7.6mm	*
Hindlimb duty cycle	3	Males	55.9±2.6%	65.3±1.5%	62.9±8.1%	*
	10	Females	47.6±6.2%	58.4±5.6%	61.9±7.6%	****
Hindlimb swing time	6	Males	0.133±0.025s	0.088±0.004s	0.086±0.009s	****
	10	Males	0.105±0.03s	0.075±0.008s	0.069±0.01s	***
	6	Females	0.141±0.017s	0.093±0.018s	0.093±0.015s	****
Forelimb BOS	10	Females	15.4±1.2mm	12.8±1.5mm	13.6±1.4mm	*
Hindlimb BOS	6	Males	34.3±5.1mm	28.1±2.5mm	27.6±2mm	**
	10	Males	36.6±7.1mm	28.6±3mm	28.5±2.5mm	****
	6	Females	32.7±3mm	25.5±2.2mm	27.5±1.8mm	***
	10	Females	35.8±5.1mm	26.4±3.1mm	28.3±2.8mm	****
Duration	6	Males	3.4±0.9s	1.8±0.2s	2.0±0.4s	****
	10	Males	3.6±1.6s	2.1±0.3s	1.9±0.4s	****
	3	Females	2.8±0.7s	1.9±0.6s	1.7±0.4s	*
	6	Females	3.0±0.8s	1.7±0.5s	1.4±0.3s	***
	10	Females	4.7±1.5s	1.6±0.2s	1.5±0.3s	****
Diagonal walking	6	Males	54.9±11.7%	70.7±4.4%	65.6±8.2%	*
	10	Males	41.6±14.9%	56.1±5.9%	52.7±8.4%	*

	10	Females	30.7±15.9%	69.1±9.1%	65.3±11%	****
Three paw walking	10	Females	35±8.4%	20.5±7.7%	20.3±5.7%	*

2.4.9. Variability of Parameters

In order to determine the group sizes required for therapeutic testing, statistical power analysis was conducted on all of the readouts using G*Power 3.1.9.2. (Faul et al., 2009) (*table 2.4*). Coefficients of variation are relatively low (<16%) for the majority of parameters measured. Power analysis (student's t-test, two-tailed, $\alpha = 0.05$, $\beta = 0.8$) was conducted on data at 6 and 10 months of age for most parameters and the N number required to detect a 10, 15 and 20% difference from TDP-43^{Q331K} mice calculated. For rotarod data we have previously found in $SOD1^{G93A}$ mice that the time taken to reach a 20% decline in performance is the least variable measure, and so this was used again here. The analysis suggests an N of 14 per group would be sufficient to detect a difference of at least 15% for all parameters. Overall, the data suggest that a study length of 10 months does not offer many advantages over a study length of 6 months with most of the effect sizes relatively unchanged between 6 and 10 months of age. Overall a study length of 6 months with group sizes of 14 is sufficient for the investigation of therapeutic agents in preclinical studies in this model.

Table 2. 5: Coefficient of variation and power analysis. Coefficient of variation and power analysis for all measured parameters at 6 and 10 months of age in female mice. Power = 80%.

Parameter	Age (months)	Mean values in TDP-43^{Q331K} mice (±s.d.)	Coefficient of Variation	Mean difference TDP-43^{WT} vs TDDP-43^{Q331K}	N required to detect an x% improvement
Time to reach a neuroscore of 2 (severe waddle)	N/A	26.43 weeks ± 0.535	2.02%	N/A	10% = 3
					15% = 2
					20% = 2
Weight	6	35.27g ± 3.651	10.4%	+55%	10% = 14
					15% = 7
					20% = 5
	10	43.8g ± 4.418	10.09%	+54%	10% = 14
					15% = 7
					20% = 5
Increase by 2 weeks in time to reach a 20% decline in rotarod performance from maximum	N/A	11.43 weeks ± 1.813	15.86%	N/A	11
Catwalk hindlimb base of support	6	32.651 ± 3.006	9.2%	+28%	10% = 12
					15% = 6
					20% = 4
	10	35.843 ± 5.143	14.3%	+36%	10% = 27
					15% = 13
					20% = 8

2.4.10. Litter Statistics

Litter size, percentage of transgenic pups, and percentage of male pups were compared between the two colonies TDP-43^{WT} and TDP-43^{Q331K} (*figure 2.17*). The litter size of the TDP-43^{Q331K} colony was significantly higher than the TDP-43^{WT} colony (6±2.61 in TDP-43^{WT} vs 7±2.12 in TDP-43^{Q331K}). The percentage of transgenic (49.91±22.37% in TDP-43^{WT} vs 47.91±22.68%) and male (48.06±24.84% in TDP-43^{WT} vs 53.32±20.26%) pups within each litter were equal between the two colonies. Breeding consistently uses transgenic males with non-transgenic females. The males appear to be fertile until at least 10 months of age in both colonies.

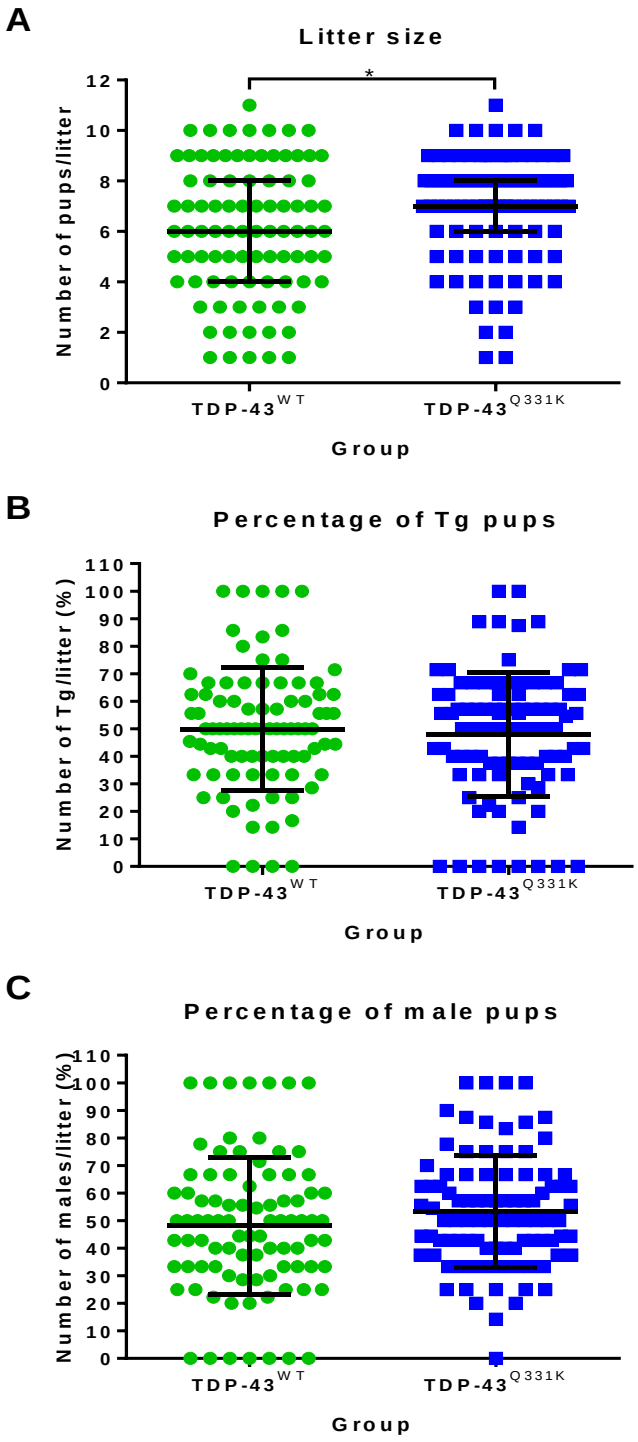

Figure 2. 17: Litter statistics for TDP-43^{WT} and TDP-43^{Q331K} colonies.

Comparisons between colonies for litter size (A), percentage of transgenic pups (B), and percentage of male pups (C). Litter size was compared using a Mann Whitney U test as the data were not normally distributed. Percentage of transgenic and male pups were compared using a student's t-test.

2.4.11. huTARDBP Gene Expression

The same cDNA samples were used to measure gene expression of huTDP-43 in the cDNA of cortex, spinal cord and hindlimb muscles of TDP-43^{WT} and TDP-43^{Q331K} mice at 10 months of age (*figure 2.18*) to assess the levels of expression compared with previously reported levels on a C57BL/6NCrl background (Arnold et al., 2013). For all tissues, TDP-43^{Q331K} values were expressed as a percentage of the TDP-43^{WT} values.

Expression of huTDP-43 was over 3-fold higher in the TDP-43^{Q331K} cortex compared to the TDP-43^{WT} cortex (100±17.3% in TDP-43^{WT} vs 308.4±36.4% in TDP-43^{Q331K}, $p<0.0001$). Expression of huTDP-43 was over 2-fold higher in the TDP-43^{Q331K} spinal cord compared to the TDP-43^{WT} spinal cord (100±13.3% in TDP-43^{WT} vs 213.3±65.8% in TDP-43^{Q331K}, $p<0.0001$). Expression of huTDP-43 was over 4-fold higher in the TDP-43^{Q331K} hindlimb muscle compared to the TDP-43^{WT} hindlimb muscle (100±19.8% in TDP-43^{WT} vs 407.6±111.9% in TDP-43^{Q331K}, $p<0.0001$). Relative huTDP-43 expression was therefore highest in the TDP-43^{Q331K} muscle, followed by cortex, and spinal cord.

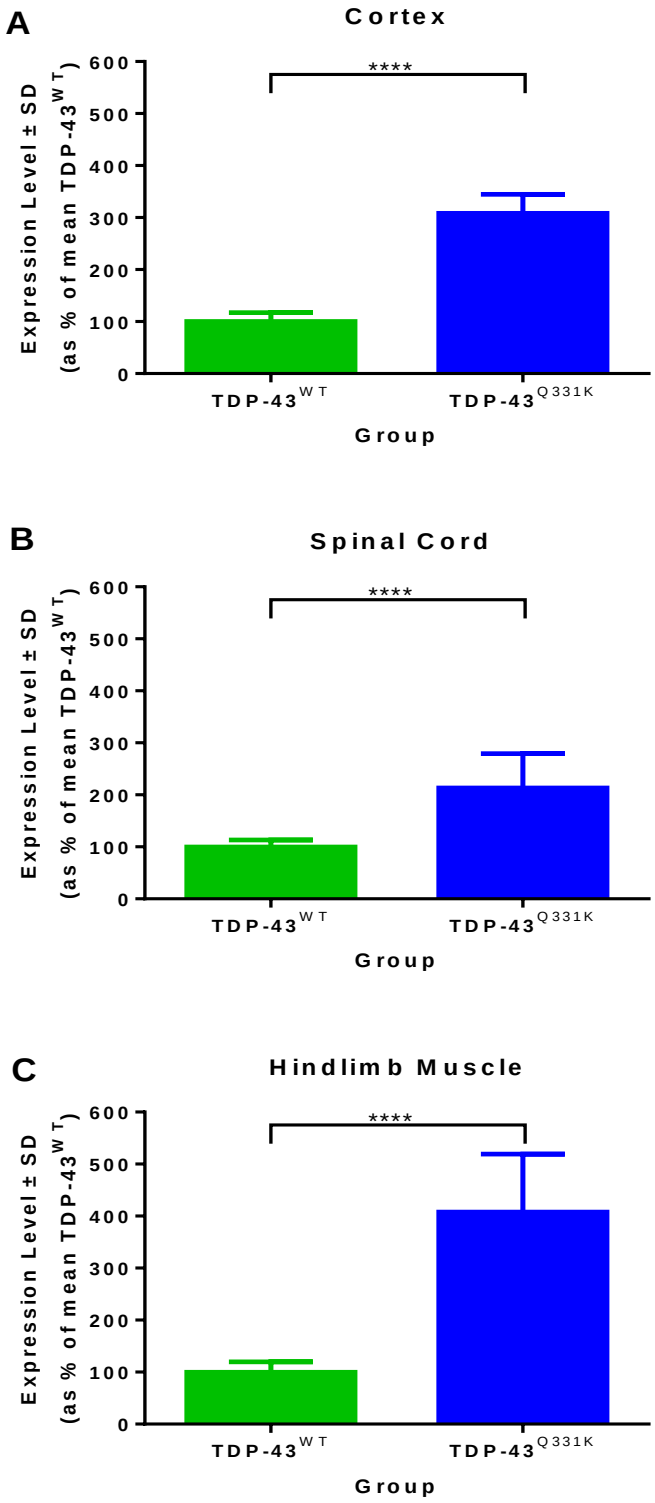

Figure 2. 18: huTDP-43 gene expression ± SD at 10 months of age.

*Gene expression of huTDP-43 as a percentage of the mean TDP-43^{WT} levels, as measured in cDNA of cortex (A), spinal cord (B) and hindlimb muscles (C) of TDP-43^{WT} and TDP-43^{Q331K} mice (n=9-12). ****p<0.0001, student's t-test.*

2.4.12. Total (mouse + human) *TARDBP* Gene Expression

Gene expression of total (mouse + human) TDP-43 was measured in the cDNA of cortex and spinal cord of non-transgenic, TDP-43^{WT} and TDP-43^{Q331K} mice at 10 months of age (*figure 2.19*), and expressed as a percentage of the mean non-transgenic value. Gene expression of total (mouse + human) TDP-43 was also measured in the hindlimb muscles of TDP-43^{WT} and TDP-43^{Q331K} mice, and expressed a percentage of the mean TDP-43^{WT} value.

Expression of TDP-43 was significantly lower in both TDP-43^{WT} and TDP-43^{Q331K} cortex compared to the non-transgenic cortex (100±28% in non-transgenic vs 77.8±23.9 in TDP-43^{WT} vs 67±18.6% in TDP-43^{Q331K}, $p<0.01$). Expression of TDP-43 was significantly lower in both TDP-43^{WT} and TDP-43^{Q331K} spinal cord compared to the non-transgenic spinal cord (100±15.7% in non-transgenic vs 69.6±8.2% in TDP-43^{WT} vs 67.6±15.2% in TDP-43^{Q331K}, $p<0.0001$). Expression of TDP-43 was significantly higher in the TDP-43^{Q331K} hindlimb muscle compared to the TDP-43^{WT} hindlimb muscle (100±19.7% in TDP-43^{WT} vs 139±51.5% in TDP-43^{Q331K}, $p<0.05$).

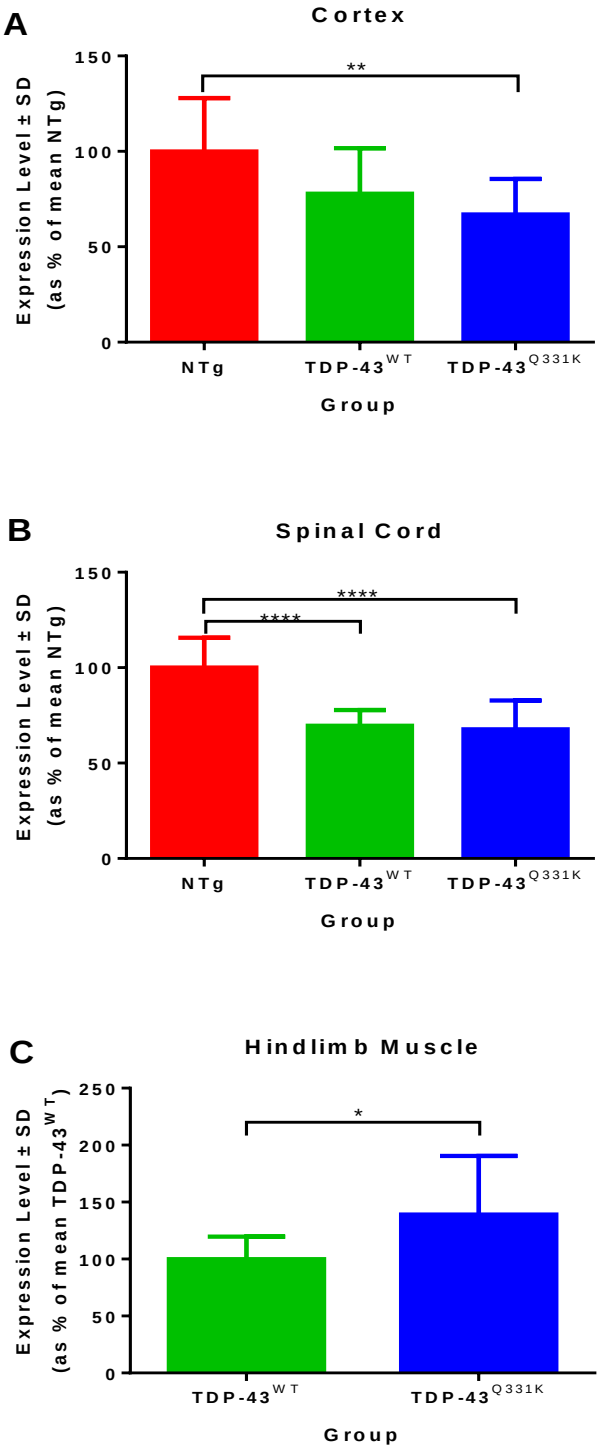

Figure 2. 19: Mouse (total) TDP-43 gene expression at 10 months of age.

*Gene expression as a percentage of the mean non-transgenic levels, measured in cDNA of cortex (A) and spinal cord (B) of non-transgenic, TDP-43^{WT} and TDP-43^{Q331K} mice (n=9-12). **<0.01, ****p<0.0001, one-way ANOVA. Gene expression as a percentage of the mean TDP-43^{WT} levels, as measured in cDNA of hindlimb muscles (C) of TDP-43^{WT} and TDP-43^{Q331K} mice (n=9-12). *p<0.05, student's t-test.*

2.4.13. TDP-43 Protein Quantification

Western blotting with an anti-TDP-43 antibody allowed for quantification of both human and mouse TDP-43 protein as separate bands due to the c-myc tag on the human protein increasing the molecular weight, as shown in *figure 2.20*. All samples used for protein quantification were the same as those used in *section 2.4.11* and *2.4.12* for protein expression quantification.

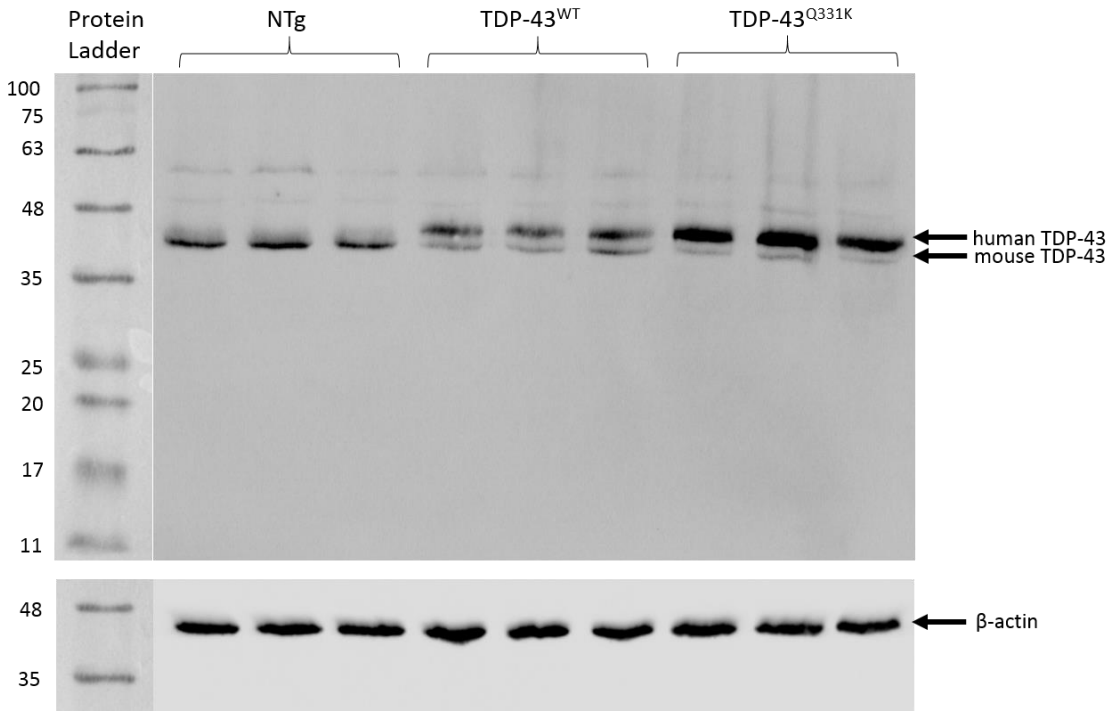

Figure 2. 20: Example of a Western blot for TDP-43.

The Western blot showed two separate bands for human (44.2kD) and mouse TDP-43 (43kD) between protein ladder markers for 35 and 48. This example shows non-transgenic, TDP-43^{WT} and TDP-43^{Q331K} 10m male cortex samples respectively (n=3).

As expected, Western blot analysis shows no human TDP-43 protein in the non-transgenic mice, and moderate levels in the TDP-43^{WT} mice (66.6±8.6% in cortex, 126.1±67.1 in cord), whilst levels in the TDP-43^{Q331K} mice were relatively high (151±23.1% in cortex, 213.9±154.1 in cord). Conversely, mouse TDP-43 was highest in the non-transgenic mice, reduced in the TDP-43^{WT} mice (47.5±16.2% in cortex, 65.5±16.3 in cord) and further reduced in the TDP-43^{Q331K} mice (13.6±2.3% in cortex, 70.7±29.6 in cord). Total TDP-43 levels are highest in the TDP-43^{Q331K} mice (164.6±23.1%

in cortex, 191.6±78.5 in cord), and moderate in the TDP-43^{WT} mice (114.1±22.8% in cortex, 284.5±173.3 in cord) (see *figure 2.21*).

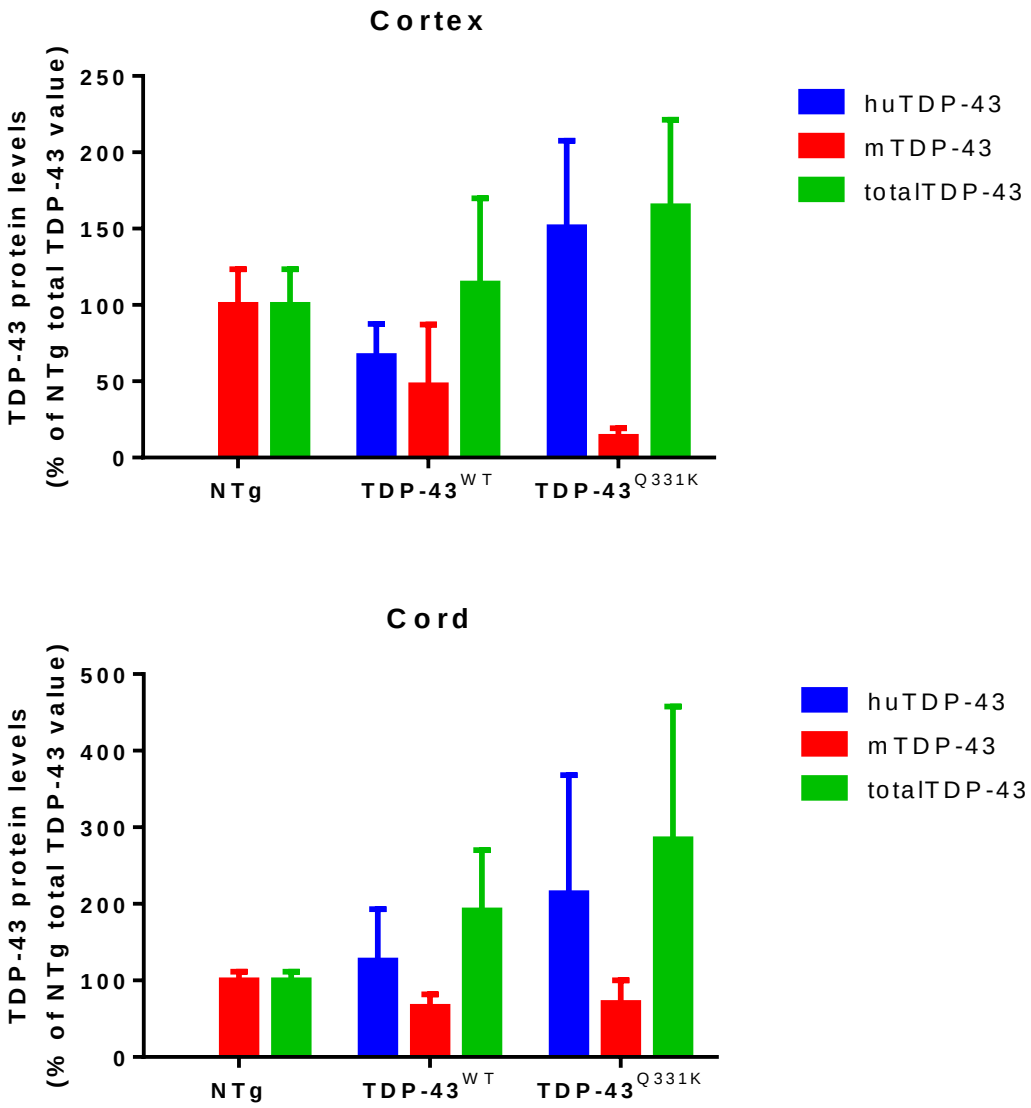

Figure 2. 21: Western blot quantification of TDP-43.

Relative human, mouse and total TDP-43 protein levels in 10m non-transgenic, TDP-43^{WT} and TDP-43^{Q331K} mice for cortex (A), and spinal cord (B), n=5-6. All samples are normalised to the non-transgenic total TDP-43 value for each Western blot. In all tissues, human TDP-43 is undetected in the non-transgenic mice, moderately detected in the TDP-43^{WT} mice and highly detected in the TDP-43^{Q331K} mice. Conversely, mouse TDP-43 is highest in the non-transgenic mice, moderate in the TDP-43^{WT} mice and low in the TDP-43^{Q331K} mice. Total TDP-43 levels are highest in the TDP-43^{Q331K} mice, and lowest in the non-transgenic.

2.4.14. Immunohistochemical Analysis of huTDP-43 Localisation

Lumbar spinal cord sections from 10 month old TDP-43^{WT} and TDP-43^{Q331K} mice show clear nuclear staining for c-myc-tagged huTDP-43 (green), representative of c-myc tagged huTDP-43 protein. C-myc-tagged huTDP-43 can also be seen in the cytoplasm of the motor neurons, which are identified by anti-NeuN staining and their large size and location (red) (*figure 2.22*). Image analysis enabled staining intensities (average grey level) of nuclear and cytoplasmic regions of motor neurons (large ventral horn neurons with size > 19.44μm²) to be determined.

Nuclear staining intensity of c-myc-tagged huTDP-43 was significantly higher (average grey level 10119±1285 in TDP-43^{WT} vs 14982±1985 in TDP-43^{Q331K}, student's t-test, $p<0.01$) in the lumbar cord motor neurons of the TDP-43^{Q331K} mice compared to the TDP-43^{WT} mice (*figure 2.23*). However, there was no significant difference between cytoplasmic staining intensity of c-myc-tagged huTDP-43 (5124±842.7 in TDP-43^{WT} vs 6102±638.9 in TDP-43^{Q331K}, student's t-test, $p>0.05$) in the lumbar cord of the TDP-43^{WT} and TDP-43^{Q331K} mice (*figure 2.23*). The ratio of nuclear/cytoplasmic staining intensity of c-myc-tagged huTDP-43 was significantly higher (1.99±0.13 in TDP-43^{WT} vs 2.479±0.24 in TDP-43^{Q331K}, student's t-test, $p<0.01$) in the lumbar spinal cord of TDP-43^{Q331K} mice compared to TDP-43^{WT} mice (*figure 2.23*).

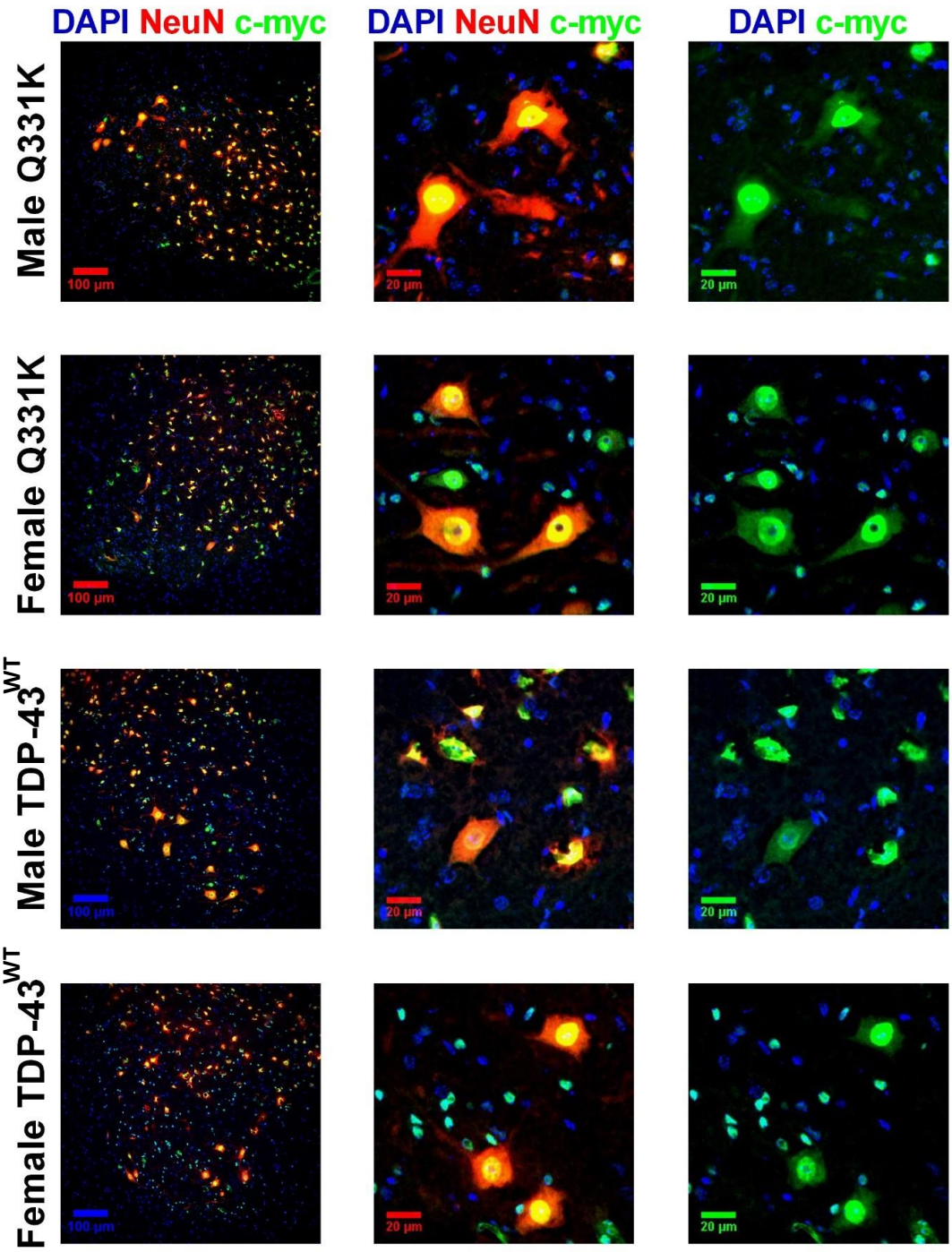

Figure 2. 22: Immunohistochemical staining of huTDP-43.

Staining of spinal cord ventral horn in 10m old mice. Nuclei are stained by DAPI in blue, motor neurons are stained by anti-NeuN in red, huTDP-43 is stained by anti-c-myc in green.

Quantification of c-myc in the nuclei and cytoplasm of spinal cord motor neurons shows the quantity of c-myc (and therefore huTDP-43) is higher in the nucleus of the motor

neurons of TDP-43^{Q331K} mice compared to the TDP-43^{WT} mice. The ratio of nuclear/cytoplasmic c-myc is also higher in the TDP-43^{Q331K} mice, suggestive of a higher proportion of c-myc in the nucleus and no cytoplasmic mislocalisation of huTDP-43 (*figure 2.23*).

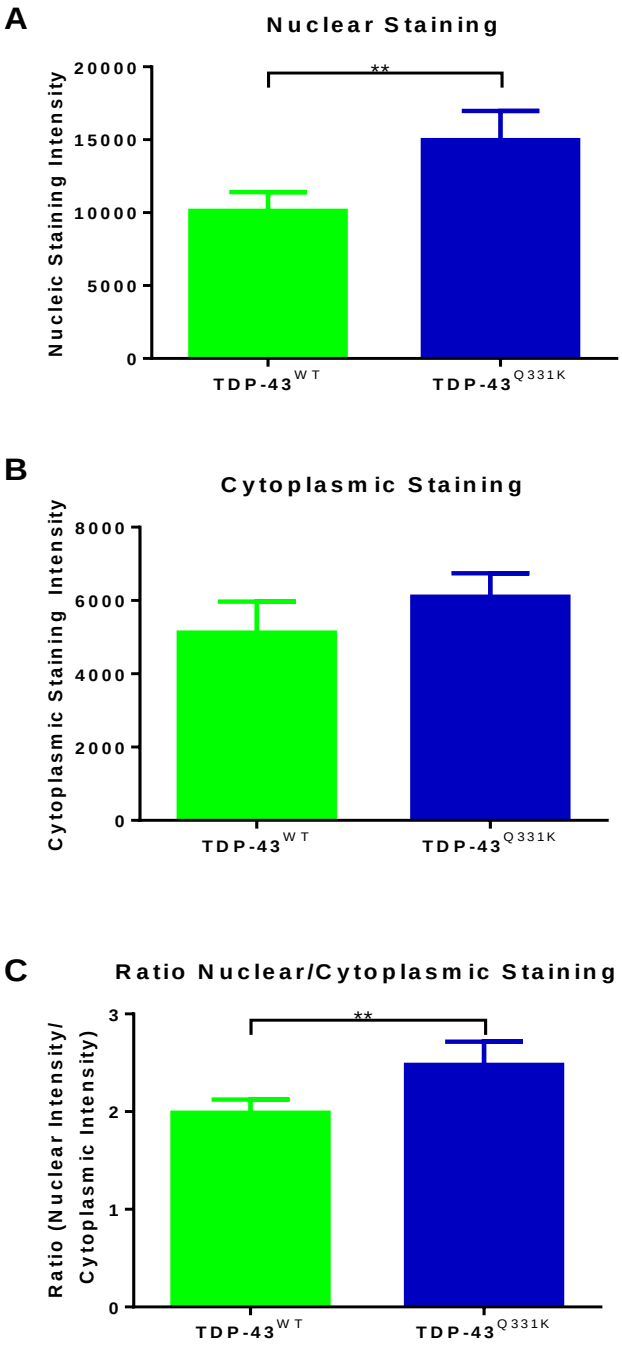

Figure 2. 23: Immunohistochemical staining localisation of huTDP-43.

*Quantification of the amount of huTDP-43 in the nuclei (A), cytoplasm (B) and nuclear/cytoplasmic ratio (C) of spinal cord motor neurons in 10m TDP-43^{WT} and TDP-43^{Q331K} mice (n=5-6). **p<0.01 vs all other groups.*

2.4.15. Immunohistochemical Analysis of Astrogliosis

Spinal cord sections from 10 month old mice were stained for GFAP immunoreactivity, for which higher staining levels (both area and intensity) are suggestive of astrogliosis. Immunohistochemical staining of GFAP showed a higher staining index of GFAP in the TDP-43^{Q331K} 10 month spinal cord, compared to the non-transgenic ($8.11x10^7 \pm 3.347x10^7$ in TDP-43^{Q331K} vs $5.356x10^7 \pm 2.827x10^7$ in non-transgenic), suggestive of astrogliosis.

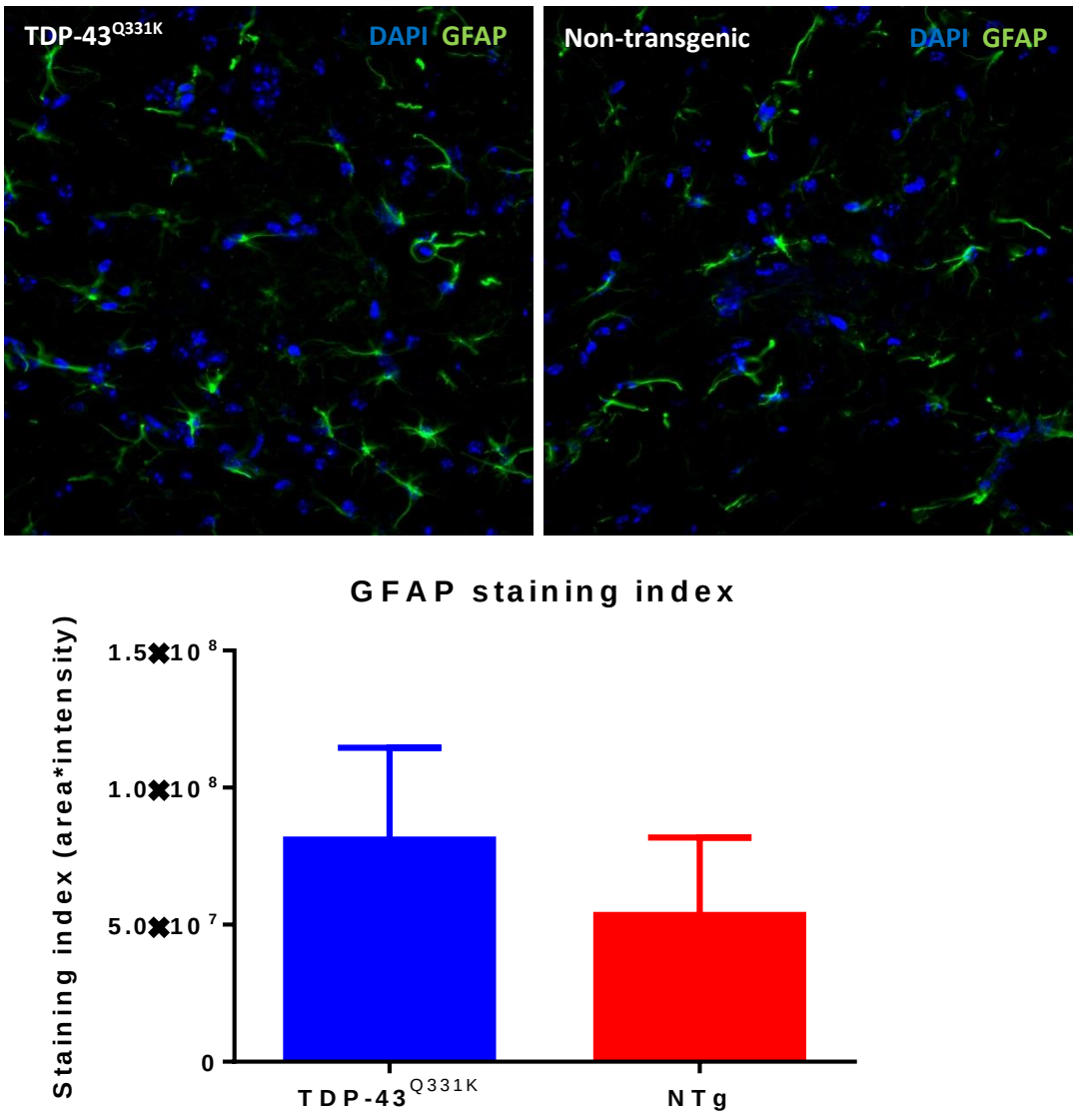

Figure 2. 24: GFAP staining and staining index.

Quantification of GFAP staining in the spinal cord of 10m TDP-43^{Q331K} and non-transgenic mice (n = 5). Non-significant on a student's t-test.

2.4.16. Immunohistochemical Analysis of Microgliosis

10 month spinal cord sections were stained for IBA-1 immunoreactivity, for which increased area of staining is suggestive of microgliosis (staining intensity is unaffected by microgliosis). Immunohistochemical staining of IBA-1 showed a significantly higher staining area of IBA-1 in the TDP-43^{Q331K} 10 month spinal cord, compared to the non-transgenic (2992±571µm^2 in TDP-43^{Q331K} vs 2213±474µm^2 in non-transgenic), suggestive of microgliosis.

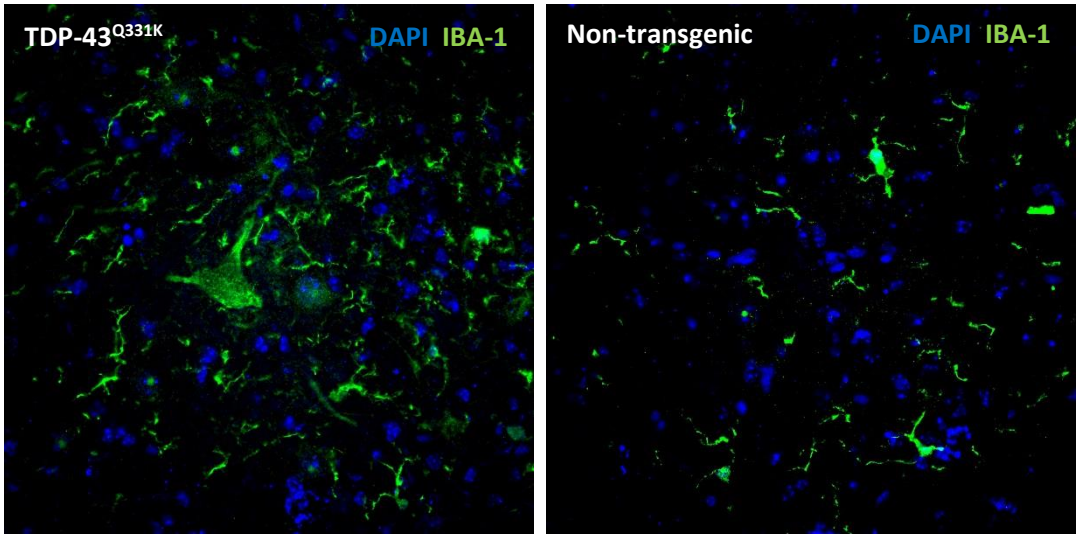

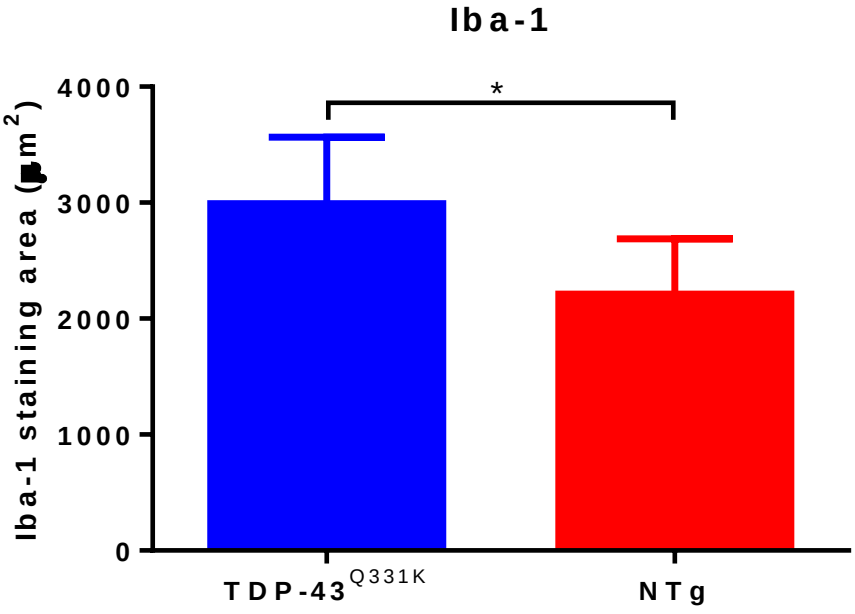

Figure 2. 25: IBA-1 staining and quantification of staining area.

*Quantification of IBA-1 staining in the spinal cord of 10m TDP-43^{Q331K} and non-transgenic mice (n = 5-6). *p<0.05 vs all other groups.*

2.5. Discussion

There is a clear need for additional mouse models of MND, not only for evaluation of potential therapeutic agents, but also to probe mechanisms of neurodegeneration. No therapies have translated to humans from the most commonly tested model, the SOD1^{G93A} mouse (Gurney et al., 1994), and no consistent effect of organic small molecule drugs have been found in this model (Ittner et al., 2015). Given the heterogeneity of MND in terms of both genotype and phenotype, trials of novel therapeutic agents would, ideally, be performed across several disease models. For the maximum efficiency of such studies, new models must be carefully characterised prior to integration into drug testing paradigms.

TDP-43 models may play an important role in testing therapeutics, given the almost ubiquitous nature of TDP-43 pathology in human MND (Gitcho et al., 2008, Mackenzie et al., 2007). Therefore, characterisation of this novel TDP-43^{Q331K} model is key in assessing its validity and reliability for therapeutic trials.

2.5.1. huTARDBP Sequencing and Copy Number

Sequence analysis found the TDP-43^{Q331K} transgene to have an adenine to cytosine nucleotide mutation, causing a glutamine to lysine amino acid change at position 331 of the human *TARDBP* gene, confirming the Q331K mutation, which was not found in the TDP-43^{WT} mice. The TDP-43^{Q331K} mice therefore carry a mutation which has previously been identified in an MND patient (Sreedharan et al., 2008).

TARDBP copy number analysis showed that although TDP-43^{WT} mice appear to consistently have just one copy of the human *TARDBP* gene, the TDP-43^{Q331K} mice potentially vary in copy number. Gene copy number has been directly correlated with disease severity in the SOD1^{G93A} mouse model (Alexander et al., 2004). However, as the subsequent data shows, there is low variance in the measured parameters in the present study. Plotting of the rotarod performance of each of the TDP-43^{Q331K} mice with a known copy number variation showed no obvious differences in rotarod performance between those mice with a low copy number and those with a high copy number. It is also worth bearing in mind that the variability seen may be due to technical issues with sample preparation or digital PCR itself. Digital PCR is very sensitive to small changes in copy number and for some samples a precise copy number estimation could not be

determined. It would appear that in general the TDP-43^{Q331K} mice have more copies and this allows for greater variation in copy number estimation, whereas TDP-43^{WT} have a single copy and so estimation of copy number is more precise. Despite this, digital PCR is more reliable than previous methods (qPCR) (Whale et al., 2012), which have been used and which in general, only identify large changes in copy number.

A comparison of mean TDP-43^{Q331K} rotarod performance and the rotarod performance of mice with an estimated copy number of one shows a slightly increased performance in the low copy number mice. However, as copy number was not estimated for all mice on the study, it is possible that there are other low copy number mice in the mean data.

It can therefore be concluded that in this model, copy number variation may have a slight impact on motor phenotype, but this requires further investigation and monitoring.

2.5.2. Variability of Parameters

As shown in *table 2.3*, the coefficient of variation (the standard deviation as a percentage of the mean) was relatively low for all the parameters measured, providing reassurance that the model has low phenotypic variability. The data shown in the table were for females, as they had a lower variance than the males and any therapeutic trials will therefore use females only, in order to reduce the number of mice required per group.

Power analysis suggests group sizes of 14 would be sufficient to detect a 10% difference in neuroscores, weight, rotarod and a 15% difference in hindlimb base of support on the catwalk. This would be an ideal group size for therapeutic trials as it would allow for a therapeutic effect size of 15% to be detected using the described parameters. This group size of 14 is relatively low compared to the suggested group size for SOD1^{G93A} mice of 24 animals per group (Scott et al., 2008).

2.5.3. The Effect of huTARDBP Copy Number on Phenotype

TDP-43^{WT} mice showed no significant differences in neuroscores, weight, rotarod performance or catwalk gait analysis when compared to the non-transgenic mice. It

would appear that for these parameters, carrying a huTARDBP had no effect on motor phenotype.

The TDP-43^{WT} mice are therefore an ideal control line and the findings in TDP-43^{Q331K} mice are specific to the mutation, rather than due to the expression of huTARDBP.

2.5.4. Disease Severity and Onset

As found previously (Arnold et al., 2013), the disease phenotype in the TDP-43^{Q331K} mice is mild. There were no signs of distress in the animals and no mice reached a humane endpoint, as defined within our Home Office License. Differences in phenotype are evident by 6 months in all the parameters measured, and rate of progression is slow beyond 6 months of age.

A significant tremor is detectable by 10 weeks of age in the TDP-43^{Q331K} mice, as was found previously at 3 months of age (Arnold et al., 2013), and a significant reduction in rotarod performance can be detected by 12 weeks of age. This indicates that onset of visible signs of disease in the TDP-43^{Q331K} mice is around 10-12 weeks of age.

2.5.5. Weight

Unexpectedly the TDP-43^{Q331K} mice became overweight with age, as reflected in the weight data. Dissection of the mice for tissue confirmed that the weight gain was due to increased white fat, particularly in the abdominal area. This was not reported previously but has been found in another TDP-43 mouse model carrying an A315T mutation (Stallings et al., 2013). Conversely, knockout of TDP-43 in another mouse model found that a lack of fat deposition led to early death (Chiang et al., 2010). Both studies related fat metabolism to expression of the gene TBC1D1, which was tightly coupled with TDP-43 levels. This weight gain will therefore be a focus of further study, as reported in chapter 3.

2.5.6. Rotarod Deficit vs Weight

It is possible that rotarod findings are partially influenced by the weight of the mice, as a study in 3xTg-AD mice found a correlation between increased weight and decreased

rotarod performance (Stover et al., 2015). However, clinical signs of disease including tremor and muscular atrophy are already present at the onset of rotarod decline in TDP-43^{Q331K} mice and a significant difference was found in rotarod performance before a significant difference in weight became evident (compare *figures 2.4 and 2.5*).

When weight is taken into account by plotting rotarod performance/weight , the decline in performance is still evident in the TDP-43^{Q331K} mice compared to the other groups, suggesting that the decline in rotarod performance is indicative of motor dysfunction, despite the influence of weight.

2.5.7. Correlation of Neuroscore with Other Measures

Decreased rotarod performance is evident in both male and female TDP-43^{Q331K} mice by 10 weeks of age and many differences are found in catwalk gait analysis at both 3 and 6 months of age. However, differences in neuroscores did not become apparent until 27 weeks (post the 3 and 6 month time points), suggesting that neuroscoring is not sensitive to onset of disease, as measured by motor function. This is also seen in the $SOD1^{G93A}$ model where a significant rotarod deficit is obvious before the onset of visible signs of disease (Mead et al., 2011), and running wheel performance declines before symptom onset (Bruestle et al., 2009). Indeed, it is often noted by MND patients that they felt different long before onset of their first clinical sign of MND. A classic example of this is Lou Gehrig, the famous American baseball player, whose home-run average declined dramatically before symptom onset and diagnosis of MND (Kasarskis and Winslow, 1989).

Previously published work found significant hindlimb clasping in the TDP-43^{Q331K} mice from 3 months of age (Arnold et al., 2013) and initially hindlimb clasping was measured in this study. However, hindlimb clasping was highly variable within each mouse, so it was deemed unreliable in this model and measurement was stopped.

It must be considered that at the time of neuroscoring in this study, a model-specific neuroscoring protocol had not been developed and therefore, a more specific neuroscoring protocol was subsequently developed for future studies (see chapter 4).

2.5.8. Catwalk Gait Analysis

Gait analysis has been used to detect early signs of disease in the SOD1^{G93A} mouse model, consistently finding increased stand time in the SOD1^{G93A} mice compared to controls (Wooley et al., 2005, Mead et al., 2011), increased base of support (BOS) (Mancuso et al., 2011a, Guillot et al., 2008), and decreased stride length (Mead et al., 2011, Wooley et al., 2005), to the extent of being used as a therapeutic trial readout (Lee et al., 2013, Sun et al., 2014).

2.5.8.1. Differences in Forelimb Gait

Forelimb paw intensity shows a tendency to increase in all groups of males at 10 months of age, possibly due to the increase in weight of all males. This increase is more exaggerated in the TDP-43^{Q331K} females, possibly due to the larger difference in weight between the TDP-43^{Q331K} and other groups. However, weight is significantly increased in TDP-43^{Q331K} males and females by 10 weeks of age, yet no difference in forelimb intensity is found at 3 or 6 months of age. Therefore, although weight may be a contributing factor, it is possible that the forelimb intensity is affected by the unsteadiness of the mice and greater reliance on forepaws.

No differences were found with age, group or gender in forelimb print length, which is to be expected as the size of the paws would not be expected to change post maturity.

Forelimb stride length showed no differences in males with age or group. However, in females, the stride length appeared to increase slightly in the TDP-43^{WT} and non-transgenic groups, whilst reducing slightly in the TDP-43^{Q331K} mice (no findings were significant), as found in SOD1^{G93A} mice (Mead et al., 2011). The forelimbs of SOD1^{G93A} mice tend to be relatively unaffected, whereas there is potentially an effect in the forelimbs of the TDP-43^{Q331K} mice. The reason for an increase in stride length of the TDP-43^{WT} and non-transgenic mice is unknown. It is possible that the decrease in stride length of the TDP-43^{Q331K} mice is due to weakness of the forelimbs, limiting the amount of lift given to each paw, and therefore the amount of distance covered.

An increase in duty cycle may represent a decreased ability to initiate movement of the limb off the ground, as found in TDP-43^{Q331K} males at 10 months of age, and TDP-43^{Q331K} females at 6 and 10 months of age. A decrease in duty cycle of all groups was found in

females at 6 months of age, possibly due to an increased swing time, affectively decreasing the proportion of time spent with the paws on the surface and in turn, decreasing the duty cycle.

Forelimb swing time is increased in the TDP-43^{Q331K} male and female mice at 3, 6 and 10 months. This is suggestive of a generalised slowing of movement, likely due to weakness of the forelimbs. Forelimb swing time shows a slight increase in all groups at 6 months compared to all other time points. The reason for this is unknown.

Forelimb BOS increases in all groups with age in both males and females, possibly due to an increase in size of the mice with age, increasing the distance between the paws. Forelimb BOS is significantly higher in the female TDP-43^{Q331K} mice at 10 months of age. In the forepaws, a swimming gait was not observed and cannot therefore explain this finding. It is possible that an increased weight has caused a wider stance. However, this is not evident at 6 months of age, despite a significantly increased weight at this timepoint.

2.5.8.2. Differences in Hindlimb Gait

Hindlimb paw intensity shows a decrease in all groups of both males and females at 6 months of age for an unknown reason. Hindlimb intensity is significantly lower in the TDP-43^{Q331K} mice compared to all other groups at 10 months of age, suggesting that less weight is being placed on the hind paws, despite an increase in the weight of the animal. This is consistent with a slight increase in forelimb paw intensity at 10 months of age, suggesting that the mice are placing more weight on to the forelimbs, possibly because the hindlimbs are weaker than the forelimbs, increasing reliance on forelimb strength. However, this finding is not seen in female mice, despite an increase in forelimb intensity.

Hindlimb print length showed no differences with age, group or sex, other than an increase in the TDP-43^{Q331K} females at 10 months of age, the reason for which is unknown as it is not expected that paw size would change post maturity.

Hindlimb stride length showed no differences in males with age or group. However, in females, the stride length appeared to increase slightly in the TDP-43^{WT} and non-transgenic groups, whilst reducing slightly in the TDP-43^{Q331K} mice. As with the forelimb

findings, this is in keeping with findings in SOD1^{G93A} mice (Mead et al., 2011). The reason for an increase in stride length of the TDP-43^{WT} and non-transgenic mice is unknown. It is possible that the decrease in stride length of the TDP-43^{Q331K} mice is due to weakness of the hindlimbs, limiting the amount of lift given to each paw, and therefore the amount of distance covered.

Hindlimb duty cycle expresses the hindlimb stance time as a percentage of the step cycle duration and is as such representative of the amount of time a paw remains on the surface within each stride. A decreased duty cycle was found in TDP-43^{Q331K} males at 3 months of age, the reason for which is unknown. An increase in duty cycle may represent a decreased ability to initiate movement of the limb off the ground, as found in both TDP-43^{Q331K} males at 10 months of age, and females at 6 and 10 months of age. A decrease in duty cycle of all groups was found in females at 6 months of age, possibly due to an increased swing time, effectively decreasing the percentage of duty cycle.

Hindlimb swing time is increased in the TDP-43^{Q331K} male and female mice at 6 and 10 months of age. This is suggestive of a generalised slowing of movement, likely due to weakness of the muscles, as found in the forelimbs.

Hindlimb BOS increases in all groups with age in both males and females, possibly due to an increase in size of the mice, increasing the distance between the hindpaws. At 6 and 10 months the TDP-43^{Q331K} male and female mice show a larger hindlimb BOS compared to other groups, likely due to their increased weight, which is mainly evident in the lower torso, resulting in an increased distance between the hindlimbs. The waddling gait of the mice will also increase the distance between hindpaw placements, increasing hindlimb BOS further.

2.5.8.3. Differences in Overall Gait Pattern and Duration

Walking duration, indicative of walking speed, remains similar with age in the TDP-43^{WT} and non-transgenic mice. However, in the TDP-43^{Q331K} mice, walking duration increases with age in both males and females, indicating a slowing down of the mice, consistent with the decrease in swing time. This general slowing in walking pace is suggestive of limb weakness and/or a lack of motivation to move.

Ordinarily, mice will spend most of their time walking in a diagonal stepping pattern, meaning they will step with the left forepaw whilst stepping with the right hindpaw; then step with the right forepaw whilst stepping with the left hindpaw. When a mouse becomes less stable, they may become more reliant on a three paw stepping pattern, spending more time with three paws on the ground. A tendency towards three paw stepping was found in both male and female TDP-43^{Q331K} mice. A decrease in diagonal stepping coincided with an increase in three paw stepping in males at 6 and 10 months, and in females at 10 months of age.

These results indicate that the TDP-43^{Q331K} mice become slower and more unsteady with age.

2.5.9. Litter Statistics

No records could be found for litter size, percentage of transgenic pups and percentage of male pups for the C57BL/6NJ genetic background or for the TDP-43^{Q331K} mouse model. Our own data in SOD1^{G93A} mice indicates a reduction in the percentage of transgenic pups from the expected 50% to approximately 40%.

The TDP-43^{WT} colony have an average litter size of 6 with 50% of pups being transgenic and 48% of pups being male. The TDP-43^{Q331K} colony have an average litter size of 7 with 48% of pups being transgenic and 53% of pups being male. This suggests that there is no particular biological preference specific to gender or genotype. The reason for an increased litter size in the TDP-43^{Q331K} colony is unknown, but may be due to bias in the original breeding trios, which has subsequently been inherited by the following generations.

2.5.10. huTARDBP Gene Expression

Previously published data described the huTARDBP expression levels in TDP-43^{Q331K} mice as being 1-1.5 fold compared to the levels of endogenous expression in non-transgenic mice (Arnold et al., 2013). The non-transgenic mice do not carry any huTDP-43 so ideally, total levels of TDP-43 (both human and mouse) would be compared. However, primer pairs with an equal affinity for both human and mouse TDP-43 could not be

designed (see *section 3.5.11*. below). Hence, huTDP-43 expression was compared between the TDP-43^{WT} and TDP-43^{Q331K} mice.

The huTDP-43 gene is expressed under a murine prion promotor, which is primarily expressed in the CNS, hence huTDP-43 expression levels were measured in the cortex and spinal cord. Expression levels were also measured in the hindlimb muscle, as this is a potential target tissue for the induction of pathology by the TDP-43^{Q331K} mutation.

In comparison to the TDP-43^{WT} tissue, expression of huTDP-43 in the TDP-43^{Q331K} mice was found to be approximately 2-fold in the spinal cord, 3-fold in the cortex, and 4-fold in the hindlimb muscles. It seems that there is a significantly increased expression of huTDP-43 in the TDP-43^{Q331K} mice as compared to the TDP-43^{WT} mice, which may translate to an increased protein level which could lead to toxicity independent of mutation status.

It is surprising that the highest expression was found in the hindlimb muscle, despite the murine prion promotor being primarily expressed in the CNS (Arnold et al., 2013), and the previously published data suggested that levels of huTDP-43 were relatively low in muscle (Arnold et al., 2013). The reason for the difference in these findings is unclear.

2.5.11. Total (mouse + human) TDP-43 Gene Expression

Due to the self-regulatory nature of the *TARDBP* gene, the presence of huTDP-43 may result in a decrease in endogenous TDP-43 (Ayala et al., 2011). In the previously published data, total TDP-43 mRNA and protein levels in the spinal cord were found to be approximately 2-fold in the TDP-43^{WT} and 3-fold in the TDP-43^{Q331K} mice, when compared to endogenous levels in the non-transgenic (Arnold et al., 2013). It was then expected that the total TDP-43 cDNA would be highest in the TDP-43^{Q331K} mice, and lowest in the non-transgenic mice. However, the total TDP-43 cDNA was shown to be highest in the non-transgenic mice.

In-house data showed that the TDP-43 primers used were complimentary to human and mouse TDP-43, with R-squared values of 0.98 and 0.97 respectively when tested against a human or mouse cDNA template dilution in a qPCR reaction to test specificity. However, upon closer inspection of the sequences, the primer pair has 3 mismatches with the human cDNA sequence, whereas they are fully complimentary to the mouse

cDNA sequence (see *table 2.5*). It is assumed that the primers may preferentially bind to mouse TDP-43 when both mouse and human TDP-43 are present. The data therefore, are mostly representative of endogenous mouse TDP-43 expression but it cannot be assumed that the data is solely representative of mouse TDP-43 expression alone. The specificity of these primers must be checked before a conclusion is drawn.

Table 2. 6: Primer sequences vs complimentary cDNA. *Mismatches between the primers and huTDP-43 are highlighted in blue.*

	Forward primer sequence/ complimentary cDNA sequence	**(Reverse primer sequence)/ complimentary cDNA sequence**
Mouse cDNA	TACCGGAATCCCGTGTCTCA	TGGATGAGACAGATGCTTCCTC
Human cDNA	TACAGGAATCCAGTGTCTCA	TGGATGAGACAGATGCTTCATC
Primer pair	TACCGGAATCCCGTGTCTCA	(GAGGAAGCATCTGTCTCATCCA) TGGATGAGACAGATGCTTCCTC

2.5.12. TDP-43 Protein Levels

In both cord and cortex, total TDP-43 levels were highest in the TDP-43^{Q331K} mice at approximately 1.5-3 fold that of non-transgenic mice, and TDP-43^{WT} mice had 1.1-1.9-fold that of non-transgenic mice, similar to levels found in a previous study of the mice on a different genetic background (Arnold et al., 2013). As found in the gene expression data, endogenous mouse TDP-43 levels decreased as human TDP-43 protein levels increased, due to the self-regulatory nature of TDP-43 (Ayala et al., 2011).

Protein levels of human TDP-43 were found to be 1.5-2.1-fold that of the non-transgenic in TDP-43^{Q331K} mice, considerably more than the 1-1.5-fold increase found previously (Arnold et al., 2013).

Overall, protein levels were in keeping with the data recorded for gene expression, and showed similar results to those published previously. The TDP-43^{WT} mice do carry a slight overexpression of TDP-43, and the TDP-43^{Q331K} mice more so but the levels recorded are not excessively high compared to many other TDP-43 mouse models (see *table 1.4*).

It must be considered that the TDP-43 antibody affinity to mouse and human TDP-43 was assumed to be equal. It is important to check the antibody affinity if further study of protein levels are carried out.

2.5.13. Immunohistochemical Analysis

Unfortunately the quality of tissue used in this analysis was poor, which reduced the number of spinal cords which could be used for analysis. Future tissue collection will use different methods of tissue collection for better quality of immunostaining.

2.5.13.1. Immunohistochemical Analysis of huTDP-43 Localisation

Localisation of huTDP-43 was carried out using immunohistochemical staining of the c-myc tag. Previous investigations of TDP-43^{Q331K} mice on a C57BL/6NCrl background found small cytoplasmic inclusions of TDP-43 in the lumbar spinal cord but no evidence of nuclear clearing (Arnold et al., 2013). Another study, in which the TDP-43^{Q331K} mice were crossed with TDP-43^{WT} mice found cytoplasmic mislocalisation of TDP-43, alongside cytoplasmic inclusions in the TDP-43$^{Q331K/WT}$ spinal cord (Mitchell et al., 2015). Interestingly this study suggested that nuclear clearance of TDP-43 may accelerate disease, but is not a necessary feature, seeing as the TDP-43^{Q331K} mice have no nuclear clearance of TDP-43 and a slow progression of disease; whereas the TDP-43$^{Q331K/WT}$ mice had nuclear clearance of TDP-43 and a rapid disease progression.

Increased cytoplasmic huTDP-43 was not found in this study in the TDP-43^{Q331K} mice compared to the TDP-43^{WT} mice at 10 months of age. Increased nuclear huTDP-43 was reported in the TDP-43^{Q331K} mice compared to the TDP-43^{WT} mice, which has not been described previously. This confirms that nuclear clearance of TDP-43 is not critical for a neurodegenerative phenotype, although found in several other TDP-43 mouse models (Wegorzewska et al., 2009, Xu et al., 2010, Wils et al., 2010, Igaz et al., 2011).

It must be noted that in this study quantification of TDP-43 was the aim of this immunohistochemical investigation and no search was carried out for cytoplasmic inclusions of TDP-43. There may therefore have been inclusions in the tissue, as found previously (Arnold et al., 2013), and in most other mouse models of TDP-43 (see *table*

1.4 for details) (Tsai et al., 2010, Stallings et al., 2010, Xu et al., 2010, Wils et al., 2010, Shan et al., 2010, Swarup et al., 2011, Igaz et al., 2011, Xu et al., 2011, Wu et al., 2012b).

2.5.13.2. Immunohistochemical Analysis of GFAP

GFAP has long been used as a marker of astrocytes, which increases in reactivity with astrogliosis (Eng and Ghirnikar, 1994), as found in other models of MND (Ferraiuolo et al., 2011, Yamanaka et al., 2008a) and most TDP-43 mouse models (see *table 1.4* for more details) (Wegorzewska et al., 2009, Tsai et al., 2010, Stallings et al., 2010, Xu et al., 2010, Wils et al., 2010, Swarup et al., 2011, Igaz et al., 2011, Xu et al., 2011, Wu et al., 2012b). Therefore, immunohistochemical GFAP quantification requires a measurement of intensity and area of staining, for which a staining index was used.

GFAP immunoreactivity was found to be non-significantly higher in the ventral horn of 10 month TDP-43^{Q331K} mice compared to non-transgenic mice, as found in the spinal cord of young TDP-43^{Q331K} mice on a C57BL/6NCrl background (Arnold et al., 2013). It is therefore likely that astrogliosis may be evident from an early stage in the TDP-43^{Q331K} mice.

2.5.13.3. Immunohistochemical Analysis of IBA-1

IBA-1 is recognised as a marker of microglia (Ahmed et al., 2007), and microgliosis is evident in several models of MND (Boillee et al., 2006), including a TDP-43 mouse model (Swarup et al., 2011). The intensity of IBA-1 immunoreactivity does not increase with microgliosis. The area of IBA-1 immunoreactivity was measured and found to be higher in the spinal cord of 10 month old TDP-43^{Q331K} mice compared to non-transgenic mice, suggestive of microgliosis.

These findings are consistent with those of young TDP-43^{Q331K} mice on a C57BL/6NCrl background (Arnold et al., 2013), indicating likelihood that microgliosis is present from an early stage of disease in the TDP-43^{Q331K} mice.

2.6. Conclusion

In conclusion, this study showed that the TDP-43^{Q331K} mice have a progressive mild motor phenotype in both the forelimbs and hindlimbs, with low variability, especially in female mice. There appears to be no significant difference between the motor phenotype of TDP-43^{WT} and non-transgenic mice, suggesting the presence of huTARDBP is not responsible for the motor phenotype found in TDP-43^{Q331K} mice.

Expression of huTDP-43 cDNA is increased in TDP-43^{Q331K} cortex, spinal cord and muscle, and this is correlated with TDP-43 protein levels.

Astrogliosis and microgliosis is evident in the spinal cords of TDP-43^{Q331K} mice by 10 months of age along with increased nucleic TDP-43 levels, but there is no discernible cytoplasmic mislocalisation.

3. Running Wheel Activity and Food Intake

3.1. Introduction

Although unreported in previous papers, the initial characterisation study in these mice found a striking weight gain in the TDP-43^{Q331K} mice compared to the TDP-43^{WT} and non-transgenic mice (see chapter 2).

Previously, the level of huTARDBP protein in TDP-43^{Q331K} mice has been described as being slightly higher than the endogenous expression, with similar levels of total TDP-43 as the control line TDP-43^{WT} (Arnold et al., 2013). A link between *TARDBP* and fat metabolism has been identified in previous studies, which have reported that a conditional knockout of *TARDBP* in mice causes a lethal decrease in fat metabolism due to downregulation of TBC1 domain family member 1 (TBC1D1) (Chiang et al., 2010). Conversely, another mouse model which showed an overexpression of TARDBP with an A315T mutation had increased fat deposition, correlated with increased TBC1D1 expression, increased food intake (although the increase was relative to body weight), and decreased activity levels (Stallings et al., 2013).

TBC1D1 is an obesity candidate gene (Taylor et al., 2008, Stone et al., 2006) involved in regulating the translocation of the glucose transporter type 4 (GLUT4) (Sakamoto and Holman, 2008, Taylor et al., 2008). Expression of TBC1D1 is predominantly in muscle (Chadt et al., 2008, Taylor et al., 2008) and its activity is increased in the presence of insulin and muscle contraction (An et al., 2010, Taylor et al., 2008, Sakamoto and Holman, 2008).

It appears to be well established that knockout of TBC1D1 increases fatty acid uptake and oxidation, causing weight loss (Chadt et al., 2008, Chiang et al., 2010); whereas overexpression decreases fatty acid uptake and oxidation, causing weight gain (Chadt et al., 2008, Stallings et al., 2013). Therefore, as expression of TBC1D1 appears to be linked with TDP-43 expression (Stallings et al., 2013), an investigation of TBC1D1 gene expression, food intake and activity levels in the TDP-43^{Q331K} mouse model could provide insights into the mechanisms causing increased weight.

Motor function tests such as rotarod provide an indication of forced activity capabilities. However, voluntary activity provides an indicator of the more natural, habitual activity levels of the mice. An ideal way to investigate this is by using home cage running wheels,

which the mice can use at their will (De Bono et al., 2006). An increase in activity levels due to running wheel access may decrease weight in the mice (Bennett et al., 2014), especially in males (De Bono et al., 2006). However, not all studies have found a difference in weight between mice that have access to wheels and those that do not (Allen et al., 2001).

Earlier studies of running wheel activity in C57BL/6 mice have shown that the mice will run considerable distances, almost exclusively during the night (Lapvetelainen et al., 1997). Mice usually run in short bouts, and have a tendency to maintain a regular cruising speed (De Bono et al., 2006). In one study, female mice ran consistently throughout the night and ran on average 40% further than male mice, whilst male mice ran mostly during the first half of the night. However, running activity was more varied in female mice, possibly due to the oestrous cycle (De Bono et al., 2006), as supported by in-house data for specific strains.

A running wheel study in SOD1^{G93A} mice showed low variability and a reliable decline in running time and distance with disease progression, consistent with a decline in rotarod performance (Bennett et al., 2014). Previous studies have consistently shown a steady increase in running time and distance at the beginning of a running wheel study, suggestive of a training period (Bennett et al., 2014, De Bono et al., 2006, Allen et al., 2001). However, it must be considered that the mouse model under investigation here is on a different genetic background to the mice used in previous running wheel studies and the mouse strain may have a large impact on voluntary running activity (Massett and Berk, 2005, Turner et al., 2005).

It is expected that running wheel activity in the TDP-43^{Q331K} and TDP-43^{WT} mice will increase with time at the beginning of the study, with females showing higher levels of activity compared to males. Running activity and evaluation of food intake may provide an indicator of the mechanisms involved in the increased weight of TDP-43^{Q331K} mice compared to their counterparts.

3.2. Aims

1. To assess activity levels of male and female TDP-43^{Q331K} mice in comparison to TDP-43^{WT} mice.

2. To assess the food intake of male and female TDP-43^{Q331K} mice in comparison to TDP-43^{WT} mice.

3. To assess TBC1D1 expression in the cortex, spinal cord and muscle of TDP-43^{WT} and TDP-43^{Q331K} mice.

3.3. Materials and methods

3.3.1. Ethics Statement

All mouse experiments were carried out under the terms of the UK Animals (Scientific Procedures) Act 1986 and under a UK Home Office project license. Mice were housed and cared for in accordance with the Home Office Code of Practice for Housing and Care of Animals Used in Scientific Procedures. All procedures were carried out under under an appropriate UK Project Licence by personal licence holders. ARRIVE guidelines (Kilkenny et al., 2010) were adhered to during this report.

3.3.2. Transgenic C57BL/6NJ Mice

TDP-43^{WT} and TDP-43^{Q331K} mice *(Mus musculus)* were originally generated on a C57BL/6NCrl background by insertion of c-myc-tagged human *TARDBP* (Arnold et al., 2013) and were subsequently backcrossed on to a C57BL/6NJ background before being deposited at the Jackson Laboratory (stock numbers 017907 and 017933, respectively).

The running wheel study was carried out with 6 males and 6 females per group (TDP-43^{WT} and TDP-43^{Q331K}). Mice were recruited at 30 days of age and remained under evaluation until 300 days of age.

For genotyping methods see section 2.3.4.

3.3.3. Housing

Mice were bred in a SPF environment, and transferred to a conventional facility for the studies described here. The facility uses a 12 h light/dark cycle, and room temperature is set to 21˚C. Cages (L36 x W21 x H18.5cm) were lined with fine sawdust (eco-pure flakes 6, Datesand, UK), which was changed every 2 weeks, a plastic house was placed in each cage and paper wool (Datesand, UK) was used as bedding material.

Each cage contained a 37.8cm circumference Fast Trac running wheel (LBS Biotech, UK) mounted at 25˚ below horizontal on a 4cm fixed post. The wheel was placed in the corner of each cage where the circumference was 5-10mm from the edge of two perpendicular sides of the cage. A 5 x 10mm neodymium magnet was glued to the underside of each Fast Trac wheel and a bicycle computer (Cateye Velo, Japan) with reed switch was fixed to the side of the cage (see *figure 3.1*). Time spent running, distance run and average running speed were recorded daily. This set up was based on the in-house protocol used in a previous study (Bennett et al., 2014).

All mice were housed separately due to the use of running wheels in the home cage. Mice were fed 2018 rodent diet (Harlan, UK) ad libitum. Water was provided ad libitum and changed weekly. Fresh bottles were provided every four weeks.

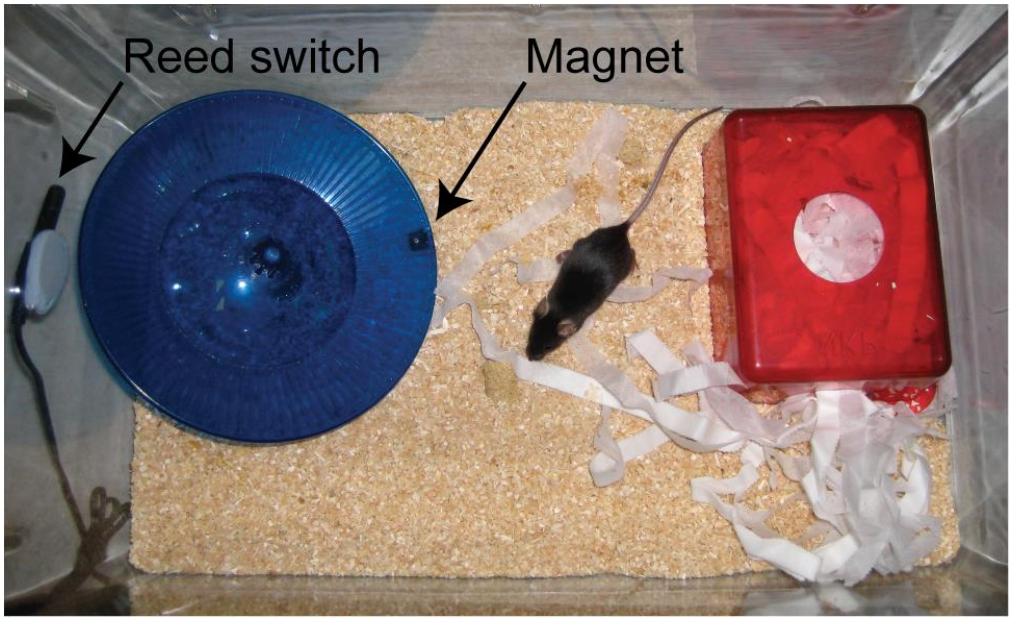

Figure 3. 1: Running wheel cage set-up (Bennett et al., 2014).

The Fast Trac running wheel is fixed in the corner of the cage, with a magnet attached to the underside, detected by a reed switch on the side of the cage which is connected to a cycle computer.

3.3.4. Weight and Food Intake Monitoring

Weight was monitored weekly by placing the mice in a box on a set of scales (Kern, Germany) pre-set to zero. Food intake was monitored fortnightly by weighing the food on a set of scales (Kern, Germany), and re-weighing the food approximately 72 hours later. During the 72 hour period, the sawdust in the cage was replaced with paper towelling, to ensure that any small pieces of food which may have dropped from the top of the hopper could be included for weighing.

3.3.5. Tissue Collection

Mice were sacrificed at 10 months of age by overdose using an intraperitoneal injection of pentobarbitone (2.5ml/kg) and exsanguination via cardiac puncture using a 25 gauge 0.5 x 16mm needle (BD Microlance, Ireland) and a 1ml syringe (Terumo Europe, Belgium,) after cessation of the pedal reflex. The head was decapitated and the brain removed and placed on a plastic square, wrapped in wet paper towel. The blunt edge of a steel back industrial single edge blade (Fisher Scientific, UK) was used to peel off the cortex from the remaining brain. An incision was made over the spine at the level of the hips and PBS was pushed in to the spinal cavity using a 20ml syringe (BD Plastipak, UK) fixed with a pipette tip (Fisherbrand, UK), ejecting the spinal cord from the rostral end of the spinal column.

Triceps surae muscles were removed by dissection. Cortex, spinal cord and muscles were immediately snap frozen in liquid nitrogen and then stored at -80˚C. Cortex and spinal cord from non-transgenic mice had been prepared using these methods from a previous cohort. Unfortunately non-transgenic snap frozen muscle tissue was unavailable, as non-transgenic mice were not used in this study.

3.3.6. RNA Extraction

RNA was extracted using an RNeasy® lipid tissue mini kit (74804, Qiagen, UK) as per the manufacturer's instructions. Firstly, tissues were homogenised using a pellet pestle motor (Fisher Scientific, UK) in 1ml of QIAzol lysis reagent and incubated at room temperature (RT) for 5 mins. 200µl of chloroform was added to each sample and the

samples were shaken for 15 seconds before incubating at RT for 2 mins, followed by centrifugation at 12000 x g for 15 mins at 4˚C. The supernatant was then transferred and mixed with one volume of 70% ethanol. This solution was centrifuged through an RNeasy® spin column at 8000 x g for 15 seconds at RT. Buffer RW1 was then centrifuged through the spin column at 8000 x g for 15 seconds at RT, followed by buffer RPE at 8000 x g for 15 seconds at RT and again at 8000 x g for 2 mins at RT. In a fresh tube, 50µl of RNase-free water was then centrifuged through the spin column at 8000 x g for 1 min at RT, the product of which was the RNA, which was stored at -80˚C.

3.3.7. cDNA Extraction

Sample RNA concentrations were estimated using the nanodrop spectrophotometer ND-1000 (Labtech International, UK). cDNA was extracted from RNA using a high capacity RNA-to-cDNA kit (4387406, Applied Biosystems, USA). Solutions were made of 10µl of RT buffer mix 20x (Applied Biosystems, USA), 1µl of RT enzyme mix 2x (Applied Biosystems, USA) and a 9µl dilution of 2µg of sample in water. Samples were placed in the PCR machine (G-storm, UK) for 1 hour at 37˚C, followed by 5 mins at 95˚C. 60µl of water was added to each sample and then stored at -20˚C.

3.3.8. qPCR

Primer pairs were mixed and diluted to 5µM (see *table 3.1* for primer sequences).

Samples were plated in duplicate in non-skirted, frosted, thin-wall 0.2ml low profile 96 well plates (P3-0402, Geneflow, UK) and covered with optical wide area 8-cap strips (P3-0051, Geneflow, UK). Each well contained 1µl cDNA, 1µl primer mix, 3µl water and 5µl brilliant III ultra-fast SYBR® green QPCR master mix (600882, Agilent Technologies, USA). GAPDH was used as the house-keeping gene. A non-template control was plated for each primer pair.

Samples were placed in the qPCR machine (Mx 3000P, Stratagene, USA) and run on the following protocol: 95˚C for 10 mins, 45 cycles (95˚C for 30 seconds, 58˚C for 1 min, 72˚C for 1 min), 95˚C for 1 min, 55˚C for 30 seconds, 95˚C for 30 seconds.

Table 3. 1: Primer sequences. *Forward and reverse primer sequences used for qPCR analysis.*

Primer pair	Forward	Reverse
TBC1D1	GTGAGGAAGAGGCGTTCAAG	AGGTCTCGGTGGTAATCGTG
GAPDH	ATGGTGAAGGTCGGTGTGAA	TGGCAACAATCTCCACTTTGC

3.3.9. qPCR Analysis

Cycle threshold (Ct) values were extracted using MxPro Mx3000P software version 4.10 (Stratagene, USA). Further analysis was carried out using Microsoft Excel 2013 (Microsoft, USA) and GraphPad Prism 6 (GraphPad, USA).

Mean Ct values were calculated for each sample from the duplicates. Data were not used if duplicate Ct values differed by ≥1. The relative concentration was calculated using the equation: $1/2^{(\text{gene of interest Ct} - \text{GAPDH Ct})}$. Values were presented as a percentage of the mean TDP-43^{WT} value for each sample, or as a percentage of the mean non-transgenic value wherever possible.

3.3.10. Statistical Analysis

Running activity was variable across days, consequently the maximum running time, distance and speed run each week was used as a representation of running activity. Age to a 20% decline in running time, distance and speed were calculated by determining the age at which a consistent 20% decline from the initial readout (week 5) was detected.

The relative concentration of each sample was calculated for gene expression in cortex, spinal cord and muscles from non-transgenic, TDP-43^{Q331K} and TDP-43^{WT} mice (n = 6-12/group).

GraphPad Prism 6 was used for all statistical analyses (GraphPad, USA). Two-way ANOVA with repeated measures and a Sidak post-test was used for all data with multiple time points; Students's t-test was used for all data with a normal distribution in which there were 2 groups at one timepoint; the Mann-Whitney U test was used for all data with non-normal distribution in which there were 2 groups at one timepoint. All data are represented as mean and standard deviation.

3.4. Results

3.4.1. Running Time

In both TDP-43^{Q331K} and TDP-43^{WT} males and females, mean running time declined with age (*figure 3.2A & B*). The male data showed a slight increase in running time at the beginning of the study, suggestive of a training period; whereas the females showed an age-dependent decline from the beginning of the study. There was no significant difference in running time between TDP-43^{Q331K} and TDP-43^{WT} mice in males or females on a two-way ANOVA with repeated measures (Sidak post-test).

Male TDP-43^{Q331K} mice reached a mean maximum running time at 6 weeks of age (162 ± 79.2 minutes) followed by a steady decline to a minimum mean running time at 30 weeks of age (5.3 ± 7.3 minutes). In contrast, male TDP-43^{WT} mice had an increase in running time from 5 weeks of age until reaching a maximum mean running time at 10 weeks of age (243 ± 106.1 minutes), then gradually declining to a minimum mean running time at 41 weeks of age (37.3 ± 25.3 minutes).

Female TDP-43^{Q331K} mice reached a mean maximum running time at 5 weeks of age (338 ± 78.7 minutes) followed by a steady decline to a minimum mean running time at 43 weeks of age (6.1 ± 3.6 minutes). In contrast, female TDP-43^{WT} mice reached a mean maximum running time at 6 weeks of age (269 ± 107.6 minutes) followed by a steady decline to a minimum mean running time at 43 weeks of age (28.8 ± 21.5 minutes).

Age to reach a 20% decline in running time (*figure 3.2C & D*) was higher in TDP-43^{WT} mice compared to TDP-43^{Q331K} mice but also showed much more variability in both males (9.8 ± 2.2 weeks in TDP-43^{Q331K} vs 20.5 ± 12.9 weeks in TDP-43^{WT}, $p<0.05$) and females (12.2 ± 4.1 weeks in TDP-43^{Q331K} vs 18.9 ± 13.9 weeks in TDP-43^{WT}).

When comparing male and female mice (*figure 3.2E & F*), female mice ran for longer than male mice in the TDP-43^{Q331K} group, however, this was not significant on a two-way ANOVA with repeated measures (Sidak post-test). In the TDP-43^{WT} mice, there was no difference between males and females on a two-way ANOVA with repeated measures (Sidak post-test).

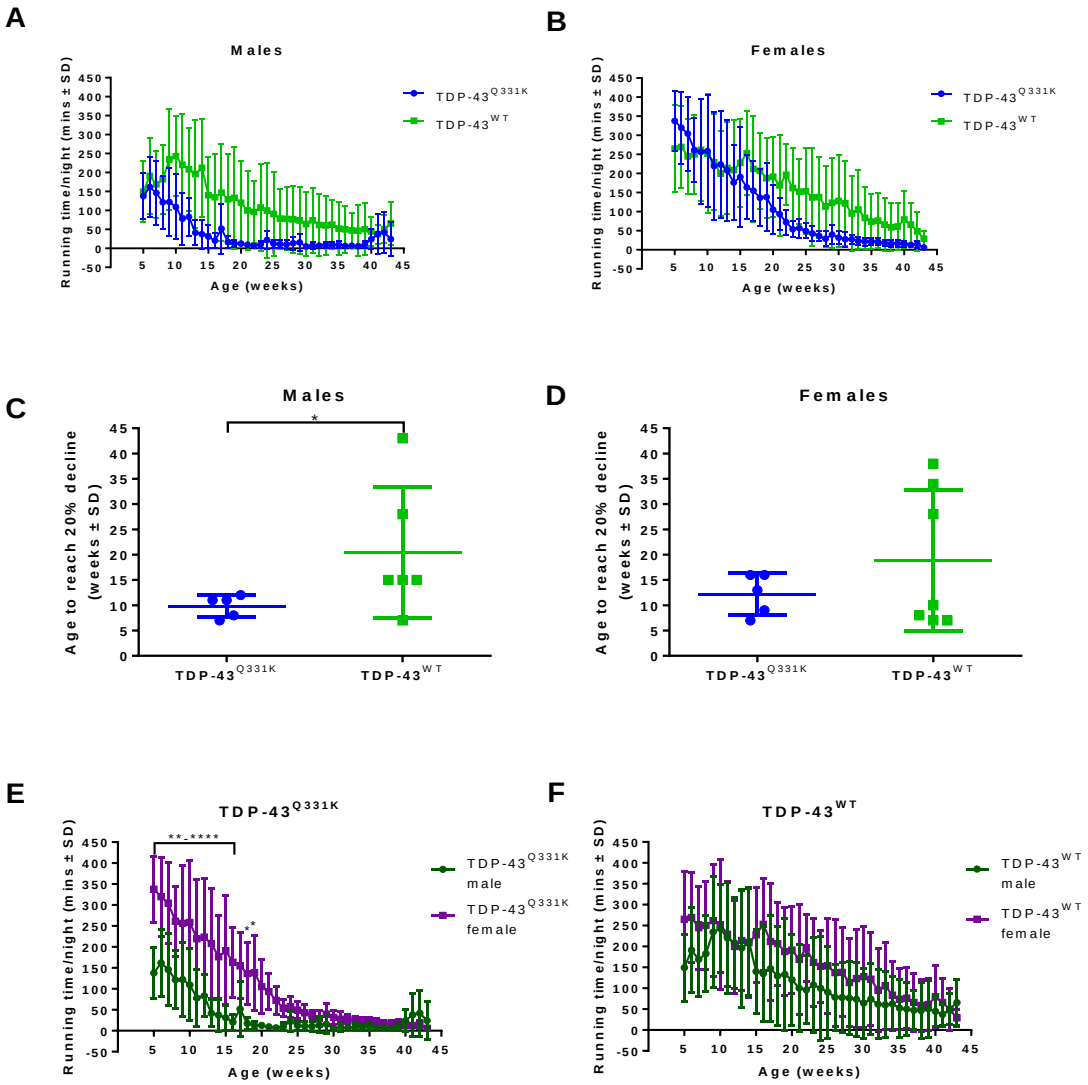

Figure 3. 2: Maximum running time/night within each week ± SD.

*Maximum time spent running per night within each week (n=6) of male and female TDP-43^{WT} and TDP-43^{Q331K} mice. A & B: there was no significant difference in running time between TDP-43^{Q331K} and TDP-43^{WT} mice on a two-way ANOVA with repeated measures and Sidak post-test but there was a decline in running time with age in all groups ($p<0.0001$). C & D: there was a significant difference in age to reach a 20% decline in running time between TDP-43^{Q331K} and TDP-43^{WT} male mice ($p<0.05$) but not in female mice on a Mann-Whitney U test. E & F: there was no significant difference in running time between males and females in the TDP-43^{Q331K} or TDP-43^{WT} groups on a two-way ANOVA with repeated measures and Sidak post-test, multiple comparisons showed increased running time in the TDP-43^{Q331K} females compared to males, *$p<0.05$ vs all other groups, **$p<0.01$ vs all other groups, ***$p<0.001$ vs all other groups, ****$p<0.0001$ vs all other groups.*

3.4.2. Running Distance

In both TDP-43^{Q331K} and TDP-43^{WT} males and females, mean running distance declined significantly with age (*figure 3.3A & B*, $p<0.0001$). The male data showed a slight increase in running distance at the beginning of the study, suggestive of a training period; whereas the females showed an age-dependent decline from the beginning of the study. There was no significant difference in running distance between TDP-43^{Q331K} and TDP-43^{WT} mice in males or females on a two-way ANOVA with repeated measures (Sidak post-test).

Male TDP-43^{Q331K} mice reached a mean maximum running distance at 6 weeks of age (4.25 ± 2.7km) followed by a steady decline to a minimum mean running distance at 38 weeks of age (0.03 ± 0.02km). In contrast, male TDP-43^{WT} mice had an increase in running distance from 5 weeks of age until reaching a maximum mean running distance at 10 weeks of age (7.85 ± 7.5km), then gradually declining to a minimum mean running distance at 41 weeks of age (0.82 ± 1km).

Female TDP-43^{Q331K} mice reached a mean maximum running distance at 5 weeks of age (11.58 ± 5.8km) followed by a steady decline to a minimum mean running distance at 42 weeks of age (0.07 ± 0.06km). In contrast, female TDP-43^{WT} mice reached a mean maximum running distance at 5 weeks of age (8.11 ± 5.5km) followed by a steady decline to a minimum mean running distance at 42 weeks of age (0.77 ± 1.1km).

Age to reach a 20% decline in running distance (*figure 3.3C & D*) showed no difference between TDP-43^{WT} mice and TDP-43^{Q331K} mice in males (19.5 ± 13 weeks in TDP-43^{Q331K} vs 9.6 ± 2.9 weeks in TDP-43^{WT}) or females (19.5 ± 13 weeks in TDP-43^{Q331K} vs 18.7 ± 12.3 weeks in TDP-43^{WT}).

When comparing male and female mice (*figure 3.3E & F*), female mice ran further than male mice in the TDP-43^{Q331K} group, however this was not significant on a two-way ANOVA with repeated measures (Sidak post-test). In the TDP-43^{WT} mice, there was no difference between males and females on a two-way ANOVA with repeated measures (Sidak post-test).

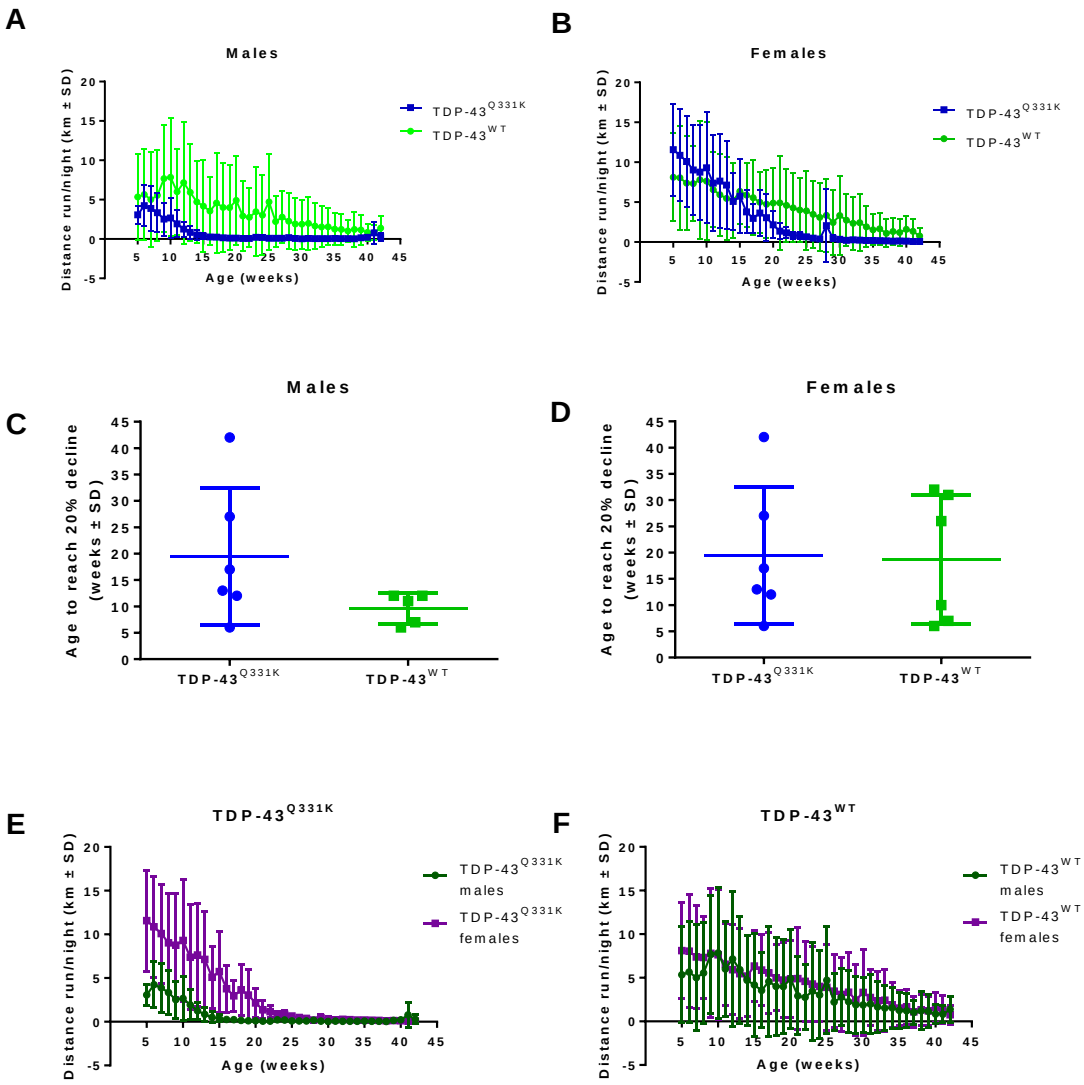

Figure 3. 3: Maximum distance/night within each week ± SD.

Maximum distance run per night within each week (n=6) of male and female TDP-43^{WT} and TDP-43^{Q331K} mice. A & B: there was no significant difference in running distance between TDP-43^{Q331K} and TDP-43^{WT} mice on a two-way ANOVA with repeated measures and Sidak post-test but there was a decline in running time with age in all groups ($p<0.0001$). C & D: there was no significant difference in age to reach a 20% decline in running distance between TDP-43^{Q331K} and TDP-43^{WT} mice on a Mann-Whitney U test. E & F: there was no significant difference in running time between males and females in the TDP-43^{Q331K} or TDP-43^{WT} groups on a two-way ANOVA with repeated measures and Sidak post-test.

3.4.3. Running Speed

In both TDP-43^{Q331K} and TDP-43^{WT} males and females, the mean running speed significantly declined with age after a short period of increasing speed at the beginning of the study, suggestive of a training period (*figure 3.4A & B*, p<0.0001). The decline in speed with age appeared steeper in females when compared to males, but there was no significant difference in average running speed between TDP-43^{Q331K} and TDP-43^{WT} mice in males or females on a two-way ANOVA with repeated measures (Sidak post-test).

Male TDP-43^{Q331K} mice reached a mean maximum running speed at 7 weeks of age (1.61 ± 0.5km/hr) followed by a steady decline to a minimum mean running speed at 30 weeks of age (0.29 ± 0.3km/hr). In contrast, male TDP-43^{WT} mice had an increase in running speed from 5 weeks of age until reaching a maximum mean running speed at 13 weeks of age (1.78 ± 0.8km/hr), then gradually declining to a minimum mean running speed at 38 weeks of age (0.88 ± 0.7km/hr).

Female TDP-43^{Q331K} mice reached a mean maximum running speed at 7 weeks of age (2.02 ± 0.7km/hr) followed by a steady decline to a minimum mean running speed at 43 weeks of age (0.18 ± 0.2km/hr). In contrast, female TDP-43^{WT} mice reached a mean maximum running speed at 11 weeks of age (1.89 ± 0.5km/hr) followed by a steady decline to a minimum mean running speed at 37 and 40 weeks of age (0.69 ± 0.6/0.7km/hr).

Age to reach a 20% decline in average running speed (*figure 3.4C & D*) showed no difference between TDP-43^{WT} and TDP-43^{Q331K} mice in males (12.8 ± 2.8 weeks in TDP-43^{Q331K} vs 23.7 ± 17.1 weeks in TDP-43^{WT}) or females (17.3 ± 3.4 weeks in TDP-43^{Q331K} vs 31 ± 15 weeks in TDP-43^{WT}).

When comparing male and female mice (*figure 3.4E & F*), female mice ran faster than male mice in the TDP-43^{Q331K} group, however, this was not significant on a two-way ANOVA with repeated measures (Sidak post-test). In the TDP-43^{WT} mice, there was no difference between males and females on a two-way ANOVA with repeated measures (Sidak post-test).

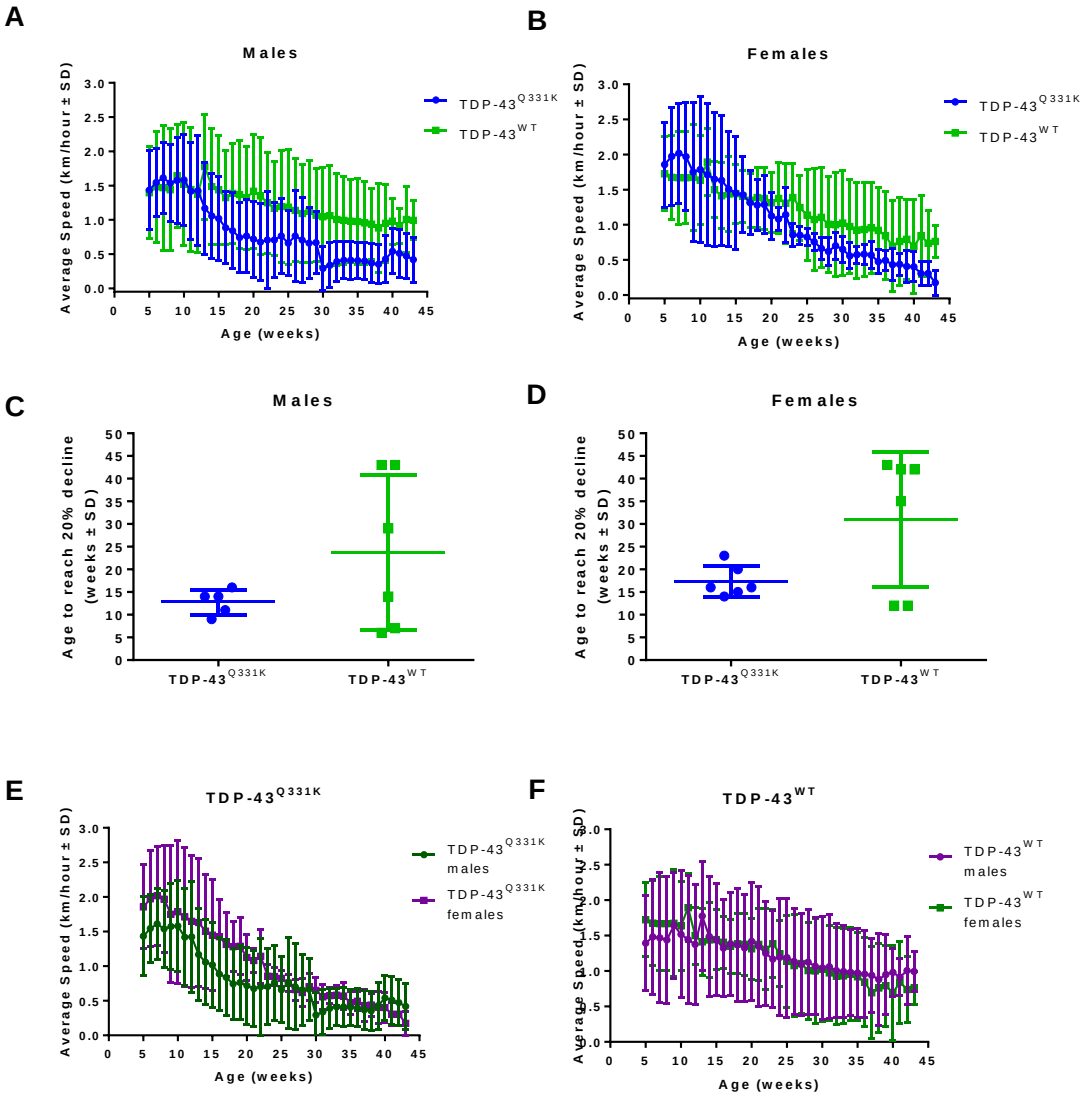

Figure 3. 4: Maximum average speed/night within each week ± SD.

A & B: there was no significant difference in average running speed between TDP-43^{Q331K} and TDP-43^{WT} mice on a two-way ANOVA with repeated measures and Sidak post-test but there was a decline in running time with age in all groups ($p<0.0001$). C & D: there was no significant difference in age to reach a 20% decline in average running speed between TDP-43^{Q331K} and TDP-43^{WT} mice on a Mann-Whitney U test. E & F: there was no significant difference in average running speed between males and females in the TDP-43^{Q331K} or TDP-43^{WT} groups on a two-way ANOVA with repeated measures and Sidak post-test.

3.4.4. TDP-43^{Q331K} Mice are Heavier than TDP-43^{WT} Mice

Male and female TDP-43^{Q331K} and TDP-43^{WT} mice showed a significant increase in weight with age (*figure 3.5*). In both male and female mice, the TDP-43^{Q331K} mice are heavier than the TDP-43^{WT} mice. In the male mice, the weight difference between the two groups begins to disappear at around 36 weeks of age when the TDP-43^{Q331K} weight plateaus, whilst the TDP-43^{WT} weight continues to increase, closing the gap between the weights of the two groups. Conversely, the female TDP-43^{Q331K} mice increase in weight throughout the study at a much steeper incline than the TDP-43^{WT} mice, making the difference significant from 18 weeks of age (26 ± 1.7g TDP-43^{Q331K} vs 21.2 ± 1.6g TDP-43^{WT}, $p<0.05$).

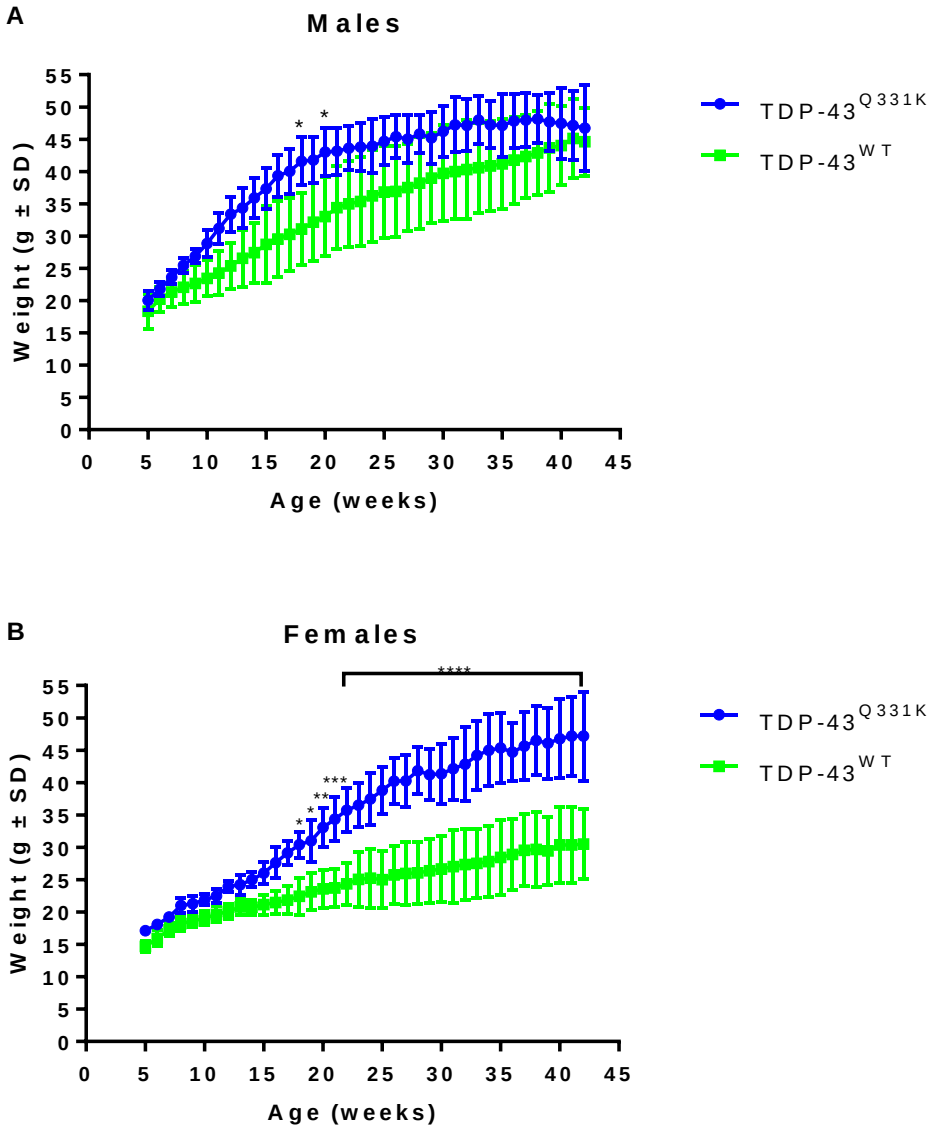

Figure 3. 5: Whole body weight ± SD.

*Body weight, as measured each week (n=6) in male and female TDP-43^{WT} and TDP-43^{Q331K} mice. In males (A), the data were significantly different on a two-way ANOVA with repeated measures and Sidak post-test for the effects of group ($p<0.05$) and age ($p<0.0001$). In females (B), the data were significantly different on a two-way ANOVA with repeated measures and Sidak post-test for the effects of group ($p<0.001$) and age ($p<0.0001$). *p<0.05 vs all other groups, **p<0.01 vs all other groups, ***p<0.001 vs all other groups, ****p<0.0001 vs all other groups, two-way ANOVA with repeated measures (Sidak post-test).*

3.4.5. Food Intake

Male and female TDP-43^{Q331K} mice showed a significantly increased food intake compared to the TDP-43^{WT} mice on a two-way ANOVA with repeated measures and Sidak post-test (*figure 3.6*). All male mice, and the female TDP-43^{Q331K} mice show an upwards trend in food intake at the beginning of the study from 7 weeks, plateauing at 11 weeks of age. Towards the end of the study, food intake appears to increase in the TDP-43^{WT} mice.

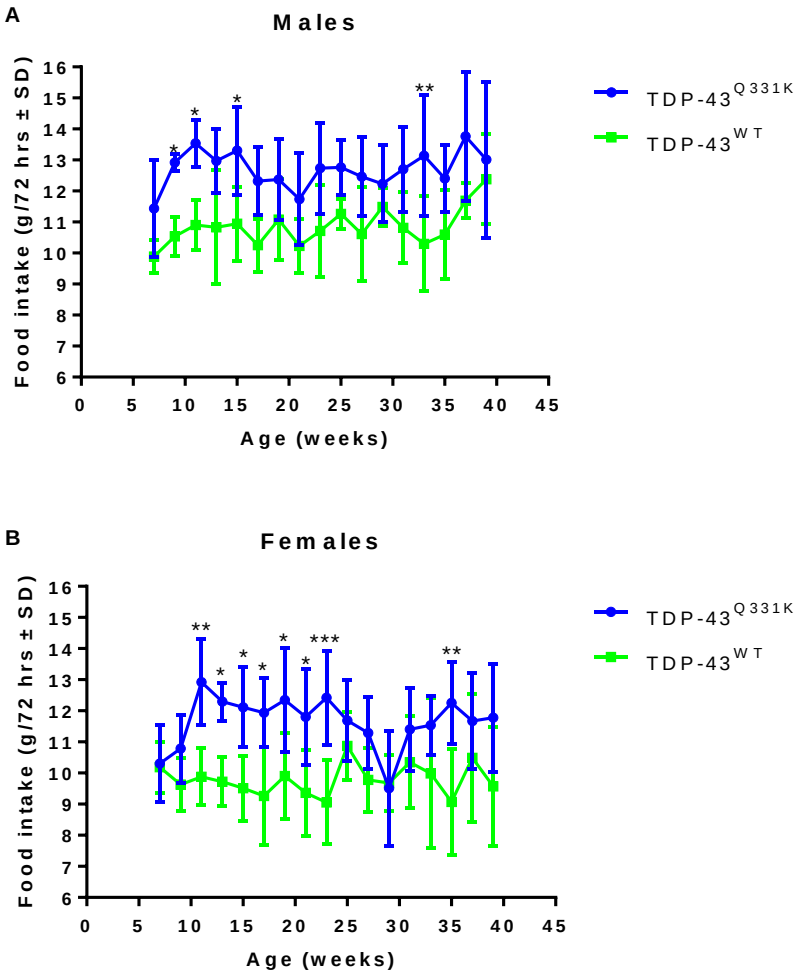

Figure 3. 6: Food intake ± SD.

*Food intake over a 72 hour period, as measured every 2 weeks (n=6) in male and female TDP-43^{WT} and TDP-43^{Q331K} mice. In both males (A) and females (B), the data were significantly different on a two-way ANOVA with repeated measures (Sidak post-test) for the effect of group (p<0.01). *p<0.05 vs all other groups, **p<0.01 vs all other groups, ***p<0.001 vs all other groups, two-way ANOVA with repeated measures (Sidak post-test).*

3.4.6. Weight of Running vs Non-running Mice

Comparison of weight from the running wheel study and the previous characterisation study (see chapter 2) shows mice on the running wheels appeared to be heavier than those which did not have wheels in the characterisation study (*figure 3.7*). Wheel mice appeared heavier in males and females of both TDP-43^{Q331K} and TDP-43^{WT} mice. These data suggest that running wheel use does not decrease weight in these mice. Statistical analysis could not be performed as the data were not collected as part of the same study. A separate study would be needed to confirm the effect of wheel use on weight in these mice.

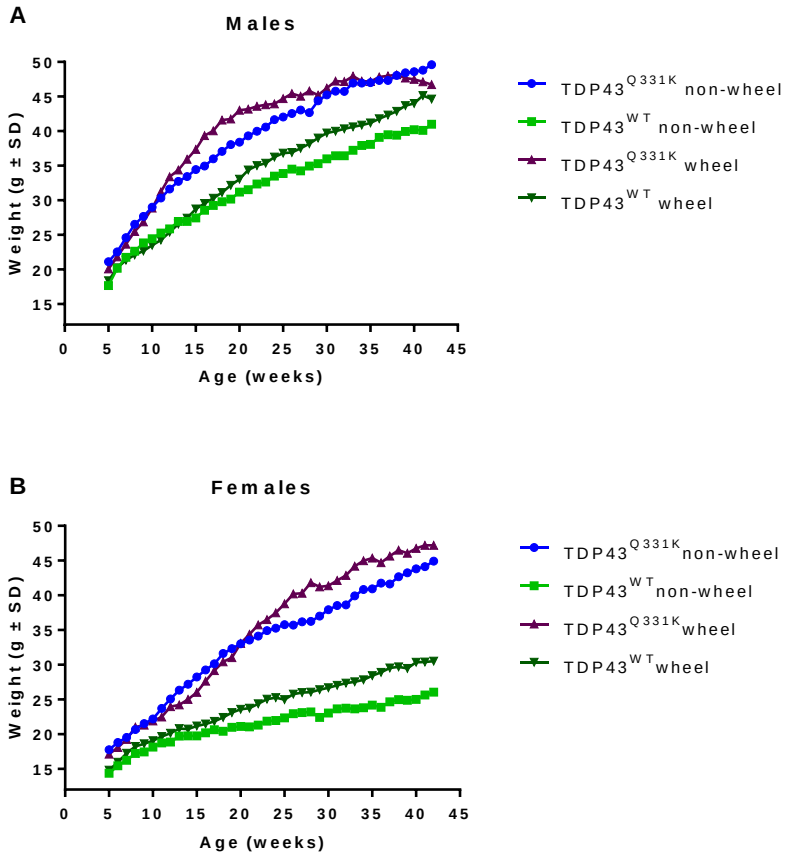

Figure 3. 7: Whole body weight of running wheel mice vs non-running mice (from previous study).

Body weight, as measured each week in male (A) and female (B) TDP-43^{WT} and TDP-43^{Q331K} mice in both the running wheel study and the previous characterisation study (described in chapter 2). Statistical analysis could not be performed as data were not collected as part of the same study.

3.4.7. TBC1D1 Gene Expression

Gene expression of TBC1D1 was measured in the cDNA of cortex and spinal cord from non-transgenic, TDP-43^{WT} and TDP-43^{Q331K} mice at 10 months of age (*figure 3.8*), expressed as a percentage of the non-transgenic values. Gene expression of TBC1D1 was also measured in the cDNA of hindlimb muscles of TDP-43^{WT} and TDP-43^{Q331K} mice, expressed as a percentage of the TDP-43^{WT} values.

Expression of TBC1D1 was not significantly different in the TDP-43^{WT} or TDP-43^{Q331K} cortex compared to the non-transgenic cortex (100 ± 23.1% in non-transgenic vs 97.9 ± 13.4% in TDP-43^{WT} vs 100 ± 8.9% in TDP-43^{Q331K}) or TDP-43^{WT} and TDP-43^{Q331K} spinal cord compared to the non-transgenic spinal cord (100 ± 12.5% in non-transgenic vs 95.5 ± 11.5% in TDP-43^{WT} vs 91.2 ± 8.2% in TDP-43^{Q331K}). Expression of TBC1D1 was not significantly different in the TDP-43^{Q331K} hindlimb muscle compared to the TDP-43^{WT} hindlimb muscle (100 ± 24.2% in TDP-43^{WT} vs 108.4 ± 34.1% in TDP-43^{Q331K}).

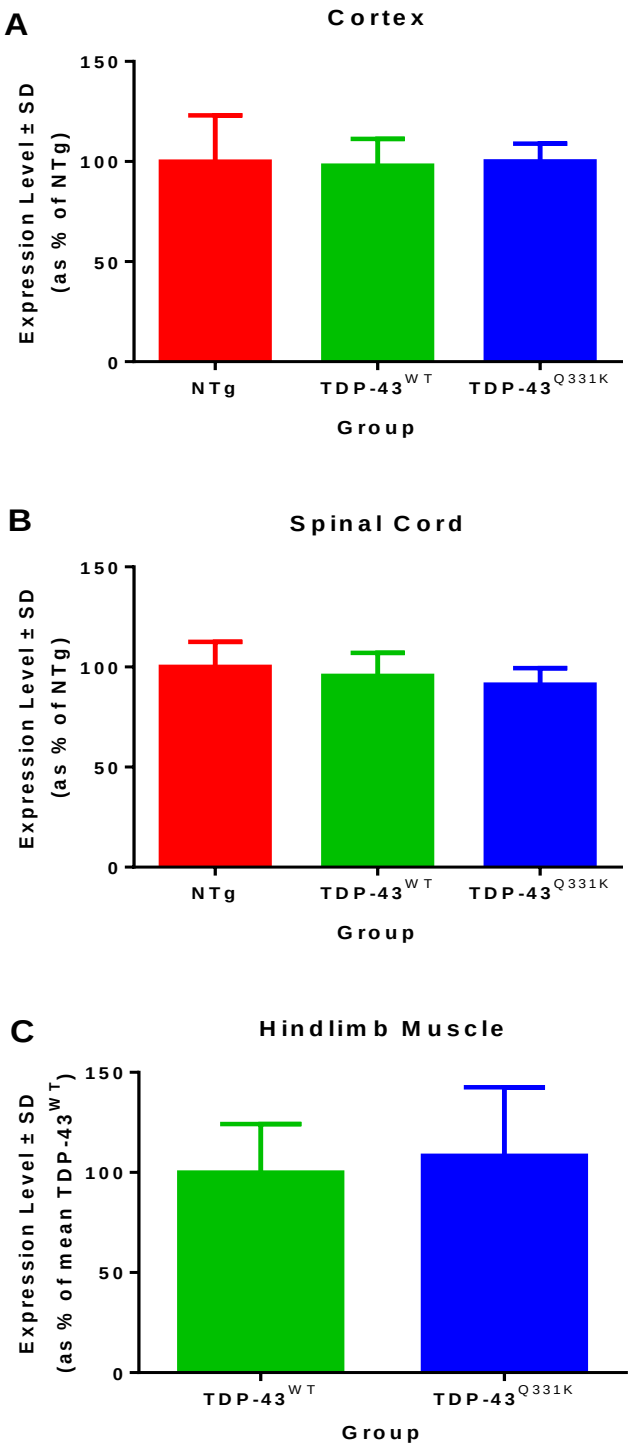

Figure 3. 8: TBC1D1 gene expression ± SD at 10 months of age.

Gene expression as a percentage of the mean non-transgenic levels, as measured in cDNA of cortex (A) and spinal cord (B) of TDP-43^{WT} and TDP-43^{Q331K} mice (n=9-12) showed no differences on a one-way ANOVA. Gene expression as a percentage of the mean TDP-43^{WT} levels, as measured in cDNA of hindlimb muscles (C) of TDP-43^{WT} and TDP-43^{Q331K} mice (n=9-12) showed no differences on a Student's t-test.

3.5. Discussion

3.5.1. Running Activity Over Time

As found in a previous running wheel study in SOD1^{G93A} mice (Bennett et al., 2014), running time and distance declined with age and disease severity in both the TDP-43^{WT} and TDP-43^{Q331K} mice.

Several running wheel studies have described an initial training period in which the running activity gradually increases when the mice are first housed with a running wheel (De Bono et al., 2006, Bennett et al., 2014, Allen et al., 2001). In the study conducted here, a slight training period was seen in both the TDP-43^{WT} and TDP-43^{Q331K} male mice for time, distance and average speed. However, a training period was not seen in the TDP-43^{WT} and TDP-43^{Q331K} female mice, other than for average speed in the TDP-43^{Q331K} mice. It is unclear why there would be a difference between male and female training as the previous studies showed a training period in both male and female mice.

3.5.2. Gender Effects on Running Activity

A previous study which compared male and female running wheel activity found that female mice ran considerably further than male mice (De Bono et al., 2006). This was also found in the study described here in the TDP-43^{Q331K} mice, as females ran for a longer time and distance compared to males and had a higher maximum distance during the disease course, but no differences were found in the TDP-43^{WT} group.

The oestrous cycle of female mice has been suggested to influence running wheel activity (De Bono et al., 2006) and to increase the variability in this activity measure. In this study the female running wheel activity showed no more variability than the male running wheel activity. However, any variance due to the oestrous cycle may have been eliminated by the use of a weekly maximum time, distance and speed reached.

3.5.3. Running Activity and Disease

Running time, distance and average speed were all non-significantly lower in both male and female TDP-43^{Q331K} mice compared to the TDP-43^{WT} mice, suggesting that voluntary activity levels were slightly reduced in the TDP-43^{Q331K} mice due to disease. Lower

activity levels have also been found in another overweight mutant TDP-43 mouse model (Stallings et al., 2013). The decreased activity levels are likely to be a contributing factor to the increased weight of TDP-43^{Q331K} mice.

As suggested in the SOD1^{G93A} mice (Bennett et al., 2014), reduced activity could also be due to motor dysfunction. However, the disease phenotype is very mild in this model so unlikely to be the cause of reduced activity. It is well documented that normal mice are highly motivated to run on a wheel (Sherwin, 1998), and it is therefore also possible that reduced running in the TDP-43^{Q331K} mice is due to a cognitive aspect of their disease such as lack of motivation.

The overall running wheel activity of both TDP-43^{WT} and TDP-43^{Q331K} mice was considerably lower than that found in other studies, in which mice ran for a time period of 4-6 hours per night (Bennett et al., 2014), compared to a matter of 0-4 hours in the study discussed here. This is likely to be due to the background strain of the model as it has been shown that genetic background has a large influence on running wheel activity in mice (Turner et al., 2005, Massett and Berk, 2005). No record could be found of running wheel activity in C57BL/6N mice and this study shows it to be relatively low compared to other strains.

3.5.4. Weight

As found in a previous study (chapter 2), the mice gained weight with age, significantly more so in the TDP-43^{Q331K} mice compared to the TDP-43^{WT} mice.

Surprisingly, when comparing the weight of the mice on running wheels in this study, with the mice which were not on running wheels in the previous study (chapter 2), it appears that the mice on running wheels were heavier than those which were not in males and females of both TDP-43^{Q331K} and TDP-43^{WT} mice. The wheel running activity therefore, did not appear to cause any relative weight loss. Conversely, most previous studies have found the mice on running wheels to be lighter than those which were not on running wheels (Bennett et al., 2014), especially in male mice (De Bono et al., 2006). However, another study found no difference in weight between the mice on wheels and the mice which were not (Allen et al., 2001). No records could be found of mice being heavier when on running wheels. It is possible that the mice were heavier due to

increased muscle mass, but the activity levels were so minimal, especially towards the end of the study, that this seems unlikely.

3.5.5. Food Intake

Food intake increased with age during the first few weeks of the study, at which time the mice were still maturing and were therefore increasing their food intake as they grew. Food intake was higher in both male and female TDP-43^{Q331K} mice compared to TDP-43^{WT} mice, as reported in another overweight mutant TDP-43 mouse model (Stallings et al., 2013). Further experiments to assess appetite and metabolic pathways could elucidate the reason for this increased food intake. The increased food intake is likely to be a contributing factor to the increased weight of TDP-43^{Q331K} mice and may be a sign of hyperphagia, a symptom which can occur in FTD in humans (Ahmed et al., 2016a).

A very interesting future study would be to restrict food intake in these mice, providing further indication of how much increased food intake is influencing the weight of the mice.

3.5.6. TBC1D1 Gene Expression

As described previously, several mouse models have identified a link between TDP-43 and TBC1D1 expression with conditional deletion decreasing TBC1D1 expression and TDP-43 overexpression increasing TBC1D1 expression, which may explain the lethal leaness and obesity seen in these two model systems respectively (Chiang et al., 2010, Stallings et al., 2013). This TDP-43^{Q331K} model shows increased weight gain and increased expression of huTDP-43 compared to the TDP-43^{WT} expression and so TBC1D1 gene expression was evaluated by qPCR, with an increase in expression anticipated.

The data (*figure 3.8*) indicated that levels of TBC1D1 expression were no different in the cortex, spinal cord and hindlimb muscles of TDP-43^{Q331K} mice when compared to TDP-43^{WT} and non-transgenic mice. There appears to be no direct link in this case between levels of huTDP-43, TBC1D1, and the observed weight gain. This leaves open the question of why these mice show increased weight gain. Certainly the reduced activity as evidenced by the poor running wheel performance and increased food intake may

explain the weight gain observed in these mice but the underlying cause of this is unknown.

3.6. Conclusion

In conclusion, the TDP-43^{Q331K} mice have increased food intake and reduced activity levels compared to TDP-43^{WT} mice. Expression of huTDP-43 cDNA is increased in TDP-43^{Q331K} but this increase in expression is not correlated with expression levels of TBC1D1. As a result, the underlying reason for increased fat deposition in the TDP-43^{Q331K} mouse model remains uncertain.

4. Riluzole and Electrophysiology Study

4.1. Introduction

4.1.1. Riluzole

As discussed previously (chapter 1), riluzole is the only drug licenced for treatment of MND, and extends life by several months (Stewart et al., 2001, Miller et al., 2003), potentially as long as 12 months (Georgoulopoulou et al., 2013). Riluzole was first published as an effective treatment for MND in 1994 (Bensimon et al., 1994) and approved by the Food and Drug Administration in 1995. The most likely mechanism of action is to reduce glutamate toxicity and modulate sodium channels, thereby reducing cortical and axonal hyperexcitability (Geevasinga et al., 2016).

The general consensus is that 100mg/day of riluzole can extend median survival and has a small beneficial effect on bulbar and limb function but not muscle strength (Miller et al., 2012). However, other studies have suggested that riluzole has little or no effect on MND (Stewart et al., 2001) and this may be related to the concept of MND consisting of multiple clinical subgroups, with riluzole only being effective in a subset of patients, limiting its overall effect on the MND populations investigated (Georgoulopoulou et al., 2013).

Some investigators test therapeutic compounds in $SOD1^{G93A}$ mice in combination with riluzole (Waibel et al., 2004, Snow et al., 2003), arguing that it is more clinically relevant as patients will remain on riluzole during clinical trials.

Studies in $SOD1^{G93A}$ mice found that riluzole has a slight effect on survival and motor function at 24 and 44mg/kg/day, dosed from 42-43 days of age, mixed into feeding pellets, prior to disease onset (Gurney et al., 1998). The improvement in motor function, measured by running wheel activity, was larger during the earlier stages of disease.

A more recent study showed dosing of riluzole at 8mg/kg/day in $SOD1^{G93A}$ mice had no effect on disease onset or survival (Li et al., 2013), as has been suggested in several other studies at varying doses (Scott et al., 2008).

Riluzole has a short half-life which can be affected by age (Le Liboux et al., 1999) and in humans the mean half-life after multiple doses is 12 hours (Bryson et al., 1996), hence patients take riluzole twice a day. Mice have a much faster metabolism than humans and clear drugs more rapidly. For this reason, previous studies have administered

riluzole to mice in the drinking water, ensuring continual dosage. In-house studies have treated SOD1^{G93A} mice with riluzole at doses ranging from 120 to 2000µg/ml of riluzole in the drinking water (equating to doses of 36 to 100mg/kg). The higher doses showed some sedative effect. A dose of 240µg/ml significantly reduced the decline in motor function in SOD1^{G93A} mice in two separate studies.

It has been shown in patients that the plasma concentrations of riluzole are strongly correlated with therapeutic effect (Le Liboux et al., 1999). Plasma levels should therefore be considered when designing a preclinical study.

Such mixed results in the SOD1^{G93A} mouse model may indicate that SOD1 patients are a subgroup of MND which may or may not benefit from taking riluzole. A preclinical trial of riluzole in TDP-43^{Q331K} mice may provide insight in to whether riluzole is effective in patients with TDP-43 mutations and/or TDP-43 pathology. To date, no riluzole studies have been recorded in a *TARDBP* mouse model.

4.1.2. Electrophysiology

Biomarkers are measurable indicators of biological processes, either of normal function, pathological processes or responses to therapeutic intervention (Turner et al., 2009). In the case of MND, the latter two processes are of interest in order to facilitate diagnosis and disease monitoring, and measure the effect of therapeutic trials.

There is currently no single diagnostic test for MND. Diagnosis relies on a history of progressive motor symptoms , supported by examination findings and the elimination of other diseases (Turner et al., 2009) through MRI, blood tests and electromyography (EMG). Due to the gradual onset of symptoms, the extensive range of tests and the level of expertise required, diagnosis of MND takes an average of one year from symptom onset (Zoccolella et al., 2006). A biomarker which could be used to make an earlier, more concrete diagnosis would help patients in future planning and allow earlier access to relevant healthcare services and symptomatic therapies.

Monitoring of the disease is key for healthcare professionals and carers to plan ahead and put in place the necessary care and practicalities needed at end of life. Disease monitoring usually consists of symptom assessment, measurement of one or more functional rating scales, respiratory function tests, and assessments of muscle strength

and patient quality of life (Costa et al., 2010). Currently, prognosis can only be inferred by observing clinical disease presentation and speed of progression (Chio et al., 2009), whereas a reliable biomarker could enable more accurate predictions.

A biomarker to carry through from trials of animal models to patients could offer invaluable insights into disease pathophysiology and enable monitoring of the response to therapeutic agents from the laboratory to the clinic. This translational approach is invaluable in increasing confidence when moving into clinical studies and has the potential to offer new insights into disease pathophysiology and, importantly, reduce the duration and cost of clinical trials in patients, allowing more potential new treatments to be tested.

Nerve conduction studies and EMG are currently one of the main diagnostic tests undertaken when patients are being investigated for suspected MND (Benatar et al., 2016). One of their key aims is to exclude other diseases which may mimic MND such as cervical myeloradiculopathy, hereditary spastic paraparesis or inclusion body myositis (Turner and Talbot, 2013). Nerve conduction studies are undertaken in both the arms and legs. Receiving electrodes are placed on the muscle and stimulating electrode needles are placed on to the nerve. A supramaximal stimulation is applied to the nerve and a compound muscle action potential (CMAP) is measured. CMAP is a standard test in nerve conduction studies, which quantifies the depolarisation of muscle fibres following supramaximal stimulation of the nerve innervating that muscle, as detected by the electrodes. Reduced CMAP amplitude usually correlates with a loss in functional motor axons and/or the fibre they innervate. In MND patients (Benatar et al., 2016), CMAP amplitudes may be reduced due to degeneration of the motor axons which in turn leads to a reduction in muscle strength and function.

Motor unit number estimation (MUNE) is an electrophysiological method which has been used for decades (McComas et al., 1971), and can be calculated in several ways. One method estimates the action potential of the whole muscle using a supramaximal stimulation, and divides this by the estimated action potential of a single motor unit, as calculated using minimal stimulation. Alternatively, the stimulus is gradually increased and with each increase in response, another motor unit is assumed to have been recruited, allowing for counting of the number of motor units. A more recently developed but similar method is motor unit number index (MUNIX) (Nandedkar et al.,

2010), in which CMAP is divided by an average motor unit size derived from surface interference patterns obtained as the patient voluntarily contracts the muscle being examined. In both MUNE and MUNIX, lower numbers of motor units are found in MND patients compared to control subjects (Neuwirth et al., 2015, Baumann et al., 2012).

A further test carried out in diagnostic investigations, most commonly when investigating neuromuscular junction (NMJ) disorders such as myasthenia gravis, is repetitive stimulation. In this, repeated stimulation is applied to the nerve. During normal activation of the NMJ, increased pre-synaptic calcium causes an increase in acetylcholine (ACh) release. As post-synaptic ACh receptors are activated, an influx of sodium occurs into the myocyte, causing an endplate potential (EPP). If the EPP is above threshold, an action potential will occur in the muscle fibre, resulting in contraction. The safety factor is defined as the difference between the EPP and the threshold potential required to produce an action potential, or the amount of excess neurotransmitter beyond the point of producing an action potential (Wood and Slater, 2001).

During repetitive stimulation, the primary store of ACh is depleted, reducing the EPP. However, so long as the EPP remains above threshold, an action potential will still occur. After approximately 1 second, a secondary store of ACh will be available for release and the EPP will rise back to normal levels. Therefore, during a slow repetitive stimulation (3Hz), a temporary reduction in EPP may be seen around the fourth stimulus. However, the CMAP amplitude will usually remain unaffected as the EPPs will always remain above threshold.

During fast repetitive stimulation or exercise (30-50Hz), the primary store of ACh is depleted very rapidly and the secondary store is activated faster, combined with an increase in calcium concentration, further increasing release of ACh; EPPs (and CMAP amplitude) remain the same throughout in healthy subjects.

In MND patients a decremental response to repetitive nerve stimulation has been reported (Iwanami et al., 2011, Wang et al., 2001). While this is incompletely understood, it is thought to reflect an underlying reduction in the safety factor, perhaps due to axons being in the process of degenerating. As the train of stimuli proceed the threshold for successful transmission is not achieved for a proportion of neuromuscular junctions. This results in fewer muscle fibres being activated and so a drop in the amplitude of the CMAP.

EMG is also utilised in the diagnostic process. In this a needle electrode is inserted in to a muscle of interest. The recording activities during both rest and voluntary muscle activation (if possible) are then recorded and analysed. When the muscle is at rest no electrical activity should be recorded by the needle electrode. If any activity is recorded this is generally held to be abnormal and a sign of denervation. Fibrillation potentials/positive sharp waves are signs of spontaneous EPPs in which an individual muscle fibre is spontaneously activated (Whittaker, 2012) and fasciculation potentials are indicators of spontaneous motor unit action potentials, both of which can be signs of the denervation that occurs in MND (Costa et al., 2012). The Awaji criteria allow for EMG data to be equated to clinical examination and historical evidence of lower motor neuron pathology (de Carvalho et al., 2008).

Motor evoked potentials (MEPs) are another useful electrophysiological measurement in mice as they give an indication of motor connectivity involving stimulation of the motor cortex and measurement of the electrical current at the spine or the muscle. However, MEPs can be invasive and require a wider range of equipment and are therefore, not as frequently used in diagnosis as other methods. In patients, transcranial magnetic stimulation can be used to evoke MEPs, reducing its invasive nature and providing useful indicators of upper motor neuron dysfunction (Menon et al., 2015).

CMAP amplitude, MUNE and fibrillation potential measurements have been reported in mouse models of neurological disease and suggested as translational biomarkers, showing similarities to measurements in human studies (Arnold et al., 2015, Arnold et al., 2014). A decremental response in repetitive stimulation has also been shown in a mouse model of spinal muscular atrophy, showing promise as a translational electrophysiological biomarker (Bogdanik et al., 2015).

Many electrophysiological studies have been carried out on MND mouse models, mostly on the $SOD1^{G93A}$ mice. Studies have found a reduction in CMAP amplitude (Mancuso et al., 2014, Alves et al., 2011, Li et al., 2013, Mancuso et al., 2011b), MUNE (Li et al., 2013, Shefner et al., 2002, Mancuso et al., 2011b) and MEPs (Mancuso et al., 2011b). Furthermore, EMG has demonstrated spontaneous fibrillations in the hindlimb muscles (Azzouz et al., 1997, Miana-Mena et al., 2005).

The published data on the TDP-43^{Q331K} model used electrophysiological studies to investigate the loss of upper/lower motor neurons (Arnold et al., 2013). Muscle MEPs

were reduced in the TDP-43^{Q331K} mice compared to control mice, demonstrating a loss of connectivity in the motor system. However, spinal MEPs were not reduced in the TDP-43^{Q331K} mice, indicating that there was no loss of upper motor neurons, only lower motor neurons. Consistent with this, EMG demonstrated spontaneous activity suggestive of fibrillations.

In summary, electrophysiological measures may provide a translational biomarker of MND, whilst concurrently providing additional insight in to the TDP-43^{Q331K} mouse model under investigation. Neurophysiological measures have been used in this study to further characterise the phenotype of the model and investigate the potential therapeutic effect of riluzole in the TDP-43^{Q331K} mouse model.

4.1.3. Marble Burying

Marble burying assays are tests in which mice are placed in a cage of deep bedding with marbles placed on the surface and the number of marbles buried in a set time are counted (Deacon, 2006). The true meaning of marble burying activity has long been debated and marble burying activity widely varies with genetic background (Deacon, 2006, Thomas et al., 2009).

Marble burying was traditionally thought of as a test of anxiety seeing as anxiolytic drugs reduce marble burying behaviour (Ichimaru et al., 1995, Nicolas et al., 2006). However, several studies propose that the marbles do not induce fear/anxiety, as mice will dig in the new environment regardless of whether marbles are present (Gyertyan, 1995, Thomas et al., 2009), repetitive exposure to the marbles does not reduce the burying response (Londei et al., 1998, Thomas et al., 2009, Njunge and Handley, 1991), mice did not avoid marbles when given the choice (Njunge and Handley, 1991), and marble burying activity does not correlate with other anxiety measures (Thomas et al., 2009).

Marble burying has frequently been used as a measure of repetitive behaviour, especially in mouse models of obsessive compulsive disorder (Angoa-Perez et al., 2013, Londei et al., 1998, Ichimaru et al., 1995, Egashira et al., 2008). Glutamate-related drugs used to treat obsessive behaviour have been shown to reduce marble burying behaviour without reducing locomotor activity, although riluzole had no effect on marble burying

behaviour (Egashira et al., 2008). Anti-psychotic drugs have also been shown to reduce marble burying behaviour (Nicolas et al., 2006).

It is now a common belief that marble burying is simply a measure of digging behaviour (Deacon, 2006, Gyertyan, 1995) and one study showed that marble burying correlated with digging behaviour and digging behaviour was unaffected by the presence of marbles (Thomas et al., 2009). It could therefore be concluded that marble burying is a measure of normal behaviour, as digging is a habitual behaviour in mice, by which they explore their environment (Deacon, 2006).

As described previously, an estimated 50% of MND patients will experience cognitive/behavioural changes (Ringholz et al., 2005), and 10-15% of MND patients will be diagnosed with MND-FTD, the symptoms of which may include repetitive behaviours and apathy (Chan et al., 2015). Symptoms of FTD may be measured in mice by using measures of normal behaviour such as mothering, nest construction and self-grooming (Cathomas et al., 2015), in which apathy is presented by a lack of normal behaviour.

No cognitive investigations have been carried out in the TDP-43^{Q331K} mice, as yet. We propose therefore, that marble burying could be considered as a measure of habitual behaviour, which could be increased by the presence of FTD in the TDP-43^{Q331K} mice, as found in FTD patients (Chan et al., 2015). Conversely, the presence of FTD may cause apathy in the mice, reducing normal digging behaviour, and consequently marble burying activity. Current data from the running wheel study (chapter 3) suggests that the mice may show signs of apathy as they demonstrate reduced running activity, again a normal behaviour in mice, although this may be complicated by any pure motor deficit which is also present.

Marble burying has been used recently in mouse models of C9ORF72, in which mice with a $(G_4C_2)_{450}$ repeat expansion showed increased marble burying behaviour compared to wild type mice, interpreted as increased levels of anxiety (Jiang et al., 2016).

4.2. Aims

1. To assess whether riluzole is an effective treatment in TDP-43^{Q331K} mice.

2. To use electrophysiology to characterise the hindlimb denervation of TDP-43^{Q331K} mice.

3. To assess marble burying behaviour in TDP-43^{Q331K} mice as a measure of normal behaviour.

4.3. Materials and Methods

4.3.1. Ethics Statement

All mouse experiments were carried out under the terms of the UK Animals (Scientific Procedures) Act 1986 and under a UK Home Office project license. Mice were housed and cared for in accord with the Home Office Code of Practice for Housing and Care of Animals Used in Scientific Procedures.

All procedures were carried out under an appropriate UK Project Licence by personal licence holders.

ARRIVE guidelines (Kilkenny et al., 2010) were adhered to during this report.

4.3.2. Transgenic C57BL/6N Mice

TDP-43^{WT} and TDP-43^{Q331K} mice *(Mus musculus)* were originally generated on a C57BL/6NCrl background by insertion of c-myc-tagged human *TARDBP* (Arnold et al., 2013) and were subsequently backcrossed on to a C57BL/6NJ background before being deposited at the Jackson Laboratory (stock numbers 017907 and 017933, respectively).

Power analysis (see *table 2.4*) was used to calculate minimum group sizes to detect differences in latency to fall on the rotarod. Required group sizes were lower in females and therefore only female mice were used in this study. 14 TDP-43^{Q331K} mice were recruited to the riluzole and vehicle groups, 7 of which were also assessed by electrophysiological investigations. A group of 7 TDP-43^{WT} and 7 non-transgenic mice were also recruited as controls for the electrophysiological investigations. The number of mice recruited to each group eventually differed slightly from that planned as one mouse was culled due to encephalitis and the replacement was accidentally recruited to a different group. Mice were recruited at 25 days of age and remained on the study until 6 months of age.

For genotyping methods see section 2.3.4.

4.3.3. Housing

Mice were bred in a SPF environment, and transferred to a conventional facility for the studies described here. The facility uses a 12 h light/dark cycle, and room temperature is set to 21˚C. Cages were lined with fine sawdust (eco-pure flakes 6, Datesand, UK), which was changed weekly, a plastic house was in each cage and paper wool (Datesand, UK) was used as bedding material. Mice were fed 2018 rodent diet (Harlan, UK) ad libitum.

All mice were housed in littermate pairs or trios whenever possible.

4.3.4. Mass Spectrometry of Riluzole Compounds

Mass spectrometry of two riluzole batches was carried out at the University of Sheffield Mass Spectrometry facility.

Liquid chromatography-mass spectrometry was carried out on 0.4mg/ml samples of riluzole (Apollo Scientific, UK). Liquid chromatography was carried out on an Agilent 1260 Infinity instrument (Agilent, UK). Mass spectrometry was carried out on an Agilent 6530 Q-ToF instrument (Agilent, UK) with an injection volume of 1µl and a flow rate of 0.4ml/min.

4.3.5. Administration of Riluzole/Vehicle

Riluzole (Apollo Scientific, UK) was administered in the drinking water at 240ug/ml (approximately 70mg/kg) in 0.1% dimethyl sulfoxide (DMSO, Sigma-Aldrich, UK). All non-transgenic, TDP-43^{WT} and vehicle mice were administered 0.1% DMSO in the drinking water.

Mice were dosed from 30 days of age. Drinking water was changed every 2/3 days and drinking bottles changed weekly.

The primary investigator (JS) was blinded to the treatment group throughout the study.

4.3.6. Riluzole PK Study

An initial pharmacokinetic (PK) study was carried out in a cohort of 6 female non-transgenic mice, all of which were administered riluzole (as described in 4.3.4.) for 7 days. On the eighth day, half of the cohort were culled at 6am; half at 6pm (anticipated to represent peak and trough exposure respectively due to lighting hours).

Mice were culled with an overdose of pentobarbitone. Blood samples were taken by cardiac puncture. Spinal cords were removed and snap frozen in liquid nitrogen. Samples were sent for riluzole quantification using ultra-high performance liquid chromatography time of flight - TOF mass spectrometry using electrospray ionisation (Pharmidex, UK).

4.3.7. Neuroscoring and Weighing

Neuroscores and weight were monitored weekly in the morning. A modified neuroscoring system was devised in which forelimb tremor was measured by holding the mouse by the tail and scoring the forelimbs on a subjective scale of 0-3 (normal-strong). Resting tremor was measured by placing the mouse in the hand (0-no tremor, 1-intermittent tremor, 2-continuous tremor, 3-continuous tremor with large, whole body convulsions). A 'neuroscore' scale was used to delineate motor dysfunction (0-normal, 1-significant resting tremor, 2-abnormal gait, 3-severe waddle). Whenever possible, this scoring was carried out by the same investigator (JS).

Weight was monitored by placing the mice in a box on a set of scales (Kern, Germany) pre-set to zero.

These measurements were taken immediately prior to rotarod testing and in the same procedure room as the rotarod.

4.3.8. Accelerating Rotarod Test

Mice were placed on the accelerating rotarod (Jones & Roberts for mice 7650) for a period of 300 seconds. In this time the rotarod accelerates from 4 to 40 rpm and latency to fall was recorded for each mouse. All rotarod testing was carried out at a similar time

of day (am) and all testing consisted of two trials, with the highest score being recorded for analysis.

Mice were initially trained on the rotarod over 3 days (27-29 days of age) and underwent the first testing day at 30 days of age, being tested each week thereafter.

4.3.9. Catwalk Gait Analysis

The catwalk gait analysis system 7.1 (Noldus Information Technology B.V., Netherlands) was used to capture gait parameters at 1, 3, 6 and 10 months of age. Mice were placed on the glass floor of the catwalk system in complete darkness and left to walk/run freely. Whenever possible, 6 straight continuous runs were recorded and the 3 straightest, most continuous runs were selected for analysis. Catwalk software 7.1 was used to analyse the gait parameters of the mice. Microsoft excel was used to collate data within groups. Walking duration is the time taken to cross the length of the recording window (43.8 cm). Base of support is the distance between the paws whilst walking. For more details see *section 2.3.9.*

4.3.10. Electrophysiology

Electrophysiology was carried out at 1, 3 and 6 months of age in all non-transgenic, TDP-43^{WT}, TDP-43^{Q331K} riluzole/electrophysiology, and TDP-43^{Q331K} vehicle /electrophysiology groups (n = 7-8 per group). Mice were placed under gaseous anaesthesia (1–2% isoflurane, flow rate 1.0 L/min oxygen and nitrous oxide continuous inhalation through a nose cone). Body temperature was maintained using an electric heat pad (CWE, USA). The fur of the left hindlimb and lower back was shaved and depilatory cream used to remove any remaining fur.

All recordings were made using a Dantec Keypoint Focus EMG System (Optima, UK). For CMAP and repetitive stimulation, supramaximal stimuli were applied subcutaneously at the sciatic notch using twisted pair subdermal electrodes (Ambu Neuroline, UK). A grounding electrode was placed in the base of the tail (Ambu Neuroline, UK), and ring recording electrodes were placed circumferentially around the distal hindlimb muscles

(Alpine Biomed, Denmark), layered with Ten20 nerve conductive paste (Pulse Medical Ltd, UK), see *figure 4.1*.

The mouse was maintained under gaseous anaesthesia with stimulating electrodes over

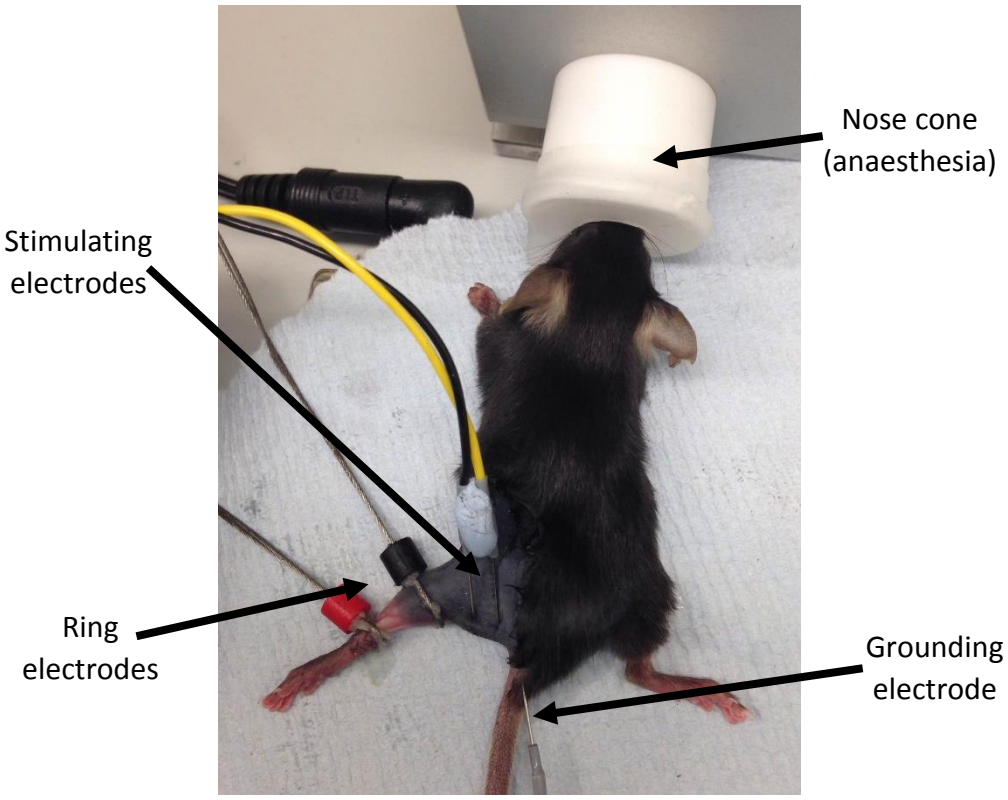

Figure 4. 1: Electrophysiology set-up.

the sciatic notch, a grounding electrode in the base of the tail and ring electrodes around the hindlimb.

CMAPs were acquired by applying a single, square wave electrical impulse of 0.1ms duration to the sciatic notch. The position of the subcutaneous stimulating electrodes was trialled to ensure that a response was obtained using a stimulating current of around 1-2mA. The stimulation intensity was then increased until no further increase in amplitude was seen and hence a supramaximal response elicited.

The electrodes were then held in the same place whilst repetitive stimulation was carried out. This involved ten pulses, applied at 3Hz, 10Hz and 50Hz. The area and amplitude of the response decrement were recorded. Analyses were undertaken using the change in amplitude/area seen on the 10th response relative to the first response (as typically employed in the clinical investigation of neuromuscular junction disorders) and also the relative change seen on the final response.

At 6 months of age, in mice for which electrophysiology was non-recovery, EMG recordings were taken using a 30 gauge concentric cable electrode (Ambu Neuroline, UK). Recordings were taken in the gastrocnemius and tibialis anterior muscles.

Electrophysiology training and analysis was carried out with the help of Dr James Alix.

4.3.11. Marble Burying

Mice were placed in a semi-light room in cages 19cm deep x 33cm long x 21cm wide, filled with sawdust approximately 8cm deep. 24 marbles were placed in 4 x 6 grid pattern on the surface of the sawdust (see *figure 4.2A*). Mice were left undisturbed for 1 hour and then returned to their home cage. Marbles were counted as buried when 2/3 covered by sawdust (see *figure 4.2B*).

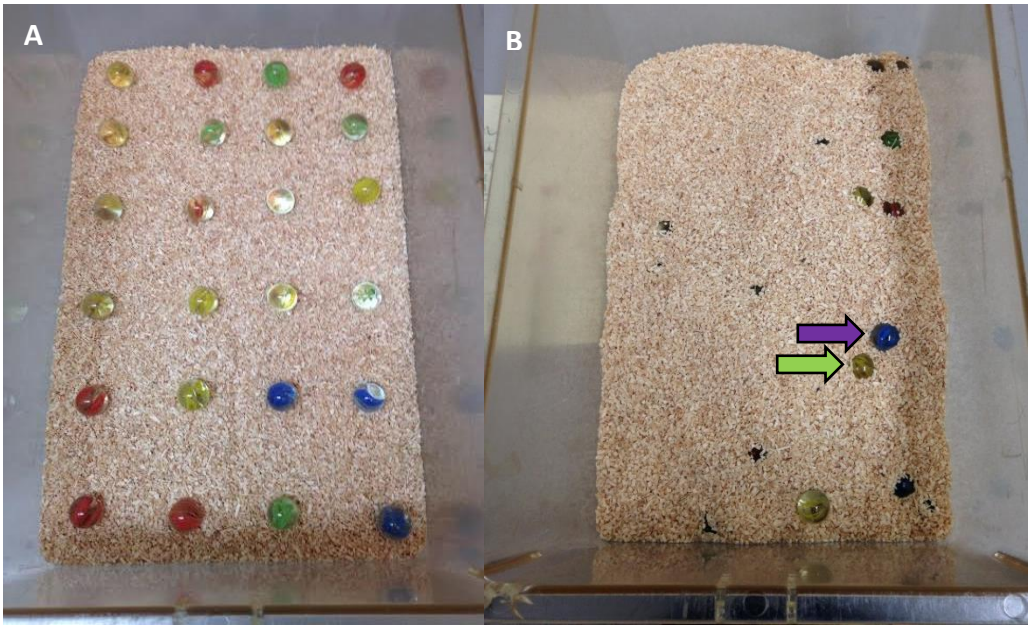

Figure 4. 2: Marble burying cage layout (A) and cage after marble burying (B).

As shown in A, marbles are placed in a 4 x 6 grid pattern. Post marble burying (B), marbles are counted as buried if 2/3 covered by sawdust (green arrow), marbles are not counted as buried if they are <2/3 covered by sawdust (purple arrow).

4.3.15. Statistics

GraphPad Prism 6 was used for all statistical analyses (GraphPad, San Diego, CA, USA). Two-way ANOVA with Tukey's post-test was used unless otherwise stated. All data are presented as a mean and standard deviation.

4.4. Results

4.4.1. Mass Spectrometry of Riluzole

Before administering riluzole to the mice, it was noted that the colour of the substance was different to that used in a simultaneous study within the department. Therefore, a sample of each riluzole batch was sent for mass spectrometry analysis to ensure they were suitably pure.

The total ion current (TIC) intensities of two riluzole samples are shown in *figure 4.3*. Both samples show a peak in the spectra at approximately 6.5 and 7.9 mins.

In both spectra the 6.5 min peak is much larger than the 7.9 min peak at approximately $4.6x10^7$, this is representative of the riluzole compound. The 7.9 min peak is larger in sample 2 at $0.4x10^7$, compared to sample 1 where it is $0.2x10^7$, this is representative of an impurity which is still within acceptable limits. These data confirm identity and purity of the riluzole batch used.

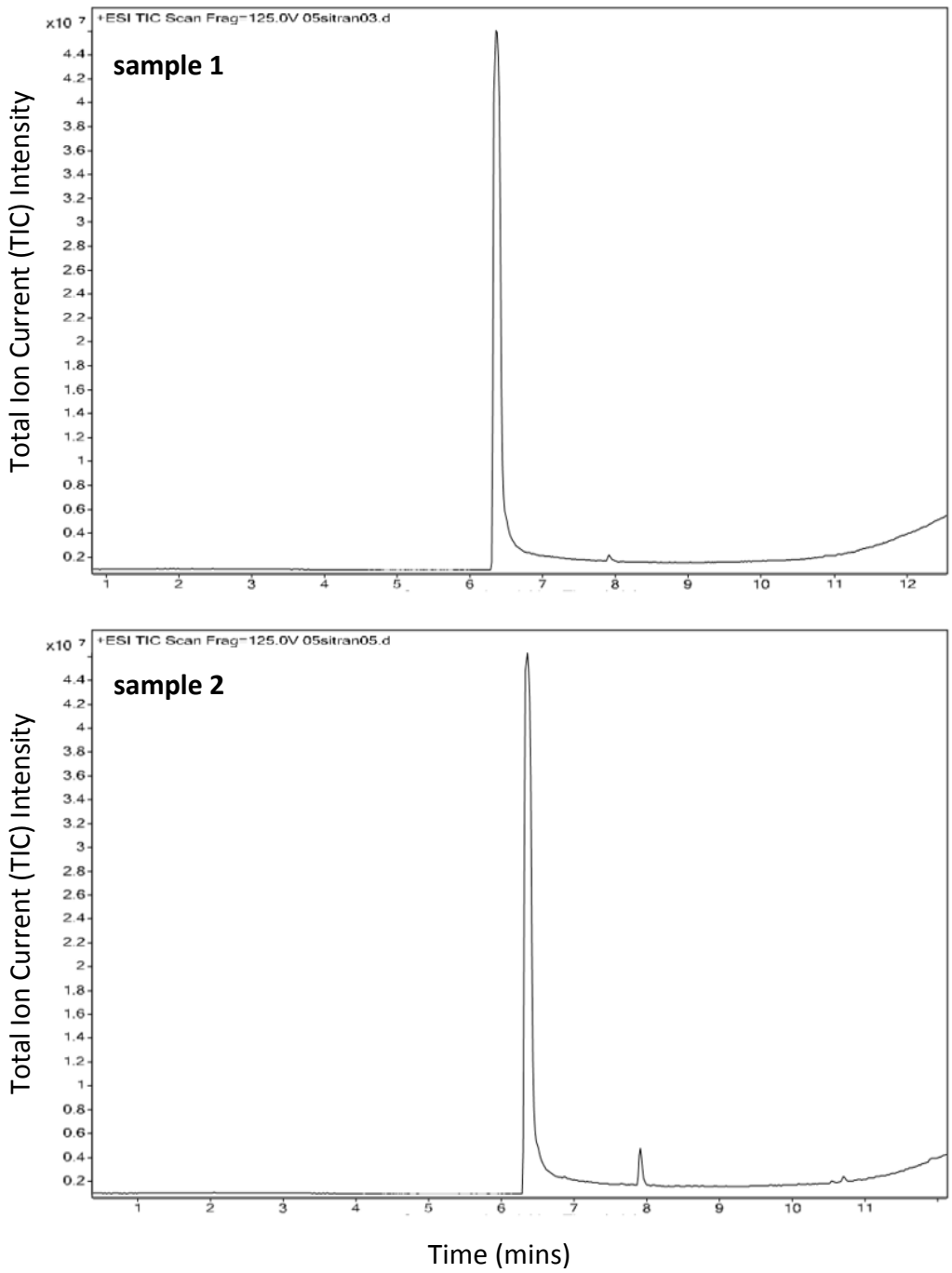

Figure 4. 3: Total ion current (TIC) intensity spectra of riluzole samples.

Mass spectrometry shows both batches contain a single major peak although the impurity peak is slightly larger in batch 2 they are both >95% pure.

4.4.2. Riluzole PK Study

A PK study was carried out to ensure that the riluzole was penetrating the blood brain barrier at therapeutic levels which match those found in humans.

Riluzole levels in blood and spinal cord were detected at anticipated peak and trough exposures at the end and the beginning of the night cycle respectively (*table 4.1*). Peak levels were higher than trough in both blood (116.2 ±54.4nM peak vs 78.7 ± 8.3nM trough) and spinal cord (307.4 ±173.6nM peak vs 220.8 ±43.8nM trough), with a similar spinal cord/blood ratio in both groups (2.5 ±0.6nM peak and 2.8 ±0.4nM trough).

Therefore, as expected, riluzole penetrated the blood brain barrier and more riluzole was consumed during the dark hours of the light-dark cycle.

Table 4. 1: Riluzole concentrations (uHPLC/TOF Mass spec). *Mean riluzole concentrations in the blood and spinal cord for 7-day dosed mice at peak and trough dosage (n = 3, mean +/- SD).*

	Blood (nM)	**Spinal cord (nM)**	**Spinal cord/blood ratio**
Peak	116.2 (±54.4)	307.4 (±173.6)	2.5 (±0.6)
Trough	78.7 (± 8.3)	220.8 (±43.8)	2.8 (±0.4)

4.4.3. Neuroscoring

Neuroscoring was carried out weekly in all TDP-43^{Q331K} mice, both riluzole and vehicle groups.

Neuroscoring consisted of 3 measurements, forelimb tremor, hindlimb tremor and an overall neuroscore, all measured on a scale of 0-3. No difference was evident between the riluzole and vehicle groups in any measurement on a two-way ANOVA.

Both groups presented with a median forelimb tremor score of 1 (mild tremor when lifted by the tail base) from the beginning of data collection (5 weeks of age) and this remained at 1 throughout the study. Some mice developed to a score of 2 (moderate tremor) but most mice maintained a forelimb tremor score of 1 throughout.

Both groups presented mostly with a hindlimb tremor score of 0, with a few mice presenting with a score of 1 at 5 weeks of age. Hindlimb tremor progressed to a median score of 3 in both groups by 25 weeks of age. Most mice progressed to a hindlimb

tremor score of 3 (continuous resting tremor with whole-body convulsions), whilst several mice progressed to a hindlimb tremor score of 2 (continuous resting tremor).

A median overall neuroscore of 0 was found in both groups at 5 weeks of age, progressing to a median neuroscore of 3 by 25 weeks of age, suggesting that most mice developed to a neuroscore of 3 (severe waddle), whilst some mice progressed to a neuroscore of 2 (abnormal gait).

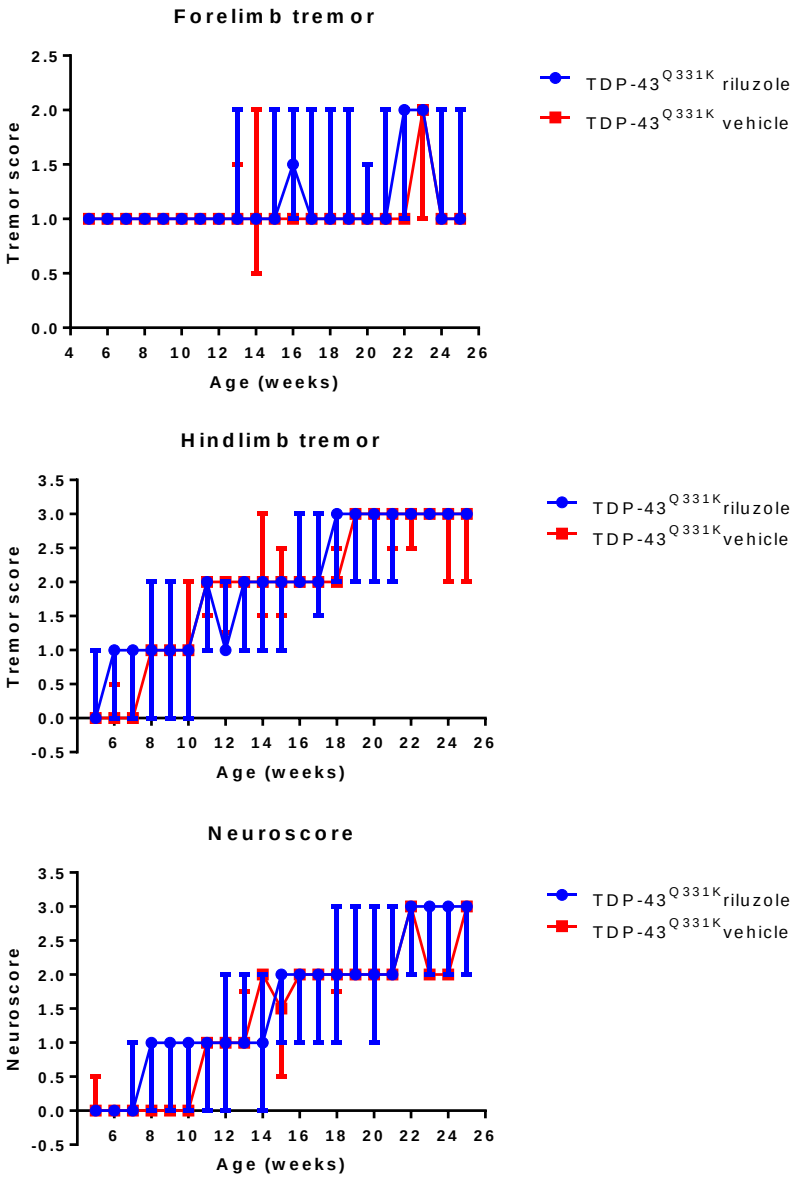

Figure 4. 4: Median neuroscores over time.

Graphs showing median (± interquartile range) forelimb tremor, hindlimb tremor and neuroscores based on a scale of 0-3 from 5-25 weeks of age in riluzole and vehicle female TDP-43^{Q331K} mice (n = 13-15).

4.4.4. Body Weight

Body weight was measured weekly in the riluzole and vehicle groups from 5-23 weeks of age (female TDP-43^{Q331K}). As found previously, weight increased with age. In the riluzole group (n = 15), weight increased from 15.4 ± 1.4g at 5 weeks, to 33.6 ± 6.8g at 23 weeks of age. In the vehicle group (n = 13), weight increased from 15.5 ± 1.2g at 5 weeks of age to 30.1 ± 5.1g at 23 weeks of age. There was no significant difference in weight between each group on a two-way ANOVA with repeated measures. Riluzole, therefore, had no effect on the weight of TDP-43^{Q331K} mice.

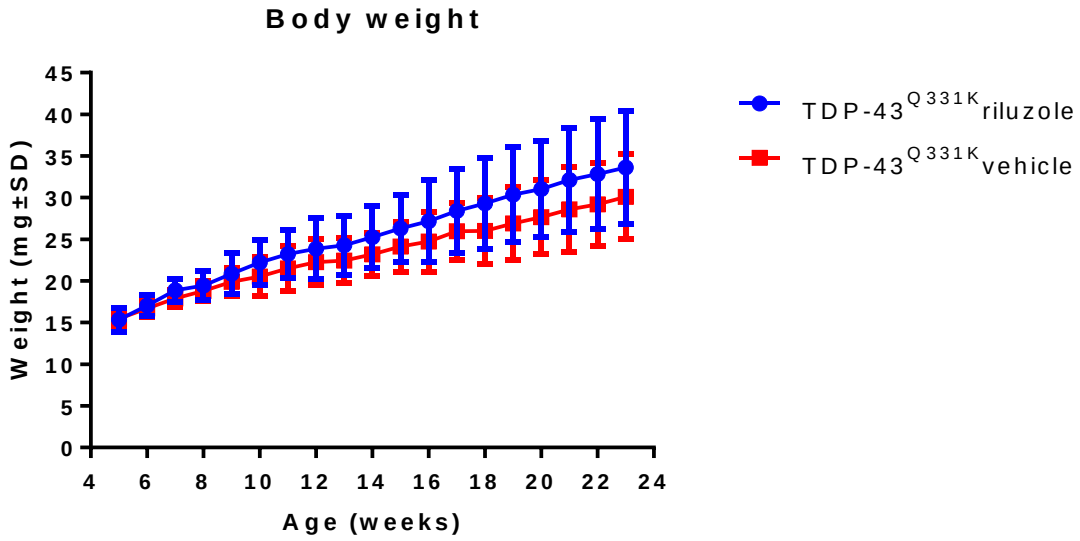

Figure 4. 5: Mean body weight (±SD) in vehicle and riluzole TDP-43^{Q331K} mice.

Body weight increased from 5-23 weeks of age in the riluzole and vehicle groups (female, TDP-43^{Q331K}, n = 13-15). There is no significant difference in weight between the two groups (two-way ANOVA with repeated measures).

4.4.5. Rotarod Performance

Rotarod performance was measured weekly in the riluzole and vehicle groups from 5-23 weeks of age (female TDP-43^{Q331K}). As found previously, rotarod performance decreased with age. In the riluzole group (n = 15), rotarod performance declined from 257.2 ± 54.3s at 5 weeks, to 168.7 ± 49.5s at 23 weeks of age. In the vehicle group (n = 13), rotarod performance declined from 264.5 ± 49.6s at 5 weeks of age to 182.5 ± 63.3s

at 23 weeks of age. There was no significant difference in rotarod performance between each group on a two-way ANOVA with repeated measures. Riluzole, therefore, showed no treatment effect on rotarod performance.

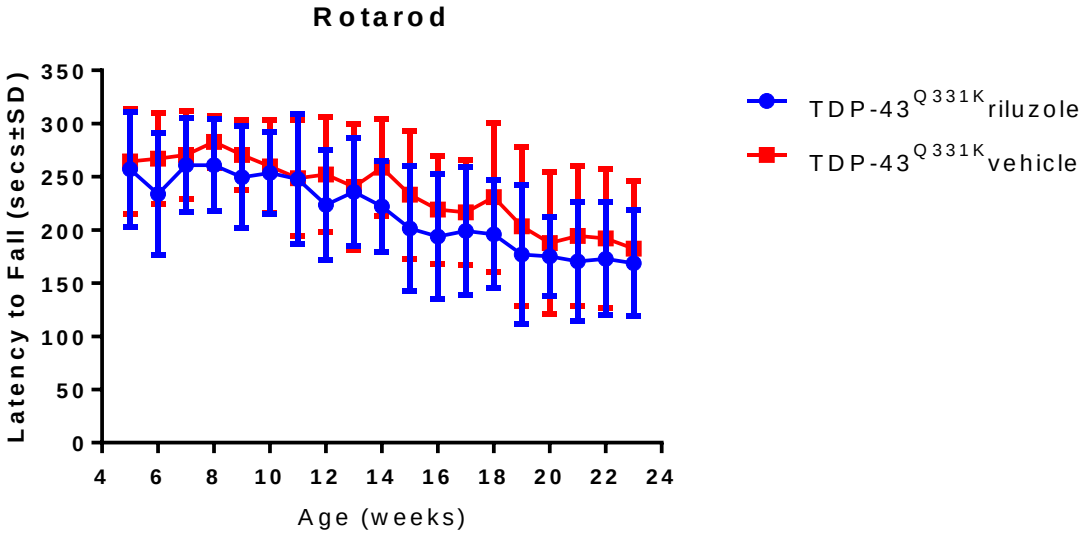

Figure 4. 6: Mean rotarod performance (±SD) in vehicle and riluzole TDP-43^{Q331K} mice.

Rotarod performance decreased from 5-23 weeks of age in the riluzole and vehicle groups (female, TDP-43^{Q331K}, n = 13-15). There is no significant difference in latency to fall between between the two groups (two-way ANOVA with repeated measures).

4.4.6. Catwalk Gait Analysis

Gait analysis was carried out in all groups at 3 and 6 months of age. All numbers for significant findings are recorded in *table 4.2*.

Duration (the time taken to cross the recording area of the catwalk equipment) showed no differences between the riluzole and vehicle dosed TDP-43^{Q331K} groups or between the non-transgenic and TDP-43^{WT} groups at 3 or 6 months of age. However, both TDP-43^{Q331K} groups had a significantly longer duration compared to the non-transgenic and TDP-43^{WT} groups at 3 and 6 months.

Forelimb base of support (the distance between the forepaws during walking) showed no differences between any of the groups at 3 or 6 months.

Hindlimb base of support (the distance between the hindpaws during walking) showed no differences between the riluzole and vehicle TDP-43^{Q331K} groups or between the non-

transgenic and TDP-43^{WT} groups at 3 or 6 months of age. However, the TDP-43^{Q331K} groups had a significantly increased hindlimb BOS compared to the control groups at 3 and 6 months of age.

Diagonal stepping (the percentage of time spent walking in a diagonal stepping pattern: left forepaw placed at the same time as right hindpaw; right forepaw placed at the same time as left hindpaw) showed no differences between the riluzole and vehicle TDP-43^{Q331K} groups or between the non-transgenic and TDP-43^{WT} groups at 3 or 6 months of age. However, both TDP-43^{Q331K} groups had significantly less diagonal stepping compared to the control groups at 3 and 6 months.

Three paw stepping (the percentage of time spent walking with three paws on the surface) showed no significant differences between any groups.

Four paw stepping (the percentage of time spent walking with four paws on the surface) showed no differences between the riluzole and vehicle TDP-43^{Q331K} groups or between the non-transgenic and TDP-43^{WT} groups at 3 or 6 months of age. However, both TDP-43^{Q331K} groups had significantly more four paw stepping compared to the control groups at 3 and 6 months.

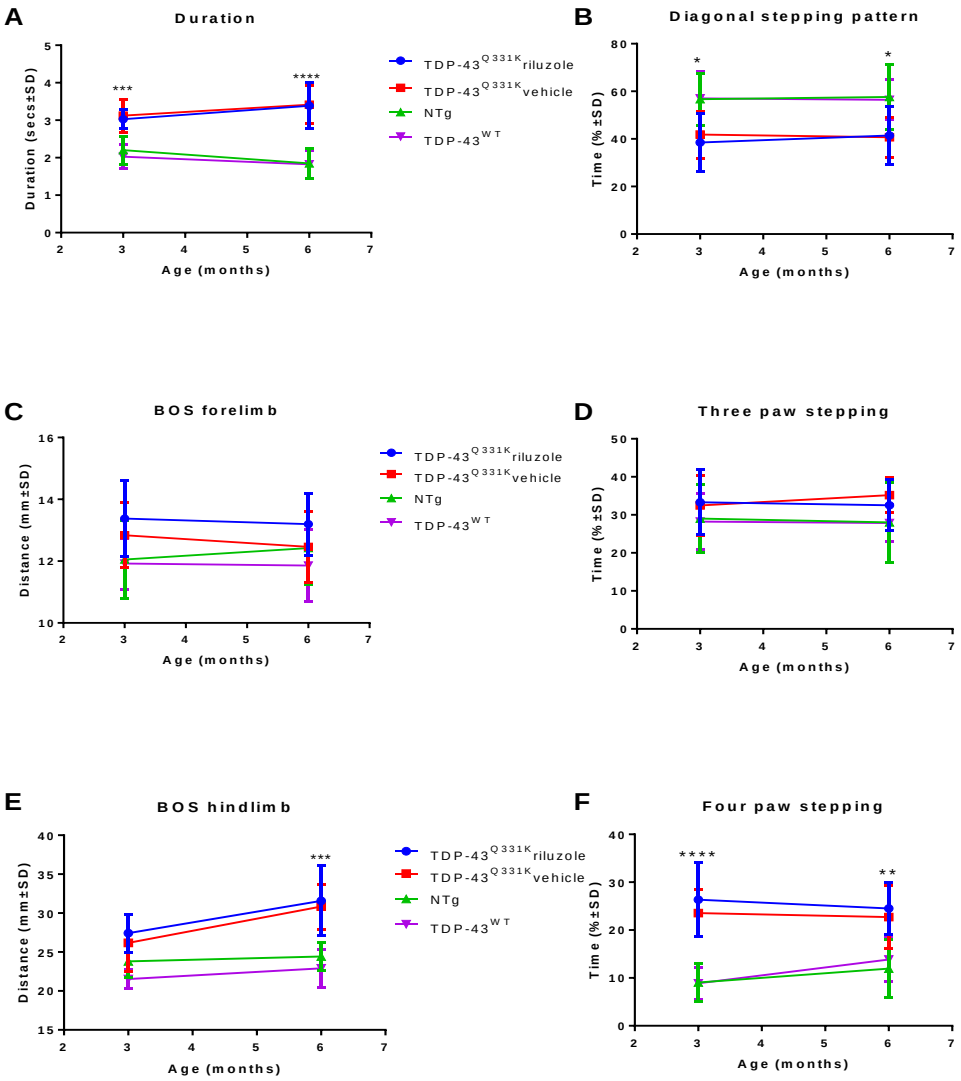

Figure 4. 7: Catwalk gait analysis: mean (±SD) duration (A), diagonal stepping (B), forelimb BOS (C), three paw stepping (D), hindlimb BOS (E) and four paw stepping (F).

Mean duration (A), forelimb BOS (C) and hindlimb BOS (E) for all groups at 3 and 6 months of age (n = 7-14) showing significantly longer walking duration in both TDP-43^{Q331K} groups at 3 and 6 months of age compared to the control groups (p<0.001, p<0.0001 respectively) and significantly increased hindlimb BOS at in both TDP-43^{Q331K} groups at 6 months of age compared to the control groups (p<0.001). Percentage of time spent stepping in a diagonal (B), three paw (D) and four paw (F) pattern for all groups at 3 and 6 months of age (n = 7-14). Diagonal stepping was significantly lower in the TDP-43^{Q331K} groups compared to the control groups at 3 and 6 months of age (p<0.05) and four paw stepping was significantly increased in the TDP-43^{Q331K} groups compared to the control groups at 3 and 6 months of age (p<0.0001, p<0.01 respectively).

Forelimb swing time (the mean time between lifting a forepaw and placing it back down) showed no significant differences between any groups at 3 months of age. However, both TDP-43^{Q331K} groups had a significantly increased forelimb swing compared to the control groups at 6 months of age.

Forelimb stride length (the mean distance between forepaw prints) showed no significant differences between any groups at 3 or 6 months of age.

Forelimb duty cycle (the length of time a paw is on the surface, expressed as a percentage of the total time taken for each stride) showed no differences between the riluzole and vehicle TDP-43^{Q331K} groups or between the non-transgenic and TDP-43^{Q331K} groups at 3 or 6 months of age. However, both TDP-43^{Q331K} groups had a significantly higher duty cycle compared to the control groups at 3 and 6 months.

Hindlimb swing time (the mean time between lifting a hindpaw and placing it back down) showed no significant differences between any groups at 3 months of age. However, both TDP-43^{Q331K} groups had a significantly increased hindlimb swing compared to the control groups at 6 months of age.

Hindlimb stride length (the mean distance between hindpaw prints) showed no significant differences between any groups at 3 or 6 months of age.

Hindlimb duty cycle (the length of time a paw is on the surface, expressed as a percentage of the total time taken for each stride) showed no differences between the riluzole and vehicle TDP-43^{Q331K} groups or between the control groups at 3 or 6 months of age. However, both TDP-43^{Q331K} groups had a significantly higher duty cycle compared to the control groups at 3 and 6 months.

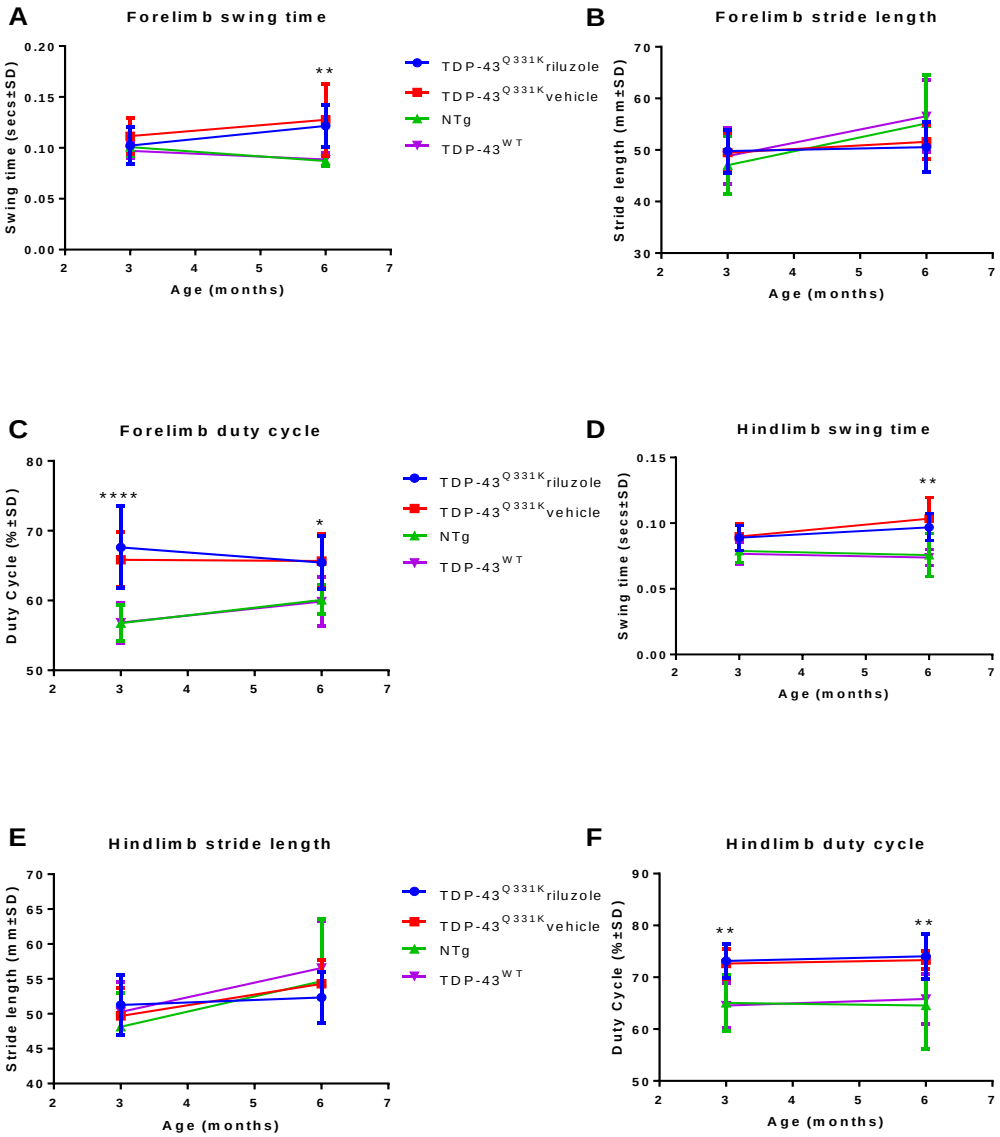

Figure 4. 8: Mean (±SD) catwalk gait analysis: forelimb swing time (A), stride length (B) and duty cycle (C), hindlimb swing time (D), stride length (E) and duty cycle (F).

Forelimb swing time (A), stride length (B) and duty cycle (C) for all groups at 3 and 6 months of age (n = 7-14). Forelimb swing time was significantly increased in the TDP-43^{Q331K} groups compared to the control groups at 6 months of age (p<0.01) and forelimb duty cycle was significantly increased in the TDP-43^{Q331K} groups compared to the control groups at both 3 and 6 months of age (p<0.0001, p<0.01 respectively). Hindlimb swing time (D), stride length (E) and duty cycle (F) for all groups at 3 and 6 months of age (n = 7-14). Hindlimb swing time was significantly increased in the TDP-43^{Q331K} groups compared to the control groups at 6 months of age (p<0.01) and hindlimb duty cycle was significantly increased in the TDP-43^{Q331K} groups compared to the control groups at both 3 and 6 months of age (p<0.01).

Table 4. 2: Table of significant catwalk gait analysis findings. ** = p<0.05, ** = p<0.01, *** = p<0.001, **** = p<0.0001.*

Catwalk parameter	**Age**	**TDP-43^{Q331K} riluzole**	**TDP-43^{Q331K} vehicle**	**TDP-43^{WT}**	**Non-transgenic**	**Significance of the difference between the TDP-43^{Q331K} and control groups**
Duration	3	3±0.3s	3.1±0.4	2±0.3s	2.2±0.4s	***
	6	3.4±0.6s	3.4±0.5s	1.8±0.4s	1.8±0.4s	****
Hindlimb BOS	6	31.6±4.5mm	30.8±2.9mm	22.9±2.5mm	24.4±1.8mm	***
Diagonal stepping	3	38.5±12.2%	41.8±9.9%	57±11.4%	56.7±11%	*
	6	41.4±12%	40.7±8.4%	56.4±8.3%	57.6±13.8%	*
Four paw stepping	3	26.3±7.7%	23.5±4.9%	8.9±3.4%	9.1±3.9%	****
	6	24.5±5.5%	22.7±6.5%	13.8±4.6%	11.9±6.1%	**
Forelimb swing time	6	0.12±0.02s	0.13±0.04s	0.09±0.01s	0.09±0.01s	**
Forelimb duty cycle	3	67.6±5.9%	65.8±4%	56.8±2.9%	56.8±2.6%	****
	6	65.4±3.8%	65.7±3.8%	59.9±3.6%	60.1±2.1%	*
Hindlimb swing time	6	0.1±0.01s	0.1±0.02s	0.07±0.01s	0.08±0.02s	**
Hindlimb duty cycle	3	73.2±3.2%	72.6±2.9%	64.6±4.4%	65.1±5.4%	**
	6	74±4.4%	73.3±1.7%	65.8±4.7%	64.6±8.4%	**

4.4.7. CMAP

CMAP amplitude, representative of the amount of functional motor axons and muscle fibres, was measured in the hindlimb of mice in all groups at 1, 3 and 6 months of age. CMAP amplitude showed no differences between the riluzole and vehicle TDP-43^{Q331K} groups or between the non-transgenic and TDP-43^{Q331K} groups at 1, 3 or 6 months of age. However, both TDP-43^{Q331K} groups had a significantly lower CMAP amplitude compared to the non-transgenic and TDP-43^{WT} groups at 1 month (22.6±6.4mV TDP-43^{Q331K} riluzole vs 24.7±6.7mV TDP-43^{Q331K} vehicle vs 34.6±2.7mV non-transgenic vs 32.9±2.4mV TDP-43^{WT}, $p<0.05$, two-way ANOVA), 3 months (26.9±4.5mV TDP-43^{Q331K} riluzole vs 26.3±6.7mV TDP-43^{Q331K} vehicle vs 49.2±8.9mV non-transgenic vs 50.1±5.1mV TDP-43^{WT}, $p<0.0001$, two-way ANOVA) and 6 months (24.6±7mV TDP-43^{Q331K} riluzole vs 25.3±5.9mV TDP-43^{Q331K} vehicle vs 46.2±5.7mV non-transgenic vs 45.7±5.2mV TDP-43^{WT}, $p<0.0001$, two-way ANOVA), suggestive of a lower number of functional motor axons in the TDP-43^{Q331K} mice throughout.

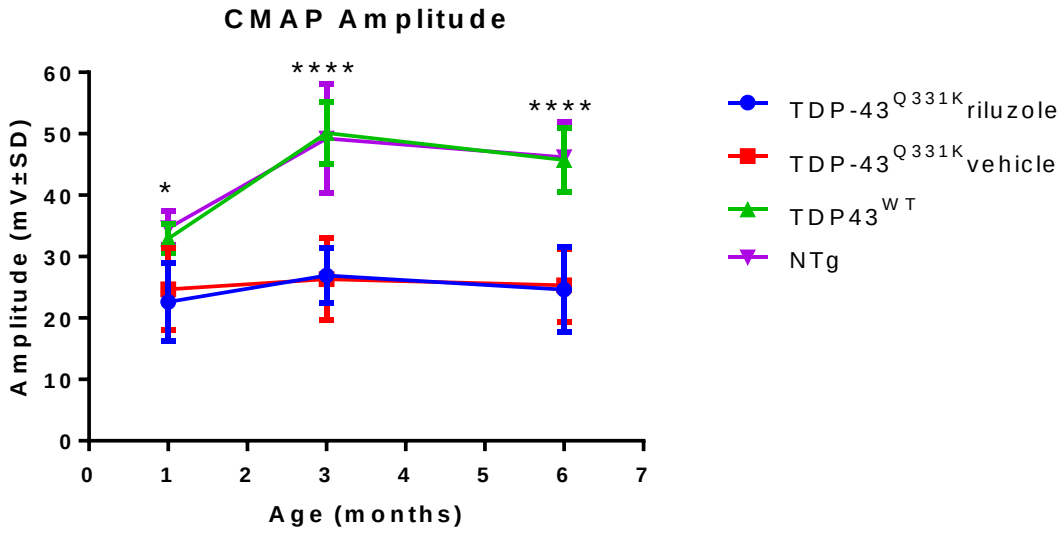

Figure 4. 9: CMAP amplitude (±SD) at 1, 3 and 6 months of age.

CMAP amplitude was recorded in the hindlimb of all mice (n = 7-8) at 1, 3 and 6 months of age. CMAP was significantly lower in TDP-43^{Q331K} groups compared to the control groups at 1 ($p<0.05$), 3 ($p<0.0001$) and 6 months ($p<0.0001$).

4.4.8. Repetitive Stimulation Total Decrement

Repetitive stimulation was carried out at 1, 3 and 6 months of age to investigate the functionality of the NMJs. In healthy subjects, the response to repetitive stimulation would be expected to remain at a steady state; a reduction in response could be suggestive of disease.

4.4.8.1. Differences with Age

Repetitive stimulation was carried out at 3Hz in all groups at 1, 3 and 6 months of age. The decrement between stimuli 1 and 10 showed no significant differences at any age between the non-transgenic and TDP-43^{WT} mice. Although non-significant, the riluzole group did show a consistently smaller decrement compared to the vehicle group throughout, indicative of a potential treatment effect. Differences between the TDP-43^{Q331K} groups and the control groups were evident throughout but not consistently significant (see *figure 4.12*). However, the TDP-43^{Q331K} groups had a larger decrement than the control groups at 1 month (-4.3±3.5% TDP-43^{Q331K} riluzole vs -3.1±3.1% TDP-43^{Q331K} vehicle vs -0.5±3.4% non-transgenic vs -0.6±5.3% TDP-43^{WT}), 3 months (-6.4±2.1% TDP-43^{Q331K} riluzole vs -4.2±2.7% TDP-43^{Q331K} vehicle vs -1.4±0.9% non-transgenic vs 0.1±2.7% TDP-43^{WT}) and 6 months (-3.2±0.4% TDP-43^{Q331K} riluzole vs -5±3.5% TDP-43^{Q331K} vehicle vs -0.7±0.9% non-transgenic vs -0.8±1.9% TDP-43^{WT}).

The data for 3Hz was very variable, and therefore difficult to assess changes over time within groups. At 10Hz, a trend can be seen in the TDP-43^{Q331K} riluzole group in which repetitive stimulation response decreases over time. However, there are no obvious trends in any other groups over time. 50Hz was only measured at 6 months and so there are no data over time for this parameter.

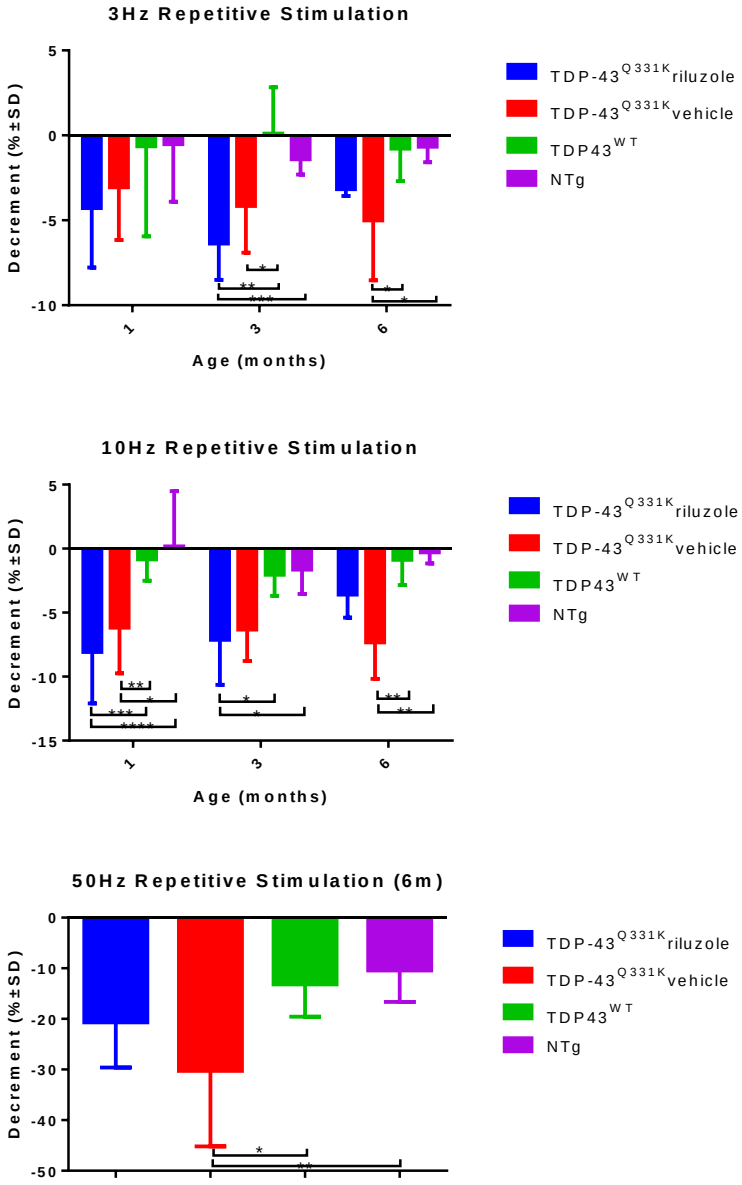

Figure 4. 10: Repetitive stimulation – total decrement from first to last stimulus.

The decrement between stimuli 1 and 10 were recorded at 3 and 10Hz in the hindlimb of all groups (n = 7-8) at 1, 3 and 6 months of age. 50Hz was carried out in the same mice at 6 months of age. Repetitive stimulation at 3Hz was significantly different for the effect of group ($p<0.001$), but not for the effect of age on a two-way ANOVA with repeated measures and Tukey's post-tests. Repetitive stimulation at 10Hz was significantly different for the effect of group ($p<0.0001$), but not for the effect of age on a two-way ANOVA with repeated measures and Tukey's post-tests. Repetitive stimulation at 50Hz was significantly different on a one-way ANOVA with Tukey's post-tests ($p<0.01$). Multiple comparisons were also made (= $p<0.05$, ** = $p<0.01$, *** = $p<0.001$, **** = $p<0.0001$).*

4.4.8.2. Analysis of Individual Stimuli at 1 Month

Analysis of each individual stimulus response was plotted to enable further interpretation and to ensure that stimulus responses were not decreasing and returning to baseline between stimuli 1 and 10.

With a stimulus of 3Hz at 1 month of age (*figure 4.13*), a slight decrement in response is shown over time in all groups in response to repeated stimuli. Overall, there is no significant difference between groups on a two-way ANOVA with repeated measures, and multiple comparisons show no differences between groups for any stimuli.

With a stimulus of 10Hz (*figure 4.13*), a decrement in response is shown over time in both TDP-43^{Q331K} groups, whereas the TDP-43^{WT} and non-transgenic groups show no decrease in response to repeated stimuli. Overall, there is a significant difference between groups on a two-way ANOVA with repeated measures ($p<0.001$), and multiple comparisons show no differences between the TDP-43^{Q331K} riluzole and vehicle groups, no differences between the TDP-43^{WT} and non-transgenic groups. Some differences were found between TDP-43^{Q331K} groups and control groups but these were inconsistent across stimuli.

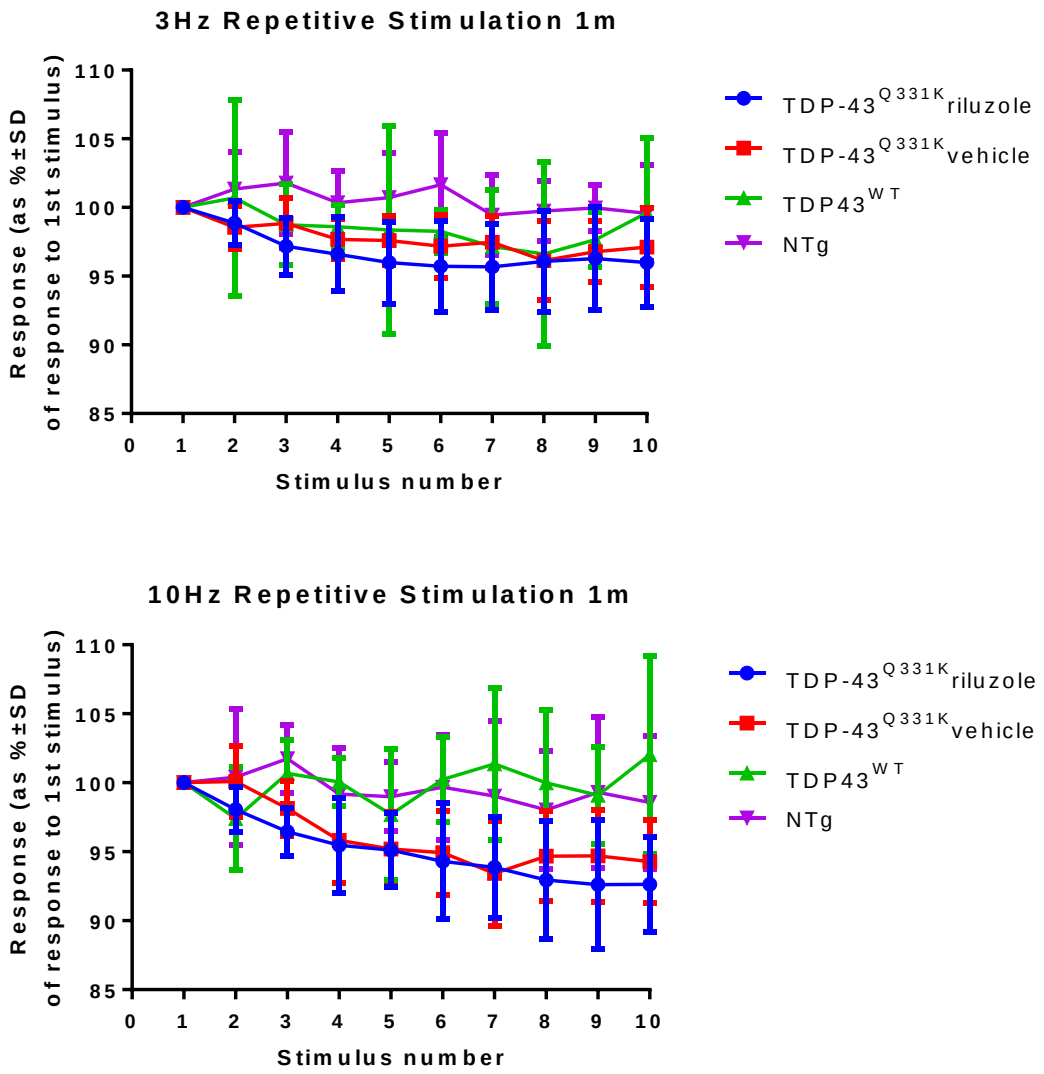

Figure 4. 11: Repetitive stimulation showing individual stimuli at 1 month.

The response (±SD) for each stimuli normalised to the first stimulus at 3, 10, and 50Hz in the hindlimb of all groups (n = 7-8) at 1 month of age. At 3Hz, no significant difference was found between groups on a two-way ANOVA with repeated measures and Tukey's post-tests. At 10Hz, there was a significant difference (p<0.001) between groups on a two-way ANOVA with repeated measures and Tukey's post-tests.

4.4.8.3. Analysis of Individual Stimuli at 3 Months

With a stimulus of 3Hz at 3 months of age (*figure 4.14*), a slight decrement in response is shown over time in both TDP-43^{Q331K} groups, whereas the TDP-43^{WT} and non-transgenic groups show little or no decrease in response to repeated stimuli. Overall, there is a significant difference between groups on a two-way ANOVA with repeated

measures ($p<0.0001$), and multiple comparisons show no differences between the TDP-43^{Q331K} riluzole and vehicle groups, no differences between the TDP-43^{WT} and non-transgenic groups, and significant differences between the TDP-43^{Q331K} riluzole group and the control groups from stimulus 3 ($p<0.01$), a consistent significant difference between the TDP-43^{Q331K} vehicle group and TDP-43^{WT} from stimulus 6 ($p<0.01$), and a significant difference between the TDP-43^{Q331K} vehicle group and non-transgenic group at stimulus 10 ($p<0.05$).

With a stimulus frequency of 10Hz (*figure 4.14*), a decrement in response is shown over time in both TDP-43^{Q331K} groups, whereas the TDP-43^{WT} and non-transgenic groups show no decrease in response to repeated stimuli. Overall, there is a significant difference between groups on a two-way ANOVA with repeated measures ($p<0.001$). Multiple comparisons show no differences between the TDP-43^{Q331K} riluzole and vehicle groups, no differences between the TDP-43^{WT} and non-transgenic groups, and no differences between the TDP-43^{Q331K} riluzole group and the control groups. Significant differences were found between the TDP-43^{Q331K} riluzole group and the control groups from stimulus 3 ($p<0.01$), a significant difference between the TDP-43^{Q331K} vehicle group and non-transgenic from stimulus 5 ($p<0.01$), and a significant difference between the TDP-43^{Q331K} vehicle group and TDP-43^{WT} non-transgenic group at stimulus 6 ($p<0.01$).

It should be noted that, although non-significant, the riluzole group show a consistently reduced decrement compared to the vehicle group throughout both the 3Hz and 10Hz stimulations, showing a potential treatment effect.

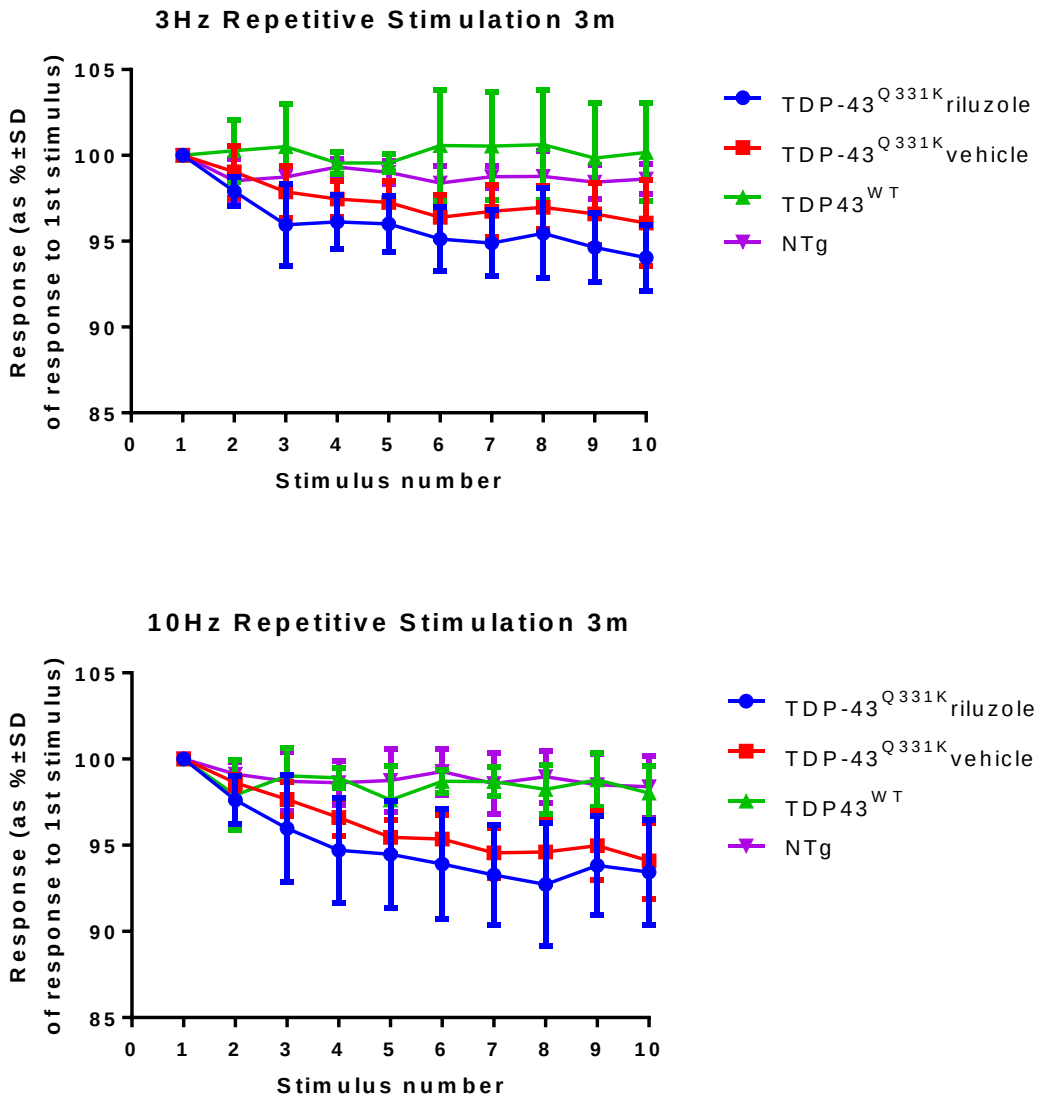

Figure 4. 12: Repetitive stimulation showing individual stimuli at 3 months.

The response (±SD) for each stimuli normalised to the first stimulus at 3, 10, and 50Hz in the hindlimb of all groups (n = 7-8) at 3 months of age. At 3Hz, there was a significant difference (p<0.0001) between groups on a two-way ANOVA with repeated measures and Tukey's post-tests. At 10Hz, there was a significant difference (p<0.001) between groups on a two-way ANOVA with repeated measures and Tukey's post-tests.

4.4.8.4. Analysis of Individual Stimuli at 6 Months

With a stimulus of 3Hz at 6 months of age (*figure 4.15*), a decrement in response is shown over time in both TDP-43^{Q331K} groups, whereas the TDP-43^{WT} and non-transgenic groups show no decrease in response to repeated stimuli. Overall, there is a significant

difference between groups on a two-way ANOVA with repeated measures ($p<0.001$). Multiple comparisons show no differences between the TDP-43^{Q331K} riluzole and vehicle groups, no differences between the TDP-43^{WT} and non-transgenic groups but significant differences between the TDP-43^{Q331K} groups and the control groups from stimulus 7 ($p<0.05$).

With a stimulus of 10Hz (*figure 4.15*), a decrement in response is shown over time in both TDP-43^{Q331K} groups, whereas the TDP-43^{WT} and non-transgenic groups show no decrease in response to repeated stimuli. Overall, there is a significant difference between groups on a two-way ANOVA with repeated measures ($p<0.001$), and multiple comparisons show no differences between the TDP-43^{Q331K} riluzole and vehicle groups, no differences between the TDP-43^{WT} and non-transgenic groups and no differences between the TDP-43^{Q331K} riluzole group and the control groups. However, there are significant differences between the TDP-43^{Q331K} vehicle group and the control groups from stimulus 6 ($p<0.05$). This shows that there is potentially a slight rescue effect in the riluzole group, given that the repetitive stimulation responses are not significantly lower compared to the control groups, whereas the vehicle group are.

With a stimulus of 50Hz (*figure 4.15*), a decrement in response is shown over time in all groups in response to repeated stimuli. Overall, there is a significant difference between groups on a two-way ANOVA with repeated measures ($p<0.01$), and multiple comparisons show no differences between the TDP-43^{Q331K} riluzole and vehicle groups, no differences between the TDP-43^{WT} and non-transgenic groups, no differences between the TDP-43^{Q331K} riluzole group and the control groups, and significant differences between the TDP-43^{Q331K} vehicle group and the control groups from stimulus 4 ($p<0.05$), again, suggestive of a slight treatment effect in the riluzole group.

As with the 3 month data, it should be noted that the riluzole group shows a significantly reduced decrement compared to the vehicle group at 3, 10 and 50Hz, showing a possible treatment effect.

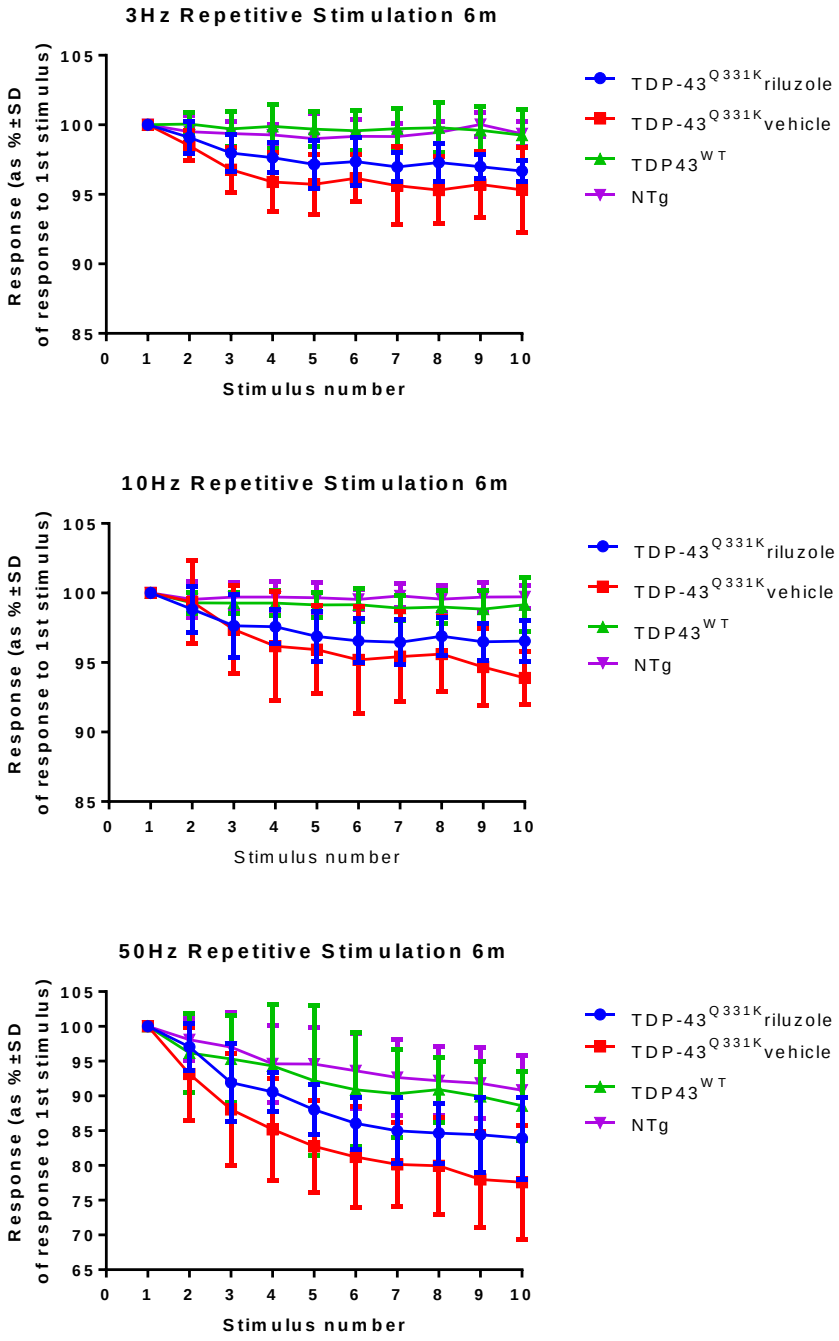

Figure 4. 13: Repetitive stimulation showing individual stimuli at 6 months.

The response (±SD) for each stimulus normalised to the first stimulus at 3, 10, and 50Hz in the hindlimb of all groups (n = 7-8) at 6 months of age. At 3Hz, there was a significant difference ($p<0.001$) between groups on a two-way ANOVA with repeated measures and Tukey's post-tests. At 10Hz, there was a significant difference ($p<0.001$) between groups on a two-way ANOVA with repeated measures and Tukey's post-tests. At 50Hz, there was a significant difference ($p<0.01$) between groups on a two-way ANOVA with repeated measures and Tukey's post-tests.

4.4.9. EMG

Spontaneous activity was investigated as its presence is usually considered indicative of denervation.

Spontaneous EMG activity was not identified in every TDP-43^{Q331K} mouse but was found in the hindlimb of seven out of the eight mice investigated and there was no obvious difference in the frequency of spontaneous activity between the riluzole and vehicle groups. Spontaneous activity included fasciculations (f*igure 4.16A & B*), heightened insertional activity (*figure 4.16C*), and positive sharp waves (*figure 4.16D*). Some possible motor unit action potentials were also seen to fire briefly (see *figure 4.16E*).

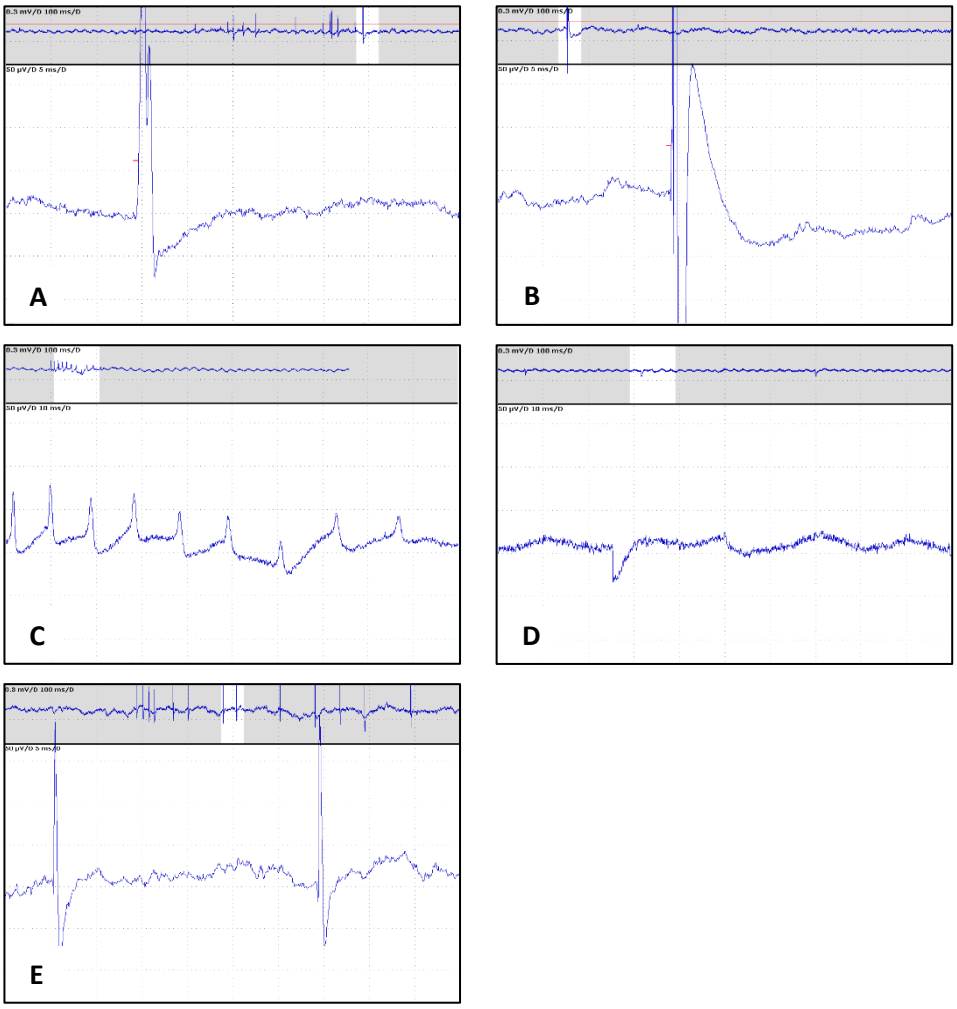

Figure 4. 14: Electrophysiological traces of spontaneous activity recorded in TDP-43^{Q331K} female mice at 6 months of age.

Examples of spontaneous activity recorded in the TDP-43^{Q331K} mice include fasciculations (A & B), heightened insertional activity in response to the EMG needle (C), positive sharp waves (D), and possible motor unit action potentials (E).

Although far less frequent, some positive sharp waves were also found in one or two of the seven TDP-43^{WT} and seven non-transgenic mice investigated. As with the TDP-43^{Q331K} mice, possible motor unit action potentials were found (see *figure 4.17*). No signs of fasciculations, fibrillations, or heightened insertional activity were found.

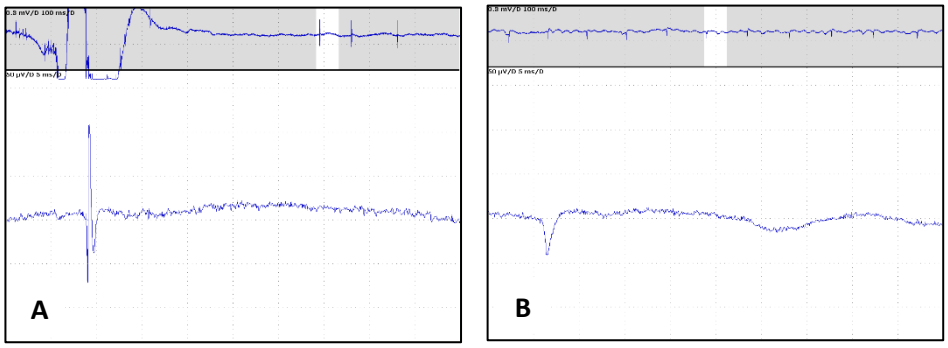

Figure 4. 15: Electrophysiological traces of spontaneous activity recorded in TDP-43^{WT} female mice at 6 months of age.

Examples of spontaneous activity recorded in the TDP-43^{WT} mice possible motor unit action potentials (A), and positive sharp waves (B).

4.4.10. Marble Burying

At 6 months of age mice were placed in new cages containing 24 evenly spaced marbles and the number of marbles buried in 1 hour was recorded. As discussed in *section 4.1.3*, the main purpose of the marble burying paradigm was to identify apathy as an indicator of FTD in the TDP-43^{Q331K} model.

The data show a much higher proportion of marbles being buried by the non-transgenic and TDP-43^{WT} mice compared to the TDP-43^{Q331K} riluzole and vehicle mice (4.7±5.1 TDP-43^{Q331K} riluzole vs 9.2±7.4 TDP-43^{Q331K} vehicle vs 13.7±8 non-transgenic vs 17.3±4.8 TDP-43^{WT}). There was a significant difference between the TDP-43^{WT} and TDP-43^{Q331K} riluzole group ($p<0.001$, one-way ANOVA), the TDP-43^{WT} and TDP-43^{Q331K} vehicle group ($p<0.05$, one-way ANOVA), and the non-transgenic and TDP-43^{Q331K} riluzole group ($p<0.05$, one-way ANOVA).

The decreased marble burying activity in TDP-43^{Q331K} groups may be indicative of apathetic behaviour or could be due to motor dysfunction.

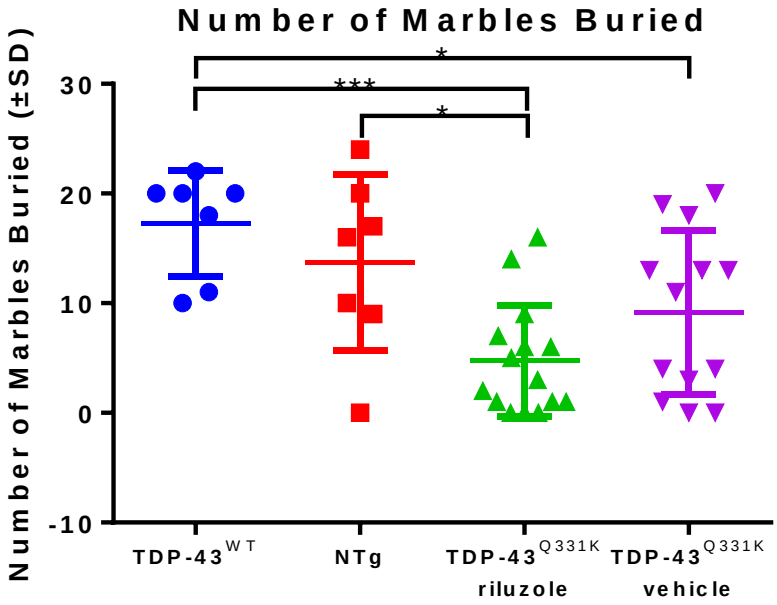

Figure 4. 16: Marble burying.

Number of marbles buried (out of 24) at 6 months of age in all groups (n = 7-15) within 1 hour. The TDP-43^{Q331K} vehicle group buried significantly fewer marbles than the TDP-43^{WT} group, and the TDP-43^{Q331K} riluzole group buried significantly less marbles than both the TDP-43^{WT}and non-transgenic group.

4.4.11. End of Study Riluzole Concentrations

Riluzole levels in blood and brain were analysed at the end of the riluzole study in mice from the dosed group (*table 4.2*). Riluzole levels in blood were found to be very similar to the earlier PK study (116.2 ± 54.4nM peak in the PK study vs 123.9 ± 54.4nM at the end of the study) and the brain concentrations recorded here were at similar levels to those found in the PK study trough spinal cord reported in section 5.4.2. (220.8 ± 43.8nM PK trough spinal cord vs 194.7 ± 115.3nM in brain). These results indicate that the CNS riluzole levels were maintained throughout the study.

Table 4. 3: Riluzole concentrations (uHPLC/TOF Mass spec). *Mean riluzole concentrations in the blood and spinal cord of TDP-43^{Q331K} mice dosed with 240µg/ml in drinking water from 1-6 months of age (blood n = 2, brain n = 5).*

Blood (nM)	Brain (nM)	Brain/Blood ratio
123.9 (±54.4)	194.7 (±115.3)	2.05 (±0.5)

4.5. Discussion

4.5.1. Mass Spectrometry of Riluzole

As seen in *figure 4.3*, riluzole batch 2 (from a previous study) was found to have a higher peak of impurity at 7.9mins retention time, when compared to batch 1. The expert opinion of the mass spectrometer was that both samples were at least 95% riluzole which correlated with the data sheets provided by the supplier. However, batch 1 had higher purity and was therefore used for this study.

4.5.2. Riluzole PK Study

The purpose of the PK study was to assess the CNS penetrance of the riluzole and ensure that the drug exposure was comparable to that in MND patients.

In patients, riluzole levels within the CNS have not been measured as far as we are aware (for example in cerebrospinal fluid). However, plasma levels have been measured in several studies. Steady state plasma concentrations are reached within 5 days of dosing in patients (Bryson et al., 1996), with highly variable serum concentrations (which correlate highly with plasma levels) among individuals (Groeneveld et al., 2008).

In healthy volunteers, mean peak serum concentrations of riluzole were reported as 0.173-0.269mg/L (0.73-1.15µM) (Le Liboux et al., 1999). In MND patients, mean trough to peak serum levels of riluzole were 0.11-0.432mg/L (0.47-1.84µM) and minimum trough to peak serum levels of riluzole were 0.013-0.034mg/L (0.056-0.145µM) (Groeneveld et al., 2001).

In the PK study carried out here, whole blood levels of riluzole were measured in the mice, which are assumed to be comparable to serum and plasma levels, as is found with many drugs (Flanagan et al., 2003). The mean trough-peak range of riluzole concentrations in the blood was 78.7-116.2nM (0.0787-0.1162µM). Therefore, although relatively low, the blood concentrations found in this study were within the minimum peak and trough range found in patients (0.056-0.145µM) (Groeneveld et al., 2001), as was the end of study mean blood concentration of riluzole (0.123µM).

Peak levels were higher than trough levels in the spinal cord and blood, showing that the mice consume more of their drinking water, and therefore more riluzole, during the

night. The high spinal cord/blood ratio in the PK study and brain/blood ratio in the end of study riluzole concentrations indicate that riluzole is highly CNS penetrant.

Overall, the PK study data suggest that an optimal riluzole concentration may require a higher dose in the TDP-43^{Q331K} mice. However, this must be approached with caution as a high dose in SOD1^{G93A} mice has been shown to have a sedative effect (in-house data).

4.5.3. Neuroscoring

In chapter 2, neuroscoring was assessed using criteria based on the SOD1^{G93A} mouse model. However, differences between TDP-43^{Q331K}, TDP-43^{WT} and non-transgenic mice were not found by this neuroscoring method until after differences were evident on both rotarod and catwalk measures, suggesting that an adjusted neuroscoring system may be required.

A new assessment protocol was created for this study and the data show consistent findings with low variability, signifying an effective system.

No differences were identified between the riluzole and vehicle TDP-43^{Q331K} groups, however, a clear phenotypic progression can now be identified through neuroscoring, in which forelimb tremor is evident from early on in the model but does not appear to progress, whilst hindlimb resting tremor progresses rapidly to a consistent continuous resting tremor at 6 months of age, and walking progresses from normal to a severe waddling gait in most mice by 6 months of age.

Since forelimb tremor shows little change with disease, measurement of hindlimb resting tremor and walking (overall neuroscore) would be sufficient in measuring disease progression in the TDP-43^{Q331K} model.

4.5.4. Body Weight and Rotarod

Body weight and rotarod data showed no significant differences between the TDP-43^{Q331K} riluzole and vehicle groups but there was a very slight trend for increased weight and decreased rotarod performance in the riluzole group.

Riluzole has been shown to reduce glutamate release and facilitate glial uptake of glutamate (Banasr et al., 2010, Chowdhury et al., 2008), in turn increasing glucose

oxidative metabolism and glutamate/glutamine cycling (Chowdhury et al., 2008), and therefore affecting metabolism. A study in rats showed a 2mg/kg dose of riluzole decreased baseline metabolic rate and motor activity (Faustino and Donnelly, 2006). One or both of these may be occurring in the TDP-43^{Q331K} riluzole group, and resulting in their slightly increased weight.

In comparison to the data presented in chapter 2 (see *sections 2.4.4.* and *2.4.5*.), the weight and rotarod data showed a considerably lower mean weight and increased rotarod performance from the beginning of the study at 5 weeks of age (weight: 17.7±1.3 in TDP-43^{Q331K} vs 15.5±1.2 in TDP-43^{Q331K} vehicle; rotarod: 230.1±50.8 in TDP-43^{Q331K} vs 264.5±49.6 in TDP-43^{Q331K} vehicle), to the end of the study at 23 weeks of age (weight: 34.9±3.7 in TDP-43^{Q331K} vs 30.1±5.1 in TDP-43^{Q331K} vehicle; rotarod: 105±30.7 in TDP-43^{Q331K} vs 182.5±63.3 in TDP-43^{Q331K} vehicle). The reason for differences in weight and rotarod between the two studies is unknown but could relate to the intake of DMSO in the drinking water, the absence of male mice in the room or genetic drift within the colony. It will be important to monitor inter-study variability between control groups over time as has been reported for the SOD1^{G93A} mouse model (Mead et al., 2011).

4.5.5. Catwalk Gait Analysis

No differences were found between the TDP-43^{Q331K} riluzole and vehicle groups, at any time point. Differences were found between the TDP-43^{Q331K} groups and control groups. Catwalk gait analysis has not been reported previously in the TDP-43^{Q331K} mice, but was described in chapter 2 (*section 2.4.8.*) of this thesis.

Duration (time taken to cross the catwalk) is significantly increased in the TDP-43^{Q331K} groups compared to control groups at 3 and 6 months of age, as found in chapter 2. Forelimb BOS showed no significant differences but a tendency towards increased BOS in the TDP-43^{Q331K} mice compared to controls, as supported by findings in chapter 2, in which forelimb BOS increased with age in the TDP-43^{Q331K} mice, with the difference becoming significant at 10 months of age. Hindlimb BOS increased in the TDP-43^{Q331K} compared to the control groups, becoming significantly larger by 6 months of age, as was also found in chapter 2. These findings signify a considerably slower walking speed in the TDP-43^{Q331K}, with a wider stance.

Diagonal walking (stepping using diagonal paws) is the most commonly used stepping pattern in mice, used approximately 80% of the time (Gruntman et al., 2007). In the TDP-43^{Q331K} mice, they use diagonal stepping significantly less compared to the control groups at 3 and 6 months of age, using significantly more three and four-paw stepping at the same ages. Interestingly, these findings appeared earlier than in the cohort of mice described in chapter 2, in which these parameters were not significantly different until 10 months of age, possibly due to smaller group sizes. It appears that the TDP-43^{Q331K} mice are becoming more unsteady and reliant on support from a third or even fourth paw whilst walking and this was more evident in this study, compared to the previous characterisation study.

Forelimb and hindlimb swing time were significantly increased in the TDP-43^{Q331K} groups compared to controls at 6 months of age, as was found in chapter 2. Tendencies towards an increased forelimb and hindlimb stride length were found in the control groups over time, whilst stride length in the TDP-43^{Q331K} groups remained the same, however, differences were significant at these time points in the earlier study (*figures 2.11 and 2.13*). Forelimb and hindlimb duty cycle were increased in the TDP-43^{Q331K} groups compared to controls at 3 and 6 months of age but were only significant at 6 months of age in chapter 2.

Overall, the catwalk gait analysis findings were very similar to those found previously (chapter 2), showing consistency in findings between studies in these mice. It appears that dosing of riluzole did not have any therapeutic effects detectable by gait analysis.

4.5.6. Electrophysiology

CMAP amplitude, repetitive stimulation and EMG were measured in all groups at 1, 3 and 6 months of age.

4.5.6.1. CMAP

CMAP amplitude quantifies the depolarisation of stimulated muscle fibres and a reduction in CMAP correlates with loss of functional motor axons or muscle fibres. A reduction in CMAP amplitude is often seen in MND patients following degeneration of motor axons (Benatar et al., 2016).

No difference was found in CMAP amplitude between the TDP-43^{Q331K} riluzole and vehicle groups. CMAP amplitude was significantly lower in both TDP-43^{Q331K} groups compared to the control group at 1, 3 and 6 months, suggestive of a loss of functional motor axons/fibres, as has been demonstrated previously in the SOD1^{G93A} mouse model (Mancuso et al., 2011b, Alves et al., 2011).

CMAP amplitude increased with age initially, and then plateaued. This initial increase may be due to an increase in muscle fibre size as the mice develop and a similar pattern with age has been documented in another mouse model (Verhamme et al., 2011).

4.5.6.2. Repetitive Stimulation

Repetitive stimulation provides a measure of the fidelity of neuromuscular transmission. In healthy subjects, no decrement in response will be seen across stimuli; in MND a decrement is seen in most patients (Wang et al., 2001, Iwanami et al., 2011, Killian et al., 1994). The exact aetiology behind this observation remains unclear but is usually interpreted as representing the presence of immature neuromuscular junctions (Iwanami et al., 2011).

A previous study using a mouse model of SMA found that repetitive stimulation at 10Hz showed a decremental response (Bogdanik et al., 2015) but no records of repetitive stimulation in a mouse model of MND could be found. In this study there was no obvious change in response to repetitive stimulation with age in any of the control groups, and no obvious decrement across stimuli was evident in the control groups at 3 or 10Hz. It is probable that the decrement seen at 50Hz in the control groups at 6 months was related to a change in confirmation of the muscle due the tetanic stimulus response.

In comparison, the TDP-43^{Q331K} mice showed a significant decrement in response at all frequencies and ages, as is consistent with findings in MND patients. This is suggestive of a reduction in the safety factor at the neuromuscular junction, potentially a sign of recent reinnervation in which endplates have a lower safety factor (Wang et al., 2001, Iwanami et al., 2011) or a lack of acetylcholine replacement after depletion (Iwanami et al., 2011).

It appears that the decremental response was less severe in the TDP-43^{Q331K} riluzole group, compared to the vehicle group at 3 and 6 months of age, indicative of a treatment

effect. It is possible that this treatment effect could have been clarified by putting more stress on the neuromuscular junction (i.e. a higher frequency of repetitive stimulation). When this was attempted at 50Hz, it is believed that the frequency was too high, affecting the confirmation of the limb. A compromise of 20 or 30Hz may have been a more appropriate frequency to investigate.

If these findings do demonstrate a treatment effect, it is interesting that no effect was found in any motor function tests such as the catwalk or rotarod. However, it has been found in MND patients that although riluzole extends survival, it does not improve functional outcome measures including motor function, lung function, fasciculations, muscle strength and motor symptoms (as stated in the Summary of Product Characteristics for riluzole). It is possible therefore that any treatment effect at the neuromuscular junction was too subtle to detect using motor function tests.

It is likely that the repetitive stimulation decrement is reduced in the riluzole group because less NMJs are unstable due to a reduction in denervation/reinnervation events, in which the safety factor for action potential conduction is impaired. Unfortunately there is no NMJ immunostaining to support this theory but it is an interesting topic for further research.

There are a number of ways in which riluzole may reduce NMJ instability. Riluzole affects many neural mechanisms and the mechanisms by which it extends life in MND patients remain unclear. The mechanisms of action include: reduced glutamate release from the pre-synaptic terminal, inhibition of voltage-gated calcium currents, potentiation of calcium-dependent potassium currents, inhibition of voltage-gated potassium current, inhibition of sodium currents (both persistent and fast) (Bellingham, 2011) and blocking of muscle ACh receptors *in vitro* (Deflorio et al., 2012).

MND patients are recorded as having increased levels of persistent sodium and a decreased potassium conductance (Vucic and Kiernan, 2006). Riluzole reduces hyperexcitability, which increases the threshold voltage, requiring further depolarization in order to produce an action potential (Kuo et al., 2006, Del Negro et al., 2002). This reduction in hyperexcitability is as a result of decreased sodium influx and potassium efflux, reducing the occurrence of over-activation of the neurons and in turn, reducing neurodegeneration, preventing NMJ instability (Stys et al., 1992). Hence,

riluzole has a neuroprotective effect, which reduces the number of unstable NMJs, increasing the muscle's ability to maintain a response to repetitive stimulation.

A second factor is whether the dose of riluzole is high enough. As shown in *table 4.1* we have achieved reasonable levels of riluzole in the CNS, but the levels of riluzole may be much higher in the CNS of patients judging by the levels in the systemic circulation in the two species (blood in mice, serum in patients). This raises the question of whether a higher dose of riluzole may show a more profound difference. However, in-house studies have found that high doses of riluzole have a sedative effect in SOD1^{G93A} mice so higher doses must be approached with caution. It is also possible that an alternative method of dosing may be more effective and should be considered.

4.5.6.3. EMG

Spontaneous EMG activity is not specific to motor neuron loss and may be seen in a range of pathologies such as neuropathies and myopathies (although fasciculation potentials are not seen in myopathic conditions).

Positive sharp waves have been found in the SOD1^{G93A} (Miana-Mena et al., 2005) and wild type SOD1 (PeledKamar et al., 1997) mouse models. However it must be considered that normal healthy mice may have some nerve injury from normal everyday life, as found in healthy people (Falck and Alaranta, 1983).

Insertional activity occurs due to discharge potentials as the cell membrane is disrupted by the EMG needle. Heightened insertional activity is considered a sign of denervation (Shi et al., 2014) and was not found in the non-transgenic or TDP-43^{WT} mice, but was identified in the TDP-43^{Q331K} mice. Heightened insertional activity has also been identified previously in a wild type SOD1 mouse model (PeledKamar et al., 1997) and a knockout SOD1 mouse model (Shi et al., 2014).

Fibrillations and fasciculations are a classic electrophysiological finding in MND and indeed in mouse models of MND (Costa et al., 2012, Azzouz et al., 1997, Miana-Mena et al., 2005). The previous study of TDP-43^{Q331K} mice reported fibrillation potentials (Arnold et al., 2013) and we also found both fasciculation and fibrillation potentials in TDP-43^{Q331K} mice in this study. While it is a little surprising to observe spontaneous activity in the wild type and non-transgenic groups, including positive sharp waves, fasciculation

and fibrillations have been recorded in healthy people (Falck and Alaranta, 1983). It is possible that this activity related to age related changes or minor injuries sustained over time in cages with other mice. It is difficult to quantify the amount of spontaneous activity as it can be subjective and also liable to sampling error, given the small recording area of the EMG needle. As a result we did not attempt quantification of spontaneous activity. However, we did not observe increased insertional activity or fasciculation potentials in the TDP-43^{WT} mice.

Overall, the spontaneous activity was evident but was not consistently found in all mice tested. This may be due to some reinnervation, as the phenotype does not progress rapidly. Carrying out EMG at earlier time points would have allowed us to investigate this further but the EMG needle is relatively large (30 gauge) and so it was deemed safest to only carry out EMG during terminal procedures (at 6 months of age).

Ultimately, the increased spontaneous activity in the TDP-43^{Q331K} group is in keeping with the MND phenotype.

4.5.7. Marble Burying

As described previously, marble burying is believed to be a surrogate marker of normal digging behaviour in mice (Deacon, 2006).

As was found in a previous study of non-transgenic mice (Egashira et al., 2008), riluzole had no impact on marble burying behaviour, as demonstrated by no difference in marble burying activity between the TDP-43^{Q331K} riluzole and vehicle groups.

The TDP-43^{Q331K} groups buried fewer marbles than the TDP-43^{WT} and non-transgenic groups, suggesting a decrease in normal digging behaviour. This was evident in the mice during the task, as the TDP-43^{Q331K} mice would often sit motionless and show no signs of exploration. It is possible that this lack of digging could be due to motor dysfunction, however, the motor phenotype in this model is mild so that appears unlikely, and little attempt at digging was observed in the TDP-43^{Q331K} mice. The lack of digging behaviour is more likely to signify a cognitive phenotype, namely apathy, or a lack of interest in digging. 10-15% of MND patients will develop a diagnosis of MND-FTD, exhibiting as signs such as inappropriate behaviour, repetitive behaviour, and/or apathy (Chan et al.,

2015). Overall, the lack of marble burying activity in the TDP-43^{Q331K} mice may be indicative of an FTD phenotype.

4.6. Conclusion

This study has allowed further characterisation of the TDP-43^{Q331K} mice and highlighted a potential FTD phenotype. The study has also allowed us to define a more reliable neuroscoring system for the TDP-43^{Q331K} and TDP-43^{WT} colonies. Riluzole appeared to have no significant effect on gross motor phenotype in the TDP-43^{Q331K} mice, but did seem to improve the NMJ safety factor, reducing the repetitive stimulation decrement and posing interesting ideas for future studies. Further investigation using immunohistochemistry is needed to determine whether riluzole treatment influences the disease pathology.

5. 31P-MRS Imaging

5.1. Introduction

5.1.1. Energy Metabolism in MND Patients

Most MND patients lose weight during their disease course, partially due to muscle loss and lowered food intake (Kasarskis et al., 1996, Slowie et al., 1983); but also, at least in some patients, due to an increased basal metabolic rate (hypermetabolism) (Dupuis et al., 2011). Hypermetabolism, along with dysphagia, can make it very hard for MND patients to maintain weight, however, maintenance of weight is crucial, as weight loss correlates with morbidity and mortality (Kasarskis et al., 1996, Koerner et al., 2013) in MND patients.

It is widely accepted that many MND patients become hypermetabolic, but it appears that it is not ubiquitous, and it is unclear which subgroups of patients are at risk. Estimates of the proportion of patients who are hypermetabolic range widely from 50% (Bouteloup et al., 2009), 62% (Desport et al., 2005), and 52% in purely sporadic cases; to 100% in familial cases (Funalot et al., 2009).

The underlying cause of hypermetabolism in MND is unknown and it appears that several metabolic pathways/elements may be implicated, including insulin signalling, glycolysis, and fatty acid oxidation (Raman et al., 2015). Many investigations have identified mitochondrial dysfunction as a key contributor to hypermetabolism in MND. In muscle biopsy samples from MND patients, mitochondria have been found to have increased volume and poor morphology (Siklos et al., 1996) with a tendency to pathological grouping in the lumbar spinal cord (Sasaki and Iwata, 1996) and sarcolemma of skeletal muscle (Afifi et al., 1966). Mutations and deletions in mitochondrial DNA have been found in patients (Comi et al., 1998, Dhaliwal and Grewal, 2000, Wiedemann et al., 2002) and axonal transport of mitochondria is often disrupted (De Vos et al., 2008).

It is also possible that the phosphocreatine (PCr) pathway is affected in MND. It has been regularly suggested that patients have increased levels of phosphocreatine kinase, suggestive of increased PCr pathway activity or muscle damage (Williams and Bruford, 1970, Felice and North, 1998, Rafiq et al., 2016). This has led to pre-clinical trials of creatine supplementation for the treatment of MND (Snow et al., 2003, Andreassen et

al., 2001), however, these results have not translated through to beneficial effects in human clinical trials (Groeneveld et al., 2003, Shefner et al., 2004).

It is likely that, whilst some energy pathways are disrupted in MND, such as glycolysis and fatty acid oxidation, activity of other components such as the PCr pathway may be upregulated in a compensatory manner, in order to provide the energy required for life.

5.1.2. 31P-MRS

Magnetic resonance spectroscopy (MRS) is an imaging method which can assess the molecular content of living tissue based on magnetic resonance signal characteristics. Some phosphorous-containing compounds can be measured using 31P-MRS, providing comparative levels of several compounds including PCr, inorganic phosphate (Pi), α-adenosine triphosphate (α-ATP), β-ATP, and γ-ATP at the positions stated in *table 5.1*.

Table 5. 1: Spectral position for each of the main 31P-MRS metabolites.

Metabolite	**Spectral position (ppm)**
PCr	0
Pi	5.14
γ-ATP	-2.389
α-ATP	-7.529
β-ATP	-16.072

The phosphocreatine pathway is a key source of rapidly available ATP (the energy currency of the cell). The enzyme phosphocreatine kinase is the catalyst for the reversible conversion of PCr + ATP ↔ Pi + creatine + adenosine diphosphate (ADP). A calculation based on the distance between peaks of Pi and PCr can be used to calculate intracellular pH (Ren et al., 2015, Petroff et al., 1985).

5.1.3. 31P-MRS in MND Patients

A number of studies using 31P-MRS of muscle have been carried out in MND patients, one of which applied the imaging after aerobic and ischaemic muscle contraction in 10 patients vs 38 controls (Grehl et al., 2007). The study showed that consumption of PCr during both exercise conditions was significantly lower in MND patients compared to controls, and hypothesised several alternate mechanisms for this observation including: a decrease in substrate availability; a decreased energy demand; or defective energy

metabolism. The ratio of PCr/ATP was significantly higher in patients than in controls. The authors stated that it was unclear whether this was due to increased PCr, decreased ATP levels, or both. They concluded that they could not confirm mitochondrial dysfunction using this method. Another study of 31P-MRS in MND patients using an exercise protocol showed pH and PCr to be lower; and Pi to be higher in patients compared to controls during the exercise phase but not during the recovery phase. However, none of these metabolic responses to exercise showed statistically significant differences (Sharma et al., 1995).

Another study was carried out in patients at rest, in which the triceps surae was studied and no differences in metabolites were found between patients and controls (Ryan et al., 2014). However, the groups were small (6 patients, 7 controls) and unmatched.

5.1.4. Energy Metabolism in Mouse Models of MND

Studies of various mouse models of MND have demonstrated evidence of hypermetabolism with increased oxygen consumption (Dupuis et al., 2004) and reduced body mass (Dupuis et al., 2004, Wong et al., 1995), despite equal or increased calorie intake compared to control animals (Dupuis et al., 2004).

At the muscle level, oxygen consumption has been shown to be increased in $SOD1^{G93A}$ mice using a Clark electrode in an oxygraphic cell containing muscle fibre bundles (Leclerc et al., 2001) but unchanged at the spinal cord level, as measured by a respirometer (Wendt et al., 2002). The $SOD1^{G93A}$ mouse model has also demonstrated reduced ATP synthesis in the brain and spinal cord measured using a luciferase/luciferin-based system (Mattiazzi et al., 2002) and muscle using an enzymatic assay (Derave et al., 2003). However, in the $SOD1^{G86R}$ mouse model, ATP synthesis in the spinal cord was not significantly different from control mice (Mattiazzi et al., 2002). In another study, energy use in muscle appeared to be derived preferentially from lipids rather than glucose at the presymptomatic stage (Palamiuc et al., 2015). These contrasting results could support the hypothesis that patterns of energy metabolism dysfunction may differ with genotype.

From an environmental perspective, diet has been shown to affect survival and disease in mouse models, with a high energy diet increasing mean survival by 20% and reducing

loss of motor neurons (Dupuis et al., 2004). Meanwhile, long term calorie restriction appears to cause earlier disease onset and hasten disease progression (Hamadeh et al., 2005), as does short term calorie restriction, when compared to an *ad libitum* diet (Hamadeh and Tarnopolsky, 2006).

As shown in patients, many mouse models of MND appear to show changes in morphology of mitochondria. In brainstem, cerebellum and forebrain of mice with high expression of human SOD1, mitochondria were swollen, with dilation of the intermembrane space and swollen cristae, from 30 weeks of age compared to controls. Axons showed vacuolated mitochondria and older mice had aggregates of degenerating mitochondria at symptomatic stages of disease (Jaarsma et al., 2000).

Motor neuronal mitochondria in the spinal cords of many mouse models of MND at onset/symptomatic stages have been found to be aggregated (Xu et al., 2010), swollen (Jaarsma et al., 2001, Bendotti et al., 2001, Wong et al., 1995) and vacuolated (Xu et al., 2010, Bendotti et al., 2001, Higgins et al., 2003, Kong and Xu, 1998) with fewer, disorganised cristae (Xu et al., 2010, Bendotti et al., 2001, Wong et al., 1995, Dalcanto and Gurney, 1995, Kong and Xu, 1998) and extended, leaking and even unravelled outer membranes (Higgins et al., 2003, Wong et al., 1995, Dalcanto and Gurney, 1995, Kong and Xu, 1998).

The morphology of mitochondria in muscle of mouse models of MND has been less extensively investigated. A $SOD1^{G93A}$ mouse model showed abnormalities in mitochondria at the neuromuscular junction and not in muscle (Gould et al., 2006), whereas another $SOD1^{G93A}$ mouse model showed clustered, swollen and vacuolated mitochondria with abnormal cristae at the end stage of disease (Dobrowolny et al., 2008). These defects in mitochondrial morphology and functionality increase generation of free radicals, causing increased oxidative stress, and impairing function of the electron transport chain, as measured histochemically in $SOD1^{G93A}$ mice (Bendotti et al., 2001, Shaw, 2005).

31P-magnetic resonance spectroscopy has not yet been investigated in mouse models of MND. However, a study which measured PCr in $SOD1^{G93A}$ mice by enzymatic analysis with standard fluorometric assays, found significantly reduced PCr in $SOD1^{G93A}$ mice compared to controls (Derave et al., 2003).

One study using enzymatic analysis found that creatine levels in muscle were higher in SOD1^{G93A} mice compared to control mice (Derave et al., 2003). However, in spinal cord, creatine kinase levels were significantly decreased (Wendt et al., 2002). In contrast to findings in patients, creatine supplementation in mouse models of MND was shown to improve survival and disease progression (Klivenyi et al., 1999, Ikeda et al., 2000).

Overall, it appears that SOD1 mouse models of MND exhibit deficits in energy metabolism which may be partially ameliorated by increased availability of energy substrates and many studies suggest this is partly due to mitochondrial dysfunction.

Clearly, there is energy dysfunction in both MND patients and SOD1 mouse models, and a large proportion of studies have focused on mitochondrial function. As demonstrated with the lack of translation of creatine as a therapeutic intervention, it must be considered that findings may not always translate between mouse models and patients, but may give an indication of subgroup pathologies. Little focus has been made on the PCr pathway in mouse models of MND and investigation of 31P-MRS in the SOD1^{G93A} mouse model would provide the opportunity to fill this gap in knowledge and compare findings in the mice with those from patients.

5.2. Aims

1. To establish a safe protocol for 31P-MRS in mice.

2. To optimise the MR sequence for 31P-MRS.

2. To investigate differences in energy metabolism of SOD1^{G93A} mice compared with controls using 31P-MRS.

5.3. Materials and methods

5.3.1. Mice

5.3.1.1. Ethics Statement

All mouse experiments were carried out in accordance with the Animals (Scientific Procedures) Act 1986 under an appropriate UK Project Licence. Animals were housed and cared for in-house at the University of Sheffield, adhering to the Home Office Code

of Practice for the Housing and Care of Animals Used in Scientific Procedures Act (ASPA 1986) in-house at the University of Sheffield.

5.3.1.2. Transgenic SOD1^{G93A} Mice

Mice were from a well-established in-house colony of C57BL/6J Ola Hsd SOD1^{G93A} mice bred by crossing C57BL/6J Ola Hsd females (Harlan, UK) with males which are hemizygous for the SOD1^{G93A} transgene. Non-transgenic littermates were used as control mice. All mice used for imaging were male.

5.3.1.3. Study Sizes

For the initial preliminary experiment, one non-transgenic mouse was scanned at 106 days of age. For the second preliminary experiment, one 113 day old non-transgenic, and one 110 day old SOD1^{G93A} mouse were scanned.

For the main pilot study, 6 SOD1^{G93A} mice were scanned together with 6 non-transgenic littermates for the 36 day time point. However, all 12 mice were culled due to welfare issues (see *section 5.4.4*). Therefore, a new cohort was established for the 73 day scan of 6 SOD1^{G93A} mice and 6 non-transgenic mice. By the 115 day time point 3 SOD1^{G93A} mice remained and 3 non-transgenic mice. The details for the changes in sample size are given below.

For the follow up experiment (using a narrower spectral width and a cotton blanket with heat pad), 2 SOD1^{G93A} mice were scanned together with 2 non-transgenic mice at 49-50 days of age.

5.3.2. Anaesthesia and Physiological Monitoring of Mice

5.3.2.1. Original Method using Heat Pad

Animals were placed on a sponge bed in a custom built Perspex magnet capsule and imaged under gaseous anaesthesia (1–2%, flow rate 1.0 L/min oxygen and nitrous oxide continuous inhalation through a nose cone). Anaesthetic level was controlled on the basis of respiratory parameters using a pressure sensitive pad under the subject's chest (SAII Model 1025 monitoring and gating system, SAII, USA).

Inside the capsule, a non-magnetic ceramic heated hot air system (SAII - MR-compatible Heater System for Small Animals, SAII, USA) and rectal temperature probe (SAII - MR-compatible Heater System for Small Animals, SAII, USA), integrated into the physiological monitoring system maintained and monitored the temperature of the animal.

Post-scanning, animals were placed in an incubator at 31-32˚C for 10-30 minutes whilst they recovered from the anaesthesia.

5.3.2.2. Modified Heat Pad Protocol Covering Tails

After some of the animals developed tail necrosis issues thought to relate to thermal injury (see *section 5.4.4.*), wet gauze was placed over the tail of the mice to reduce the temperature and increase humidity. All other aspects of the protocol remained the same.

5.3.2.3. Modified Heat Pad Protocol Placing Pad Underneath

After further issues with tail necrosis, the procedure was abandoned as unsafe and an alternative heating method was used, in which a heat pad (CWE, PA, USA) was placed under the sponge bed of the mouse within the scanner, and a rectal temperature probe (Harvard, UK) was used to supply feedback to the monitoring system (CWE, PA, USA).

5.3.2.4. Warm Water System

Due to further problems with overheating, a warm water system was trialled. The custom built Perspex magnet capsule had an incorporated hollowed-out area to allow passage of a water tube under the mouse. This system was plugged in to a water bath (Heating Circulator SC150-S5P, ThermoFisher Scientific, UK), warming the water to 60˚C, which then passed under the mouse to maintain body temperature. The rectal probe and pressure pad were used to detect body temperature and respiratory rate respectively. However, this method was insufficient.

5.3.2.5. Heat Pad Method with Cotton Blanket

A cotton blanket was wrapped around the mouse with the pressure pad to the chest. The heat pad was then placed over the back of the mice (with the cotton blanket protecting the fur of the mice from the heat pad). The rectal probe provided temperature feedback (CWE, PA, USA).

5.3.3. Scanning Parameters

The animals were scanned on a 7 Tesla MRI system (Bruker BioSpec^{AVANCEII}, 310mm bore, B/C 70/30), with pre-installed 12 channel RT-shim system (B-S30) and fitted with an actively shielded, 116mm inner diameter, water cooled, 3 coil gradient system (Bruker BioSpin MRI GmbH B-GA12S. 660 mT/m maximum strength per axis with 80µs ramps).

5.3.3.1. Long TR Method

A 31P single pulse sequence utilising a block excitation pulse was used, with centre frequency 121.57MHz, and an acquisition time of 102ms, with repetition time (TR) of 4s. The spectral width was 164ppm/20000Hz with 2048 points and 450 averages, giving a spectral resolution of 4.88Hz/pt.

The whole brain of each mouse was scanned using a 2cm diameter surface coil. Saturation slices were used to suppress signal from surrounding muscle. The total scanning time was 30 minutes.

5.3.3.2. Short TR Method

Short TR scans were carried out using the same parameters, except with a shorter repetition time of 400ms, meaning we could increase averaging to 4500 in an effort to improve signal to noise ratio.

5.3.3.3. Narrower Spectral Width Method

A 31P sinc3 pulse sequence was used with an acquisition time of 500ms, flip angle 45˚, TR 5s, spectral width 41.13ppm/20000Hz with 2500 points and 128 averages, giving a spectral resolution of 1Hz/pt. The total scanning time was 10 minutes.

5.3.4. Data Processing

Firstly, a manually identified phase shift was applied to all spectra using Matlab 7 (Mathworks Inc, USA). Spectra using the same scanning parameters had the same phase shift applied. 31P-MRS spectra were normalised along the X-axis to align the PCr peaks of each trace. Peak values were then extracted for PCr, Pi, γ-ATP, α-ATP and β-ATP (see *table 5.1*). The three ATP-peaks represent each of the phosphates bound to adenosine.

For visual comparison of the average spectra, the PCr peak was normalised to 1 because some scans produce spectra in which all peak values are high/low, so normalising to the PCr peak height compensates for this. Conventionally, in 31P-MRS, the PCr peak is used for this purpose.

ATP was measured using the β-ATP peak.

Integrals of peak values, ratios of peak values, and comparisons of ratios and integrals were calculated and plotted using Graphpad Prism 6.0. Ratios and integrals for the transgenic and non-transgenic groups were compared using unpaired t-tests. When multiple t-tests were carried out, a Bonferroni correction was applied.

5.4. Results

5.4.1. First Preliminary Scan

Firstly, a single mouse was scanned using the 31P-MRS surface coil. Whole brain acquisition was performed for 30 minutes to ensure a spectrum could be obtained. No adverse events occurred.

Figure 5.1 shows the first spectrum obtained, with no post-processing of the data. Peaks are identifiable for phosphomonoesters (PME), Pi, PCr, γ-ATP, α-ATP and β-ATP. The x-axis was not aligned to the correct position and is approximately 8ppm shifted to the right due to field drift in the MR system.

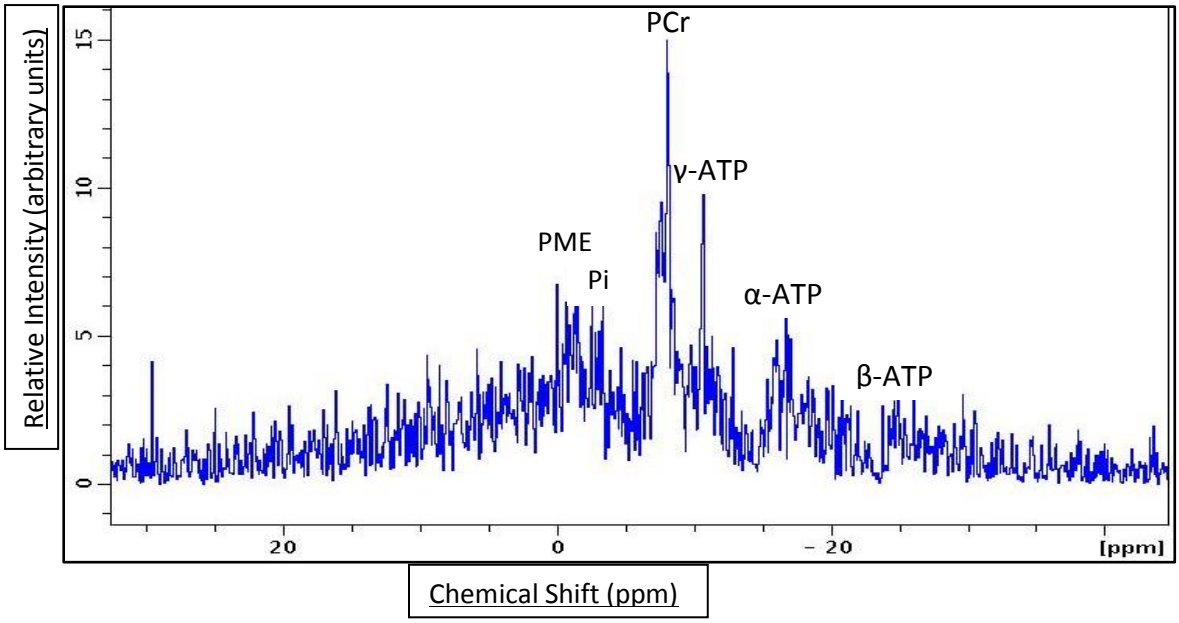

Figure 5. 1: Raw 31P-MRS spectrum from whole brain of a 106 day old non-transgenic mouse (TR = 4s).

5.4.2. Second Preliminary Scans

To ensure the scans could be replicated and the protocol ran smoothly, a second set of 31P-MRS scanning was carried out on whole brain for 30 minutes on a pair of mice, one transgenic; one non-transgenic. No adverse events occurred.

Figure 5.2 shows the non-transgenic spectrum obtained, with no post-processing of the data. Peaks are identifiable for PME, Pi, PCr, γ-ATP, α-ATP and β-ATP. The x-axis was not aligned to the correct position and is approximately 3ppm shifted to the right due to drift in the MR system.

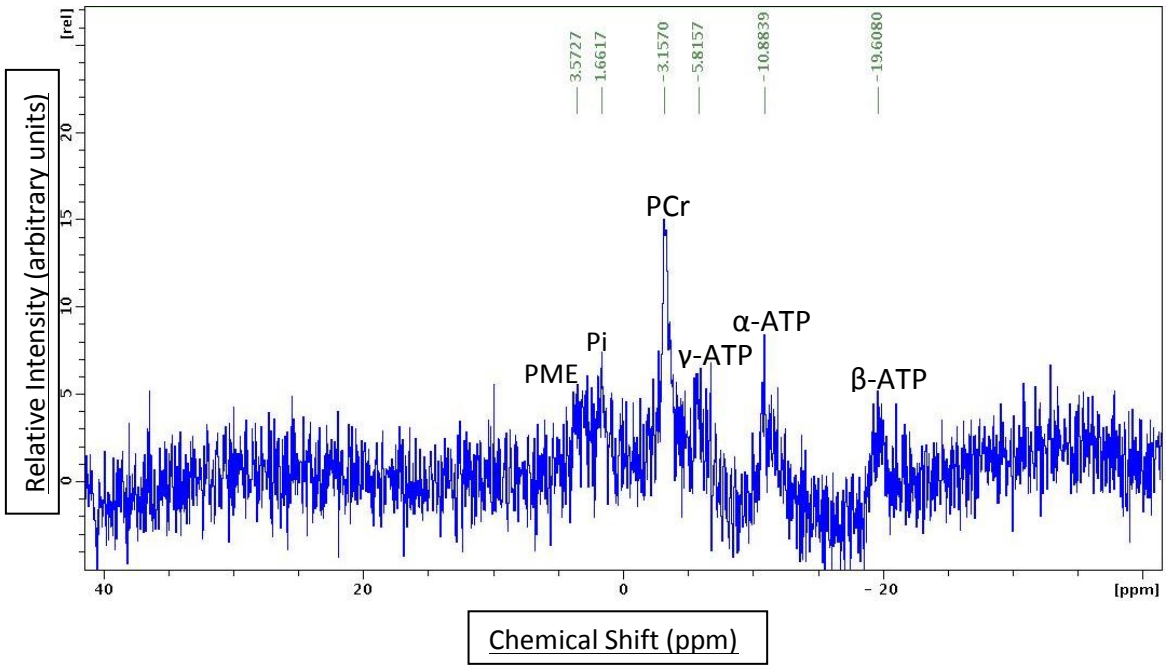

Figure 5. 2: Raw 31P-MRS spectrum from whole brain of a 113 day old non-transgenic mouse (TR = 4s).

Figure 5.3 shows the SOD1^{G93A} spectrum obtained, with no post-processing of the data. As with the non-transgenic spectrum, peaks are identifiable for PME, Pi, PCr, γ-ATP, α-ATP and β-ATP and the x-axis was not aligned to the correct position and is approximately 3ppm shifted to the right.

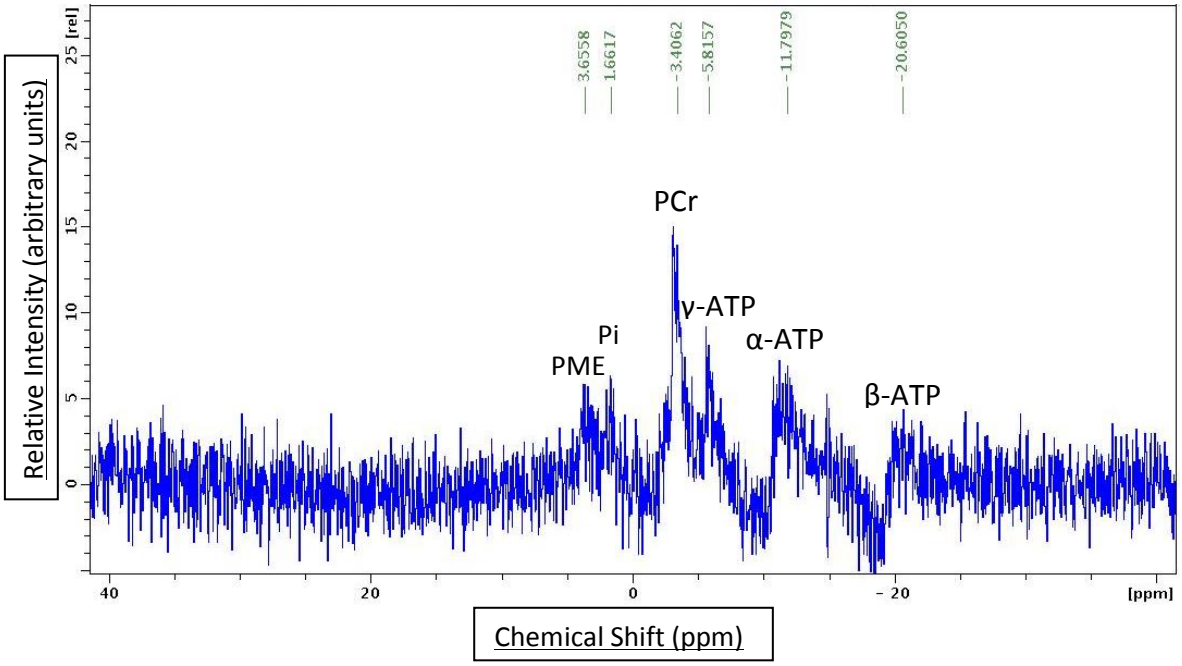

Figure 5. 3: Raw 31P-MRS spectrum from whole brain of a 110 day old SOD1^{G93A} mouse (TR = 4s).

The spectra collected were similar in height, shape and noise, providing confidence in the reproducibility of the scans, and the protocol had produced no adverse events so appeared sufficient to begin a pilot study, comparing whole brain spectroscopy in $SOD1^{G93A}$ and non-transgenic mice.

5.4.3. Pilot Study 36-Day Scanning

Six pairs of mice were scanned using a 31P-MRS surface coil placed to provide coverage of the whole brain. It was noted that, over time, noise in the spectra increased. This was thought to represent a physical effect due to the increase in temperature of the coil, caused by the hot air flow used to maintain the body temperature of the mice. Therefore, an ice pack was applied between scans to reduce the temperature of the coil. However, it is unknown what effect this warming of the coil may have had on the average spectra.

When normalised to the PCr peak height, the spectra of the transgenic brain appeared to show higher Pi, higher γ-ATP and lower α-ATP compared to the non-transgenic brain (*figure 5.4*).

However, no obvious differences could be extrapolated from the PME, PDE and β-ATP peaks.

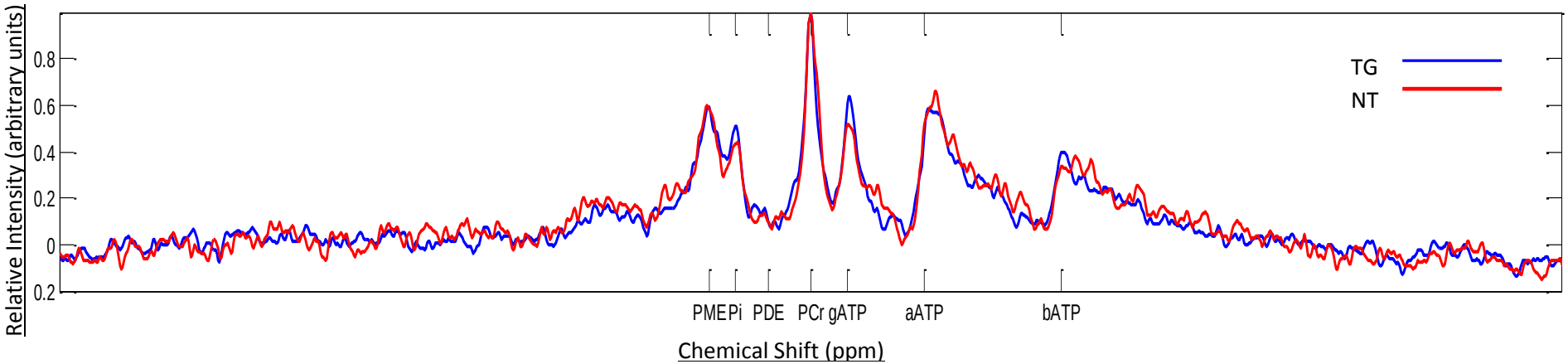

Figure 5. 4: Average 31P-MRS spectra of whole mouse brain at 36 days of age (n = 6), TR 4s.

PME: phosphomonoesters; Pi: inorganic phosphate; PDE: phosphodiesters; PCr: phosphocreatine; gATP: γ-ATP; αATP: α-ATP; bATP: β-ATP. Peak height of PCr normalised to 1.

To compare peaks quantitatively, peak height ratios and integrals for PCr, Pi and ATP (β-ATP) were derived.

Peak height ratios (*figure 5.5*) showed no significant differences between the spectra of $SOD1^{G93A}$ and non-transgenic mice for any of the ratios Pi/PCr (non-transgenic 0.71±0.10 vs $SOD1^{G93A}$ 0.71±0.09), ATP/Pi (non-transgenic 0.65±0.11 vs $SOD1^{G93A}$ 0.63±0.09) and ATP/PCr (non-transgenic 0.45±0.06 vs $SOD1^{G93A}$ 0.44±0.07). No obvious trends were present.

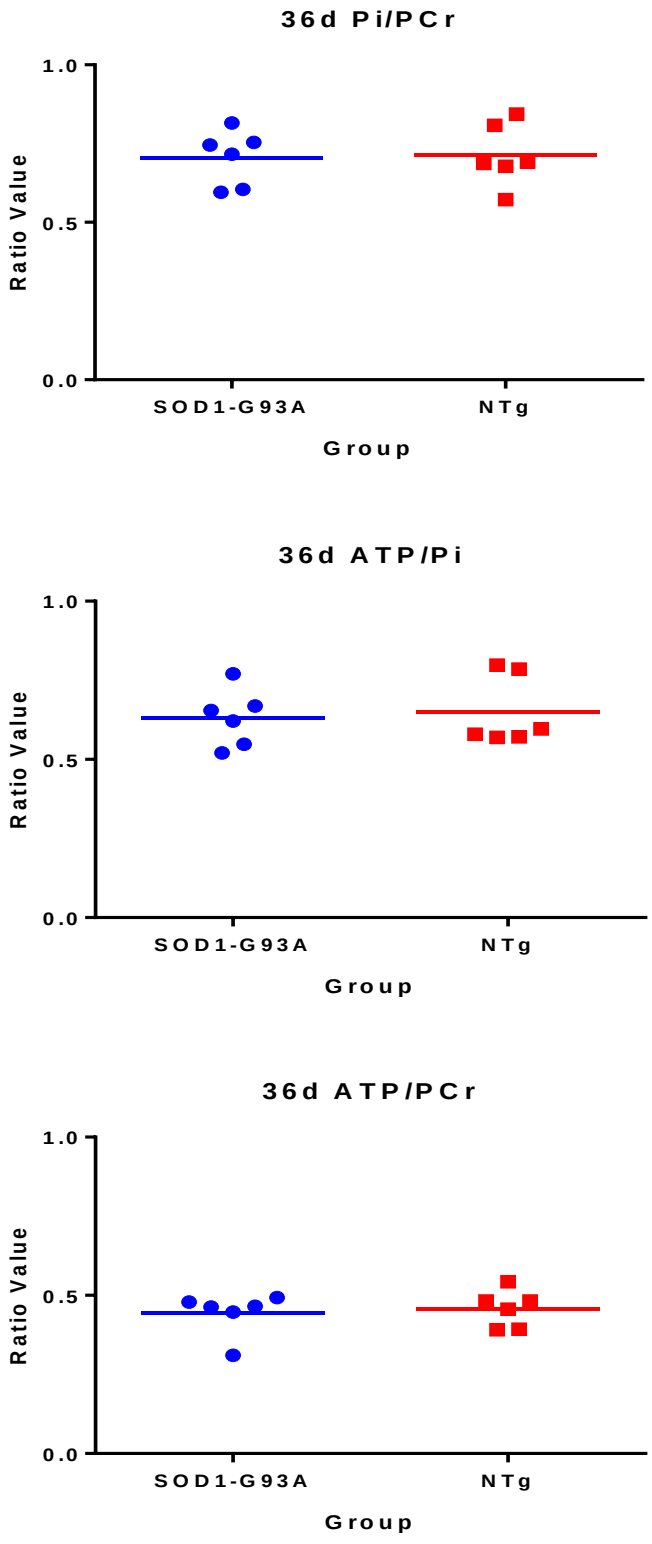

Figure 5. 5: Scatter plot graphs illustrating metabolite peak height ratios in the transgenic (Tg) and non-transgenic (NTg) (n = 6) mice groups at 36 days of age.

Unpaired t-tests showed no significant difference between groups with any of the comparisons.

Alternatively, integrals of the peaks can be investigated, as this provides a figure for the whole peak, taking width of the peak in to consideration rather than just the height. Due to slight magnetic field inhomogeneity some molecules will resonate around an approximate frequency, rather than at an exact frequency, and this method accounts for molecules resonating slightly above or below the estimated frequency.

Interestingly, each of the integral graphs (*figure 5.6*) demonstrates a higher mean integral for the $SOD1^{G93A}$ compared to the non-transgenic spectra for PCr (non-transgenic $1.9x10^7 \pm 4.1x10^6$ vs $SOD1^{G93A}$ $2.2x10^7 \pm 4.6x10^6$), Pi (non-transgenic $1.6x10^7 \pm 3.3x10^6$ vs $SOD1^{G93A}$ $1.8x10^7 \pm 3.8x10^6$), and ATP (non-transgenic $5.3x10^7 \pm 1.2x10^7$ vs $SOD1^{G93A}$ $6.5x10^7 \pm 1.2x10^7$). This appears most marked for ATP. However, these differences were not statistically significant.

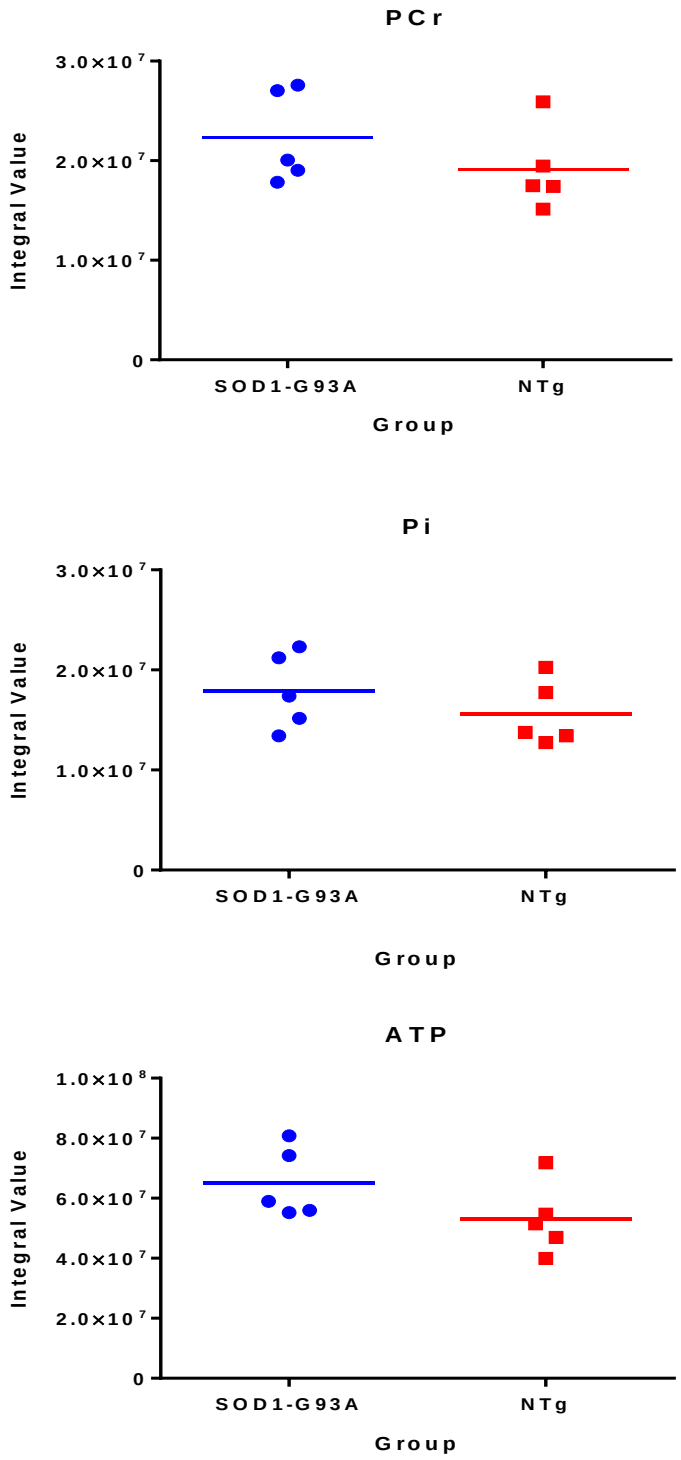

Figure 5. 6: Scatter plot graphs illustrating metabolite integrals for PCr, Pi and ATP in the SOD1^{G93A} and non-transgenic (NTg) (n = 6) mice at 36 days of age.

Unpaired t-tests showed no significant difference between groups with any of the metabolites.

5.4.4. Adverse Events

During the week after scanning, several mice developed a necrotic-like appearance to the tail. These mice were immediately humanely sacrificed. To determine whether this might be caused by air flow in the scanner we scanned a single mouse with its tail covered by a wet gauze. This modification to the technique prevented the adverse event from occurring, and was used for subsequent scans.

5.4.5. Pilot Study 73-Day Scanning

Six pairs of mice were scanned at 73 days of age using the 31P-MRS surface coil to obtain whole brain coverage. An ice pack was applied between scans to reduce the temperature of the coil. The tails of the mice were covered with wet gauze in an attempt to avoid tail necrosis. Two mice died during scanning under anaesthesia, reducing the number of mice in the non-transgenic group to 4.

When normalised to the PCr peak, the brain spectra from the transgenic mice appeared to show higher PME, Pi, γ-ATP, α-ATP and β-ATP compared to the non-transgenic mice (*figure 5.7*). There was no difference in PDE. However, it appears likely that these differences in spectra are due to a lower PCr peak in the transgenic spectra, consequentially increasing the other peaks when the PCr peaks are normalised to 1. To compare peaks more easily, ratios of peaks heights and integrals of peaks were compared.

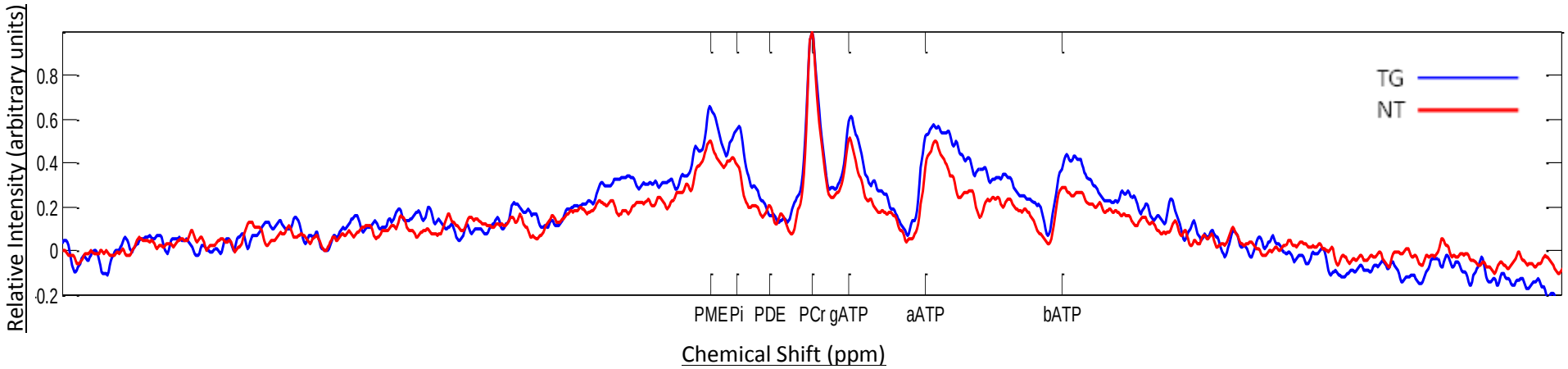

Figure 5. 7: Average 31P-MRS spectra of whole mouse brain at 73 days of age (6 SOD1^{G93A}, 4 NTg), TR = 4s.

PME: phosphomonoesters; Pi: inorganic phosphate; PDE: phosphodiesters; PCr: phosphocreatine; gATP: γ-ATP; αATP: α-ATP; bATP: β-ATP. Peak height of PCr normalised to 1.

The main pattern evident in the ratios of peak heights at 73 days of age (*figure 5.8*) is that ATP/PCr (non-transgenic 0.66±0.19 vs SOD1^{G93A} 0.79±0.09) appears higher in the SOD1^{G93A} group than in the non-transgenic group. In contrast, ATP/Pi ratios (non-transgenic 0.61±0.11 vs SOD1^{G93A} 0.61±0.08) appear lower in the transgenic group and Pi/PCr (non-transgenic 0.39±0.06 vs SOD1^{G93A} 0.47±0.05) is slightly higher in the SOD1^{G93A} group compared to the non-transgenic.

Although the ATP/PCr ratio initially appears significantly higher in SOD1^{G93A} mice compared to the non-transgenic mice on a student's t-test ($p<0.05$), the significant difference between the peak height ratio ATP/PCr is no longer significant when calculations are adjusted using a bonferroni correction.

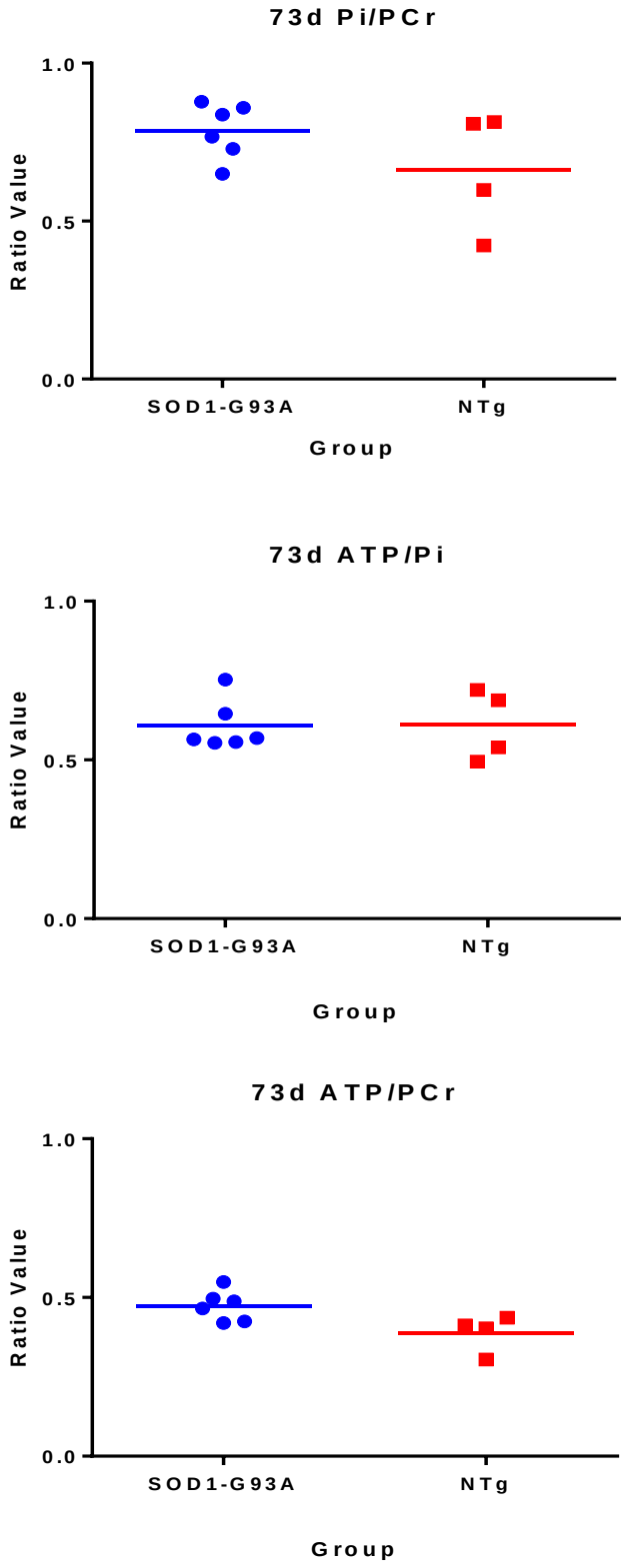

Figure 5. 8: Scatter plot graphs illustrating metabolite peak height ratios in the SOD1^{G93A} (n = 6) and non-transgenic (NTg) (n = 4) mice groups at 73 days of age.

Unpaired t-tests showed no significant difference between Tg and NTg spectra for any ratios.

Interestingly, each of the integral graphs for 73 days of age (*figure 5.9*) show a slightly higher mean integral for the non-transgenic spectra compared to the $SOD1^{G93A}$ spectra for PCr (non-transgenic $2.2x10^7 \pm 1x10^7$ vs $SOD1^{G93A}$ $1.9x10^7 \pm 8.1x10^6$), Pi (non-transgenic $1.7x10^7 \pm 8.2x10^6$ vs $SOD1^{G93A}$ $1.6x10^7 \pm 6.8x10^6$), and ATP (non-transgenic $6x10^7 \pm 3x10^7$ vs $SOD1^{G93A}$ $5.7x10^7 \pm 2.5x10^7$), showing the opposite trend to the 36-day integral values. However, these differences are non-significant.

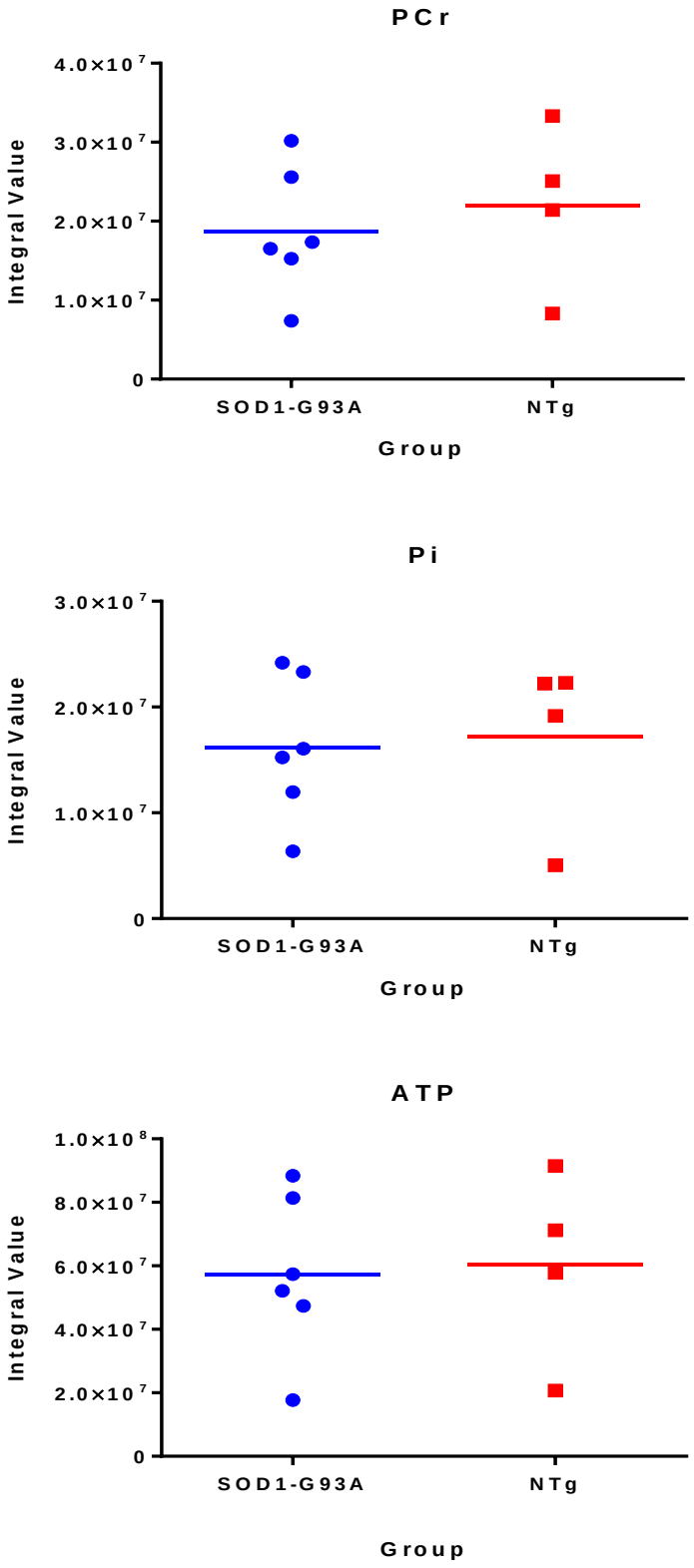

Figure 5.9: Scatter plot graphs illustrating metabolite integrals for PCr, Pi and ATP in the SOD1^{G93A} (n = 6) and non-transgenic (NTg) (n = 4) mice at 73 days of age.

Unpaired t-tests showed no significant difference between groups with any of the metabolites.

5.4.6. Adverse Events

During the week after scanning, despite use of the wet gauze, several mice developed a necrotic-like appearance to the tail. These mice were immediately humanely sacrificed.

5.4.7. Pilot Study 115-Day Scanning

Three pairs of mice were scanned at 115 days of age using the 31P-MRS surface coil to achieve whole brain coverage. The core temperature of the mice was maintained using a heat pad rather than the hot air system. One mouse died during scanning as it did not survive the anaesthesia and one mouse was scanned using a shorter TR so could not be grouped with other scans. Therefore, data were collected from 4 mice only.

When normalised to the PCr peak, the spectra of the $SOD1^{G93A}$ brain appeared to show lower PME, PDE and Pi compared to the non-transgenic brain (*figure 5.10*). However, no obvious differences can be observed between the γ-ATP, α-ATP and β-ATP peaks. To compare peaks more quantitatively, ratios of peak heights and integrals of peaks were compared.

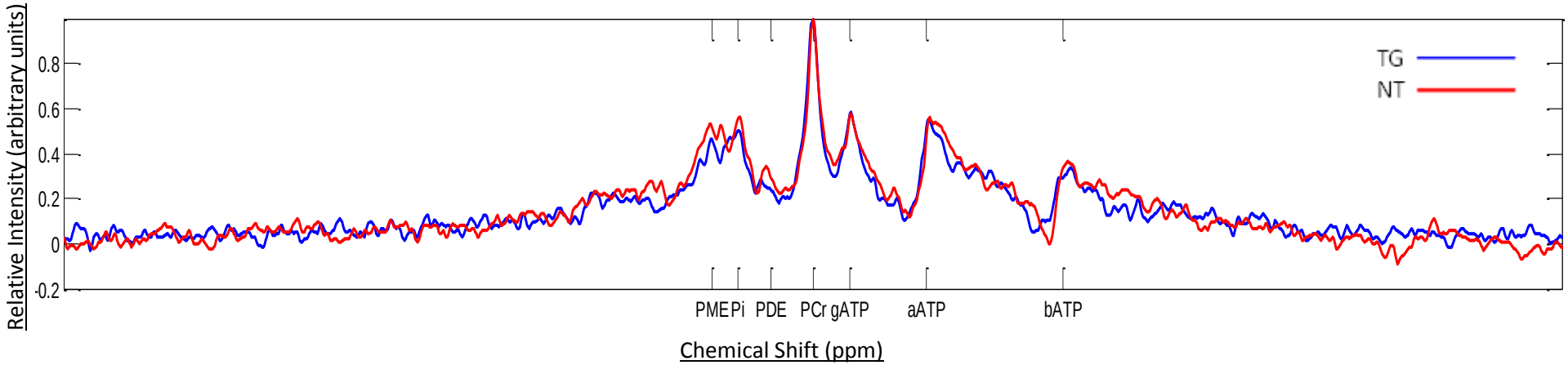

Figure 5. 70: Average 31P-MRS spectra of whole mouse brain at 115 days of age (1 SOD1^{G93A}, 3 NTg), TR = 4s.

PME: phosphomonoesters; Pi: inorganic phosphate; PDE: phosphodiesters; PCr: phosphocreatine; gATP: γ-ATP; aATP: α-ATP; bATP: β-ATP. Peak height of PCr normalised to 1.

The peak heights data for 115 days of age are shown in *figure 5.11* for comparison with previous time points. However, there are insufficient data to draw any conclusions or conduct statistical analysis between groups.

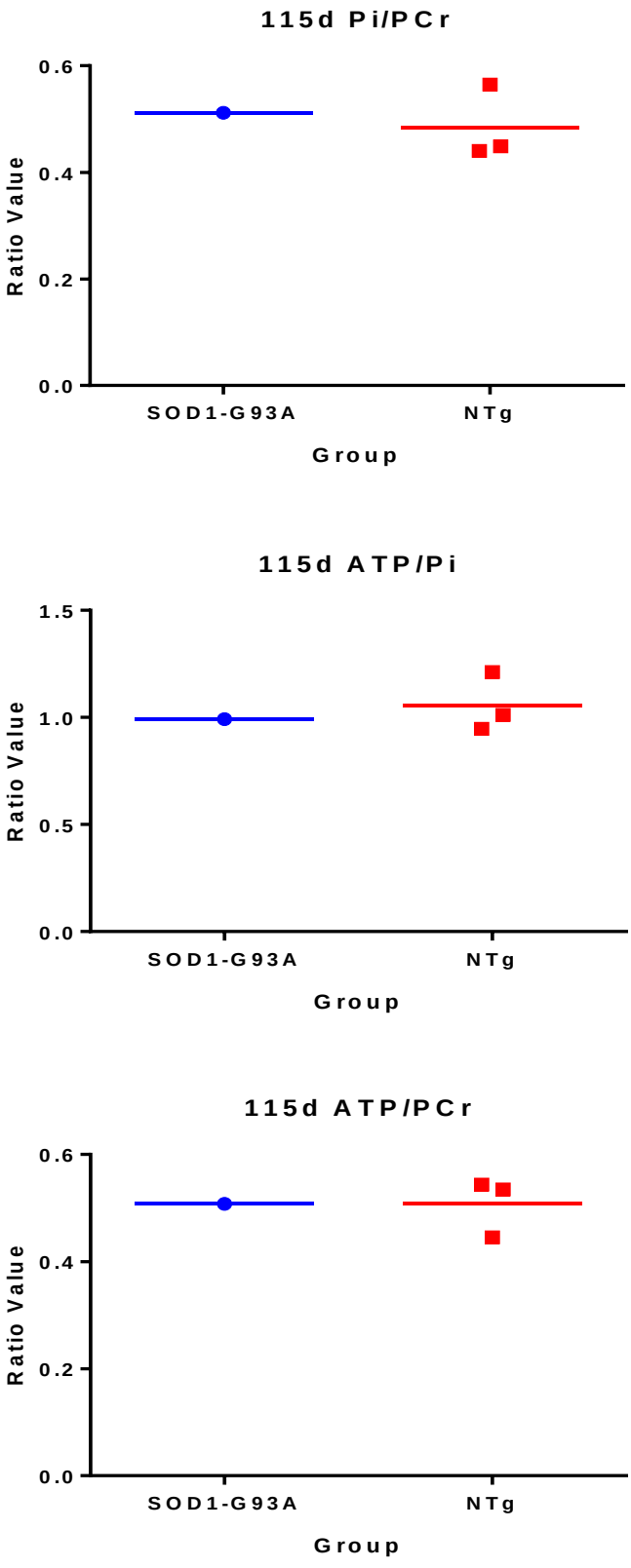

Figure 5. 81: Scatter plot graphs illustrating metabolite peak height ratios in the SOD1^{G93A} (n = 1) and non-transgenic (NTg) (n = 3) mice groups at 115 days of age.

There were insufficient numbers to perform formal statistical testing.

The peak integral graphs at 115 days of age are shown in *figure 5.12* below. Again, there are no obvious differences between groups and insufficient data to draw conclusions.

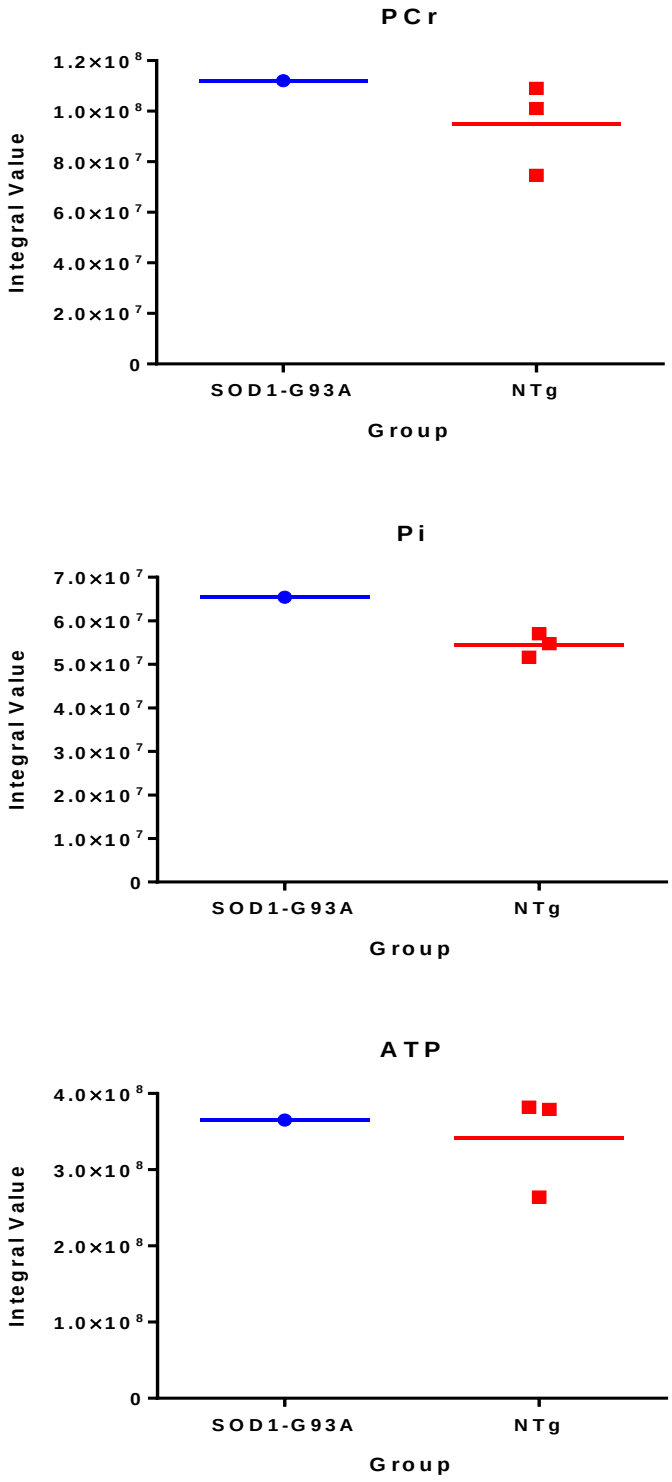

Figure 5. 92: Scatter plot graphs illustrating metabolite integrals for PCr, Pi and ATP in the SOD1^{G93A} (n = 1) and non-transgenic (NTg) (n = 3) mice at 115 days of age.

There were insufficient numbers to perform formal statistical testing.

5.4.8. Adverse Events

During the week after scanning, several mice developed a necrotic-like appearance to the tail and feet. These mice were immediately humanely sacrificed.

5.4.9. Changes in 31P-MRS Over Time

The changes in 31P-MRS peak height ratios over time show no statistically significant changes between 36 and 73 days of age using a two-way ANOVA (*figure 5.13*). 115 day data was not plotted as there was only one mouse in the $SOD1^{G93A}$ group.

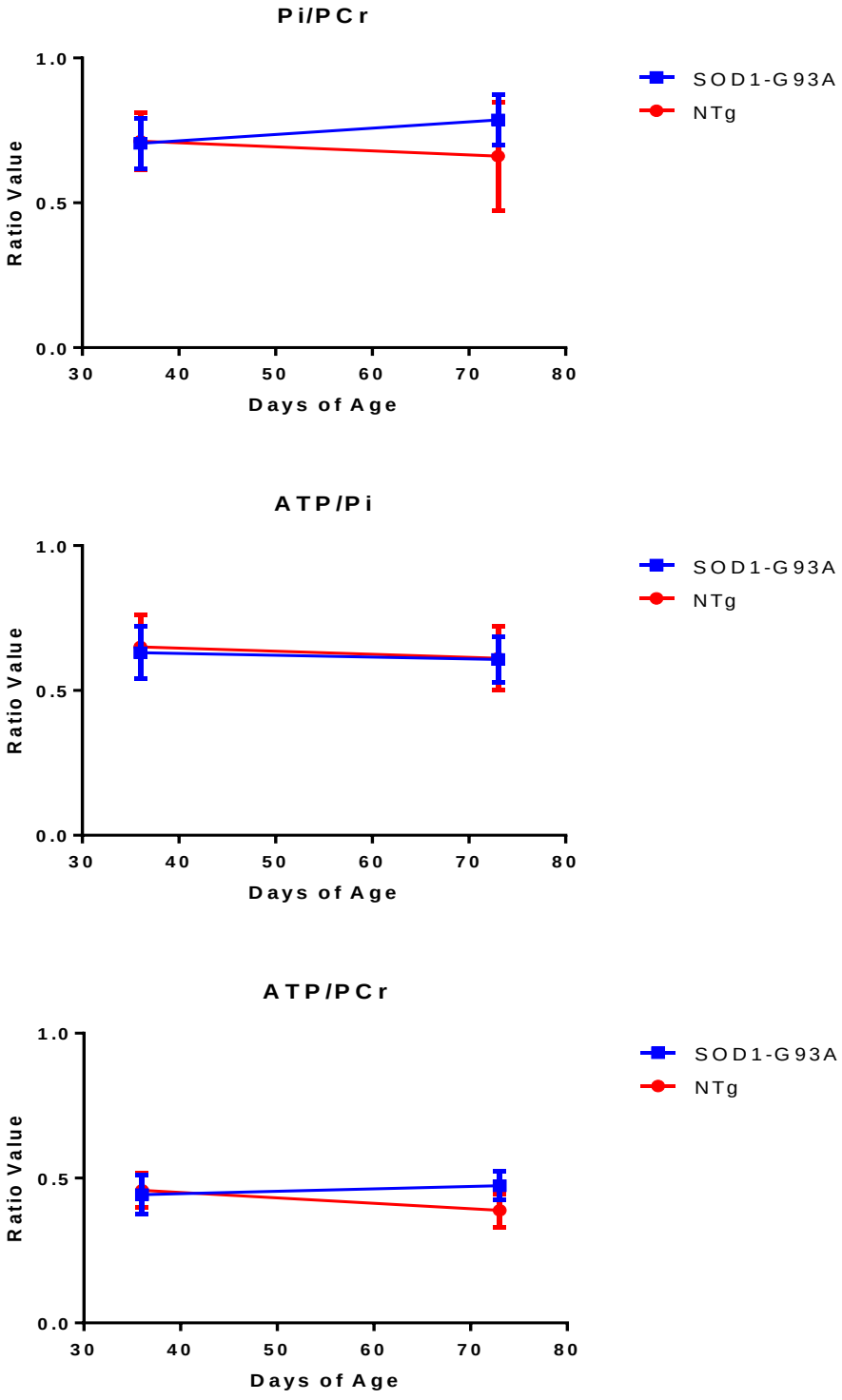

Figure 5. 103: Changes in 31P-MRS peak height ratios from 36 days of age (SOD1^{G93A} n = 6, NTg n = 6) to 73 days of age (Tg n = 6, NTg n = 4). TR = 4s.

The changes in 31P-MRS integrals over time also show no statistically significant changes between 36 and 73 days of age on a two-way ANOVA (*figure 5.14*).

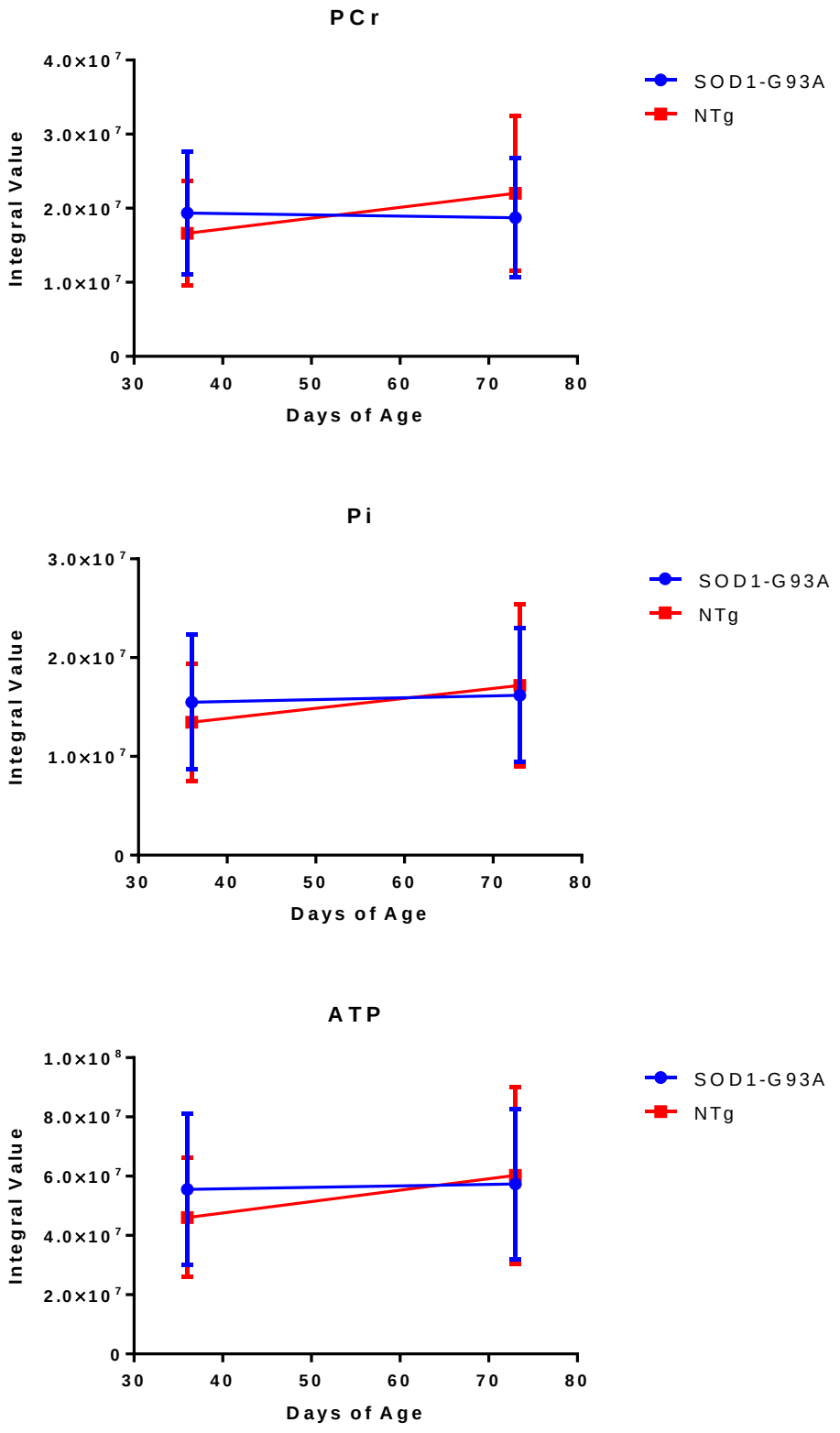

Figure 5. 114: Changes in 31P-MRS peak integrals from 36 days of age (SOD1^{G93A} n = 6, NTg n = 6) to 73 days of age (Tg n = 6, NTg n = 4). TR = 4s.

5.4.10. Water Bath Method

The water bath tubing within the mouse scanning bed did not cover the whole area in which the mouse lays. Therefore, an attempt was made to maintain body temperature of the mouse using this method outside of the magnet, prior to any attempts within the magnet, where the temperature is lower.

Unfortunately, the mouse could not maintain body temperature using this method and had to be removed from the bed and placed in the incubator. This heating method was therefore deemed unsafe for use.

5.4.11. 31P-MRS Findings from Final Experiment

At a much later time point and after several discussions with the vet, project licence holder, and head of Biological Services, a final attempt was made to collect 31P-MRS data from 2 pairs of mice at 49-50 days of age. In this experiment the mice were wrapped in a cotton blanket before the heat pad was placed over the back of the mouse.

The mean spectra suggest decreased Pi concentrations in the SOD1^{G93A} mice compared to the non-transgenic but no obvious differences in any other peaks. However, due to normalisation to the PCr peak, it is more informative to look at peak ratio values.

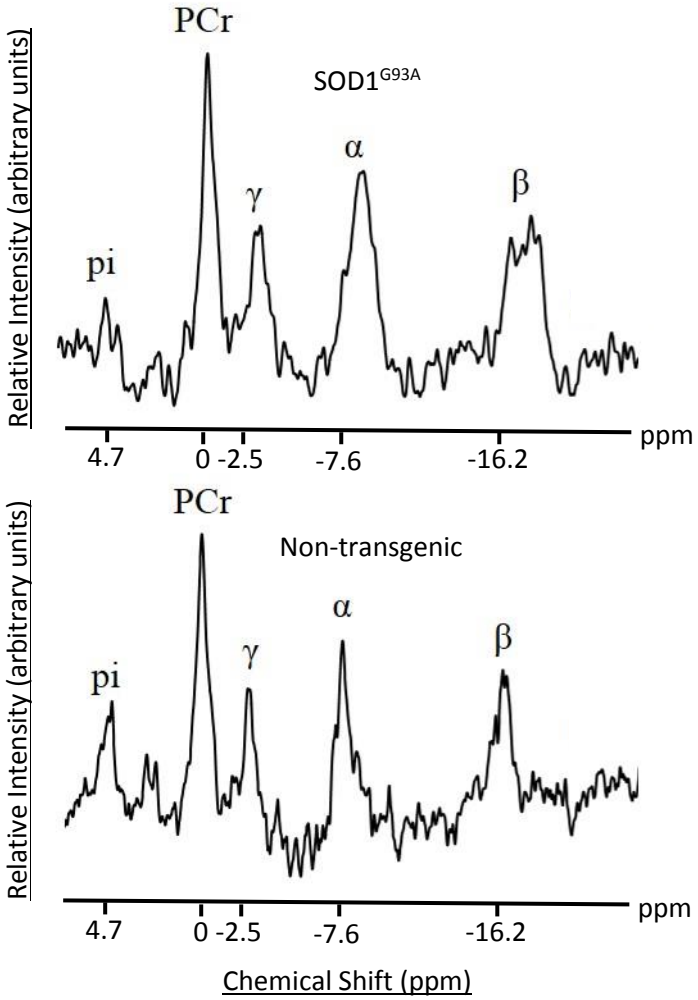

Figure 5. 15: Mean 31P-MRS spectra for 49-50 day old SOD1^{G93A} and non-transgenic mice (n = 2).

Spectra are normalised to PCr peaks. Peaks are identified for Pi, PCr, γ-ATP, α-ATP, and β-ATP.

The ratio values (*figure 5.16*) show a lower Pi/PCr for the SOD1^{G93A} mice compared to the non-transgenic, and a higher ATP/Pi, whilst ATP/PCr looks to be similar. Considering the small numbers of mice in each group (n = 2), statistical differences were not calculated.

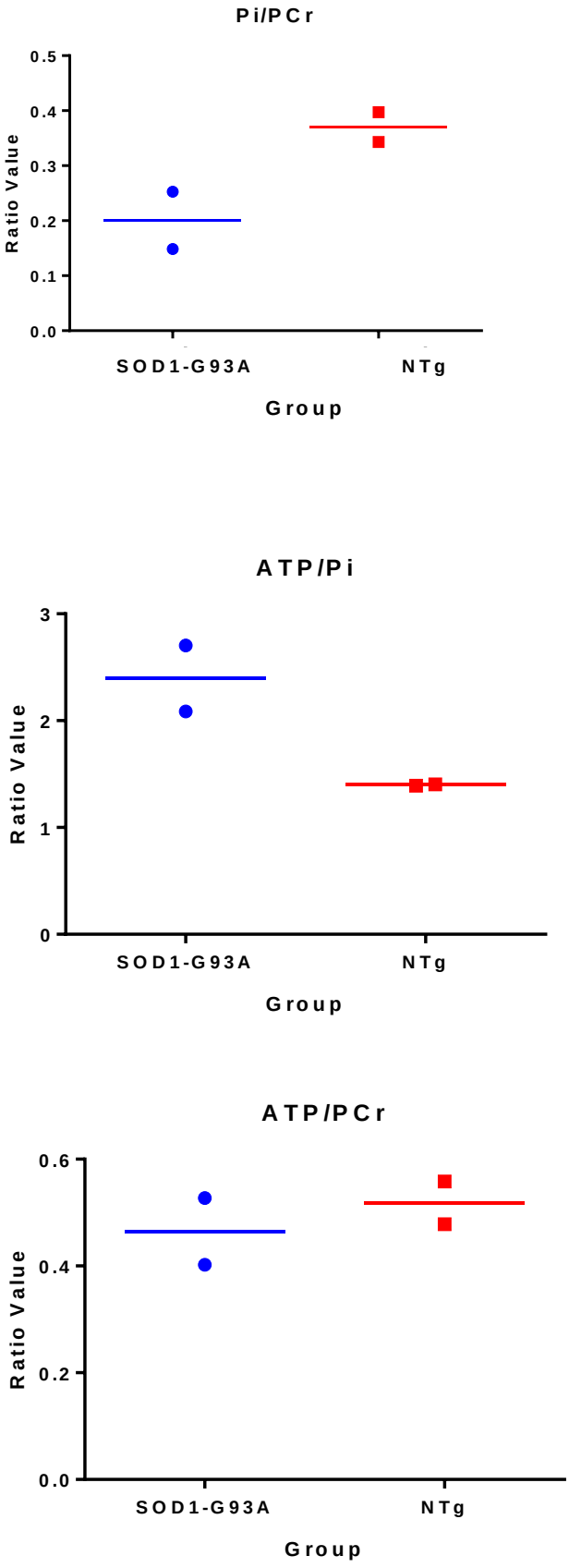

Figure 5. 16: Ratio values for mean spectra of the final set of scanning (n = 2).

There were insufficient data to calculate statistical differences.

5.4.12. Final Heat Pad Method

With this method, the mouse was wrapped in a cotton blanket before application of the heat pad to the back. It was ensured that the heat pad was kept well away from the tail of the mouse. Despite this, within 24 hours, damage to the tail was evident.

After the mouse was culled, the tail was removed and sent to Central Diagnostic Services at the University of Cambridge for histological analysis. The report stated a diagnosis of severe extensive coagulation necrosis oedema and perivascular inflammation consistent with thermal injury. From this, it can be concluded that overheating is a problem, but no solution has been found thus far.

5.4.13. Comparison of Scanning Parameters

One of the major limitations of this technique in mice is the lack of signal from such a small volume of tissue, requiring long sequences with multiple scans averaged to improve signal to noise ratio. During discussions with colleagues at the nuclear magnetic resonance (NMR) facility at the University of Sheffield it was suggested that a shorter TR would allow for more data points to be collected within the same time frame, possibly increasing the signal to noise ratio and eliminating the 'phospholipid bump' seen in *figure 5.17* (black spectra).

Subsequently, a shorter TR of 0.4s, collecting 4000 data points, was used. The main limitation of this method is that a short TR may prevent the molecules relaxing back to their original state between scanning points, so may not represent the number of phosphates present in the tissue, making the data less quantitative. As shown by the red spectra in *figure 5.17*, this method eliminates the 'phospholipid bump', reducing the amount of post-processing required for analysis.

During the final period of scanning, a third set of parameters were used, with a narrower spectral width (*figure 5.17*, green spectra), allowing for higher resolution. This method acquired a similar resolution of scanning with a much shorter scanning time, when compared to the previous scanning parameters.

The purpose of this comparison was to investigate whether the larger number of averages in the 0.4s TR scan would improve the signal-to-noise ratio of the spectra whilst

maintaining a spectrum which is representative of the tissue phosphates and therefore, similar to the scans which used a 4s TR.

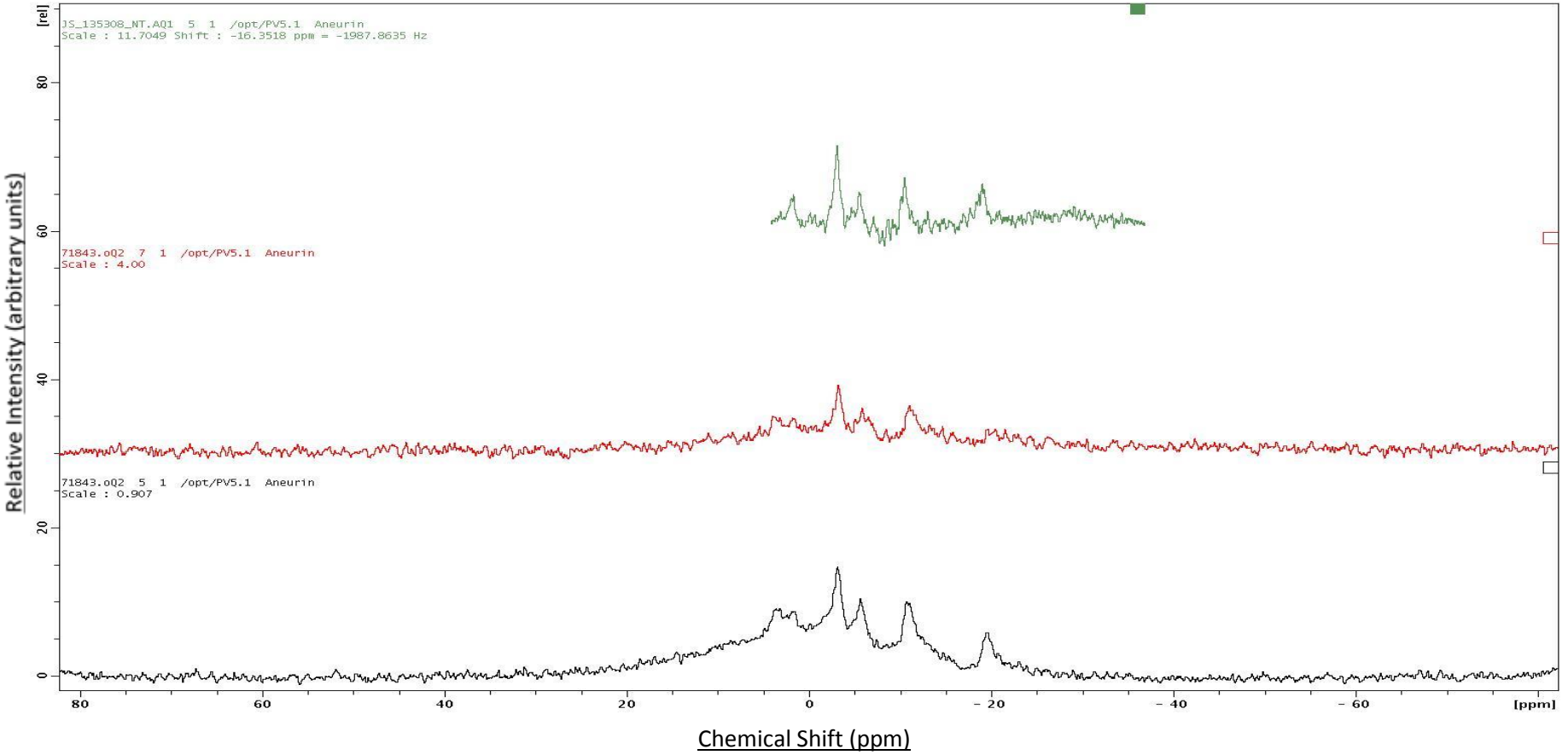

Figure 5.17: Raw spectra from each set of scanning parameters.

The original scanning parameters (long TR) shown in black, short TR shown in red, and a shorter spectral width shown in green. All spectra are from whole brain, male non-transgenic mice.

5.5. Discussion

5.5.1. Feasibility of 31P-MRS

This pilot study investigating 31P-MRS scanning in mice demonstrated technical feasibility as spectra were reproducible, with similar profiles and peak locations to previously published work in mice (Renema et al., 2003, Tracey et al., 1996). However, the experiment was limited by significant and recurrent problems relating to mouse welfare, which are discussed below.

When attempting to work up a 31P-MRS protocol, it may have been more appropriate to use mouse models of metabolic disease, in which the differences in metabolite levels between non-transgenic and disease groups would have been far greater and predictions of differences could have been made. 31P-MRS findings would then have been further validated. This may be worthy of consideration for any further studies in to 31P-MRS in mice, prior to looking for subtle differences in metabolites.

5.5.2. Adverse Events

No studies could be found which reported necrosis of rodents caused by MRS, anaesthesia, or by use of any similar heating systems. Other groups conducting MRI in mice at other academic centres have used circulating warmed water, so this technique was attempted. However, our water system proved insufficient to maintain body temperature in the mice.

Previous experience from our group using the same mouse model applying MRI to detect muscle volume changes at 30, 60, 90 and 120 days, had not identified any issues (Mead et al., 2011), so this problem was not foreseen. However, since these studies were performed, a new magnet was purchased which ran at a colder temperature and we hypothesise that this made the heating system insufficient and during the initial equilibrium phase, additional demands on the system may have led to higher local temperatures. This decreased temperature of the magnet system was adjusted by the

manufacturers after our initial issues. However, we continued to have serious problems despite switching to a water system and then a heat pad with cotton blanket. Therefore, it appears that despite the temperature of the magnet bore being as warm as possible, the heating systems were still having to work very hard, causing necrosis with the heat pad and cotton blanket protocol, as confirmed by a diagnostic report.

The reasons for necrotic-like appearance to the tail in MRS studies remains a mystery. Several attempts were made to resolve this issue, but none were successful. We therefore conclude that this approach is not suitable for further investigation in our models.

5.5.3. Comparison of 31P-MRS in SOD1^{G93A} and Non-Transgenic Mice

Due to the issues described above, the conclusions drawn from our experiments are limited. No ratios of peak heights were found to have significant differences between the transgenic and non-transgenic groups, at 36, 73 or 115 days of age. No significant findings were found in the differences between transgenic and non-transgenic peak integrals at 36, 73 or 115 days of age. The limitations of small sample size reached their peak at 115 days of age, at which time only one mouse was in the transgenic group, precluding statistical analysis. The last set of scanning was also carried out with too few mice to analyse the data statistically but no recurrent trends were found in the data as a whole.

In a previous study using this mouse model, ATP was found to be lower in the brain at end stage (17 weeks of age) using a luciferase/luciferin based assay (Mattiazzi et al., 2002). Therefore, with larger group sizes, it would be hypothesised that a decrease in ATP-values may be found at the end stage of disease. We can neither confirm nor refute this hypothesis with the data acquired in this study. Overall, no conclusions can be made with regard to differences in 31P-MRS spectra between transgenic and non-transgenic mice, without testing larger group sizes. It must also be considered that these scans were of whole brain, whereas MND affects some, but not all brain areas. Therefore, scans of specific brain regions, such as the forebrain, may represent an alternative approach.

5.5.4. Changes in 31P-MRS over Time

The 115 day scan results could not be included in the comparison of 31P-MRS over time due to attrition of the sample size. Comparison of peak heights and peak integrals between 36 and 73 days of age in the pilot study showed no significant differences. However, as mentioned previously, increased group sizes would be necessary to find out whether there are any differences in peaks over time.

This is a novel area of investigation in MND mouse models and in the human disease. No reports could be found in the literature for 31P-MRS in mouse or human brains with age, therefore, it is unknown what may be expected if 31P-MRS was investigated further in $SOD1^{G93A}$ mice.

5.5.5. Comparison of 31P-MRS Scanning Parameters

Throughout the study, scanning parameters were adjusted to improve the quality of the spectra by firstly shortening the TR, then shortening the spectral width.

It is possible that the long TR scanning provides more quantitative peaks, as the phosphorus molecules can fully relax between scans, providing a similar signal with each scan. Whereas, with the short TR, phosphorus molecules may not have time to fully relax between scans, resulting in peak heights which do not represent the absolute number of phosphorus molecules in a particular environment but are relative to the number of phosphorus molecules. However, the long TR results in a large bump under the spectra, deemed to be a 'phospholipid bump', and shortening the TR eliminates this bump.

Shortening of the spectral width prevents the scans recording activity from areas of the spectra which are not of interest and subsequently, shortens the scanning time. In the interests of welfare, a shorter scanning time is always preferable as it reduces the chance of the mice failing to recover from the anaesthesia. In future studies, a shorter scanning time would therefore be recommended.

5.6. Conclusions

This study revealed a problem with the methods used to maintain mouse body temperature during MRS imaging that proved to be intractable.

The best scanning parameters were the final set in which the spectral width was reduced, producing a good quality spectra whilst decreasing the amount time the mice spend in the scanner. These parameters would be preferable for future studies.

6. Discussion

6.1. Was the TDP-43^{Q331K} Mouse Model an Appropriate Choice?

As discussed in chapter 1, the main reason for choosing this TDP-43^{Q331K} mouse model (Arnold et al., 2013) was to avoid a knockout or a high overexpression of TDP-43, ensuring that the genotype of the mice was as close to the human MND genotype as possible (i.e. a mutation in the endogenous gene). Since the acquisition of this model, CRISPR/Cas9 technology has been developed for use in mouse models, enabling the knock-in of specific mutations in the endogenous mouse gene with relative ease (Wu et al., 2013, Platt et al., 2014). This technology provides a fast method of creating mouse models without the overexpression caused by most other techniques, and could provide the ideal disease model genotype. However, at the time of choosing a TDP-43 mouse model, this technique was not available and no other knock-in TDP-43 mouse models had been created.

Investigations made here have found that the overexpression of TDP-43 in this model was slightly higher than expected from previous findings (Arnold et al., 2013). However, this overexpression is still moderately low compared to the overexpression levels in other models (see *table 1.4*).

The main qualities required in a TDP-43 model were defined in chapter 1 as: being on a defined genetic background, having a reproducible phenotype with low variability in readouts, disease homogeneity, a mild-moderate disease severity, a moderate disease length, having an appropriate control line, having a degenerative phenotype due to loss of motor neurons, and signs of MND pathology.

Many of these criteria were already met by choosing the TDP-43^{Q331K} mouse model over other models, including the defined genetic background (due to backcrossing at Jackson laboratories), which in turn increases disease homogeneity, and an appropriate control line was also available; the TDP-43^{WT} line. During this project, three *in vivo* studies were carried out to investigate the remaining characteristics. The low variability was evident in the coefficients of variation for most of the phenotypic readouts, including rotarod performance, catwalk gait analysis, running wheel performance and marble burying, as well as by the relatively low numbers of animals required to achieve good statistical power for detecting changes of 10-20% from the baseline.

The data were similar between studies, particularly for catwalk gait analysis. However, there was a noticeable drift in weight and rotarod data across studies, by which the increase in weight and decline in rotarod performance were not as large in the later studies of TDP-43^{Q331K} mice. There is a need here for replication studies to establish the reason for these shifts in data and to assess the influence of these on preclinical trial data. It is also important to replicate studies at different centres to ensure the model is robust.

Copy number showed some variability in the TDP-43^{Q331K} line and it is known that copy number can cause wide variability in phenotype in mutant SOD1 transgenic mice (Alexander et al., 2004). Tissue was not available to investigate the TDP-43 expression levels and pathological differences between the mice tested for TDP-43 copy number, hence only rotarod differences were investigated, which were not suggestive of a difference in phenotype. This, coupled with the low variability found in all three *in vivo* studies, indicates that the low copy number observed in two TDP-43^{Q331K} mice was likely due to a technical error. Ideally, further investigation would be made by sending a larger number of samples for gene copy number estimation.

As expected from previous studies (Arnold et al., 2013, Mitchell et al., 2015), the disease phenotype of TDP-43^{Q331K} mice was relatively mild and did not progress to a state of paralysis or a humane end point, ensuring minimal distress. Our studies suggested that the disease progression beyond 6 months of age was minimal, and that a 6 month study, as opposed to 10 months, provided a big enough window in phenotype to measure neuroprotective agents or to investigate the mechanisms of pathogenesis. This greatly reduces the cost and time required for studies in this model, and also reduces the total distress experienced by the mice under study, satisfying the refinement aspect of *in vivo* studies.

A degenerative phenotype was evident in the TDP-43^{Q331K} mice which showed reduced rotarod performance, reduced muscle mass, reduced CMAP, reduced repetitive stimulation response, and spontaneous EMG activity. However, this cannot be supported by a reduced number of motor neurons as, although this investigation was planned, it was not completed due to issues with tissue quality and time constraints. A reduced number of motor neurons is to be expected as a 35% reduction in motor neurons at 12 months of age was recorded previously in this model when on a

C57BL/6NCrl background (Arnold et al., 2013). Furthermore, a reduction in CMAP amplitude (as reported in chapter 4) is suggestive of motor axon loss. Despite this, the counting of motor neurons is a key investigation for further study as it would confirm whether the cell body of the motor neurons are also lost. Investigation of NMJ integrity (suggested by the reduced response to repetitive stimulation shown in chapter 4) is also of importance, as it could confirm the presence of a 'dying back' axonopathy, as found in both MND patients and the $SOD1^{G93A}$ mouse model (Dadon-Nachum et al., 2011, Fischer et al., 2004).

Pathological investigations confirmed the presence of astrogliosis and microgliosis in the spinal cord of TDP-43^{Q331K} mice, as found previously (Arnold et al., 2013, Mitchell et al., 2015). Although nuclear clearing of TDP-43 with increased cytoplasmic levels are found in motor neurons in MND (Neumann et al., 2006), we identified elevated TDP-43 levels in the nucleus of spinal motor neurons in the TDP-43^{Q331K} mice, which is the converse of findings in MND patient motor neurons (Neumann et al., 2006, Tollervey et al., 2011). It is interesting that a degenerative phenotype is present in such a scenario and may suggest the absolute level of TDP-43 in either compartment (nucleus or cytoplasm), or overall, is the critical factor.

The absolute level of TDP-43 expression, as described in the introduction, has been clearly linked to neurodegeneration and in models with significant wild type overexpression, a very severe phenotype is found. This was the reason why one the main criteria for choosing this model was that the total TDP-43 gene expression and protein levels were deemed to be similar to those in the wild type and non-transgenic mice (Arnold et al., 2013). However, upon investigation we found that total TDP-43 levels in the wild-type mice were approximately 2-fold that of the non-transgenic mice, and 3-fold in the TDP-43^{Q331K} mice, differing depending on tissue type and considerably higher than the levels reported previously. This poses potential for an influence of the overexpression on the TDP-43^{Q331K} mice which is independent of the mutation, however this is expected to be of little relevance as these overexpression levels are still relatively low compared to wild type overexpression models (Wils et al., 2010, Shan et al., 2010). The importance of total TDP-43 expression levels is perhaps best emphasised by the report in which TDP-43^{Q331K} mice were crossed with TDP-43^{WT}, creating a TDP-$43^{Q331K/WT}$ mouse with a severe phenotype, resulting in a total TDP-43 expression in the brain of

over 4-fold that of non-transgenic mice, and death by 8-10 weeks of age (Mitchell et al., 2015). Although this overexpression is not dramatically higher than seen here in the TDP-43^{Q331K} mice, the effect on the phenotype is dramatic. It appears that a 4-fold total TDP-43 expression level pushes the TDP-43 levels beyond a threshold, which accelerates the disease course and causes severe motor dysfunction with a striking TDP-43 pathology.

Further investigation for TDP-43 pathology is required in the TDP-43^{Q331K} model as aggregates and inclusions were not identified in this project, although cytoplasmic ubiquitin and p62-positive inclusions of TDP-43 have been identified in TDP-43$^{Q331K/WT}$ motor cortex and spinal cord at 8 weeks of age (Mitchell et al., 2015). Immunostaining for phospho-TDP-43, p62 and ubiquitin should be conducted in the brain and spinal cord of TDP-43^{Q331K} mice, all of which have been identified in motor neurons of MND patients (Neumann et al., 2006, Arai et al., 2006).

All-in-all, this model met most of the requirements expected of a TDP-43 mouse model and presented as the best available model at the time of choosing. However, more investigation is required to confirm the pathology and pattern of motor neuron death in this model, as well the potential for genetic drift within the colonies.

6.2. Utility of the TDP-43^{Q331K} Mouse Model for Pre-clinical Trials

As described in *table 2.4*, many readouts measured in this model have provided data with low variability, which is ideal when looking for a treatment effect in preclinical trials. Based on this, power analysis has suggested group sizes of 14 females, which is a relatively low number of animals per group for pre-clinical trials, when compared to the SOD1^{G93A} model (Scott et al., 2008).

Treatment effects in therapeutic preclinical trials of TDP-43^{Q331K} mice can be identified by measuring motor phenotype, which can be easily and reliably measured using rotarod (Hamm et al., 1994, Gilli et al., 2016). These findings can also be supported using more time consuming measurements such as neuroscoring, Catwalk gait analysis and electrophysiological studies. Pathologically, a treatment effect may be identified by a reduction in astrogliosis, microgliosis or cytoplasmic TDP-43 levels. Added to this, further pathological studies of spinal cord, brain and muscle in this model may add to

the pathological readouts which may identify treatment effects. Electrophysiological studies may be of particular relevance for preclinical trials as this is a measurement which can also be monitored in patients, increasing the translational aspects of the transition from preclinical to patient trials.

The TDP-43^{Q331K} mouse model was characterised in this project in the hope that it may be representative of a larger population of MND patients compared to the SOD1^{G93A} mouse model, increasing translation from MND models to patients. We showed here that the TDP-43^{Q331K} mice have increased cytoplasmic TDP-43 in spinal cord motor neurons, as found in MND patients (Neumann et al., 2006, Arai et al., 2006), and clear signs of a neurodegenerative phenotype, coupled with a potential FTD phenotype, all of which can be reliably monitored. The TDP-43^{Q331K} mouse model is therefore well suited to pre-clinical trials due to the low variability, moderate length disease course and reliability of readouts.

However, it is key to replicate studies within the centre and across centres to establish the robustness of the model, prior to its use in preclinical trials.

6.3. How Problematic is the Increased Weight of TDP-43^{Q331K} Mice?

An unexpected finding in this project was the increased weight of TDP-43^{Q331K} mice compared to their TDP-43^{WT} counterparts, the reason for which remains unknown. Slightly decreased voluntary activity levels and increased food intake were found, which may be indicative of FTD (see chapter 3) and in part, explain the increased weight.

The increased weight was a concern as it may confound other findings such as the rotarod (Stover et al., 2015) and catwalk gait analysis (Deumens et al., 2007). However, after a number of methods were considered, the rotarod data were normalised for weight, and a decline in rotarod performance was still evident. Also, weight is unlikely to impact on electrophysiological and pathological investigations, providing reliable measures of neurodegeneration, regardless of weight. Furthermore, reduced muscle mass was identified in the hindlimb, which is certainly not linked with the increased body weight.

We therefore suggest that motor function testing should always be supported by electrophysiological and/or pathological studies in therapeutic trials using the TDP-

43^{Q331K} mouse model and weight should always be monitored so it can be taken in to account for rotarod measurements.

6.4. Does the TDP-43^{Q331K} Mouse Model the MND-FTD Continuum?

Signs of apathy, reduced activity levels and over-eating are found in FTD patients (Ahmed et al., 2016b, Chan et al., 2015), and led to an investigation of cognitive function in the TDP-43^{Q331K} mice. Marble burying was chosen as a simple, yet effective measurement of normal exploratory behaviour (digging). As hypothesised, TDP-43^{Q331K} mice buried significantly less marbles than TDP-43^{WT} mice, suggesting reduced digging behaviour, which may be interpreted as a sign of apathy.

Apathy combined with over-eating is highly suggestive of FTD in the TDP-43^{Q331K} mice. However, other measurements of FTD such as a lack of social interaction, anxiety, repetitive behaviour, and a lack of fear response must be carried out in these mice before an assumption of FTD can be made. Further studies could include a three chamber social approach test (Gascon et al., 2014, Yin et al., 2010), which may confirm or refute the hypothesis that reduced marble burying may be interpreted as a sign of FTD.

6.5. The Implications of Riluzole Having no Treatment Effect on Motor Function in TDP-43^{Q331K} Mice

Riluzole is the only drug which has been licenced for treatment of MND and has been predicted to extend life by as long as 12 months (Georgoulopoulou et al., 2013, Miller et al., 2012). However, other studies have suggested riluzole has little or no effect on MND (Stewart et al., 2001) and this may be related to the concept of subgroups, limiting its overall effect on the MND population (Georgoulopoulou et al., 2013).

Studies on the effect of riluzole in $SOD1^{G93A}$ mice have reported mixed findings (Gurney et al., 1998, Li et al., 2013, Scott et al., 2008), so it is debatable whether riluzole is an effective treatment in this model. It is interesting therefore, that riluzole appeared to have no significant effect on motor function in TDP-43^{Q331K} mice. However, as discussed in the Summary of Product Characteristics for riluzole, no effect has been found on motor function in MND patients, only on survival. A potential treatment effect was

identified here in the repetitive stimulation results for TDP-43^{Q331K} mice, suggestive of a subtle rescue effect at the NMJ, but this finding requires further investigation, including NMJ histology.

It could be that a higher dose of riluzole is required to see a more definite treatment effect in the TDP-43^{Q331K} mouse model but such an effect may never appear as a clear rescue of motor function. The possibility of using a higher dose is highlighted by comparing the riluzole PK concentrations to studies in SOD1^{G93A} mice (in-house data), for which the TDP-43^{Q331K} data is within the trough range for both blood and brain. Future studies should include the administration of riluzole at a higher dose, in which the blood levels of riluzole reach the mid-high levels of those found in patients and equate more to the levels found in SOD1^{G93A} mice.

6.6. 31P-MRS as a Pre-clinical Biomarker

This study was the first known attempt at measuring 31P-MRS in a mouse model of MND (chapter 5) which could be a useful translational biomarker, indicative of underlying metabolic changes during disease (Grehl et al., 2007, Sharma et al., 1995, Ryan et al., 2014). SOD1^{G93A} mice were used for this investigation as the TDP-43^{Q331K} and TDP-43^{WT} mice were not available at that point and they have a more profound phenotype with well described metabolic changes (Leclerc et al., 2001, Derave et al., 2003, Mattiazzi et al., 2002).

Issues with animal welfare resulted in low numbers of mice at later time points, limiting the conclusions which could be drawn. Furthermore, the scanning parameters were frequently changed to improve the quality of scanning, reducing consistency between scans. Now that scanning parameters have been optimised, repeated scanning of a cohort of mice at different time points is required, to assess the utility of 31P-MRS as a translational biomarker.

In order to scan a cohort of mice, the animal welfare issues must be addressed by installing a safe and suitable heating system. The hot water system (see *section 4.3.2.4.*) which was used in one of the scanning sessions was unsuitable as the warm water beneath the mouse only covered half of the body area, and the mouse lost temperature very quickly. We suggest a modification to this method in which the water flows under the whole of the mouse by adjusting the layout of the scanning bed. This modification

has already been made but has not been tested. This would be a logical technique to test in the first instance.

6.7. Future Work

This project had limitations which could be overcome with future work, primarily by a thorough investigation of the brain, spinal cord and muscle of the TDP-43^{Q331K} mice. Pathological investigations should include NMJ staining, motor neuron counts and motor neuron staining for p62, ubiquitin and phospho-TDP-43, as well as careful examination for TDP-43 inclusions and aggregates. These investigations could further elucidate the underlying mechanisms involved in neurodegeneration in the TDP-43^{Q331K} model, and potentially provide insights in to the development of TDP-43 pathology in MND patients.

Further investigations of gene copy number are required by sending a large number of samples for quantification. Studies in to the potential FTD phenotype of TDP-43^{Q331K} mice using a variety of tests could be very informative, as well as another riluzole study using a higher dose. Further testing of a heating system is required for future 31P-MRS imaging.

6.8. Overall Conclusions

Overall, this project has provided new insights into the TDP-43^{Q331K} mouse model and showed potential benefits of using this model in future pre-clinical trials. Detailed phenotypic characterisation has provided a number of novel readouts of disease in this model and shown that an increase of nuclear TDP-43 may be sufficient to cause neurodegeneration. The EMG readouts provide a useful measure which can be implemented in an identical manner to human studies, facilitating the translation of therapeutic effects from one species to another. The fact that riluzole was able to improve the reduction in CMAP amplitude on repetitive stimulation may indicate that this is a useful translational readout for riluzole mimics or other compounds that can act on this pathway. There is also room for the identification of therapeutics which modify the motor phenotype (as riluzole did not, similar to the human disease). Finally the identification of a phenotype which may mimic MND-FTD to an extent is intriguing and

worthy of further investigation and again, may make this model particularly valuable for investigation of therapeutics and mechanisms across the MND-FTD disease spectrum. The TDP-43^{Q331K} model has a reliable and reproducible motor phenotype, signs of pathology, and a potential FTD-like phenotype. Further studies of pathology and signs of FTD in this model could be very beneficial to increase the number of readouts available for monitoring in pre-clinical therapeutic trials.

7. References

ACOSTA, J. R., GOLDSBURY, C., WINNICK, C., BADROCK, A. P., FRASER, S. T., LAIRD, A. S., HALL, T. E., DON, E. K., FIFITA, J. A., BLAIR, I. P., NICHOLSON, G. A. & COLE, N. J. 2014. Mutant human FUS is ubiquitously mislocalized and generates persistent stress granules in primary cultured transgenic zebrafish cells. *Plos One,* 9.6.

AFIFI, A. K., ALEU, F. P., GOODGOLD, J. & MACKAY, B. 1966. Ultrastructure of atrophic muscle in amyotrophic lateral sclerosis. *Neurology,* 16**,** 475-475.

AHMED, R. M., IRISH, M., PIGUET, O., HALLIDAY, G. M., ITTNER, L. M., FAROOQI, S., HODGES, J. R. & KIERNAN, M. C. 2016. Amyotrophic lateral sclerosis and frontotemporal dementia: distinct and overlapping changes in eating behaviour and metabolism. *Lancet Neurol,* 15**,** 332-42.

AHMED, Z., SHAW, G., SHARMA, V. P., YANG, C., MCGOWAN, E. & DICKSON, D. W. 2007. Actin-binding proteins coronin-1a and IBA-1 are effective microglial markers for immunohistochemistry. *Journal of Histochemistry & Cytochemistry,* 55**,** 687-700.

AL-CHALABI, A., JONES, A., TROAKES, C., KING, A., AL-SARRAJ, S. & VAN DEN BERG, L. H. 2012. The genetics and neuropathology of amyotrophic lateral sclerosis. *Acta Neuropathologica,* 124**,** 339-352.

ALEXANDER, G. M., ERWIN, K. L., BYERS, N., DEITCH, J. S., AUGELLI, B. J., BLANKENHORN, E. P. & HEIMAN-PATTERSON, T. D. 2004. Effect of transgene copy number on survival in the G93A SOD1 transgenic mouse model of ALS. *Molecular Brain Research,* 130**,** 7-15.

ALLEN, D. L., HARRISON, B. C., MAASS, A. H., BELL, M. L., BYRNES, W. C. & LEINWAND, L. A. 2001. Cardiac and skeletal muscle adaptations to voluntary wheel running in the mouse. *Journal of Applied Physiology,* 90**,** 1900-1908.

ALVES, C. J., DE SANTANA, L. P., DIAS DOS SANTOS, A. J., DE OLIVEIRA, G. P., DUOBLES, T., SCORISA, J. M., MARTINS, R. S., MAXIMINO, J. R. & CHADI, G. 2011. Early motor and electrophysiological changes in transgenic mouse model of amyotrophic lateral sclerosis and gender differences on clinical outcome. *Brain Research,* 1394**,** 90-104.

AN, D., TOYODA, T., TAYLOR, E. B., YU, H., FUJII, N., HIRSHMAN, M. F. & GOODYEAR, L. J. 2010. TBC1D1 regulates insulin- and contraction-induced glucose transport in mouse skeletal muscle. *Diabetes,* 59**,** 1358-1365.

ANDERSEN, P. M., NILSSON, P., ALAHURULA, V., KERANEN, M. L., TARVAINEN, I., HALTIA, T., NILSSON, L., BINZER, M., FORSGREN, L. & MARKLUND, S. L. 1995. Amyotrophic lateral sclerosis associated with homozygosity for an ASP90ALA mutation in CuZn-superoxide dismutase. *Nature Genetics,* 10**,** 61-66.

ANDREASSEN, O. A., JENKINS, B. G., DEDEOGLU, A., FERRANTE, K. L., BOGDANOV, M. B., KADDURAH-DAOUK, R. & BEAL, M. F. 2001. Increases in cortical glutamate concentrations in transgenic amyotrophic lateral sclerosis mice are attenuated by creatine supplementation. *Journal of Neurochemistry,* 77**,** 383-390.

ANGOA-PEREZ, M., KANE, M. J., BRIGGS, D. I., FRANCESCUTTI, D. M. & KUHN, D. M. 2013. Marble burying and nestlet shredding as tests of repetitive, compulsive-like behaviors in mice. *Jove-Journal of Visualized Experiments, 82, e50978-e50978.*

ARAI, T., HASEGAWA, M., AKIYAMA, H., IKEDA, K., NONAKA, T., MORI, H., MANN, D., TSUCHIYA, K., YOSHIDA, M., HASHIZUME, Y. & ODA, T. 2006. TDP-43 is a component of ubiquitin-positive tau-negative inclusions in frontotemporal lobar degeneration and amyotrophic lateral sclerosis. *Biochemical and Biophysical Research Communications,* 351**,** 602-611.

ARMON, C. 2003. An evidence-based medicine approach to the evaluation of the role of exogenous risk factors in sporadic amyotrophic lateral sclerosis. *Neuroepidemiology,* 22**,** 217-228.

ARMON, C. 2009. Smoking may be considered an established risk factor for sporadic ALS. *Neurology,* 73**,** 1693-1698.

ARNOLD, E. S., LING, S.-C., HUELGA, S. C., LAGIER-TOURENNE, C., POLYMENIDOU, M., DITSWORTH, D., KORDASIEWICZ, H. B., MCALONIS-DOWNES, M., PLATOSHYN, O., PARONE, P. A., DA CRUZ, S., CLUTARIO, K. M., SWING, D., TESSAROLLO, L., MARSALA,

M., SHAW, C. E., YEO, G. W. & CLEVELAND, D. W. 2013. ALS-linked TDP-43 mutations produce aberrant RNA splicing and adult-onset motor neuron disease without aggregation or loss of nuclear TDP-43. *Proceedings of the National Academy of Sciences of the United States of America,* 110**,** E736-E745.

ARNOLD, W. D., PORENSKY, P. N., MCGOVERN, V. L., IYER, C. C., DUQUE, S., LI, X., MEYER, K., SCHMELZER, L., KASPAR, B. K., KOLB, S. J., KISSEL, J. T. & BURGHES, A. H. 2014. Electrophysiological biomarkers in spinal muscular atrophy: preclinical proof of concept. *Ann Clin Transl Neurol.,* 1**,** 34-44.

ARNOLD, W. D., SHETH, K. A., WIER, C. G., KISSEL, J. T., BURGHES, A. H. & KOLB, S. J. 2015. Electrophysiological motor unit number estimation (MUNE) measuring compound muscle action potential (CMAP) in mouse hindlimb muscles. *Journal of visualized experiments : JoVE,* 103, e52899-e52899.

ATANASIO, A., DECMAN, V., WHITE, D., RAMOS, M., IKIZ, B., LEE, H.-C., SIAO, C.-J., BRYDGES, S., LAROSA, E., BAI, Y., FURY, W., BURFEIND, P., ZAMFIROVA, R., WARSHAW, G., ORENGO, J., OYEJIDE, A., FRALISH, M., AUERBACH, W., POUEYMIROU, W., FREUDENBERG, J., GONG, G., ZAMBROWICZ, B., VALENZUELA, D., YANCOPOULOS, G., MURPHY, A., THURSTON, G. & LAI, K.-M. V. 2016. C9orf72 ablation causes immune dysregulation characterized by leukocyte expansion, autoantibody production, and glomerulonephropathy in mice. *Scientific Reports,* 6, 23204-23204.

AYALA, Y. M., DE CONTI, L., AVENDANO-VAZQUEZ, S. E., DHIR, A., ROMANO, M., D'AMBROGIO, A., TOLLERVEY, J., ULE, J., BARALLE, M., BURATTI, E. & BARALLE, F. E. 2011. TDP-43 regulates its mRNA levels through a negative feedback loop. *Embo Journal,* 30**,** 277-288.

AYALA, Y. M., ZAGO, P., D'AMBROGIO, A., XU, Y.-F., PETRUCELLI, L., BURATTI, E. & BARALLE, F. E. 2008. Structural determinants of the cellular localization and shuttling of TDP-43. *Journal of Cell Science,* 121**,** 3778-3785.

AZZOUZ, M., LECLERC, N., GURNEY, M., WARTER, J. M., POINDRON, P. & BORG, J. 1997. Progressive motor neuron impairment in an animal model of familial amyotrophic lateral sclerosis. *Muscle & Nerve,* 20**,** 45-51.

BANASR, M., CHOWDHURY, G. M. I., TERWILLIGER, R., NEWTON, S. S., DUMAN, R. S., BEHAR, K. L. & SANACORA, G. 2010. Glial pathology in an animal model of depression: reversal of stress-induced cellular, metabolic and behavioral deficits by the glutamate-modulating drug riluzole. *Molecular Psychiatry,* 15**,** 501-511.

BANNWARTH, S., AIT-EL-MKADEM, S., CHAUSSENOT, A., GENIN, E. C., LACAS-GERVAIS, S., FRAGAKI, K., BERG-ALONSO, L., KAGEYAMA, Y., SERRE, V., MOORE, D. G., VERSCHUEREN, A., ROUZIER, C., LE BER, I., AUGE, G., COCHAUD, C., LESPINASSE, F., N'GUYEN, K., DE SEPTENVILLE, A., BRICE, A., YU-WAI-MAN, P., SESAKI, H., POUGET, J. & PAQUIS-FLUCKLINGER, V. 2014. A mitochondrial origin for frontotemporal dementia and amyotrophic lateral sclerosis through CHCHD10 involvement. *Brain,* 137**,** 2329-2345.

BARMADA, S. J., SKIBINSKI, G., KORB, E., RAO, E. J., WU, J. Y. & FINKBEINER, S. 2010. Cytoplasmic mislocalization of TDP-43 is toxic to neurons and enhanced by a mutation associated with familial amyotrophic lateral sclerosis. *Journal of Neuroscience,* 30**,** 639-649.

BAUMANN, F., HENDERSON, R. D., RIDALL, P. G., PETTITT, A. N. & MCCOMBE, P. A. 2012. Use of Bayesian MUNE to show differing rate of loss of motor units in subgroups of ALS. *Clinical Neurophysiology,* 123**,** 2446-2453.

BEGHI, E., LOGROSCINO, G., CHIO, A., HARDIMAN, O., MITCHELL, D., SWINGLER, R., TRAYNOR, B. J. & CONSORTIUM, E. 2006. The epidemiology of ALS and the role of population-based registries. *Biochimica Et Biophysica Acta-Molecular Basis of Disease,* 1762**,** 1150-1157.

BELLINGHAM, M. C. 2011. A review of the neural mechanisms of action and clinical efficiency of riluzole in treating amyotrophic lateral sclerosis: what have we learned in the last decade? *Cns Neuroscience & Therapeutics,* 17**,** 4-31.

BENATAR, M. 2007. Lost in translation: Treatment trials in the SOD1 mouse and in human ALS. *Neurobiology of Disease,* 26**,** 1-13.

BENATAR, M., BOYLAN, K., JEROMIN, A., RUTKOVE, S. B., BERRY, J., ATASSI, N. & BRUIJN, L. 2016. ALS Biomarkers for therapy development: state of the field and future directions. *Muscle & Nerve,* 53**,** 169-182.

BENDOTTI, C., CALVARESI, N., CHIVERI, L., PRELLE, A., MOGGIO, M., BRAGA, M., SILANI, V. & DE BIASI, S. 2001. Early vacuolization and mitochondrial damage in motor neurons of FALS mice are not associated with apoptosis or with changes in cytochrome oxidase histochemical reactivity. *Journal of the Neurological Sciences,* 191**,** 25-33.

BENNETT, E. J., MEAD, R. J., AZZOUZ, M., SHAW, P. J. & GRIERSON, A. J. 2014. Early detection of motor dysfunction in the SOD1(G93A) mouse model of amyotrophic lateral sclerosis (ALS) using home cage running wheels. *Plos One,* 9.9, e107918.

BENSIMON, G., LACOMBLEZ, L., MEININGER, V., BOUCHE, P., DELWAIDE, C., COURATIER, P., BLIN, O., VIADER, F., PEYROSTPAUL, H., DAVID, J., MALOTEAUX, J. M., HUGON, J., LATERRE, E. C., RASCOL, A., CLANET, M., VALLAT, J. M., DUMAS, A., SERRATRICE, G., LECHEVALLIER, B., PEUCH, A. J., NGUYEN, T., SHU, C., BASTIEN, P., PAPILLON, C., DURRLEMAN, S., LOUVEL, E., GUILLET, P., LEDOUX, L., ORVOENFRIJA, E. & DIB, M. 1994. A controlled trial of riluzole in amyotrophic lateral sclerosis. *New England Journal of Medicine,* 330**,** 585-591.

BERETTA, S., SALA, G., MATTAVELLI, L., CERESA, C., CASCIATI, A., FERRI, A., CARRI, M. T. & FERRARESE, C. 2003. Mitochondrial dysfunction due to mutant copper/zinc superoxide dismutase associated with amyotrophic lateral sclerosis is reversed by N-acetylcysteine. *Neurobiology of Disease,* 13**,** 213-221.

BERGMAN, B. P., MACKAY, D. F. & PELL, J. P. 2015. Motor neurone disease and military service: evidence from the Scottish Veterans Health Study. *Occupational and Environmental Medicine,* 72**,** 877-879.

BERLOWITZ, D. J., HOWARD, M. E., FIORE, J. F., JR., HOORN, S. V., O'DONOGHUE, F. J., WESTLAKE, J., SMITH, A., BEER, F., MATHERS, S. & TALMAN, P. 2016. Identifying who will benefit from non-invasive ventilation in amyotrophic lateral sclerosis/motor neurone disease in a clinical cohort. *Journal of Neurology Neurosurgery and Psychiatry,* 87**,** 280-286.

BOGDANIK, L. P., OSBORNE, M. A., DAVIS, C., MARTIN, W. P., AUSTIN, A., RIGO, F., BENNETT, C. F. & LUTZ, C. M. 2015. Systemic, postsymptomatic antisense oligonucleotide rescues motor unit maturation delay in a new mouse model for type II/III spinal muscular atrophy. *Proceedings of the National Academy of Sciences of the United States of America,* 112**,** E5863-E5872.

BOILLEE, S., YAMANAKA, K., LOBSIGER, C. S., COPELAND, N. G., JENKINS, N. A., KASSIOTIS, G., KOLLIAS, G. & CLEVELAND, D. W. 2006. Onset and progression in inherited ALS determined by motor neurons and microglia. *Science,* 312**,** 1389-1392.

BORCHELT, D. R., DAVIS, J., FISCHER, M., LEE, M. K., SLUNT, H. H., RATOVITSKY, T., REGARD, J., COPELAND, N. G., JENKINS, N. A., SISODIA, S. S. & PRICE, D. L. 1996. A vector for expressing foreign genes in the brains and hearts of transgenic mice. *Genetic Analysis-Biomolecular Engineering,* 13**,** 159-163.

BOURKE, S. C., TOMLINSON, M., WILLIAMS, T. L., BULLOCK, R. E., SHAW, P. J. & GIBSON, G. J. 2006. Effects of non-invasive ventilation on survival and quality of life in patients with amyotrophic lateral sclerosis. *Lancet Neurology,* 5**,** 140-147.

BOUTELOUP, C., DESPORT, J. C., CLAVELOU, P., GUY, N., DERUMEAUX-BUREL, H., FERRIER, A. & COURATIER, P. 2009. Hypermetabolism in ALS patients: an early and persistent phenomenon. *Journal of Neurology,* 256**,** 1236-1242.

BROOKS, B. R., MILLER, R. G., SWASH, M., MUNSAT, T. L. & WORLD FEDERATION NEUROLOGY RES, G. 2000. El Escorial revisited: Revised criteria for the diagnosis of amyotrophic lateral sclerosis. *Amyotrophic Lateral Sclerosis and Other Motor Neuron Disorders,* 1**,** 293-299.

BROOKS, S. P. & DUNNETT, S. B. 2009. Tests to assess motor phenotype in mice: a user's guide. *Nature Reviews Neuroscience,* 10**,** 519-529.

BROTHERTON, T., POLAK, M., KELLY, C., BIRVE, A., ANDERSEN, P., MARKLUND, S. L. & GLASS, J. D. 2011. A novel ALS SOD1 C6S mutation with implications for aggregation related toxicity and genetic counseling. *Amyotrophic Lateral Sclerosis,* 12**,** 215-219.

BRUESTLE, D. A., CUTLER, R. G., TELLJOHANN, R. S. & MATTSON, M. P. 2009. Decline in daily running distance presages disease onset in a mouse model of ALS. *Neuromolecular Medicine,* 11**,** 58-62.

BRUIJN, L. I., BECHER, M. W., LEE, M. K., ANDERSON, K. L., JENKINS, N. A., COPELAND, N. G., SISODIA, S. S., ROTHSTEIN, J. D., BORCHELT, D. R., PRICE, D. L. & CLEVELAND, D. W. 1997. ALS-linked SOD1 mutant G85R mediates damage to astrocytes and promotes rapidly progressive disease with SOD1-containing inclusions. *Neuron,* 18**,** 327-338.

BRYSON, H. M., FULTON, B. & BENFIELD, P. 1996. Riluzole - A review of its pharmacodynamic and pharmacokinetic properties and therapeutic potential in amyotrophic lateral sclerosis. *Drugs,* 52**,** 549-563.

BUDINI, M., ROMANO, V., QUADRI, Z., BURATTI, E. & BARALLE, F. E. 2015. TDP-43 loss of cellular function through aggregation requires additional structural determinants beyond its C-terminal Q/N prion-like domain. *Human Molecular Genetics,* 24**,** 9-20.

BURATTI, E. & BARALLE, F. E. 2010. The multiple roles of TDP-43 in pre-mRNA processing and gene expression regulation. *Rna Biology,* 7**,** 420-429.

BURATTI, E. & BARALLE, F. E. 2012. TDP-43: gumming up neurons through protein-protein and protein-RNA interactions. *Trends in Biochemical Sciences,* 37**,** 237-247.

CATHOMAS, F., HARTMANN, M. N., SEIFRITZ, E., PRYCE, C. R. & KAISER, S. 2015. The translational study of apathy-an ecological approach. *Frontiers in Behavioral Neuroscience,* 9, 241-241.

CHADT, A., LEICHT, K., DESHMUKH, A., JIANG, L. Q., SCHERNECK, S., BERNHARDT, U., DREJA, T., VOGEL, H., SCHMOLZ, K., KLUGE, R., ZIERATH, J. R., HULTSCHIG, C., HOEBEN, R. C., SCHUERMANN, A., JOOST, H.-G. & AL-HASANI, H. 2008. Tbc1d1 mutation in lean mouse strain confers leanness and protects from diet-induced obesity. *Nature Genetics,* 40**,** 1354-1359.

CHAN, H.-M., STOLWYK, R., NEATH, J., KELSO, W., WALTERFANG, M., MOCELLIN, R., PANTELIS, C. & VELAKOULIS, D. 2015. Neurocognitive similarities between severe chronic schizophrenia and behavioural variant frontotemporal dementia. *Psychiatry Research,* 225**,** 658-666.

CHANG, C.-K., WU, T.-H., WU, C.-Y., CHIANG, M.-H., TOH, E. K.-W., HSU, Y.-C., LIN, K.-F., LIAO, Y.-H., HUANG, T.-H. & HUANG, J. J.-T. 2012. The N-terminus of TDP-43 promotes its oligomerization and enhances DNA binding affinity. *Biochemical and Biophysical Research Communications,* 425**,** 219-224.

CHANG, H.-Y., HOU, S.-C., WAY, T.-D., WONG, C.-H. & WANG, I. F. 2013. Heat-shock protein dysregulation is associated with functional and pathological TDP-43 aggregation. *Nature Communications,* 4, 2757-2757.

CHEN, Y., YANG, M., DENG, J., CHEN, X., YE, Y., ZHU, L., LIU, J., YE, H., SHEN, Y., LI, Y., RAO, E. J., FUSHIMI, K., ZHOU, X., BIGIO, E. H., MESULAM, M., XU, Q. & WU, J. Y. 2011. Expression of human FUS protein in Drosophila leads to progressive neurodegeneration. *Protein & Cell,* 2**,** 477-486.

CHEW, J., GENDRON, T. F., PRUDENCIO, M., SASAGURI, H., ZHANG, Y.-J., CASTANEDES-CASEY, M., LEE, C., JANSEN-WEST, K., KURTI, A., MURRAY, M. E., BIENIEK, K. F., BAUER, P. O., WHITELAW, E. C., ROUSSEAU, L., STANKOWSKI, J. N., STETLER, C., DAUGHRITY, L. M., PERKERSON, E. A., DESARO, P., JOHNSTON, A., OVERSTREET, K., EDBAUER, D., RADEMAKERS, R., BOYLAN, K. B., DICKSON, D. W., FRYER, J. D. & PETRUCELLI, L. 2015. C9ORF72 repeat expansions in mice cause TDP-43 pathology, neuronal loss, and behavioral deficits. *Science,* 348**,** 1151-1154.

CHIANG, P.-M., LING, J., JEONG, Y. H., PRICE, D. L., AJA, S. M. & WONG, P. C. 2010. Deletion of TDP-43 down-regulates Tbc1d1, a gene linked to obesity, and alters body fat metabolism. *Proceedings of the National Academy of Sciences of the United States of America,* 107**,** 16320-16324.

CHIO, A., BENZI, G., DOSSENA, M., MUTANI, R. & MORA, G. 2005. Severely increased risk of amyotrophic lateral sclerosis among Italian professional football players. *Brain,* 128**,** 472-476.

CHIO, A., LOGROSCINO, G., HARDIMAN, O., SWINGLER, R., MITCHELL, D., BEGHI, E., TRAYNOR, B. G. & EURALS, C. 2009. Prognostic factors in ALS: A critical review. *Amyotrophic Lateral Sclerosis,* 10**,** 310-323.

CHIO, A. & TRAYNOR, B. J. 2015. Biomarkers for ALS-in search of the Promised Land. *Nature Reviews Neurology,* 11.2, 72-74.

CHOWDHURY, G. M. I., BANASR, M., DE GRAAF, R. A., ROTHMAN, D. L., BEHAR, K. L. & SANACORA, G. 2008. Chronic riluzole treatment increases glucose metabolism in rat prefrontal cortex and hippocampus. *Journal of Cerebral Blood Flow and Metabolism,* 28**,** 1892-1897.

CIURA, S., LATTANTE, S., LE BER, I., LATOUCHE, M., TOSTIVINT, H., BRICE, A. & KABASHI, E. 2013. Loss of function of C9orf72 causes motor deficits in a zebrafish model of amyotrophic lateral sclerosis. *Annals of Neurology,* 74**,** 180-187.

COLOMBRITA, C., ZENNARO, E., FALLINI, C., WEBER, M., SOMMACAL, A., BURATTI, E., SILANI, V. & RATTI, A. 2009. TDP-43 is recruited to stress granules in conditions of oxidative insult. *Journal of Neurochemistry,* 111**,** 1051-1061.

COMI, G. P., BORDONI, A., SALANI, S., FRANCESCHINA, L., SCIACCO, M., PRELLE, A., FORTUNATO, F., ZEVIANI, M., NAPOLI, L., BRESOLIN, N., MOGGIO, M., AUSENDA, C. D., TAANMAN, J. W. & SCARLATO, G. 1998. Cytochrome c oxidase subunit I microdeletion in a patient with motor neuron disease. *Annals of Neurology,* 43**,** 110-116.

COOKSON, M. R. & SHAW, P. J. 1999. Oxidative stress and motor neurone disease. *Brain Pathology,* 9**,** 165-186.

COOPER-KNOCK, J., SHAW, P. J. & KIRBY, J. 2014. The widening spectrum of C9ORF72-related disease; genotype/phenotype correlations and potential modifiers of clinical phenotype. *Acta Neuropathologica,* 127**,** 333-345.

CORCIA, P., VALDMANIS, P., MILLECAMPS, S., LIONNET, C., BLASCO, H., MOUZAT, K., DAOUD, H., BELZIL, V., MORALES, R., PAGEOT, N., DANEL-BRUNAUD, V., VANDENBERGHE, N., PRADAT, P. F., COURATIER, P., SALACHAS, F., LUMBROSO, S., ROULEAU, G. A., MEININGER, V. & CAMU, W. 2012. Phenotype and genotype analysis in amyotrophic lateral sclerosis with TARDBP gene mutations. *Neurology,* 78**,** 1519-1526.

COSTA, J., GOMES, C. & DE CARVALHO, M. 2010. Diagnosis, pathogenesis and therapeutic targets in amyotrophic lateral sclerosis. *Cns & Neurological Disorders-Drug Targets,* 9**,** 764-778.

COSTA, J., SWASH, M. & DE CARVALHO, M. 2012. Awaji criteria for the diagnosis of amyotrophic lateral sclerosis a systematic review. *Archives of Neurology,* 69**,** 1410-1416.

COX, P. A., RICHER, R., METCALF, J. S., BANACK, S. A., CODD, G. A. & BRADLEY, W. G. 2009. Cyanobacteria and BMAA exposure from desert dust: A possible link to sporadic ALS among Gulf War veterans. *Amyotrophic Lateral Sclerosis,* 10**,** 109-117.

DADON-NACHUM, M., MELAMED, E. & OFFEN, D. 2011. The "dying-back" phenomenon of motor neurons in ALS. *Journal of Molecular Neuroscience,* 43**,** 470-477.

DALCANTO, M. C. & GURNEY, M. E. 1995. Neuropathological changes in 2 lines of mice carrying a transgene for mutant human Cu,Zn SOD and in mice overexpressing wild-type human SOD - a model of familial amyotrophic lateral sclerosis (FALS). *Brain Research,* 676**,** 25-40.

DE BONO, J. P., ADLAM, D., PATERSON, D. J. & CHANNON, K. M. 2006. Novel quantitative phenotypes of exercise training in mouse models. *American Journal of Physiology-Regulatory Integrative and Comparative Physiology,* 290**,** R926-R934.

DE CARVALHO, M., DENGLER, R., EISEN, A., ENGLAND, J. D., KAJI, R., KIMURA, J., MILLS, K., MITSUMOTO, H., NODERA, H., SHEFNER, J. & SWASH, M. 2008. Electrodiagnostic criteria for diagnosis of ALS. *Clinical Neurophysiology,* 119**,** 497-503.

DE CONTI, L., AKINYI, M. V., MENDOZA-MALDONADO, R., ROMANO, M., BARALLE, M. & BURATTI, E. 2015. TDP-43 affects splicing profiles and isoform production of genes

involved in the apoptotic and mitotic cellular pathways. *Nucleic Acids Research,* 43**,** 8990-9005.

DE VOS, K. J., GRIERSON, A. J., ACKERLEY, S. & MILLER, C. C. J. 2008. Role of axonal transport in neurodegenerative diseases. *Annual Review of Neuroscience,* 31**,** 151-173.

DEACON, R. M. J. 2006. Digging and marble burying in mice: simple methods for in vivo identification of biological impacts. *Nature Protocols,* 1**,** 122-124.

DEFLORIO, C., PALMA, E., CONTI, L., ROSETI, C., MANTECA, A., GIACOMELLI, E., CATALANO, M., LIMATOLA, C., INGHILLERI, M. & GRASSI, F. 2012. Riluzole blocks human muscle acetylcholine receptors. *Journal of Physiology-London,* 590**,** 2519-2528.

DEJESUS-HERNANDEZ, M., MACKENZIE, I. R., BOEVE, B. F., BOXER, A. L., BAKER, M., RUTHERFORD, N. J., NICHOLSON, A. M., FINCH, N. A., FLYNN, H., ADAMSON, J., KOURI, N., WOJTAS, A., SENGDY, P., HSIUNG, G.-Y. R., KARYDAS, A., SEELEY, W. W., JOSEPHS, K. A., COPPOLA, G., GESCHWIND, D. H., WSZOLEK, Z. K., FELDMAN, H., KNOPMAN, D. S., PETERSEN, R. C., MILLER, B. L., DICKSON, D. W., BOYLAN, K. B., GRAFF-RADFORD, N. R. & RADEMAKERS, R. 2011. Expanded GGGGCC Hexanucleotide repeat in noncoding region of C9ORF72 causes chromosome 9p-linked FTD and ALS. *Neuron,* 72.2, 245-256.

DEKKER, A. M., SEELEN, M., VAN DOORMAAL, P. T. C., VAN RHEENEN, W., BOTHOF, R. J. P., VAN RIESSEN, T., BRANDS, W. J., VAN DER KOOI, A. J., DE VISSER, M., VOERMANS, N. C., PASTERKAMP, R. J., VELDINK, J. H., VAN DEN BERG, L. H. & VAN ES, M. A. 2016. Large-scale screening in sporadic amyotrophic lateral sclerosis identifies genetic modifiers in C9orf72 repeat carriers. *Neurobiology of Aging,* 39, 220-e9.

DEL AGUILA, M. A., LONGSTRETH, W. T., MCGUIRE, V., KOEPSELL, T. D. & VAN BELLE, G. 2003. Prognosis in amyotrophic lateral sclerosis - A population-based study. *Neurology,* 60**,** 813-819.

DEL NEGRO, C. A., MORGADO-VALLE, C. & FELDMAN, J. L. 2002. Respiratory rhythm: An emergent network property? *Neuron,* 34**,** 821-830.

DENG, H.-X., CHEN, W., HONG, S.-T., BOYCOTT, K. M., GORRIE, G. H., SIDDIQUE, N., YANG, Y., FECTO, F., SHI, Y., ZHAI, H., JIANG, H., HIRANO, M., RAMPERSAUD, E., JANSEN, G. H., DONKERVOORT, S., BIGIO, E. H., BROOKS, B. R., AJROUD, K., SUFIT, R. L., HAINES, J. L., MUGNAINI, E., PERICAK-VANCE, M. A. & SIDDIQUE, T. 2011. Mutations in UBQLN2 cause dominant X-linked juvenile and adult-onset ALS and ALS/dementia. *Nature,* 477**,** 211-U113.

DERAVE, W., VAN DEN BOSCH, L., LEMMENS, G., EIJNDE, B. O., ROBBERECHT, W. & HESPEL, P. 2003. Skeletal muscle properties in a transgenic mouse model for amyotrophic lateral sclerosis: effects of creatine treatment. *Neurobiology of Disease,* 13**,** 264-272.

DESNUELLE, C., DIB, M., GARREL, C., FAVIER, A. & GRP, A. L. S. R.-T. S. 2001. A double-blind, placebo-controlled randomized clinical trial of alpha-tocopherol (vitamin E) in the treatment of amyotrophic lateral sclerosis. *Amyotrophic Lateral Sclerosis and Other Motor Neuron Disorders,* 2**,** 9-18.

DESPORT, J.-C., TORNY, F., LACOSTE, M., PREUX, P.-M. & COURATIER, P. 2005. Hypermetabolism in ALS: correlations with clinical and paraclinical parameters. *Neurodegenerative Diseases,* 2**,** 202-207.

DESPORT, J. C., PREUX, P. M., TRUONG, C. T., COURAT, L., VALLAT, J. M. & COURATIER, P. 2000. Nutritional assessment and survival in ALS patients. *Amyotrophic Lateral Sclerosis and Other Motor Neuron Disorders,* 1**,** 91-96.

DEUMENS, R., JAKEN, R. J. P., MARCUS, M. A. E. & JOOSTEN, E. A. J. 2007. The CatWalk gait analysis in assessment of both dynamic and static gait changes after adult rat sciatic nerve resection. *Journal of Neuroscience Methods,* 164**,** 120-130.

DHALIWAL, G. K. & GREWAL, R. P. 2000. Mitochondrial DNA deletion mutation levels are elevated in ALS brains. *Neuroreport,* 11**,** 2507-2509.

DIAPER, D. C., ADACHI, Y., SUTCLIFFE, B., HUMPHREY, D. M., ELLIOTT, C. J. H., STEPTO, A., LUDLOW, Z. N., VANDEN BROECK, L., CALLAERTS, P., DERMAUT, B., AL-CHALABI, A., SHAW, C. E., ROBINSON, I. M. & HIRTH, F. 2013. Loss and gain of Drosophila TDP-43

impair synaptic efficacy and motor control leading to age-related neurodegeneration by loss-of-function phenotypes. *Human Molecular Genetics,* 22**,** 1539-1557.

DOBROWOLNY, G., AUCELLO, M., RIZZUTO, E., BECCAFICO, S., MAMMUCARI, C., BONCONPAGNI, S., BELIA, S., WANNENES, F., NICOLETTI, C., DEL PRETE, Z., ROSENTHAL, N., MOLINARO, M., PROTASI, F., FANO, G., SANDRI, M. & MUSARO, A. 2008. Skeletal muscle is a primary target of SOD1(G93A)-mediated toxicity. *Cell Metabolism,* 8**,** 425-436.

DORMANN, D., CAPELL, A., CARLSON, A. M., SHANKARAN, S. S., RODDE, R., NEUMANN, M., KREMMER, E., MATSUWAKI, T., YAMANOUCHI, K., NISHIHARA, M. & HAASS, C. 2009. Proteolytic processing of TAR DNA binding protein-43 by caspases produces C-terminal fragments with disease defining properties independent of progranulin. *Journal of Neurochemistry,* 110**,** 1082-1094.

DUCHEN, L. W. & STRICH, S. J. 1968. An hereditary motor neurone disease with progressive denervation of muscle in mouse - mutant wobbler. *Journal of Neurology Neurosurgery and Psychiatry,* 31.6**,** 535-542.

DUPUIS, L., OUDART, H., RENE, F., DE AGUILAR, J. L. G. & LOEFFLER, J. P. 2004. Evidence for defective energy homeostasis in amyotrophic lateral sclerosis: benefit of a high-energy diet in a transgenic mouse. *Proceedings of the National Academy of Sciences of the United States of America,* 101**,** 11159-11164.

DUPUIS, L., PRADAT, P.-F., LUDOLPH, A. C. & LOEFFLER, J.-P. 2011. Energy metabolism in amyotrophic lateral sclerosis. *Lancet Neurology,* 10**,** 75-82.

EGASHIRA, N., OKUNO, R., HARADA, S., MATSUSHITA, M., MISHIMA, K., IWASAKI, K., NISHIMURA, R., OISHI, R. & FUJIWARA, M. 2008. Effects of glutamate-related drugs on marble-burying behavior in mice: Implications for obsessive-compulsive disorder. *European Journal of Pharmacology,* 586**,** 164-170.

EL-KADI, A. M., SOURA, V. & HAFEZPARAST, M. 2007. Defective axonal transport in motor neuron disease. *Journal of Neuroscience Research,* 85**,** 2557-2566.

ELDEN, A. C., KIM, H.-J., HART, M. P., CHEN-PLOTKIN, A. S., JOHNSON, B. S., FANG, X., ARMAKOLA, M., GESER, F., GREENE, R., LU, M. M., PADMANABHAN, A., CLAY-FALCONE, D., MCCLUSKEY, L., ELMAN, L., JUHR, D., GRUBER, P. J., RUEB, U., AUBURGER, G., TROJANOWSKI, J. Q., LEE, V. M. Y., VAN DEERLIN, V. M., BONINI, N. M. & GITLER, A. D. 2010. Ataxin-2 intermediate-length polyglutamine expansions are associated with increased risk for ALS. *Nature,* 466**,** 1069-U77.

ENG, L. F. & GHIRNIKAR, R. S. 1994. GFAP and astrogliosis. *Brain Pathology,* 4**,** 229-237.

FALCK, B. & ALARANTA, H. 1983. Fibrillation potentials, positive sharp waves and fasciculation in intrinsic muscles of the foot in healthy subjects. *Journal of Neurology Neurosurgery and Psychiatry,* 46**,** 681-683.

FAUL, F., ERDFELDER, E., BUCHNER, A. & LANG, A. G. 2009. Statistical power analyses using G*Power 3.1: Tests for correlation and regression analyses. *Behavior Research Methods,* 41**,** 1149-1160.

FAUSTINO, E. V. S. & DONNELLY, D. F. 2006. An important functional role of persistent Na+ current in carotid body hypoxia transduction. *Journal of Applied Physiology,* 101**,** 1076-1084.

FECTO, F., YAN, J., VEMULA, S. P., LIU, E., YANG, Y., CHEN, W., ZHENG, J. G., SHI, Y., SIDDIQUE, N., ARRAT, H., DONKERVOORT, S., AJROUD-DRISS, S., SUFIT, R. L., HELLER, S. L., DENG, H.-X. & SIDDIQUE, T. 2011. SQSTM1 mutations in familial and sporadic amyotrophic lateral sclerosis. *Archives of Neurology,* 68**,** 1440-1446.

FEILER, M. S., STROBEL, B., FREISCHMIDT, A., HELFERICH, A. M., KAPPEL, J., BREWER, B. M., LI, D., THAL, D. R., WALTHER, P., LUDOLPH, A. C., DANZER, K. M. & WEISHAUPT, J. H. 2015. TDP-43 is intercellularly transmitted across axon terminals. *Journal of Cell Biology,* 211**,** 897-911.

FELICE, K. J. & NORTH, W. A. 1998. Creatine kinase values in amyotrophic lateral sclerosis. *Journal of the Neurological Sciences,* 160**,** S30-S32.

FERRAIUOLO, L., HIGGINBOTTOM, A., HEATH, P. R., BARBER, S., GREENALD, D., KIRBY, J. & SHAW, P. J. 2011. Dysregulation of astrocyte-motoneuron cross-talk in mutant superoxide dismutase 1-related amyotrophic lateral sclerosis. *Brain,* 134**,** 2627-2641.

FISCHER, L. R., CULVER, D. G., TENNANT, P., DAVIS, A. A., WANG, M. S., CASTELLANO-SANCHEZ, A., KHAN, J., POLAK, M. A. & GLASS, J. D. 2004. Amyotrophic lateral sclerosis is a distal axonopathy: evidence in mice and man. *Experimental Neurology,* 185**,** 232-240.

FLANAGAN, R. J., YUSUFI, B. & BARNES, T. R. E. 2003. Comparability of whole-blood and plasma clozapine and norclozapine concentrations. *British Journal of Clinical Pharmacology,* 56**,** 135-138.

FREISCHMIDT, A., WIELAND, T., RICHTER, B., RUF, W., SCHAEFFER, V., MUELLER, K., MARROQUIN, N., NORDIN, F., HUEBERS, A., WEYDT, P., PINTO, S., PRESS, R., MILLECAMPS, S., MOLKO, N., BERNARD, E., DESNUELLE, C., SORIANI, M.-H., DORST, J., GRAF, E., NORDSTROM, U., FEILER, M. S., PUTZ, S., BOECKERS, T. M., MEYER, T., WINKLER, A. S., WINKELMAN, J., DE CARVALHO, M., THAL, D. R., OTTO, M., BRANNSTROM, T., VOLK, A. E., KURSULA, P., DANZER, K. M., LICHTNER, P., DIKIC, I., MEITINGER, T., LUDOLPH, A. C., STROM, T. M., ANDERSEN, P. M. & WEISHAUPT, J. H. 2015. Haploinsufficiency of TBK1 causes familial ALS and fronto-temporal dementia. *Nature Neuroscience,* 18.5**,** 631-636.

FUJII, R., OKABE, S., URUSHIDO, T., INOUE, K., YOSHIMURA, A., TACHIBANA, T., NISHIKAWA, T., HICKS, G. G. & TAKUMI, T. 2005. The RNA binding protein TLS is translocated to dendritic spines by mGluR5 activation and regulates spine morphology. *Current Biology,* 15**,** 587-593.

FUNALOT, B., DESPORT, J.-C., STURTZ, F., CAMU, W. & COURATIER, P. 2009. High metabolic level in patients with familial amyotrophic lateral sclerosis. *Amyotrophic Lateral Sclerosis,* 10**,** 113-117.

GASCON, E., LYNCH, K., RUAN, H., ALMEIDA, S., VERHEYDEN, J. M., SEELEY, W. W., DICKSON, D. W., PETRUCELLI, L., SUN, D., JIAO, J., ZHOU, H., JAKOVCEVSKI, M., AKBARIAN, S., YAO, W.-D. & GAO, F.-B. 2014. Alterations in microRNA-124 and AMPA receptors contribute to social behavioral deficits in frontotemp oral dementia. *Nature Medicine,* 20**,** 1444-1451.

GAUTIER, G., VERSCHUEREN, A., MONNIER, A., ATTARIAN, S., SALORT-CAMPANA, E. & POUGET, J. 2010. ALS with respiratory onset: Clinical features and effects of non-invasive ventilation on the prognosis. *Amyotrophic Lateral Sclerosis,* 11**,** 379-382.

GEEVASINGA, N., MENON, P., NG, K., VAN DEN BOS, M., BYTH, K., KIERNAN, M. C. & VUCIC, S. 2016. Riluzole exerts transient modulating effects on cortical and axonal hyperexcitability in ALS. *Amyotrophic Lateral Sclerosis Frontotemporal Degeneration,* 1**,** 1-9.

GEORGOULOPOULOU, E., FINI, N., VINCETI, M., MONELLI, M., VACONDIO, P., BIANCONI, G., SOLA, P., NICHELLI, P. & MANDRIOLI, J. 2013. The impact of clinical factors, riluzole and therapeutic interventions on ALS survival: A population based study in Modena, Italy. *Amyotrophic Lateral Sclerosis and Frontotemporal Degeneration,* 14**,** 338-345.

GILLI, F., ROYCE, D. B. & PACHNER, A. R. 2016. Measuring progressive neurological disability in a mouse model of multiple sclerosis. *J Vis Exp.,* (117). 10.3791/54616.

GITCHO, M. A., BALOH, R. H., CHAKRAVERTY, S., MAYO, K., NORTON, J. B., LEVITCH, D., HATANPAA, K. J., WHITE, C. L., III, BIGIO, E. H., CASELLI, R., BAKER, M., AL-LOZI, M. T., MORRIS, J. C., PESTRONK, A., RADEMAKERS, R., GOATE, A. M. & CAIRNS, N. J. 2008. TDP-43 A315T mutation in familial motor neuron disease. *Annals of Neurology,* 63**,** 535-538.

GONG, Y. H., PARSADANIAN, A. S., ANDREEVA, A., SNIDER, W. D. & ELLIOTT, J. L. 2000. Restricted expression of G86R Cu/Zn superoxide dismutase in astrocytes results in astrocytosis but does not cause motoneuron degeneration. *Journal of Neuroscience,* 20.2, 660-665.

GORDON, P. H. 2013. Amyotrophic lateral sclerosis: An update for 2013 clinical features, pathophysiology, management and therapeutic trials. *Aging and Disease,* 4**,** 295-310.

GORDON, P. H., MOORE, D. H., MILLER, R. G., FLORENCE, J. M., VERHEIJDE, J. L., DOORISH, C., HILTON, J. F., SPITALNY, G. M., MACARTHUR, R. B., MITSUMOTO, H., NEVILLE, H. E.,

BOYLAN, K., MOZAFFAR, T., BELSH, J. M., RAVITS, J., BEDLACK, R. S., GRAVES, M. C., MCCLUSKEY, L. F., BAROHN, R. J., TANDAN, R. & WESTERN, A. L. S. S. G. 2007. Efficacy of minocycline in patients with amyotrophic lateral sclerosis: a phase III randomised trial. *Lancet Neurology,* 6**,** 1045-1053.

GOULD, T. W., BUSS, R. R., VINSANT, S., PREVETTE, D., SUN, W., KNUDSON, C. M., MILLIGAN, C. E. & OPPENHEIM, R. W. 2006. Complete dissociation of motor neuron death from motor dysfunction by Bax deletion in a mouse model of ALS. *Journal of Neuroscience,* 26**,** 8774-8786.

GRAF, M., ECKER, D., HOROWSKI, R., KRAMER, B., RIEDERER, P., GERLACH, M., HAGER, C., LUDOLPH, A. C. & GERMAN VITAMIN, E. A. L. S. S. G. 2005. High dose vitamin E therapy in amyotrophic lateral sclerosis as add-on therapy to riluzole: results of a placebo-controlled double-blind study. *Journal of Neural Transmission,* 112**,** 649-660.

GREENWAY, M. J., ANDERSEN, P. M., RUSS, C., ENNIS, S., CASHMAN, S., DONAGHY, C., PATTERSON, V., SWINGLER, R., KIERAN, D., PREHN, J., MORRISON, K. E., GREEN, A., ACHARYA, K. R., BROWN, R. H. & HARDIMAN, O. 2006. ANG mutations segregate with familial and 'sporadic' amyotrophic lateral sclerosis. *Nature Genetics,* 38**,** 411-413.

GREHL, T., FISCHER, S., MUELLER, K., MALIN, J.-P. & ZANGE, J. 2007. A prospective study to evaluate the impact of P-31-MRS to determinate mitochondrial dysfunction in skeletal muscle of ALS patients. *Amyotrophic Lateral Sclerosis,* 8**,** 4-8.

GROENEVELD, G. J., VAN KAN, H., LIE-A-HUEN, L., GUCHELAAR, H. J. & VAN DEN BERG, L. H. 2008. An association study of riluzole serum concentration and survival and disease progression in patients with ALS. *Clinical Pharmacology & Therapeutics,* 83**,** 718-722.

GROENEVELD, G. J., VAN KAN, H. J. M., TORANO, J. S., VELDINK, J. H., GUCHELAAR, H. J., WOKKE, J. H. J. & VAN DEN BERG, L. H. 2001. Inter- and intraindividual variability of riluzole serum concentrations in patients with ALS. *Journal of the Neurological Sciences,* 191**,** 121-125.

GROENEVELD, G. J., VELDINK, J. H., VAN DER TWEEL, I., KALMIJN, S., BEIJER, C., DE VISSER, M., WOKKE, J. H. J., FRANSSEN, H. & VAN DEN BERG, L. H. 2003. A randomized sequential trial of creatine in amyotrophic lateral sclerosis. *Annals of Neurology,* 53**,** 437-445.

GRUNTMAN, E., BENJAMINI, Y. & GOLANI, I. 2007. Coordination of steering in a free-trotting quadruped. *Journal of Comparative Physiology α-Neuroethology Sensory Neural and Behavioral Physiology,* 193**,** 331-345.

GUILLOT, T. S., ASRESS, S. A., RICHARDSON, J. R., GLASS, J. D. & MILLER, G. W. 2008. Treadmill gait analysis does not detect motor deficits in animal models of Parkinson's disease or amyotrophic lateral sclerosis. *Journal of Motor Behavior,* 40**,** 568-577.

GUNNARSSON, L. G., BODIN, L., SODERFELDT, B. & AXELSON, O. 1992. A case-control study of motor neuron disease - its relation to heritability, and occupational exposures, particularly to solvents. *British Journal of Industrial Medicine,* 49**,** 791-798.

GURNEY, M. E., CUTTING, F. B., ZHAI, P., DOBLE, A., TAYLOR, C. P., ANDRUS, P. K. & HALL, E. D. 1996. Benefit of vitamin E, riluzole, and gabapentin in a transgenic model of familiar amyotrophic lateral sclerosis. *Annals of Neurology,* 39**,** 147-157.

GURNEY, M. E., FLECK, T. J., HIMES, C. S. & HALL, E. D. 1998. Riluzole preserves motor function in a transgenic model of familial amyotrophic lateral sclerosis. *Neurology,* 50**,** 62-66.

GURNEY, M. E., PU, H. F., CHIU, A. Y., DALCANTO, M. C., POLCHOW, C. Y., ALEXANDER, D. D., CALIENDO, J., HENTATI, A., KWON, Y. W., DENG, H. X., CHEN, W. J., ZHAI, P., SUFIT, R. L. & SIDDIQUE, T. 1994. Motor-neuron degeneration in mice that express a human Cu,Zn superoxide-dismutase mutation. *Science,* 264**,** 1772-1775.

GYERTYAN, I. 1995. Analysis of the marble burying response - marbles serve to measure digging rather than evoke burying. *Behavioural Pharmacology,* 6**,** 24-31.

HAEUSLER, A. R., DONNELLY, C. J. & ROTHSTEIN, J. D. 2016. The expanding biology of the C9orf72 nucleotide repeat expansion in neurodegenerative disease. *Nature Reviews Neuroscience,* 17**,** 383-U79.

HALEY, R. W. 2003. Excess incidence of ALS in young Gulf War veterans. *Neurology,* 61**,** 750-756.

HAMADEH, M. J., RODRIGUEZ, M. C., KACZOR, J. J. & TARNOPOLSKY, M. A. 2005. Caloric restriction transiently improves motor performance but hastens clinical onset of disease in the Cu/Zn-superoxide dismutase mutant G93A mouse. *Muscle & Nerve,* 31**,** 214-220.

HAMADEH, M. J. & TARNOPOLSKY, M. A. 2006. Transient caloric restriction in early adulthood hastens disease endpoint in male, but not female, Cu/Zn-sod mutant G93A mice. *Muscle & Nerve,* 34**,** 709-719.

HAMM, R. J., PIKE, B. R., ODELL, D. M., LYETH, B. G. & JENKINS, L. W. 1994. The rotarod test - an evaluation of its effectiveness in assessing motor deficits following traumatic brain injury. *Journal of Neurotrauma,* 11**,** 187-196.

HARWOOD, C. A., MCDERMOTT, C. J. & SHAW, P. J. 2009. Physical activity as an exogenous risk factor in motor neuron disease (MND): A review of the evidence. *Amyotrophic Lateral Sclerosis,* 10**,** 191-204.

HARWOOD, C. A., WESTGATE, K., GUNSTONE, S., BRAGE, S., WAREHAM, N. J., MCDERMOTT, C. J. & SHAW, P. J. 2016. Long-term physical activity: an exogenous risk factor for sporadic amyotrophic lateral sclerosis? *Amyotrophic Lateral Sclerosis and Frontotemporal Degeneration***,** 17.5-6, 377-384.

HATZIPETROS, T., BOGDANIK, L. P., TASSINARI, V. R., KIDD, J. D., MORENO, A. J., DAVIS, C., OSBORNE, M., AUSTIN, A., VIEIRA, F. G., LUTZ, C. & PERRIN, S. 2014. C57BL/6J congenic Prp-TDP43A315T mice develop progressive neurodegeneration in the myenteric plexus of the colon without exhibiting key features of ALS. *Brain Research,* 1584**,** 59-72.

HAYES, L. R. & ROTHSTEIN, J. D. 2016. C9ORF72-ALS/FTD: Transgenic mice make a come-BAC. *Neuron,* 90**,** 427-431.

HEIMAN-PATTERSON, T. D., DEITCH, J. S., BLANKENHORN, E. P., ERWIN, K. L., PERREAULT, M. J., ALEXANDER, B. K., BYERS, N., TOMAN, I. & ALEXANDER, G. M. 2005. Background and gender effects on survival in the TgN(SOD1-G93A) 1 Gur mouse model of ALS. *Journal of the Neurological Sciences,* 236**,** 1-7.

HIGGINS, C. M. J., JUNG, C. W. & XU, Z. S. 2003. ALS-associated mutant SOD1G93A causes mitochondrial vacuolation by expansion of the intermembrane space and by involvement of SOD1 aggregation and peroxisomes. *Bmc Neuroscience,* 4.1, 16-16.

HIGHLEY, J. R., KIRBY, J., JANSWEIJER, J. A., WEBB, P. S., HEWAMADDUMA, C. A., HEATH, P. R., HIGGINBOTTOM, A., RAMAN, R., FERRAIUOLO, L., COOPER-KNOCK, J., MCDERMOTT, C. J., WHARTON, S. B., SHAW, P. J. & INCE, P. G. 2014. Loss of nuclear TDP-43 in amyotrophic lateral sclerosis (ALS) causes altered expression of splicing machinery and widespread dysregulation of RNA splicing in motor neurones. *Neuropathology and Applied Neurobiology,* 40**,** 670-685.

HOOTEN, K. G., BEERS, D. R., ZHAO, W. & APPEL, S. H. 2015. Protective and toxic neuroinflammation in amyotrophic lateral sclerosis. *Neurotherapeutics,* 12**,** 364-375.

HOPPITT, T., PALL, H., CALVERT, M., GILL, P., YAO, G. Q., RAMSAY, J., JAMES, G., CONDUIT, J. & SACKLEY, C. 2011. A systematic review of the incidence and prevalence of long-term neurological conditions in the UK. *Neuroepidemiology,* 36**,** 19-28.

HOWE, K., CLARK, M. D., TORROJA, C. F., TORRANCE, J., BERTHELOT, C., MUFFATO, M., COLLINS, J. E., HUMPHRAY, S., MCLAREN, K., MATTHEWS, L., MCLAREN, S., SEALY, I., CACCAMO, M., CHURCHER, C., SCOTT, C., BARRETT, J. C., KOCH, R., RAUCH, G.-J., WHITE, S., CHOW, W., KILIAN, B., QUINTAIS, L. T., GUERRA-ASSUNCAO, J. A., ZHOU, Y., GU, Y., YEN, J., VOGEL, J.-H., EYRE, T., REDMOND, S., BANERJEE, R., CHI, J., FU, B., LANGLEY, E., MAGUIRE, S. F., LAIRD, G. K., LLOYD, D., KENYON, E., DONALDSON, S., SEHRA, H., ALMEIDA-KING, J., LOVELAND, J., TREVANION, S., JONES, M., QUAIL, M., WILLEY, D., HUNT, A., BURTON, J., SIMS, S., MCLAY, K., PLUMB, B., DAVIS, J., CLEE, C., OLIVER, K., CLARK, R., RIDDLE, C., ELIOTT, D., THREADGOLD, G., HARDEN, G., WARE, D., MORTIMER, B., KERRY, G., HEATH, P., PHILLIMORE, B., TRACEY, A., CORBY, N., DUNN, M., JOHNSON, C., WOOD, J., CLARK, S., PELAN, S., GRIFFITHS, G., SMITH, M., GLITHERO, R., HOWDEN, P., BARKER, N., STEVENS, C., HARLEY, J., HOLT, K., PANAGIOTIDIS, G., LOVELL, J., BEASLEY, H., HENDERSON, C., GORDON, D., AUGER, K., WRIGHT, D., COLLINS, J., RAISEN, C., DYER, L., LEUNG, K., ROBERTSON, L., AMBRIDGE, K., LEONGAMORNLERT, D.,

MCGUIRE, S., GILDERTHORP, R., GRIFFITHS, C., MANTHRAVADI, D., NICHOL, S., BARKER, G., WHITEHEAD, S., KAY, M., et al. 2013. The zebrafish reference genome sequence and its relationship to the human genome. *Nature,* 496**,** 498-503.

HUANG, C., ZHOU, H., TONG, J., CHEN, H., LIU, Y.-J., WANG, D., WEI, X. & XIA, X.-G. 2011. FUS transgenic rats develop the phenotypes of amyotrophic lateral sclerosis and frontotemporal lobar degeneration. *Plos Genetics,* 7.3, e1002011.

HUKEMA, R. K., RIEMSLAGH, F. W., MELHEM, S., VAN DER LINDE, H. C., SEVERIJNEN, L.-A. W., EDBAUER, D., MAAS, A., CHARLET-BERGUERAND, N., WILLEMSEN, R. & VAN SWIETEN, J. C. 2014. A new inducible transgenic mouse model for C9orf72-associated GGGGCC repeat expansion supports a gain-of-function mechanism in C9orf72-associated ALS and FTD. *Acta neuropathologica communications,* 2**,** 166-166.

ICHIMARU, Y., EGAWA, T. & SAWA, A. 1995. 5-HT1A-receptor subtype mediates the effect of fluvoxamine, a selective serotonin reuptake inhibitor, on marble-burying behaviour in mice. *Japanese Journal of Pharmacology,* 68**,** 65-70.

IGAZ, L. M., KWONG, L. K., LEE, E. B., CHEN-PLOTKIN, A., SWANSON, E., UNGER, T., MALUNDA, J., XU, Y., WINTON, M. J., TROJANOWSKI, J. Q. & LEE, V. M. Y. 2011. Dysregulation of the ALS-associated gene TDP-43 leads to neuronal death and degeneration in mice. *Journal of Clinical Investigation,* 121**,** 726-738.

IGUCHI, Y., KATSUNO, M., NIWA, J.-I., TAKAGI, S., ISHIGAKI, S., IKENAKA, K., KAWAI, K., WATANABE, H., YAMANAKA, K., TAKAHASHI, R., MISAWA, H., SASAKI, S., TANAKA, F. & SOBUE, G. 2013. Loss of TDP-43 causes age-dependent progressive motor neuron degeneration. *Brain,* 136**,** 1371-1382.

IKEDA, K., IWASAKI, Y. & KINOSHITA, M. 2000. Oral administration of creatine monohydrate retards progression of motor neuron disease in the wobbler mouse. *Amyotrophic Lateral Sclerosis and Other Motor Neuron Disorders,* 1**,** 207-212.

ITTNER, L. M., HALLIDAY, G. M., KRIL, J. J., GOETZ, J., HODGES, J. R. & KIERNAN, M. C. 2015. OPINION FTD and ALS-translating mouse studies into clinical trials. *Nature Reviews Neurology,* 11**,** 360-366.

IWANAMI, T., SONOO, M., HATANAKA, Y., HOKKOKU, K., OISHI, C. & SHIMIZU, T. 2011. Decremental responses to repetitive nerve stimulation (RNS) in motor neuron disease. *Clinical Neurophysiology,* 122**,** 2530-2536.

JAARSMA, D., HAASDIJK, E. D., GRASHORN, J. A. C., HAWKINS, R., VAN DUIJN, W., VERSPAGET, H. W., LONDON, J. & HOLSTEGE, J. C. 2000. Human Cu/Zn superoxide dismutase (SOD1) overexpression in mice causes mitochondrial vacuolization, axonal degeneration, and premature motoneuron death and accelerates motoneuron disease in mice expressing a familial amyotrophic lateral sclerosis mutant SOD1. *Neurobiology of Disease,* 7**,** 623-643.

JAARSMA, D., ROGNONI, F., VAN DUIJN, W., VERSPAGET, H. W., HAASDIJK, E. D. & HOLSTEGE, J. C. 2001. CuZn superoxide dismutase (SOD1) accumulates in vacuolated mitochondria in transgenic mice expressing amyotrophic lateral sclerosis-linked SOD1 mutations. *Acta Neuropathologica,* 102**,** 293-305.

JANSSENS, J., WILS, H., KLEINBERGER, G., JORIS, G., CUIJT, I., CEUTERICK-DE GROOTE, C., VAN BROECKHOVEN, C. & KUMAR-SINGH, S. 2013. Overexpression of ALS-associated p.M337V human TDP-43 in mice worsens disease features compared to wild-type human TDP-43 mice. *Molecular Neurobiology,* 48**,** 22-35.

JIANG, J., ZHU, Q., GENDRON, T. F., SABERI, S., MCALONIS-DOWNES, M., SEELMAN, A., STAUFFER, J. E., JAFAR-NEJAD, P., DRENNER, K., SCHULTE, D., CHUN, S., SUN, S., LING, S.-C., MYERS, B., ENGELHARDT, J., KATZ, M., BAUGHN, M., PLATOSHYN, O., MARSALA, M., WATT, A., HEYSER, C. J., ARD, M. C., DE MUYNCK, L., DAUGHRITY, L. M., SWING, D. A., TESSAROLLO, L., JUNG, C. J., DELPOUX, A., UTZSCHNEIDER, D. T., HEDRICK, S. M., DE JONG, P. J., EDBAUER, D., VAN DAMME, P., PETRUCELLI, L., SHAW, C. E., BENNETT, C. F., DA CRUZ, S., RAVITS, J., RIGO, F., CLEVELAND, D. W. & LAGIER-TOURENNE, C. 2016. Gain of toxicity from ALS/FTD-linked repeat expansions in C9ORF72 is alleviated by antisense oligonucleotides targeting GGGGCC-containing RNAs. *Neuron,* 90**,** 535-550.

JOHNSON, J. O., MANDRIOLI, J., BENATAR, M., ABRAMZON, Y., VAN DEERLIN, V. M., TROJANOWSKI, J. Q., GIBBS, J. R., BRUNETTI, M., GRONKA, S., WUU, J., DING, J., MCCLUSKEY, L., MARTINEZ-LAGE, M., FALCONE, D., HERNANDEZ, D. G., AREPALLI, S., CHONG, S., SCHYMICK, J. C., ROTHSTEIN, J., LANDI, F., WANG, Y.-D., CALVO, A., MORA, G., SABATELLI, M., MONSURRO, M. R., BATTISTINI, S., SALVI, F., SPATARO, R., SOLA, P., BORGHERO, G., GALASSI, G., SCHOLZ, S. W., TAYLOR, J. P., RESTAGNO, G., CHIO, A., TRAYNOR, B. J. & CONSORTIUM, I. 2010. Exome sequencing reveals VCP mutations as a cause of familial ALS. *Neuron,* 68**,** 857-864.

JOHNSON, J. O., PIORO, E. P., BOEHRINGER, A., CHIA, R., FEIT, H., RENTON, A. E., PLINER, H. A., ABRAMZON, Y., MARANGI, G., WINBORN, B. J., GIBBS, J. R., NALLS, M. A., MORGAN, S., SHOAI, M., HARDY, J., PITTMAN, A., ORRELL, R. W., MALASPINA, A., SIDLE, K. C., FRATTA, P., HARMS, M. B., BALOH, R. H., PESTRONK, A., WEIHL, C. C., ROGAEVA, E., ZINMAN, L., DRORY, V. E., BORGHERO, G., MORA, G., CALVO, A., ROTHSTEIN, J. D., DREPPER, C., SENDTNER, M., SINGLETON, A. B., TAYLOR, J. P., COOKSON, M. R., RESTAGNO, G., SABATELLI, M., BOWSER, R., CHIO, A., TRAYNOR, B. J. & ITALSGEN 2014. Mutations in the Matrin 3 gene cause familial amyotrophic lateral sclerosis. *Nature Neuroscience,* 17.5**,** 664-666.

JOYCE, P. I., MCGOLDRICK, P., SACCON, R. A., WEBER, W., FRATTA, P., WEST, S. J., ZHU, N., CARTER, S., PHATAK, V., STEWART, M., SIMON, M., KUMAR, S., HEISE, I., BROS-FACER, V., DICK, J., CORROCHANO, S., STANFORD, M. J., TU VINH, L., NOLAN, P. M., MEYER, T., BRANDNER, S., BENNETT, D. L. H., OZDINLER, P. H., GREENSMITH, L., FISHER, E. M. C. & ACEVEDO-AROZENA, A. 2015. A novel SOD1-ALS mutation separates central and peripheral effects of mutant SOD1 toxicity. *Human Molecular Genetics,* 24**,** 1883-1897.

KABASHI, E., LIN, L., TRADEWELL, M. L., DION, P. A., BERCIER, V., BOURGOUIN, P., ROCHEFORT, D., HADJ, S. B., DURHAM, H. D., VELDE, C. V., ROULEAU, G. A. & DRAPEAU, P. 2010. Gain and loss of function of ALS-related mutations of TARDBP (TDP-43) cause motor deficits in vivo. *Human Molecular Genetics,* 19**,** 671-683.

KABASHI, E., VALDMANIS, P. N., DION, P., SPIEGELMAN, D., MCCONKEY, B. J., VELDE, C. V., BOUCHARD, J.-P., LACOMBLEZ, L., POCHIGAEVA, K., SALACHAS, F., PRADAT, P.-F., CAMU, W., MEININGER, V., DUPRE, N. & ROULEAU, G. A. 2008. TARDBP mutations in individuals with sporadic and familial amyotrophic lateral sclerosis. *Nature Genetics,* 40**,** 572-574.

KARAM, C., SCELSA, S. N. & MACGOWAN, D. J. L. 2010. The clinical course of progressive bulbar palsy. *Amyotrophic Lateral Sclerosis,* 11**,** 364-368.

KASARSKIS, E. J., BERRYMAN, S., VANDERLEEST, J. G., SCHNEIDER, A. R. & MCCLAIN, C. J. 1996. Nutritional status of patients with amyotrophic lateral sclerosis: Relation to the proximity of death. *American Journal of Clinical Nutrition,* 63**,** 130-137.

KASARSKIS, E. J. & WINSLOW, M. 1989. When did Lou Gehrig's personal illness begin. *Neurology,* 39**,** 1243-1245.

KELLER, A. F., GRAVEL, M. & KRIZ, J. 2011. Treatment with minocycline after disease onset alters astrocyte reactivity and increases microgliosis in SOD1 mutant mice. *Experimental Neurology,* 228**,** 69-79.

KILKENNY, C., BROWNE, W. J., CUTHILL, I. C., EMERSON, M. & ALTMAN, D. G. 2010. Improving bioscience research reporting: The ARRIVE guidelines for reporting animal research. *Plos Biology,* 8.6, e1000412.

KILLIAN, J. M., WILFONG, A. A., BURNETT, L., APPEL, S. H. & BOLAND, D. 1994. Decremental motor-responses to repetitive nerve-stimulation in ALS. *Muscle & Nerve,* 17**,** 747-754.

KIM, H. J., KIM, N. C., WANG, Y.-D., SCARBOROUGH, E. A., MOORE, J., DIAZ, Z., MACLEA, K. S., FREIBAUM, B., LI, S., MOLLIEX, A., KANAGARAJ, A. P., CARTER, R., BOYLAN, K. B., WOJTAS, A. M., RADEMAKERS, R., PINKUS, J. L., GREENBERG, S. A., TROJANOWSKI, J. Q., TRAYNOR, B. J., SMITH, B. N., TOPP, S., GKAZI, A.-S., MILLER, J., SHAW, C. E., KOTTLORS, M., KIRSCHNER, J., PESTRONK, A., LI, Y. R., FORD, A. F., GITLER, A. D., BENATAR, M., KING, O. D., KIMONIS, V. E., ROSS, E. D., WEIHL, C. C., SHORTER, J. & TAYLOR, J. P. 2013. Mutations in prion-like domains in hnRNPA2B1 and hnRNPA1 cause multisystem proteinopathy and ALS. *Nature,* 495.7442**,** 467-473.

KLIVENYI, P., FERRANTE, R. J., MATTHEWS, R. T., BOGDANOV, M. B., KLEIN, A. M., ANDREASSEN, O. A., MUELLER, G., WERMER, M., KADDURAH-DAOUK, R. & BEAL, M. F. 1999. Neuroprotective effects of creatine in a transgenic animal model of amyotrophic lateral sclerosis. *Nature Medicine,* 5**,** 347-350.

KOERNER, S., HENDRICKS, M., KOLLEWE, K., ZAPF, A., DENGLER, R., SILANI, V. & PETRI, S. 2013. Weight loss, dysphagia and supplement intake in patients with amyotrophic lateral sclerosis (ALS): impact on quality of life and therapeutic options. *Bmc Neurology,* 13.1, 84-84.

KONG, J. M. & XU, Z. S. 1998. Massive mitochondrial degeneration in motor neurons triggers the onset of amyotrophic lateral sclerosis in mice expressing a mutant SOD1. *Journal of Neuroscience,* 18**,** 3241-3250.

KOPPERS, M., BLOKHUIS, A. M., WESTENENG, H.-J., TERPSTRA, M. L., ZUNDEL, C. A. C., DE SA, R. V., SCHELLEVIS, R. D., WAITE, A. J., BLAKE, D. J., VELDINK, J. H., VAN DEN BERG, L. H. & PASTERKAMP, R. J. 2015. C9orf72 ablation in mice does not cause motor neuron degeneration or motor deficits. *Annals of Neurology,* 78**,** 426-438.

KOYAMA, A., SUGAI, A., KATO, T., ISHIHARA, T., SHIGA, A., TOYOSHIMA, Y., KOYAMA, M., KONNO, T., HIROKAWA, S., YOKOSEKI, A., NISHIZAWA, M., KAKITA, A., TAKAHASHI, H. & ONODERA, O. 2016. Increased cytoplasmic TARDBP mRNA in affected spinal motor neurons in ALS caused by abnormal autoregulation of TDP-43. *Nucleic Acids Research,* 44**,** 5820-5836.

KRAEMER, B. C., SCHUCK, T., WHEELER, J. M., ROBINSON, L. C., TROJANOWSKI, J. Q., LEE, V. M. Y. & SCHELLENBERG, G. D. 2010. Loss of murine TDP-43 disrupts motor function and plays an essential role in embryogenesis. *Acta Neuropathologica,* 119**,** 409-419.

KRECIC, A. M. & SWANSON, M. S. 1999. hnRNP complexes: composition, structure, and function. *Current Opinion in Cell Biology,* 11**,** 363-371.

KRIZ, J., NGUYEN, M. D. & JULIEN, J. P. 2002. Minocycline slows disease progression in a mouse model of arnyotrophic lateral sclerosis. *Neurobiology of Disease,* 10**,** 268-278.

KUO, J. J., LEE, R. H., ZHANG, L. & HECKMAN, C. J. 2006. Essential role of the persistent sodium current in spike initiation during slowly rising inputs in mouse spinal neurones. *Journal of Physiology-London,* 574**,** 819-834.

KWIATKOWSKI, T. J., JR., BOSCO, D. A., LECLERC, A. L., TAMRAZIAN, E., VANDERBURG, C. R., RUSS, C., DAVIS, A., GILCHRIST, J., KASARSKIS, E. J., MUNSAT, T., VALDMANIS, P., ROULEAU, G. A., HOSLER, B. A., CORTELLI, P., DE JONG, P. J., YOSHINAGA, Y., HAINES, J. L., PERICAK-VANCE, M. A., YAN, J., TICOZZI, N., SIDDIQUE, T., MCKENNA-YASEK, D., SAPP, P. C., HORVITZ, H. R., LANDERS, J. E. & BROWN, R. H., JR. 2009. Mutations in the FUS/TLS gene on chromosome 16 cause familial amyotrophic lateral sclerosis. *Science,* 323**,** 1205-1208.

LAGIER-TOURENNE, C., BAUGHN, M., RIGO, F., SUN, S., LIU, P., LI, H.-R., JIANG, J., WATT, A. T., CHUN, S., KATZ, M., QIU, J., SUN, Y., LING, S.-C., ZHU, Q., POLYMENIDOU, M., DRENNER, K., ARTATES, J. W., MCALONIS-DOWNES, M., MARKMILLER, S., HUTT, K. R., PIZZO, D. P., CADY, J., HARMS, M. B., BALOH, R. H., VANDENBERG, S. R., YEO, G. W., FU, X.-D., BENNETT, C. F., CLEVELAND, D. W. & RAVITS, J. 2013. Targeted degradation of sense and antisense C9orf72 RNA foci as therapy for ALS and frontotemporal degeneration. *Proceedings of the National Academy of Sciences of the United States of America,* 110**,** E4530-E4539.

LAPVETELAINEN, T., TIIHONEN, A., KOSKELA, P., NEVALAINEN, T., LINDBLOM, J., KIRALY, K., HALONEN, P. & HELMINEN, H. J. 1997. Training a large number of laboratory mice using running wheels and analyzing running behavior by use of a computer-assisted system. *Laboratory Animal Science,* 47**,** 172-179.

LE LIBOUX, A., CACHIA, J. P., KIRKESSELI, S., GAUTIER, J. Y., GUIMART, C., MONTAY, G., PEETERS, P. A. M., GROEN, E., JONKMAN, J. H. G. & WEMER, J. 1999. A comparison of the pharmacokinetics and tolerability of riluzole after repeat dose administration in healthy elderly and young volunteers. *Journal of Clinical Pharmacology,* 39**,** 480-486.

LECLERC, N., RIBERA, F., ZOLL, J., WARTER, J. M., POINDRON, P., LAMPERT, E. & BORG, J. 2001. Selective changes in mitochondria respiratory properties in oxidative or glycolytic muscle fibers isolated from G93AhumanSOD1 transgenic mice. *Neuromuscular Disorders,* 11**,** 722-727.

LEE, J. K., SHIN, J. H., HWANG, S. G., GWAG, B. J., MCKEE, A. C., LEE, J., KOWALL, N. W., RYU, H., LIM, D.-S. & CHOI, E.-J. 2013. MST1 functions as a key modulator of neurodegeneration in a mouse model of ALS. *Proceedings of the National Academy of Sciences of the United States of America,* 110**,** 12066-12071.

LEMMENS, R., VAN HOECKE, A., HERSMUS, N., GEELEN, V., D'HOLLANDER, I., THIJS, V., VAN DEN BOSCH, L. & CARMELIET, P. 2007. Overexpression of mutant superoxide dismutase 1 causes a motor axonopathy in the zebrafish. *Human Molecular Genetics,* 16**,** 2359-2365.

LI, J., SUNG, M. & RUTKOVE, S. B. 2013. Electrophysiologic biomarkers for assessing disease progression and the effect of riluzole in SOD1 G93A ALS mice. *Plos One,* 8.6, e65976.

LING, J. P., PLETNIKOVA, O., TRONCOSO, J. C. & WONG, P. C. 2015. TDP-43 repression of nonconserved cryptic exons is compromised in ALS-FTD. *Science,* 349**,** 650-655.

LING, S.-C., POLYMENIDOU, M. & CLEVELAND, D. W. 2013. Converging mechanisms in ALS and FTD: disrupted RNA and protein homeostasis. *Neuron,* 79**,** 416-438.

LINO, M. M., SCHNEIDER, C. & CARONI, P. 2002. Accumulation of SOD1 mutants in postnatal motoneurons does not cause motoneuron pathology or motoneuron disease. *Journal of Neuroscience,* 22**,** 4825-4832.

LIU, Q., SHU, S., WANG, R. R., LIU, F., CUI, B., GUO, X. N., LU, C. X., LI, X. G., LIU, M. S., PENG, B., CUI, L.-Y. & ZHANG, X. 2016a. Whole-exome sequencing identifies a missense mutation in hnRNPA1 in a family with flail arm ALS. *Neurology,* 87**,** 1763-1769.

LIU, Y., PATTAMATTA, A., ZU, T., REID, T., BARDHI, O., BORCHELT, D. R., YACHNIS, A. T. & RANUM, L. P. W. 2016b. C9orf72 BAC mouse model with motor deficits and neurodegenerative features of ALS/FTD. *Neuron,* 90**,** 521-534.

LLADO, J., HAENGGELI, C., PARDO, A., WONG, V., BENSON, L., COCCIA, C., ROTHSTEIN, J. D., SHEFNER, J. M. & MARAGAKIS, N. J. 2006. Degeneration of respiratory motor neurons in the SOD1 G93A transgenic rat model of ALS. *Neurobiology of Disease,* 21**,** 110-118.

LONDEI, T., VALENTINI, A. M. V. & LEONE, V. G. 1998. Investigative burying by laboratory mice may involve non-functional, compulsive, behaviour. *Behavioural Brain Research,* 94**,** 249-254.

LONGSTRETH, W. T., MCGUIRE, V., KOEPSELL, T. D., WANG, Y. & VAN BELLE, G. 1998. Risk of amyotrophic lateral sclerosis and history of physical activity - A population-based case-control study. *Archives of Neurology,* 55**,** 201-206.

LUDOLPH, A. C., BENDOTTI, C., BLAUGRUND, E., CHIO, A., GREENSMITH, L., LOEFFLER, J.-P., MEAD, R., NIESSEN, H. G., PETRI, S., PRADAT, P.-F., ROBBERECHT, W., RUEGG, M., SCHWALENSTOECKER, B., STILLER, D., VAN DEN BERG, L., VIEIRA, F. & VON HORSTEN, S. 2010. Guidelines for preclinical animal research in ALS/MND: A consensus meeting. *Amyotrophic Lateral Sclerosis,* 11**,** 38-45.

LUDOLPH, A. C., BENDOTTI, C., BLAUGRUND, E., HENGERER, B., LOFFLER, J.-P., MARTIN, J., MEININGER, V., MEYER, T., MOUSSAOUI, S., ROBBERECHT, W., SCOTT, S., SILANI, V., VAN DEN BERG, L. H., OF, E. G. F. T. E. O. G. F. T. C. & PRECLINICAL AND PROOF OF CONCEPT STUDIES IN, A. L. S. M. N. D. M. 2007. Guidelines for the preclinical in vivo evaluation of pharmacological active drugs for ALS/MND: report on the 142nd ENMC international workshop. *Amyotrophic lateral sclerosis : official publication of the World Federation of Neurology Research Group on Motor Neuron Diseases,* 8**,** 217-23.

MACKENZIE, I. R. A., BIGIO, E. H., INCE, P. G., GESER, F., NEUMANN, M., CAIRNS, N. J., KWONG, L. K., FORMAN, M. S., RAVITS, J., STEWART, H., EISEN, A., MCCLUSKY, L., KRETZSCHMAR, H. A., MONORANU, C. M., HIGHLEY, J. R., KIRBY, J., SIDDIQUE, T., SHAW, P. J., LEE, V. M. Y. & TROJANOWSKI, J. Q. 2007. Pathological TDP-43 distinguishes sporadic amyotrophic lateral sclerosis from amyotrophic lateral sclerosis with SOD1 mutations. *Annals of Neurology,* 61**,** 427-434.

MAJOUNIE, E., RENTON, A. E., MOK, K., DOPPER, E. G. P., WAITE, A., ROLLINSON, S., CHIO, A., RESTAGNO, G., NICOLAOU, N., SIMON-SANCHEZ, J., VAN SWIETEN, J. C., ABRAMZON, Y., JOHNSON, J. O., SENDTNER, M., PAMPHLETT, R., ORRELL, R. W., MEAD, S., SIDLE, K. C., HOULDEN, H., ROHRER, J. D., MORRISON, K. E., PALL, H., TALBOT, K., ANSORGE, O., HERNANDEZ, D. G., AREPALLI, S., SABATELLI, M., MORA, G., CORBO, M., GIANNINI, F., CALVO, A., ENGLUND, E., BORGHERO, G., FORIS, G. L., REMES, A. M., LAAKSOVIRTA, H., MCCLUSKEY, L., TROJANOWSKI, J. Q., VAN DEERLIN, V. M., SCHELLENBERG, G. D., NALLS, M. A., DRORY, V. E., LU, C.-S., YEH, T.-H., ISHIURA, H., TAKAHASHI, Y., TSUJI, S., LE BER, I., BRICE, A., DREPPER, C., WILLIAMS, N., KIRBY, J., SHAW, P., HARDY, J., TIENARI, P. J., HEUTINK, P., MORRIS, H. R., PICKERING-BROWN, S., TRAYNOR, B. J., CHROMOSOME, A. L. S. F. T. D. C., FRENCH RES NETWORK, F. F. A. & CONSORTIUM, I. 2012. Frequency of the C9orf72 hexanucleotide repeat expansion in patients with amyotrophic lateral sclerosis and frontotemporal dementia: a cross-sectional study. *Lancet Neurology,* 11**,** 323-330.

MANCUSO, R., OLIVAN, S., OSTA, R. & NAVARRO, X. 2011a. Evolution of gait abnormalities in SOD1(G93A) transgenic mice. *Brain Research,* 1406**,** 65-73.

MANCUSO, R., OSTA, R. & NAVARRO, X. 2014. Presymptomatic electrophysiological tests predict clinical onset and survival in SOD1(G93A) ALS mice. *Muscle & Nerve,* 50**,** 943-949.

MANCUSO, R., SANTOS-NOGUEIRA, E., OSTA, R. & NAVARRO, X. 2011b. Electrophysiological analysis of a murine model of motoneuron disease. *Clinical Neurophysiology,* 122**,** 1660-1670.

MANUEL VIDAL-TABOADA, J., LOPEZ-LOPEZ, A., SALVADO, M., LORENZO, L., GARCIA, C., MAHY, N., RODRIGUEZ, M. J. & GAMEZ, J. 2015. UNC13A confers risk for sporadic ALS and influences survival in a Spanish cohort. *Journal of Neurology,* 262**,** 2285-2292.

MARUYAMA, H., MORINO, H., ITO, H., IZUMI, Y., KATO, H., WATANABE, Y., KINOSHITA, Y., KAMADA, M., NODERA, H., SUZUKI, H., KOMURE, O., MATSUURA, S., KOBATAKE, K., MORIMOTO, N., ABE, K., SUZUKI, N., AOKI, M., KAWATA, A., HIRAI, T., KATO, T., OGASAWARA, K., HIRANO, A., TAKUMI, T., KUSAKA, H., HAGIWARA, K., KAJI, R. & KAWAKAMI, H. 2010. Mutations of optineurin in amyotrophic lateral sclerosis. *Nature,* 465**,** 223-U109.

MASSETT, M. P. & BERK, B. C. 2005. Strain-dependent differences in responses to exercise training in inbred and hybrid mice. *American Journal of Physiology-Regulatory Integrative and Comparative Physiology,* 288**,** R1006-R1013.

MATTIAZZI, M., D'AURELIO, M., GAJEWSKI, C. D., MARTUSHOVA, K., KIAEI, M., BEAL, M. F. & MANFREDI, G. 2002. Mutated human SOD1 causes dysfunction of oxidative phosphorylation in mitochondria of transgenic mice. *Journal of Biological Chemistry,* 277**,** 29626-29633.

MCCOMAS, A. J., FAWCETT, P. R. W., CAMPBELL, M. J. & SICA, R. E. P. 1971. Electrophysiological estimation of number of motor units within a human muscle. *Journal of Neurology Neurosurgery and Psychiatry,* 34**,** 121-131.

MCDERMOTT, C. J., SHAW, P. J., COOPER, C. L., DIXON, S., BAIRD, W. O., BRADBURN, M. J., FITZGERALD, P., MAGUIRE, C., WILLIAMS, T., BAUDOUIN, S. V., KARAT, D., TALBOT, K., STRADLING, J., MAYNARD, N., TURNER, M., BIANCHI, S., ACKROYD, R., BOURKE, S. C., EALING, J., HAMDALLA, H., BENTLEY, A., GALLOWAY, S., ORRELL, R. W., WEDZICHA, W., ELLIOT, M., HUGHES, P., HANEMANN, C. O. & DI, P. S. G. C. 2015a. Safety and efficacy of diaphragm pacing in patients with respiratory insufficiency due to amyotrophic lateral sclerosis (DiPALS): a multicentre, open-label, randomised controlled trial. *Lancet Neurology,* 14**,** 883-892.

MCDERMOTT, C. J., SHAW, P. J., STAVROULAKIS, T., WALTERS, S. J., AL-CHALABI, A., CHANDRAN, S., CRAWLEY, F., DICK, D., DONAGHY, C., EAMES, P., FISH, M., GENT, C., GORRIE, G., HAMDALLA, H., HANEMANN, C. O., JOHNSON, M., MAJEED, T., MALASPINA, A., MORRISON, K., ORRELL, R., PINTO, A., RADUNOVIC, A., ROBERTS, M., TALBOT, K., TURNER, M. R., WILLIAMS, T., YOUNG, C. & PROGAS STUDY, G. 2015b. Gastrostomy in

patients with amyotrophic lateral sclerosis (ProGas): a prospective cohort study. *Lancet Neurology,* 14**,** 702-709.

MEAD, R. J., BENNETT, E. J., KENNERLEY, A. J., SHARP, P., SUNYACH, C., KASHER, P., BERWICK, J., PETTMANN, B., BATTAGLIA, G., AZZOUZ, M., GRIERSON, A. & SHAW, P. J. 2011. Optimised and rapid pre-clinical screening in the SOD1(G93A) transgenic mouse model of amyotrophic lateral sclerosis (ALS). *Plos One,* 6.8, e23244.

MENON, P., GEEVASINGA, N., YIANNIKAS, C., HOWELL, J., KIERNAN, M. C. & VUCIC, S. 2015. Sensitivity and specificity of threshold tracking transcranial magnetic stimulation for diagnosis of amyotrophic lateral sclerosis: a prospective study. *Lancet Neurology,* 14**,** 478-484.

MIANA-MENA, F. J., MUNOS, M. J., YAGUE, G., MENDEZ, M., MORENO, M., CIRIZA, J., ZARAGOZA, P. & OSTA, R. 2005. Optimal methods to characterize the G93A mouse model of ALS. *Amyotrophic Lateral Sclerosis and Other Motor Neuron Disorders,* 6**,** 55-62.

MILLECAMPS, S., SALACHAS, F., CAZENEUVE, C., GORDON, P., BRICKA, B., CAMUZAT, A., GUILLOT-NOEL, L., RUSSAOUEN, O., BRUNETEAU, G., PRADAT, P.-F., LE FORESTIER, N., VANDENBERGHE, N., DANEL-BRUNAUD, V., GUY, N., THAUVIN-ROBINET, C., LACOMBLEZ, L., COURATIER, P., HANNEQUIN, D., SEILHEAN, D., LE BER, I., CORCIA, P., CAMU, W., BRICE, A., ROULEAU, G., LEGUERN, E. & MEININGER, V. 2010. SOD1, ANG, VAPB, TARDBP, and FUS mutations in familial amyotrophic lateral sclerosis: genotyp-phenotype correlations. *Journal of Medical Genetics,* 47**,** 554-560.

MILLER, R. G., MITCHELL, J. D., LYON, M. & MOORE, D. H. 2003. Riluzole for amyotrophic lateral sclerosis (ALS)/motor neuron disease (MND). *Amyotrophic Lateral Sclerosis and Other Motor Neuron Disorders,* 4**,** 191-206.

MILLER, R. G., MITCHELL, J. D. & MOORE, D. H. 2012. Riluzole for amyotrophic lateral sclerosis (ALS)/motor neuron disease (MND). *Cochrane Database Syst Rev.***,** CD001447. doi: 10.1002/14651858.CD001447.pub3.

MILLER, R. G., MOORE, D. H., GELINAS, D. F., DRONSKY, V., MENDOZA, M., BAROHN, R. J., BRYAN, W., RAVITS, J., YUEN, E., NEVILLE, H., RINGEL, S., BROMBERG, M., PETAJAN, J., AMATO, A. A., JACKSON, C., JOHNSON, W., MANDLER, R., BOSCH, P., SMITH, B., GRAVES, M., ROSS, M., SORENSON, E. J., KELKAR, P., PARRY, G., OLNEY, R. & GRP, W. S. 2001. Phase III randomized trial of gabapentin in patients with amyotrophic lateral sclerosis. *Neurology,* 56**,** 843-848.

MITCHELL, J. C., CONSTABLE, R., SO, E., VANCE, C., SCOTTER, E., GLOVER, L., HORTOBAGYI, T., ARNOLD, E. S., LING, S.-C., MCALONIS, M., DA CRUZ, S., POLYMENIDOU, M., TESSAROLO, L., CLEVELAND, D. W. & SHAW, C. E. 2015. Wild type human TDP-43 potentiates ALS-linked mutant TDP-43 driven progressive motor and cortical neuron degeneration with pathological features of ALS. *Acta Neuropathologica Communications,* 3.1, 36.

MITCHELL, J. C., MCGOLDRICK, P., VANCE, C., HORTOBAGYI, T., SREEDHARAN, J., ROGELJ, B., TUDOR, E. L., SMITH, B. N., KLASEN, C., MILLER, C. C. J., COOPER, J. D., GREENSMITH, L. & SHAW, C. E. 2013. Overexpression of human wild-type FUS causes progressive motor neuron degeneration in an age- and dose-dependent fashion. *Acta Neuropathologica,* 125**,** 273-288.

MITCHELL, J. D. & BORASIO, G. D. 2007. Amyotrophic lateral sclerosis. *Lancet,* 369**,** 2031-2041.

MITCHELL, J. D., CALLAGHER, P., GARDHAM, J., MITCHELL, C., DIXON, M., ADDISON-JONES, R., BENNETT, W. & O'BRIEN, M. R. 2010. Timelines in the diagnostic evaluation of people with suspected amyotrophic lateral sclerosis (ALS)/motor neuron disease (MND) - a 20-year review: Can we do better? *Amyotrophic Lateral Sclerosis,* 11**,** 537-541.

MIZIELINSKA, S., GROENKE, S., NICCOLI, T., RIDLER, C. E., CLAYTON, E. L., DEVOY, A., MOENS, T., NORONA, F. E., WOOLLACOTT, I. O. C., PIETRZYK, J., CLEVERLEY, K., NICOLL, A. J., PICKERING-BROWN, S., DOLS, J., CABECINHA, M., HENDRICH, O., FRATTA, P., FISHER, E. M. C., PARTRIDGE, L. & ISAACS, A. M. 2014. C9orf72 repeat expansions cause neurodegeneration in Drosophila through arginine-rich proteins. *Science,* 345**,** 1192-1194.

MOSER, J. M., BIGINI, P. & SCHMITT-JOHN, T. 2013. The wobbler mouse, an ALS animal model. *Molecular Genetics and Genomics,* 288**,** 207-229.

MURAKAMI, T., YANG, S.-P., XIE, L., KAWANO, T., FU, D., MUKAI, A., BOHM, C., CHEN, F., ROBERTSON, J., SUZUKI, H., TARTAGLIA, G. G., VENDRUSCOLO, M., SCHIERLE, G. S. K., CHAN, F. T. S., MOLONEY, A., CROWTHER, D., KAMINSKI, C. F., ZHEN, M. & ST GEORGE-HYSLOP, P. 2012. ALS mutations in FUS cause neuronal dysfunction and death in Caenorhabditis elegans by a dominant gain-of-function mechanism. *Human Molecular Genetics,* 21**,** 1-9.

NAGAI, M., RE, D. B., NAGATA, T., CHALAZONITIS, A., JESSELL, T. M., WICHTERLE, H. & PRZEDBORSKI, S. 2007. Astrocytes expressing ALS-linked mutated SOD1 release factors selectively toxic to motor neurons. *Nature Neuroscience,* 10**,** 615-622.

NANDEDKAR, S. D., BARKHAUS, P. E. & STALBERG, E. V. 2010. Motor unit number index (MUNIX): principle, method, and findings in healthy subjects and in patients with motor neuron disease. *Muscle & Nerve,* 42**,** 798-807.

NEUMANN, M., SAMPATHU, D. M., KWONG, L. K., TRUAX, A. C., MICSENYI, M. C., CHOU, T. T., BRUCE, J., SCHUCK, T., GROSSMAN, M., CLARK, C. M., MCCLUSKEY, L. F., MILLER, B. L., MASLIAH, E., MACKENZIE, I. R., FELDMAN, H., FEIDEN, W., KRETZSCHMAR, H. A., TROJANOWSKI, J. Q. & LEE, V. M. Y. 2006. Ubiquitinated TDP-43 in frontotemporal lobar degeneration and amyotrophic lateral sclerosis. *Science,* 314**,** 130-133.

NEUWIRTH, C., BARKHAUS, P. E., BURKHARDT, C., CASTRO, J., CZELL, D., DE CARVALHO, M., NANDEDKAR, S., STALBERG, E. & WEBER, M. 2015. Tracking motor neuron loss in a set of six muscles in amyotrophic lateral sclerosis using the Motor Unit Number Index (MUNIX): a 15-month longitudinal multicentre trial. *Journal of Neurology Neurosurgery and Psychiatry,* 86**,** 1172-1179.

NICOLAS, L. B., KOLB, Y. & PRINSSEN, E. P. M. 2006. A combined marble burying-locomotor activity test in mice: A practical screening test with sensitivity to different classes of anxiolytics and antidepressants. *European Journal of Pharmacology,* 547**,** 106-115.

NJUNGE, K. & HANDLEY, S. L. 1991. Evaluation of marble-burying behaviour as a model of anxiety. *Pharmacology Biochemistry and Behavior,* 38**,** 63-67.

O'ROURKE, J. G., BOGDANIK, L., MUHAMMAD, A. K. M. G., GENDRON, T. F., KIM, K. J., AUSTIN, A., CADY, J., LIU, E. Y., ZARROW, J., GRANT, S., HO, R., BELL, S., CARMONA, S., SIMPKINSON, M., LALL, D., WU, K., DAUGHRITY, L., DICKSON, D. W., HARMS, M. B., PETRUCELLI, L., LEE, E. B., LUTZ, C. M. & BALOH, R. H. 2015. C9orf72 BAC Transgenic mice display typical pathologic features of ALS/FTD. *Neuron,* 88**,** 892-901.

O'ROURKE, J. G., BOGDANIK, L., YANEZ, A., LALL, D., WOLF, A. J., MUHAMMAD, A. K. M. G., HO, R., CARMONA, S., VIT, J. P., ZARROW, J., KIM, K. J., BELL, S., HARMS, M. B., MILLER, T. M., DANGLER, C. A., UNDERHILL, D. M., GOODRIDGE, H. S., LUTZ, C. M. & BALOH, R. H. 2016. C9orf72 is required for proper macrophage and microglial function in mice. *Science,* 351**,** 1324-1329.

OU, S. H. I., WU, F., HARRICH, D., GARCIA-MARTINEZ, L. F. & GAYNOR, R. G. 1995. Cloning and characterization of a novel cellular protein, TDP-43, that binds to human immunodeficiency virus type 1 TAR DNA sequence motifs. *Journal of Virology,* 69**,** 3584-3596.

PALAMIUC, L., SCHLAGOWSKI, A., NGO, S. T., VERNAY, A., DIRRIG-GROSCH, S., HENRIQUES, A., BOUTILLIER, A. L., ZOLL, J., ECHANIZ-LAGUNA, A., LOEFFLER, J. P. & RENE, F. 2015. A metabolic switch toward lipid use in glycolytic muscle is an early pathologic event in a mouse model of amyotrophic lateral sclerosis. *Embo Molecular Medicine,* 7**,** 526-546.

PELEDKAMAR, M., LOTEM, J., WIRGUIN, I., WEINER, L., HERMALIN, A. & GRONER, Y. 1997. Oxidative stress mediates impairment of muscle function in transgenic mice with elevated level of wild-type Cu/Zn superoxide dismutase. *Proceedings of the National Academy of Sciences of the United States of America,* 94**,** 3883-3887.

PENSATO, V., TILOCA, C., CORRADO, L., BERTOLIN, C., SARDONE, V., DEL BO, R., CALINI, D., MANDRIOLI, J., LAURIA, G., MAZZINI, L., QUERIN, G., CERONI, M., CANTELLO, R., CORTI, S., CASTELLOTTI, B., SOLDA, G., DUGA, S., COMI, G. P., CEREDA, C., SORARU, G.,

D'ALFONSO, S., TARONI, F., SHAW, C. E., LANDERS, J. E., TICOZZI, N., RATTI, A., GELLERA, C., SILANI, V. & CONSORTIUM, S. 2015. TUBA4A gene analysis in sporadic amyotrophic lateral sclerosis: identification of novel mutations. *Journal of Neurology,* 262**,** 1376-1378.

PETERS, O. M., CABRERA, G. T., TRAN, H., GENDRON, T. F., MCKEON, J. E., METTERVILLE, J., WEISS, A., WIGHTMAN, N., SALAMEH, J., KIM, J., SUN, H., BOYLAN, K. B., DICKSON, D., KENNEDY, Z., LIN, Z., ZHANG, Y. J., DAUGHRITY, L., JUNG, C., GAO, F. B., SAPP, P. C., HORVITZ, H. R., BOSCO, D. A., BROWN, S. P., DE JONG, P., PETRUCELLI, L., MUELLER, C. & BROWN, R. H., JR. 2015. Human C9ORF72 hexanucleotide expansion reproduces RNA foci and dipeptide repeat proteins but not neurodegeneration in BAC transgenic mice. *Neuron.,* 88**,** 902-9. doi: 10.1016/j.neuron.2015.11.018.

PETROFF, O. A. C., PRICHARD, J. W., BEHAR, K. L., ALGER, J. R., DENHOLLANDER, J. A. & SHULMAN, R. G. 1985. Cerebral intracellular pH by P-31 nuclear magnetic-resonance spectroscopy. *Neurology,* 35**,** 781-788.

PLATT, R. J., CHEN, S., ZHOU, Y., YIM, M. J., SWIECH, L., KEMPTON, H. R., DAHLMAN, J. E., PARNAS, O., EISENHAURE, T. M., JOVANOVIC, M., GRAHAM, D. B., JHUNJHUNWALA, S., HEIDENREICH, M., XAVIER, R. J., LANGER, R., ANDERSON, D. G., HACOHEN, N., REGEV, A., FENG, G., SHARP, P. A. & ZHANG, F. 2014. CRISPR-Cas9 knockin mice for genome editing and cancer modeling. *Cell,* 159**,** 440-455.

POLYMENIDOU, M., LAGIER-TOURENNE, C., HUTT, K. R., BENNETT, C. F., CLEVELAND, D. W. & YEO, G. W. 2012. Misregulated RNA processing in amyotrophic lateral sclerosis. *Brain Research,* 1462**,** 3-15.

POLYMENIDOU, M., LAGIER-TOURENNE, C., HUTT, K. R., HUELGA, S. C., MORAN, J., LIANG, T. Y., LING, S.-C., SUN, E., WANCEWICZ, E., MAZUR, C., KORDASIEWICZ, H., SEDAGHAT, Y., DONOHUE, J. P., SHIUE, L., BENNETT, C. F., YEO, G. W. & CLEVELAND, D. W. 2011. Long pre-mRNA depletion and RNA missplicing contribute to neuronal vulnerability from loss of TDP-43. *Nature Neuroscience,* 14**,** 459-U92.

PRUDLO, J., KONIG, J., SCHUSTER, C., KASPER, E., BUTTNER, A., TEIPEL, S. & NEUMANN, M. 2016. TDP-43 pathology and cognition in ALS: A prospective clinicopathologic correlation study. *Neurology,* 87.10, 1019-1023.

PULS, I., JONNAKUTY, C., LAMONTE, B. H., HOLZBAUR, E. L. F., TOKITO, M., MANN, E., FLOETER, M. K., BIDUS, K., DRAYNA, D., OH, S. J., BROWN, R. H., LUDLOW, C. L. & FISCHBECK, K. H. 2003. Mutant dynactin in motor neuron disease. *Nature Genetics,* 33**,** 455-456.

RAFIQ, M. K., LEE, E., BRADBURN, M., MCDERMOTT, C. J. & SHAW, P. J. 2016. Creatine kinase enzyme level correlates positively with serum creatinine and lean body mass, and is a prognostic factor for survival in amyotrophic lateral sclerosis. *European Journal of Neurology,* 23**,** 1071-1078.

RAMAN, R., ALLEN, S. P., GOODALL, E. F., KRAMER, S., PONGER, L. L., HEATH, P. R., MILO, M., HOLLINGER, H. C., WALSH, T., HIGHLEY, J. R., OLPIN, S., MCDERMOTT, C. J., SHAW, P. J. & KIRBY, J. 2015. Gene expression signatures in motor neurone disease fibroblasts reveal dysregulation of metabolism, hypoxia-response and RNA processing functions. *Neuropathology and Applied Neurobiology,* 41**,** 201-226.

RAMESH, T., LYON, A. N., PINEDA, R. H., WANG, C., JANSSEN, P. M. L., CANAN, B. D., BURGHES, A. H. M. & BEATTIE, C. E. 2010. A genetic model of amyotrophic lateral sclerosis in zebrafish displays phenotypic hallmarks of motoneuron disease. *Disease Models & Mechanisms,* 3**,** 652-662.

REN, J., SHERRY, A. D. & MALLOY, C. R. 2015. P-31-MRS of healthy human brain: ATP synthesis, metabolite concentrations, pH, and T-1 relaxation times. *Nmr in Biomedicine,* 28**,** 1455-1462.

RENEMA, W. K. J., SCHMIDT, A., VAN ASTEN, J. J. A., OERLEMANS, F., ULLRICH, K., WIERINGA, B., ISBRANDT, D. & HEERSCHAP, A. 2003. MR spectroscopy of muscle and brain in guanidinoacetate methyltransferase (GAMT)-deficient mice: Validation of an animal model to study creatine deficiency. *Magnetic Resonance in Medicine,* 50**,** 936-943.

RENTON, A. E., CHIO, A. & TRAYNOR, B. J. 2014. State of play in amyotrophic lateral sclerosis genetics. *Nature Neuroscience,* 17**,** 17-23.

RENTON, A. E., MAJOUNIE, E., WAITE, A., SIMON-SANCHEZ, J., ROLLINSON, S., GIBBS, J. R., SCHYMICK, J. C., LAAKSOVIRTA, H., VAN SWIETEN, J. C., MYLLYKANGAS, L., KALIMO, H., PAETAU, A., ABRAMZON, Y., REMES, A. M., KAGANOVICH, A., SCHOLZ, S. W., DUCKWORTH, J., DING, J., HARMER, D. W., HERNANDEZ, D. G., JOHNSON, J. O., MOK, K., RYTEN, M., TRABZUNI, D., GUERREIRO, R. J., ORRELL, R. W., NEAL, J., MURRAY, A., PEARSON, J., JANSEN, I. E., SONDERVAN, D., SEELAAR, H., BLAKE, D., YOUNG, K., HALLIWELL, N., CALLISTER, J. B., TOULSON, G., RICHARDSON, A., GERHARD, A., SNOWDEN, J., MANN, D., NEARY, D., NALLS, M. A., PEURALINNA, T., JANSSON, L., ISOVIITA, V.-M., KAIVORINNE, A.-L., HOLTTA-VUORI, M., IKONEN, E., SULKAVA, R., BENATAR, M., WUU, J., CHIO, A., RESTAGNO, G., BORGHERO, G., SABATELLI, M., HECKERMAN, D., ROGAEVA, E., ZINMAN, L., ROTHSTEIN, J. D., SENDTNER, M., DREPPER, C., EICHLER, E. E., ALKAN, C., ABDULLAEV, Z., PACK, S. D., DUTRA, A., PAK, E., HARDY, J., SINGLETON, A., WILLIAMS, N. M., HEUTINK, P., PICKERING-BROWN, S., MORRIS, H. R., TIENARI, P. J., TRAYNOR, B. J. & CONSORTIUM, I. 2011. A hexanucleotide repeat expansion in C9ORF72 is the cause of chromosome 9p21-linked ALS-FTD. *Neuron,* 72**,** 257-268.

RICKETTS, T., MCGOLDRICK, P., FRATTA, P., DE OLIVEIRA, H. M., KENT, R., PHATAK, V., BRANDNER, S., BLANCO, G., GREENSMITH, L., ACEVEDO-AROZENA, A. & FISHER, E. M. C. 2014. A nonsense mutation in mouse Tardbp affects TDP43 alternative splicing activity and causes limb-clasping and body tone defects. *Plos One,* 9.1, e85962.

RINGHOLZ, G. M., APPEL, S. H., BRADSHAW, M., COOKE, N. A., MOSNIK, D. M. & SCHULZ, P. E. 2005. Prevalence and patterns of cognitive impairment in sporadic ALS. *Neurology,* 65**,** 586-590.

RIPPS, M. E., HUNTLEY, G. W., HOF, P. R., MORRISON, J. H. & GORDON, J. W. 1995. Transgenic mice expressing an altered murine superoxide-dismutase gene provide an animal-model of amyotrophic lateral sclerosis. *Proceedings of the National Academy of Sciences of the United States of America,* 92**,** 689-693.

ROSEN, D. R., SIDDIQUE, T., PATTERSON, D., FIGLEWICZ, D. A., SAPP, P., HENTATI, A., DONALDSON, D., GOTO, J., OREGAN, J. P., DENG, H. X., RAHMANI, Z., KRIZUS, A., MCKENNAYASEK, D., CAYABYAB, A., GASTON, S. M., BERGER, R., TANZI, R. E., HALPERIN, J. J., HERZFELDT, B., VANDENBERGH, R., HUNG, W. Y., BIRD, T., DENG, G., MULDER, D. W., SMYTH, C., LAING, N. G., SORIANO, E., PERICAKVANCE, M. A., HAINES, J., ROULEAU, G. A., GUSELLA, J. S., HORVITZ, H. R. & BROWN, R. H. 1993. Mutations in Cu/Zn superoxide-dismutase gene are associated with familial amyotrophic-lateral-sclerosis. *Nature,* 362**,** 59-62.

ROSENFELD, J. & STRONG, M. J. 2015. Challenges in the Understanding and Treatment of Amyotrophic Lateral Sclerosis/Motor Neuron Disease. *Neurotherapeutics,* 12**,** 317-325.

ROWLAND, L. P. & SHNEIDER, N. A. 2001. Medical progress: Amyotrophic lateral sclerosis. *New England Journal of Medicine,* 344**,** 1688-1700.

RUTHERFORD, N. J., ZHANG, Y.-J., BAKER, M., GASS, J. M., FINCH, N. A., XU, Y.-F., STEWART, H., KELLEY, B. J., KUNTZ, K., CROOK, R. J. P., SREEDHARAN, J., VANCE, C., SORENSON, E., LIPPA, C., BIGIO, E. H., GESCHWIND, D. H., KNOPMAN, D. S., MITSUMOTO, H., PETERSEN, R. C., CASHMAN, N. R., HUTTON, M., SHAW, C. E., BOYLAN, K. B., BOEVE, B., GRAFF-RADFORD, N. R., WSZOLEK, Z. K., CASELLI, R. J., DICKSON, D. W., MACKENZIE, I. R., PETRUCELLI, L. & RADEMAKERS, R. 2008. Novel mutations in TARDBP (TDP-43) in patients with familial amyotrophic lateral sclerosis. *Plos Genetics,* 4.9, e1000193.

RYAN, T. E., ERICKSON, M. L., VERMA, A., CHAVEZ, J., RIVNER, M. H. & MCCULLY, K. K. 2014. Skeletal muscle oxidative capacity in amyotrophic lateral sclerosis. *Muscle & nerve,* 50.5, 767-774.

SAKAMOTO, K. & HOLMAN, G. D. 2008. Emerging role for AS160/TBC1D4 and TBC1D1 in the regulation of GLUT4 traffic. *American Journal of Physiology-Endocrinology and Metabolism,* 295**,** E29-E37.

SASAGURI, H., CHEW, J., XU, Y. F., GENDRON, T. F., GARRETT, A., LEE, C. W., JANSEN-WEST, K., BAUER, P. O., PERKERSON, E. A., TONG, J., STETLER, C. & ZHANG, Y. J. 2016. The extreme N-terminus of TDP-43 mediates the cytoplasmic aggregation of TDP-43 and associated toxicity in vivo. *Brain Res,* 4**,** 30318-3.

SASAKI, S. & IWATA, M. 1996. Dendritic synapses of anterior horn neurons in amyotrophic lateral sclerosis: An ultrastructural study. *Acta Neuropathologica,* 91**,** 278-283.

SCHMITT-JOHN, T., DREPPER, C., MUSSMANN, A., HAHN, P., KUHLMANN, M., THIEL, C., HAFNER, M., LENGELING, A., HEIMANN, P., JONES, J. M., MEISLER, M. H. & JOCKUSCH, H. 2005. Mutation of Vps54 causes motor neuron disease and defective spermiogenesis in the wobbler mouse. *Nature Genetics,* 37**,** 1213-1215.

SCOTT, S., KRANZ, J. E., COLE, J., LINCECUM, J. M., THOMPSON, K., KELLY, N., BOSTROM, A., THEODOSS, J., AL-NAKHALA, B. M., VIEIRA, F. G., RAMASUBBU, J. & HEYWOOD, J. A. 2008. Design, power, and interpretation of studies in the standard murine model of ALS. *Amyotrophic Lateral Sclerosis,* 9**,** 4-15.

SCOTTER, E. L., VANCE, C., NISHIMURA, A. L., LEE, Y.-B., CHEN, H.-J., URWIN, H., SARDONE, V., MITCHELL, J. C., ROGELJ, B., RUBINSZTEIN, D. C. & SHAW, C. E. 2014. Differential roles of the ubiquitin proteasome system and autophagy in the clearance of soluble and aggregated TDP-43 species. *Journal of Cell Science,* 127**,** 1263-1278.

SEPHTON, C. F., GOOD, S. K., ATKIN, S., DEWEY, C. M., MAYER, P., III, HERZ, J. & YU, G. 2010. TDP-43 Is a developmentally regulated protein essential for early embryonic development. *Journal of Biological Chemistry,* 285**,** 6826-6834.

SHAN, X., CHIANG, P.-M., PRICE, D. L. & WONG, P. C. 2010. Altered distributions of Gemini of coiled bodies and mitochondria in motor neurons of TDP-43 transgenic mice. *Proceedings of the National Academy of Sciences of the United States of America,* 107**,** 16325-16330.

SHARMA, K. R., KENTBRAUN, J. A., MAJUMDAR, S., HUANG, Y., MYNHIER, M., WEINER, M. W. & MILLER, R. G. 1995. Physiology of fatigue in amyotrophic-lateral-sclerosis. *Neurology,* 45**,** 733-740.

SHAW, P. J. 1994. Excitotoxicity and motor-neuron disease - a review of the evidence. *Journal of the Neurological Sciences,* 124**,** 6-13.

SHAW, P. J. 2005. Molecular and cellular pathways of neurodegeneration in motor neurone disease. *Journal of Neurology Neurosurgery and Psychiatry,* 76**,** 1046-1057.

SHEFNER, J. M., CUDKOWICZ, M. E. & BROWN, R. H. 2002. Comparison of incremental with multipoint mune methods in transgenic ALS mice. *Muscle & Nerve,* 25**,** 39-42.

SHEFNER, J. M., CUDKOWICZ, M. E., SCHOENFELD, D., CONRAD, T., TAFT, J., CHILTON, M., URBINELLI, L., QURESHI, M., ZHANG, H., PESTRONK, A., CARESS, J., DONOFRIO, P., SORENSON, E., BRADLEY, W., LOMEN-HOERTH, C., PIORO, E., REZANIA, K., ROSS, M., PASCUZZI, R., HEIMAN-PATTERSON, T., TANDAN, R., MITSUMOTO, H., ROTHSTEIN, J., SMITH-PALMER, T., MACDONALD, D., BURKE, D. & CONSORTIUM, N. 2004. A clinical trial of creatine in ALS. *Neurology,* 63**,** 1656-1661.

SHERWIN, C. M. 1998. Voluntary wheel running: a review and novel interpretation. *Animal Behaviour,* 56**,** 11-27.

SHI, Y., IVANNIKOV, M. V., WALSH, M. E., LIU, Y., ZHANG, Y., JARAMILLO, C. A., MACLEOD, G. T. & VAN REMMEN, H. 2014. The lack of CuZnSOD leads to impaired neurotransmitter release, neuromuscular junction destabilization and reduced muscle strength in mice. *Plos One,* 9.6, e100834.

SHIIHASHI, G., ITO, D., YAGI, T., NIHEI, Y., EBINE, T. & SUZUKI, N. 2016. Mislocated FUS is sufficient for gain-of-toxic-function amyotrophic lateral sclerosis phenotypes in mice. *Brain,* 139.9, 2380-2394.

SIKLOS, L., ENGELHARDT, J., HARATI, Y., SMITH, R. G., JOO, F. & APPEL, S. H. 1996. Ultrastructural evidence for altered calcium in motor nerve terminals in amyotrophic lateral sclerosis. *Annals of Neurology,* 39**,** 203-216.

SLOWIE, L. A., PAIGE, M. S. & ANTEL, J. P. 1983. Nutritional considerations in the management of patients with amyotrophic lateral sclerosis (ALS). *Journal of the American Dietetic Association,* 83**,** 44-47.

SMITH, B. N., TICOZZI, N., FALLINI, C., GKAZI, A. S., TOPP, S., KENNA, K. P., SCOTTER, E. L., KOST, J., KEAGLE, P., MILLER, J. W., CALINI, D., VANCE, C., DANIELSON, E. W., TROAKES, C., TILOCA, C., AL-SARRAJ, S., LEWIS, E. A., KING, A., COLOMBRITA, C., PENSATO, V., CASTELLOTTI, B., DE BELLEROCHE, J., BAAS, F., TEN ASBROEK, A. L. M. A., SAPP, P. C., MCKENNA-YASEK, D., MCLAUGHLIN, R. L., POLAK, M., ASRESS, S., ESTEBAN-PEREZ, J., MUNOZ-BLANCO, J. L., SIMPSON, M., VAN RHEENEN, W., DIEKSTRA, F. P., LAURIA, G., DUGA, S., CORTI, S., CEREDA, C., CORRADO, L., SORARU, G., MORRISON, K. E., WILLIAMS, K. L., NICHOLSON, G. A., BLAIR, I. P., DION, P. A., LEBLOND, C. S., ROULEAU, G. A., HARDIMAN, O., VELDINK, J. H., VAN DEN BERG, L. H., AL-CHALABI, A., PALL, H., SHAW, P. J., TURNER, M. R., TALBOT, K., TARONI, F., GARCIA-REDONDO, A., WU, Z., GLASS, J. D., GELLERA, C., RATTI, A., BROWN, R. H., JR., SILANI, V., SHAW, C. E., LANDERS, J. E. & CONSORTIUM, S. 2014. Exome-wide rare variant analysis identifies TUBA4A mutations associated with familial ALS. *Neuron,* 84**,** 324-331.

SNOW, R. J., TURNBULL, J., DA SILVA, S., JIANG, F. & TARNOPOLSKY, M. A. 2003. Creatine supplementation and riluzole treatment provide similar beneficial effects in copper, zinc superoxide dismutase (G93A) transgenic mice. *Neuroscience,* 119**,** 661-667.

SREEDHARAN, J., BLAIR, I. P., TRIPATHI, V. B., HU, X., VANCE, C., ROGELJ, B., ACKERLEY, S., DURNALL, J. C., WILLIAMS, K. L., BURATTI, E., BARALLE, F., DE BELLEROCHE, J., MITCHELL, J. D., LEIGH, P. N., AL-CHALABI, A., MILLER, C. C., NICHOLSON, G. & SHAW, C. E. 2008. TDP-43 mutations in familial and sporadic amyotrophic lateral sclerosis. *Science,* 319**,** 1668-1672.

STALLINGS, N. R., PUTTAPARTHI, K., DOWLING, K. J., LUTHER, C. M., BURNS, D. K., DAVIS, K. & ELLIOTT, J. L. 2013. TDP-43, an ALS linked protein, regulates fat deposition and glucose homeostasis. *Plos One,* 8.8, e71793.

STALLINGS, N. R., PUTTAPARTHI, K., LUTHER, C. M., BURNS, D. K. & ELLIOTT, J. L. 2010. Progressive motor weakness in transgenic mice expressing human TDP-43. *Neurobiology of Disease,* 40**,** 404-414.

STEWART, A., SANDERCOCK, J., BRYAN, S., HYDE, C., BARTON, P. M., FRY-SMITH, A. & BURLS, A. 2001. The clinical effectiveness and cost-effectiveness of riluzole for motor neurone disease: a rapid and systematic review. *Health technology assessment (Winchester, England),* 5**,** 1-97.

STONE, S., ABKEVICH, V., RUSSELL, D. L., RILEY, R., TIMMS, K., TRAN, T., TREM, D., FRANK, D., JAMMULAPATI, S., NEFF, C. D., ILIEV, D., GRESS, R., HE, G., FRECH, G. C., ADAMS, T. D., SKOLNICK, M. H., LANCHBURY, J. S., GUTIN, A., HUNT, S. C. & SHATTUCK, D. 2006. TBC1D1 is a candidate for a severe obesity gene and evidence for a gene/gene interaction in obesity predisposition. *Human Molecular Genetics,* 15**,** 2709-2720.

STOVER, C., ENDO, Y., TAKAHASHI, M., LYNCH, N. J., CONSTANTINESCU, C., VORUP-JENSEN, T., THIEL, S., FRIEDL, H., HANKELN, T., HALL, R., GREGORY, S., FUJITA, T. & SCHWAEBLE, W. 2001. The human gene for mannan-binding lectin-associated serine protease-2 (MASP-2), the effector component of the lectin route of complement activation, is part of a tightly linked gene cluster on chromosome 1p36.2-3. *Genes and Immunity,* 2**,** 119-127.

STOVER, K. R., CAMPBELL, M. A., VAN WINSSEN, C. M. & BROWN, R. E. 2015. Analysis of motor function in 6-month-old male and female 3xTg-AD mice. *Behavioural Brain Research,* 281**,** 16-23.

STYS, P. K., WAXMAN, S. G. & RANSOM, B. R. 1992. Ionic mechanisms of axonic injury in mammalian CNS white matter - role of Na+ channels and Na+-Ca2+ exchanger. *Journal of Neuroscience,* 12**,** 430-439.

SUN, H., HOU, Z., YANG, H., MENG, M., LI, P., ZOU, Q., YANG, L., CHEN, Y., CHAI, H., ZHONG, H., YANG, Z. Z., ZHAO, J., LAI, L., JIANG, X. & XIAO, Z. 2014. Multiple systemic transplantations of human amniotic mesenchymal stem cells exert therapeutic effects in an ALS mouse model. *Cell and Tissue Research,* 357**,** 571-582.

SUTEDJA, N. A., FISCHER, K., VELDINK, J. H., VAN DER HEIJDEN, G. J. M. G., KROMHOUT, H., HEEDERIK, D., HUISMAN, M. H. B., WOKKE, J. J. H. & VAN DEN BERG, L. H. 2009. What we truly know about occupation as a risk factor for ALS: A critical and systematic review. *Amyotrophic Lateral Sclerosis,* 10**,** 295-U70.

SWARUP, V., PHANEUF, D., BAREIL, C., ROBERTSON, J., ROULEAU, G. A., KRIZ, J. & JULIEN, J.-P. 2011. Pathological hallmarks of amyotrophic lateral sclerosis/frontotemporal lobar degeneration in transgenic mice produced with TDP-43 genomic fragments. *Brain,* 134**,** 2610-2626.

TAYLOR, E. B., AN, D., KRAMER, H. F., YU, H., FUJII, N. L., ROECKL, K. S. C., BOWLES, N., HIRSHMAN, M. F., XIE, J., FEENER, E. P. & GOODYEAR, L. J. 2008. Discovery of TBC1D1 as an insulin-, AICAR-, and contraction-stimulated signaling nexus in mouse skeletal muscle. *Journal of Biological Chemistry,* 283**,** 9787-9796.

TAYLOR, J. P., BROWN, R. H., JR. & CLEVELAND, D. W. 2016. Decoding ALS: from genes to mechanism. *Nature,* 539**,** 197-206.

TEYSSOU, E., TAKEDA, T., LEBON, V., BOILLEE, S., DOUKOURE, B., BATAILLON, G., SAZDOVITCH, V., CAZENEUVE, C., MEININGER, V., LEGUERN, E., SALACHAS, F., SEILHEAN, D. & MILLECAMPS, S. 2013. Mutations in SQSTM1 encoding p62 in amyotrophic lateral sclerosis: genetics and neuropathology. *Acta Neuropathologica,* 125**,** 511-522.

THOMAS, A., BURANT, A., BUI, N., GRAHAM, D., YUVA-PAYLOR, L. A. & PAYLOR, R. 2009. Marble burying reflects a repetitive and perseverative behavior more than novelty-induced anxiety. *Psychopharmacology,* 204**,** 361-373.

TOLLERVEY, J. R., CURK, T., ROGELJ, B., BRIESE, M., CEREDA, M., KAYIKCI, M., KOENIG, J., HORTOBAGYI, T., NISHIMURA, A. L., ZUPUNSKI, V., PATANI, R., CHANDRAN, S., ROT, G., ZUPAN, B., SHAW, C. E. & ULE, J. 2011. Characterizing the RNA targets and position-dependent splicing regulation by TDP-43. *Nature Neuroscience,* 14**,** 452-U180.

TRACEY, I., DUNN, J. F. & RADDA, G. K. 1996. Brain metabolism is abnormal in the mdx model of Duchenne muscular dystrophy. *Brain,* 119**,** 1039-1044.

TSAI, K.-J., YANG, C.-H., FANG, Y.-H., CHO, K.-H., CHIEN, W.-L., WANG, W.-T., WU, T.-W., LIN, C.-P., FU, W.-M. & SHEN, C.-K. J. 2010. Elevated expression of TDP-43 in the forebrain of mice is sufficient to cause neurological and pathological phenotypes mimicking FTLD-U. *Journal of Experimental Medicine,* 207**,** 1661-1673.

TURNER, M. J., KLEEBERGER, S. R. & LIGHTFOOT, J. T. 2005. Influence of genetic background on daily running-wheel activity differs with aging. *Physiological Genomics,* 22**,** 76-85.

TURNER, M. R., BOWSER, R., BRUIJN, L., DUPUIS, L., LUDOLPH, A., MCGRATH, M., MANFREDI, G., MARAGAKIS, N., MILLER, R. G., PULLMAN, S. L., RUTKOVE, S. B., SHAW, P. J., SHEFNER, J. & FISCHBECK, K. H. 2013. Mechanisms, models and biomarkers in amyotrophic lateral sclerosis. *Amyotrophic Lateral Sclerosis and Frontotemporal Degeneration,* 14**,** 19-32.

TURNER, M. R., CAGNIN, A., TURKHEIMER, F. E., MILLER, C. C. J. & SHAW, C. E. 2004. Evidence of widespread cerebral microglial activation in amyotrophic lateral sclerosis: an C-11 (R)-PK11195 positron emission tomography study. *Neurobiology of Disease,* 15**,** 601-609.

TURNER, M. R., KIERNAN, M. C., LEIGH, P. N. & TALBOT, K. 2009. Biomarkers in amyotrophic lateral sclerosis. *Lancet Neurology,* 8**,** 94-109.

TURNER, M. R. & TALBOT, K. 2013. Mimics and chameleons in motor neurone disease. *Practical neurology,* 13**,** 153-64.

UCHIDA, A., SASAGURI, H., KIMURA, N., TAJIRI, M., OHKUBO, T., ONO, F., SAKAUE, F., KANAI, K., HIRAI, T., SANO, T., SHIBUYA, K., KOBAYASHI, M., YAMAMOTO, M., YOKOTA, S., KUBODERA, T., TOMORI, M., SAKAKI, K., ENOMOTO, M., HIRAI, Y., KUMAGAI, J., YASUTOMI, Y., MOCHIZUKI, H., KUWABARA, S., UCHIHARA, T., MIZUSAWA, H. & YOKOTA, T. 2012. Non-human primate model of amyotrophic lateral sclerosis with cytoplasmic mislocalization of TDP-43. *Brain,* 135**,** 833-846.

VAN RHEENEN, W., SHATUNOV, A., DEKKER, A. M., MCLAUGHLIN, R. L., DIEKSTRA, F. P., PULIT, S. L., VAN DER SPEK, R. A. A., VOSA, U., DE JONG, S., ROBINSON, M. R., YANG, J., FOGH, I., VAN DOORMAAL, P. T. C., TAZELAAR, G. H. P., KOPPERS, M., BLOKHUIS, A. M., SPROVIERO, W., JONES, A. R., KENNA, K. P., VAN EIJK, K. R., HARSCHNITZ, O., SCHELLEVIS,

R. D., BRANDS, W. J., MEDIC, J., MENELAOU, A., VAJDA, A., TICOZZI, N., LIN, K., ROGELJ, B., VRABEC, K., RAVNIK-GLAVAC, M., KORITNIK, B., ZIDAR, J., LEONARDIS, L., GROSELJ, L. D., MILLECAMPS, S., SALACHAS, F., MEININGER, V., DE CARVALHO, M., PINTO, S., MORA, J. S., ROJAS-GARCIA, R., POLAK, M., CHANDRAN, S., COLVILLE, S., SWINGLER, R., MORRISON, K. E., SHAW, P. J., HARDY, J., ORRELL, R. W., PITTMAN, A., SIDLE, K., FRATTA, P., MALASPINA, A., TOPP, S., PETRI, S., ABDULLA, S., DREPPER, C., SENDTNER, M., MEYER, T., OPHOFF, R. A., STAATS, K. A., WIEDAU-PAZOS, M., LOMEN-HOERTH, C., VAN DEERLIN, V. M., TROJANOWSKI, J. Q., ELMAN, L., MCCLUSKEY, L., BASAK, A. N., TUNCA, C., HAMZEIY, H., PARMAN, Y., MEITINGER, T., LICHTNER, P., RADIVOJKOV-BLAGOJEVIC, M., ANDRES, C. R., MAUREL, C., BENSIMON, G., LANDWEHRMEYER, B., BRICE, A., PAYAN, C. A. M., SAKER-DELYE, S., DUERR, A., WOOD, N. W., TITTMANN, L., LIEB, W., FRANKE, A., RIETSCHEL, M., CICHON, S., NOETHEN, M. M., AMOUYEL, P., TZOURIO, C., DARTIGUES, J.-F., UITTERLINDEN, A. G., RIVADENEIRA, F., ESTRADA, K., HOFMAN, A., CURTIS, C., BLAUW, H. M., VAN DER KOOI, A. J., et al. 2016. Genome-wide association analyses identify new risk variants and the genetic architecture of amyotrophic lateral sclerosis. *Nature Genetics,* 48.9**,** 1043-1048.

VANCE, C., ROGELJ, B., HORTOBAGYI, T., DE VOS, K. J., NISHIMURA, A. L., SREEDHARAN, J., HU, X., SMITH, B., RUDDY, D., WRIGHT, P., GANESALINGAM, J., WILLIAMS, K. L., TRIPATHI, V., AL-SARAJ, S., AL-CHALABI, A., LEIGH, P. N., BLAIR, I. P., NICHOLSON, G., DE BELLEROCHE, J., GALLO, J.-M., MILLER, C. C. & SHAW, C. E. 2009. Mutations in FUS, an RNA processing protein, cause familial amyotrophic lateral sclerosis type 6. *Science,* 323**,** 1208-1211.

VERHAMME, C., KING, R. H. M., TEN ASBROEK, A., MUDDLE, J. R., NOURALLAH, M., WOLTERMAN, R., BAAS, F. & VAN SCHAIK, I. N. 2011. Myelin and axon pathology in a long-term study of PMP22-overexpressing mice. *Journal of Neuropathology and Experimental Neurology,* 70**,** 386-398.

VUCIC, S. & KIERNAN, M. C. 2006. Novel threshold tracking techniques suggest that cortical hyperexcitability is an early feature of motor neuron disease. *Brain,* 129**,** 2436-2446.

WAIBEL, S., REUTER, A., MALESSA, S., BLAUGRUND, E. & LUDOLPH, A. C. 2004. Rasagiline alone and in combination with riluzole prolongs survival in an ALS mouse model. *Journal of Neurology,* 251**,** 1080-1084.

WALKER, A. K., SPILLER, K. J., GE, G., ZHENG, A., XU, Y., ZHOU, M., TRIPATHY, K., KWONG, L. K., TROJANOWSKI, J. Q. & LEE, V. M. Y. 2015. Functional recovery in new mouse models of ALS/FTLD after clearance of pathological cytoplasmic TDP-43. *Acta Neuropathologica,* 130**,** 643-660.

WANG, F. C., DE PASQUA, V., GERARD, P. & DELWAIDE, P. J. 2001. Prognostic value of decremental responses to repetitive nerve stimulation in ALS patients. *Neurology,* 57**,** 897-899.

WANG, H. Y., WANG, I. F., BOSE, J. & SHEN, C. K. J. 2004. Structural diversity and functional implications of the eukaryotic TDP gene family. *Genomics,* 83**,** 130-139.

WANG, J., FARR, G. W., HALL, D. H., LI, F., FURTAK, K., DREIER, L. & HORWICH, A. L. 2009. An ALS-linked mutant SOD1 produces a locomotor defect associated with aggregation and synaptic dysfunction when expressed in neurons of Caenorhabditis elegans. *Plos Genetics,* 5.1, e1000350.

WANG, J., XU, G. L., GONZALES, V., COONFIELD, M., FROMHOLT, D., COPELAND, N. G., JENKINS, N. A. & BORCHELT, D. R. 2002. Fibrillar inclusions and motor neuron degeneration in transgenic mice expressing superoxide dismutase 1 with a disrupted copper-binding site. *Neurobiology of Disease,* 10**,** 128-138.

WANG, J., XU, G. L., SLUNT, H. H., GONZALES, V., COONFIELD, M., FROMHOLT, D., COPELAND, N. G., JENKINS, N. A. & BORCHELT, D. R. 2005. Coincident thresholds of mutant protein for paralytic disease and protein aggregation caused by restrictively expressed superoxide dismutase cDNA. *Neurobiology of Disease,* 20**,** 943-952.

WANG, W., WANG, L., LU, J., SIEDLAK, S. L., FUJIOKA, H., LIANG, J., JIANG, S., MA, X., JIANG, Z., DA ROCHA, E. L., SHENG, M., CHOI, H., LEROU, P. H., LI, H. & WANG, X. 2016. The

inhibition of TDP-43 mitochondrial localization blocks its neuronal toxicity. *Nat Med,* 22.8, 869-878.

WANG, X., FAN, H., YING, Z., LI, B., WANG, H. & WANG, G. 2010. Degradation of TDP-43 and its pathogenic form by autophagy and the ubiquitin-proteasome system. *Neuroscience Letters,* 469**,** 112-116.

WANG, Y.-T., KUO, P.-H., CHIANG, C.-H., LIANG, J.-R., CHEN, Y.-R., WANG, S., SHEN, J. C. K. & YUAN, H. S. 2013. The truncated C-terminal RNA recognition motif of TDP-43 protein plays a key role in forming proteinaceous aggregates. *Journal of Biological Chemistry,* 288**,** 9049-9057.

WATSON, M. R., LAGOW, R. D., XU, K., ZHANG, B. & BONINI, N. M. 2008. A Drosophila model for amyotrophic lateral sclerosis reveals motor neuron damage by human SOD1. *Journal of Biological Chemistry,* 283**,** 24972-24981.

WEGORZEWSKA, I., BELL, S., CAIRNS, N. J., MILLER, T. M. & BALOH, R. H. 2009. TDP-43 mutant transgenic mice develop features of ALS and frontotemporal lobar degeneration. *Proceedings of the National Academy of Sciences of the United States of America,* 106**,** 18809-18814.

WEISSKOPF, M. G., MCCULLOUGH, M. L., CALLE, E. E., THUN, M. J., CUDKOWICZ, M. & ASCHERIO, A. 2004. Prospective study of cigarette smoking and amyotrophic lateral sclerosis. *American Journal of Epidemiology,* 160**,** 26-33.

WEISSKOPF, M. G., O'REILLY, E. J., MCCULLOUGH, M. L., CALLE, E. E., THUN, M. J., CUDKOWICZ, M. & ASCHERIO, A. 2005. Prospective study of military service and mortality from ALS. *Neurology,* 64**,** 32-37.

WENDT, S., DEDEOGLU, A., SPEER, O., WALLIMANN, T., BEAL, M. F. & ANDREASSEN, O. A. 2002. Reduced creatine kinase activity in transgenic amyotrophic lateral sclerosis mice. *Free Radical Biology and Medicine,* 32**,** 920-926.

WEYDT, P., HONG, S. Y., KLIOT, M. & MOLLER, T. 2003. Assessing disease onset and progression in the SODI mouse model of ALS. *Neuroreport,* 14**,** 1051-1054.

WHALE, A. S., HUGGETT, J. F., COWEN, S., SPEIRS, V., SHAW, J., ELLISON, S., FOY, C. A. & SCOTT, D. J. 2012. Comparison of microfluidic digital PCR and conventional quantitative PCR for measuring copy number variation. *Nucleic Acids Research,* 40.

WHITTAKER, R. G. 2012. The fundamentals of electromyography. *Practical neurology,* 12**,** 187-94.

WIEDEMANN, F. R., MANFREDI, G., MAWRIN, C., BEAL, F. & SCHON, E. A. 2002. Mitochondrial DNA and respiratory chain function in spinal cords of ALS patients. *Journal of Neurochemistry,* 80**,** 616-625.

WILLIAMS, E. R. & BRUFORD, A. 1970. Creatine phosphokinase in motor neurone disease. *Clinica Chimica Acta,* 27.1**,** 53-56.

WILS, H., KLEINBERGER, G., JANSSENS, J., PERESON, S., JORIS, G., CUIJT, I., SMITS, V., CEUTERICK-DE GROOTE, C., VAN BROECKHOVEN, C. & KUMAR-SINGH, S. 2010. TDP-43 transgenic mice develop spastic paralysis and neuronal inclusions characteristic of ALS and frontotemporal lobar degeneration. *Proceedings of the National Academy of Sciences of the United States of America,* 107**,** 3858-3863.

WINTON, M. J., IGAZ, L. M., WONG, M. M., KWONG, L. K., TROJANOWSKI, J. Q. & LEE, V. M. Y. 2008. Disturbance of nuclear and cytoplasmic TAR DNA-binding protein (TDP-43) induces disease-like redistribution, sequestration, and aggregate formation. *Journal of Biological Chemistry,* 283**,** 13302-13309.

WONG, P. C., PARDO, C. A., BORCHELT, D. R., LEE, M. K., COPELAND, N. G., JENKINS, N. A., SISODIA, S. S., CLEVELAND, D. W. & PRICE, D. L. 1995. An adverse property of a familial ALS-linked SOD1 mutation causes motor-neuron disease characterized by vacuolar degeneration of mitochondria. *Neuron,* 14**,** 1105-1116.

WOOD, J. D., BEAUJEUX, T. P. & SHAW, P. J. 2003. Protein aggregation in motor neurone disorders. *Neuropathology and Applied Neurobiology,* 29**,** 529-545.

WOOD, S. J. & SLATER, C. R. 2001. Safety factor at the neuromuscular junction. *Progress in Neurobiology,* 64**,** 393-429.

WOOLEY, C. M., SHER, R. B., KALE, A., FRANKEL, W. N., COX, G. A. & SEBURN, K. L. 2005. Gait analysis detects early changes in transgenic SOD1(G93A) mice. *Muscle & Nerve,* 32**,** 43-50.

WU, C.-H., FALLINI, C., TICOZZI, N., KEAGLE, P. J., SAPP, P. C., PIOTROWSKA, K., LOWE, P., KOPPERS, M., MCKENNA-YASEK, D., BARON, D. M., KOST, J. E., GONZALEZ-PEREZ, P., FOX, A. D., ADAMS, J., TARONI, F., TILOCA, C., LECLERC, A. L., CHAFE, S. C., MANGROO, D., MOORE, M. J., ZITZEWITZ, J. A., XU, Z.-S., VAN DEN BERG, L. H., GLASS, J. D., SICILIANO, G., CIRULLI, E. T., GOLDSTEIN, D. B., SALACHAS, F., MEININGER, V., ROSSOLL, W., RATTI, A., GELLERA, C., BOSCO, D. A., BASSELL, G. J., SILANI, V., DRORY, V. E., BROWN, R. H., JR. & LANDERS, J. E. 2012a. Mutations in the profilin 1 gene cause familial amyotrophic lateral sclerosis. *Nature,* 488.7412**,** 499-503.

WU, L.-S., CHENG, W.-C. & SHEN, C. K. J. 2012b. Targeted depletion of TDP-43 expression in the spinal cord motor neurons leads to the development of amyotrophic lateral sclerosis-like phenotypes in mice. *Journal of Biological Chemistry,* 287**,** 27335-27344.

WU, Y., LIANG, D., WANG, Y., BAI, M., TANG, W., BAO, S., YAN, Z., LI, D. & LI, J. 2013. Correction of a genetic disease in mouse via use of CRISPR-Cas9. *Cell Stem Cell,* 13**,** 659-662.

XU, Y.-F., GENDRON, T. F., ZHANG, Y.-J., LIN, W.-L., D'ALTON, S., SHENG, H., CASEY, M. C., TONG, J., KNIGHT, J., YU, X., RADEMAKERS, R., BOYLAN, K., HUTTON, M., MCGOWAN, E., DICKSON, D. W., LEWIS, J. & PETRUCELLI, L. 2010. Wild-type human TDP-43 expression causes TDP-43 phosphorylation, mitochondrial aggregation, motor deficits, and early mortality in transgenic mice. *Journal of Neuroscience,* 30**,** 10851-10859.

XU, Y.-F., ZHANG, Y.-J., LIN, W.-L., CAO, X., STETLER, C., DICKSON, D. W., LEWIS, J. & PETRUCELLI, L. 2011. Expression of mutant TDP-43 induces neuronal dysfunction in transgenic mice. *Molecular Neurodegeneration,* 6.1, 73.

YAMANAKA, K., CHUN, S. J., BOILLEE, S., FUJIMORI-TONOU, N., YAMASHITA, H., GUTMANN, D. H., TAKAHASHI, R., MISAWA, H. & CLEVELAND, D. W. 2008a. Astrocytes as determinants of disease progression in inherited amyotrophic lateral sclerosis. *Nature Neuroscience,* 11**,** 251-253.

YAMANAKA, K., YAMASHITA, H., FUJIMORI-TONOU, N., TAKAHASHI, R., MISAWA, H. & CLEVELAND, D. W. 2008b. Astrocytes as determinants of disease progression in inherited ALS. *Neuroscience Research,* 61**,** S45-S45.

YANG, C., WANG, H., QIAO, T., YANG, B., ALIAGA, L., QIU, L., TAN, W., SALAMEH, J., MCKENNA-YASEK, D. M., SMITH, T., PENG, L., MOORE, M. J., BROWN, R. H., JR., CAI, H. & XU, Z. 2014. Partial loss of TDP-43 function causes phenotypes of amyotrophic lateral sclerosis. *Proceedings of the National Academy of Sciences of the United States of America,* 111**,** E1121-E1129.

YIN, F., DUMONT, M., BANERJEE, R., MA, Y., LI, H., LIN, M. T., BEAL, M. F., NATHAN, C., THOMAS, B. & DING, A. 2010. Behavioral deficits and progressive neuropathology in progranulin-deficient mice: a mouse model of frontotemporal dementia. *Faseb Journal,* 24**,** 4639-4647.

YOKOSEKI, A., SHIGA, A., TAN, C.-F., TAGAWA, A., KANEKO, H., KOYAMA, A., EGUCHI, H., TSUJINO, A., IKEUCHI, T., KAKITA, A., OKAMOTO, K., NISHIZAVA, M., TAKAHASHI, H. & ONODERA, O. 2008. TDP-43 mutation in familial amyotrophic lateral sclerosis. *Annals of Neurology,* 63**,** 538-542.

ZHANG, Y.-J., CAULFIELD, T., XU, Y.-F., GENDRON, T. F., HUBBARD, J., STETLER, C., SASAGURI, H., WHITELAW, E. C., CAI, S., LEE, W. C. & PETRUCELLI, L. 2013. The dual functions of the extreme N-terminus of TDP-43 in regulating its biological activity and inclusion formation. *Human Molecular Genetics,* 22**,** 3112-3122.

ZHOU, H., HUANG, C., CHEN, H., WANG, D., LANDEL, C. P., XIA, P. Y., BOWSER, R., LIU, Y.-J. & XIA, X. G. 2010. Transgenic rat model of neurodegeneration caused by mutation in the TDP gene. *Plos Genetics,* 6.3, e1000887.

ZHU, L., XU, M., YANG, M., YANG, Y., LI, Y., DENG, J., RUAN, L., LIU, J., DU, S., LIU, X., FENG, W., FUSHIMI, K., BIGIO, E. H., MESULAM, M., WANG, C. & WU, J. Y. 2014. An ALS-mutant

TDP-43 neurotoxic peptide adopts an anti-parallel beta-structure and induces TDP-43 redistribution. *Human Molecular Genetics,* 23**,** 6863-6877.

ZOCCOLELLA, S., BEGHI, E., PALAGANO, G., FRADDOSIO, A., SAMARELLI, V., LAMBERTI, P., LEPORE, V., SERLENGA, L., LOGROSCINO, G. & REGISTRY, S. 2006. Predictors of delay in the diagnosis and clinical trial entry of amyotrophic lateral sclerosis patients: A population-based study. *Journal of the Neurological Sciences,* 250**,** 45-49.

8. Project Outputs and Achievements

- Publication in revision: Stephenson, J. et al. (2017) Detailed Phenotypic Characterisation of Human TDP-43^{Q331K} Transgenic Mice Demonstrates Potential as a Preclinical Model for Testing Therapeutic Agents. *Disease Models and Mechanisms*
- Poster presentation at the MNDA 27th International Symposium on ALS/MND (Dublin, Ireland, 11-13th Dec 2016) https://f1000research.com/posters/5-2872
- Oral presentation at the European Network for the Cure of ALS (ENCALS) meeting 2016 (Milan, Italy, 19th-21st May 2016) entitled 'Evaluation of a TDP-43^{Q331K} mouse model: is it useful for therapeutic trials in ALS?'
- Lay presentation to the Manchester MND Association's AGM (April 2016)
- Lay presentation to the South Yorkshire MND Association's AGM (Feb 2016)
- Poster presentation at the MNDA 26th International Symposium on ALS/MND (Orlando, Florida, USA, 11-13th Dec 2015) http://f1000research.com/posters/4-1501